

Francisco Javier Milagro Serrano

Noninvasive autonomic nervous
system assessment in respiratory
disorders and sport sciences
applications

Departamento
Instituto de Investigación en Ingeniería [I3A]

Director/es
Gil Herrando, Eduardo
Bailón Luesma, Raquel

<http://zaguan.unizar.es/collection/Tesis>



Reconocimiento – NoComercial – SinObraDerivada (by-nc-nd): No se permite un uso comercial de la obra original ni la generación de obras derivadas.

© Universidad de Zaragoza
Servicio de Publicaciones

ISSN 2254-7606



Universidad
Zaragoza

Tesis Doctoral

**NONINVASIVE AUTONOMIC NERVOUS SYSTEM
ASSESSMENT IN RESPIRATORY DISORDERS
AND SPORT SCIENCES APPLICATIONS**

Autor

Francisco Javier Milagro Serrano

Director/es

Gil Herrando, Eduardo
Bailón Luesma, Raquel

UNIVERSIDAD DE ZARAGOZA

Instituto de Investigación en Ingeniería [I3A]

2019



Universidad
Zaragoza

Ph.D. Thesis

**Noninvasive autonomic nervous system
assessment in respiratory disorders and
sport sciences applications**

Javier Milagro

SUPERVISORS:

Prof. Raquel Bailón

Prof. Eduardo Gil

Ph.D. in Biomedical Engineering

October, 2019

**Noninvasive autonomic
nervous system assessment in
respiratory disorders and sport
sciences applications**

Javier Milagro, 2019

Noninvasive autonomic nervous system assessment in respiratory disorders and sport sciences applications.

Date of current version: October 7, 2019

This Ph.D. thesis has been developed within the Department of Electronic Engineering and Communications and the Aragón Institute for Engineering Research (I3A) at the University of Zaragoza (Zaragoza, Spain). This thesis has been developed in the context of the BioMEP Doctoral Programme (Marie Skłodowska-Curie Actions).

The research presented in this thesis was supported by the FPI grant *BES-2015-073694* and the projects *TIN2014-53567-R* and *RTI2018-097723-B-I00* from the *Ministerio de Economía y Competitividad* (Spain). It was also funded by *Gobierno de Aragón* (Spain) through *Reference Group BSICoS T39-17R* cofunded by *FEDER 2014-2020 "Building Europe from Aragon"*, and by *CIBER in Bioengineering, Biomaterials & Nanomedicine (CIBER-BBN)* through *Instituto de Salud Carlos III*. The computation of some parts of this thesis was performed at the *High Performance Computing platform of the NANBIOSIS ICTS, CIBER-BBN and Aragón Institute of Engineering Research (I3A)*, Zaragoza, Spain.

This thesis was printed thanks to the financial support of BSICoS Group at University of Zaragoza.

Abstract

This dissertation is focused on the noninvasive analysis of cardiac and respiratory signals, aiming at assessing autonomic nervous system (ANS) activity in several clinical and non-clinical scenarios. The document is structured in three main parts. The first part consist of an introduction to the physiological and methodological aspects to be covered in the rest of the thesis. In the second part, heart rate variability (HRV) analysis is applied in the context of respiratory disorders, concretely in asthma (both in children and adults) and in sleep apnea. In the third part, some novel applications of cardiorespiratory signals analysis in the filed of sport sciences are addressed.

The first part is composed of Ch. 1 and 2. In Ch. 1, an extensive physiological framework of the functioning of the ANS and the characteristics of the biosignals analyzed throughout the thesis is provided. Also the pathophysiology of asthma and sleep apnea, their relationship with ANS functioning, and their diagnosis and treatment strategies are discussed. The chapter concludes with an introduction to exercise physiology and to the interest in the estimation of the tidal volume and the anaerobic threshold in the field of sport sciences.

Regarding Ch.2, a common framework for the contextualized analysis of HRV is presented. After a description of the HRV signal assessment and conditioning tools, it focuses on the effect of ectopic beats, respiratory sinus arrhythmia and respiratory rate in HRV analysis. Furthermore, the use of an index for the evaluation of how the power is distributed in the HRV spectra, as well as cardiorespiratory coupling measurements, are discussed.

The second part is composed of Ch. 3, 4 and 5, all of them covering the analysis of HRV in respiratory disorders. Whereas Ch. 3 and 4 focus on child and adult asthma respectively, in Ch. 5 sleep apnea is considered. Asthma is a chronic respiratory disease which is usually accompanied by airway inflammation. It affects people of any age, but it is prone to start in early ages, and in recent years it has risen as one of the most common chronic diseases of childhood. However, there is still not a feasible method for the diagnosis of asthma in young children. The important role of vagal control in the broncho-motor tone and broncho-dilation control has pointed to the parasympathetic branch of the ANS as being involved in the pathogenesis of asthma. In this way, in Ch. 3 ANS assessment was addressed through HRV analysis in two different datasets composed of pre-school children classified attending to their risk of developing asthma or their current asthma condition. The results of the analysis revealed a decreased sympathovagal balance and a peakier high-frequency spectral component in those children at higher risk of asthma. Moreover, vagal activity and cardiorespiratory coupling lowered in a group of children with reduced risk of asthma following treatment for obstructive bronchitis, whereas they kept unchanged in those children with a worse asthma prognosis.

In difference with children, the assessment of asthma in adults is performed through a well established clinical routine. However, the stratification of patients attending to their degree of control of the symptoms is generally based on self-applied questionnaires, which remain subjective. On the other hand, the evaluation of the asthma severity re-

quires from a visit to the hospital and cumbersome tests, which can not be applied in a continuous-time basis. In this way, in Ch. 4 the value of ANS assessment for the stratification of asthmatic adults was studied. Several HRV, respiratory-derived and clinical features were used for training a set of classification algorithms. The inclusion of ANS information for classifying the subjects attending to their asthma severity resulted in a similar performance than using only clinical features, outperforming them in some cases. Therefore, ANS assessment could represent a potential complement for the monitoring of asthma.

In Ch. 5, HRV is analyzed in subjects suffering from sleep apnea syndrome (SAS) and associated cardiovascular comorbidities. SAS has been related with a 5-fold increase in the risk of developing cardiovascular diseases (CVD), which could rise to 11-fold if not conveniently treated. On the other hand, altered HRV has been independently related to SAS and to several conditions that represent risk factors for the development of CVD. Therefore, this chapter is focused on evaluating whether an imbalanced autonomic activity could be related with the development of CVD in patients with SAS. The analysis revealed a decreased sympathetic dominance in those subjects suffering from SAS and CVD with respect to those without CVD. Moreover, a retrospective analysis in a dataset with subjects with SAS that will develop CVD in the future also revealed a reduced sympathetic activity, thus suggesting that an imbalanced ANS could represent an additional risk for the development of CVD in patients with SAS.

The third part is formed by Ch. 6 and 7, and it covers different applications of the analysis of cardiorespiratory signals in the field of sport sciences. Ch. 6 is focused on the estimation of the tidal volume (TV) from the electrocardiogram (ECG). Although a proper monitoring of the respiratory activity results of great interest in certain respiratory disorders and in sport sciences, the main research effort has focused on the estimation of the respiratory rate, with only a few studies concerning the TV, most of which rely on ECG-unrelated techniques. In this chapter, a methodological framework for the estimation of TV during rest and during a treadmill test using only ECG-derived features is proposed. Fitting errors lower than 14% in most of the cases and than 6% in some of them suggest that TV can be estimated from the ECG, even in non-stationary conditions.

Finally, in Ch. 7 a novel methodology for the estimation of the anaerobic threshold (AT) from the analysis of ventricular repolarization dynamics is proposed. The AT represents the frontier beyond which the cardiovascular system limits the endurance work, and whereas it was initially intended to assess the exercise capacity in patients with CVD, it is also of great interest in the field of sport sciences, in order to design better training routines or prevent from overtraining. However, the assessment of the AT requires from invasive tests or cumbersome devices. In this chapter, the AT was estimated from the analysis of the variations in ventricular repolarization dynamics during a cycle ergometer test. Estimation errors lower than 25 W, corresponding to 1 minute in this study, in a 63% of the subjects (and lower than 50 W in the 74%) suggest that AT can be estimated noninvasively, using only ECG recordings.

Resumen y conclusiones

La presente tesis está centrada en el análisis no invasivo de señales cardíacas y respiratorias, con el objetivo de evaluar la actividad del sistema nervioso autónomo (ANS) en diferentes escenarios, tanto clínicos como no clínicos. El documento está estructurado en tres partes principales. La primera parte consiste en una introducción a los aspectos fisiológicos y metodológicos que serán cubiertos en el resto de la tesis. En la segunda parte, se analiza la variabilidad del ritmo cardíaco (HRV) en el contexto de enfermedades respiratorias, concretamente asma (tanto en niños como en adultos) y apnea del sueño. En la tercera parte, se estudian algunas aplicaciones novedosas del análisis de señales cardiorespiratorias en el campo de las ciencias del deporte.

La primera parte está compuesta por los capítulos 1 y 2. El capítulo 1 consiste en una extensa introducción al funcionamiento del sistema nervioso autónomo y las características de las bioseñales analizadas a lo largo de la tesis. Por otro lado, se aborda la patofisiología del asma y la apnea del sueño, su relación con el funcionamiento del ANS y las estrategias de diagnóstico y tratamiento de las mismas. El capítulo concluye con una introducción a la fisiología del ejercicio, así como al interés en la estimación del volumen tidal y del umbral anaeróbico en el campo de las ciencias del deporte.

En cuanto al capítulo 2, se presenta un marco de trabajo para el análisis contextualizado de la HRV. Después de una descripción de las técnicas de evaluación y acondicionamiento de la señal de HRV, el capítulo se centra en el efecto de los latidos ectópicos, la arritmia sinusal respiratoria y la frecuencia respiratoria en el análisis de la HRV. Además, se discute el uso de un índice para la evaluación de la distribución de la potencia en los espectros de HRV, así como diferentes medidas de acoplo cardiorespiratorio.

La segunda parte está compuesta por los capítulos 3, 4 y 5, todos ellos relacionados con el análisis de la HRV en enfermedades respiratorias. Mientras que los capítulos 3 y 4 están centrados en asma infantil y en adultos respectivamente, el capítulo 5 aborda la apnea del sueño. El asma es una enfermedad respiratoria crónica que aparece habitualmente acompañada por una inflamación de las vías respiratorias. Aunque afecta a personas de todas las edades, normalmente se inicia en edades tempranas, y ha llegado a constituir una de las enfermedades crónicas más comunes durante la infancia. Sin embargo, todavía no existe un método adecuado para el diagnóstico de asma en niños pequeños. Por otro lado, el rol fundamental que desempeña el sistema nervioso parasimpático en el control del tono bronco-motor y la bronco-dilatación sugiere que la rama parasimpática del ANS podría estar implicada en la patogénesis del asma. De este modo, en el capítulo 3 se evalúa el ANS mediante el análisis de la HRV en dos bases de datos diferentes, compuestas por niños en edad pre-escolar clasificados en función de su riesgo de desarrollar asma, o de su condición asmática actual. Los resultados del análisis revelaron un balance simpático-vagal reducido y una componente espectral de alta frecuencia más picuda en aquellos niños con un mayor riesgo de desarrollar asma. Además, la actividad parasimpática y el acoplo cardiorespiratorio se redujeron en un grupo de niños con bajo riesgo de asma al finalizar un tratamiento para bronquitis obstructiva, mientras que estos permanecieron inalterados en aquellos niños con una peor prógnosis.

A diferencia de los niños pequeños, en el caso de adultos el diagnóstico de asma se realiza a través de una rutina clínica bien definida. Sin embargo, la estratificación de los pacientes en función de su grado de control de los síntomas se basa generalmente en el uso de cuestionarios auto-aplicados, que pueden tener un carácter subjetivo. Por otro lado, la evaluación de la severidad del asma requiere de una visita hospitalaria y de incómodas pruebas, que no pueden aplicarse de una forma continua en el tiempo. De este modo, en el capítulo 4 se estudia el valor de la evaluación del ANS para la estratificación de adultos asmáticos. Para ello, se emplearon diferentes características extraídas de la HRV y la respiración, junto con varios parámetros clínicos, para entrenar un conjunto de algoritmos de clasificación. La inclusión de características relacionadas con el ANS para clasificar los sujetos atendiendo a la severidad del asma derivó en resultados similares al caso de utilizar únicamente parámetros clínicos, superando el desempeño de estos últimos en algunos casos. Por lo tanto, la evaluación del ANS podría representar un potencial complemento para la mejora de la monitorización de sujetos asmáticos.

En el capítulo 5, se analiza la HRV en sujetos que padecen el síndrome de apnea del sueño (SAS) y comorbidades cardíacas asociadas. El SAS se ha relacionado con un incremento de 5 veces en el riesgo de desarrollar enfermedades cardiovasculares (CVD), que podría aumentar hasta 11 veces si no se trata convenientemente. Por otro lado, una HRV alterada se ha relacionado independientemente con el SAS y con numerosos factores de riesgo para el desarrollo de CVD. De este modo, este capítulo se centra en evaluar si una actividad autónoma desbalanceada podría estar relacionada con el desarrollo de CVD en pacientes de SAS. Los resultados del análisis revelaron una dominancia simpática reducida en aquellos sujetos que padecían SAS y CVD, en comparación con aquellos sin CVD. Además, un análisis retrospectivo en una base de datos de sujetos con SAS que desarrollarán CVD en el futuro también reveló una actividad simpática reducida, sugiriendo que un ANS desbalanceado podría constituir un factor de riesgo adicional para el desarrollo de CVD en pacientes de SAS.

La tercera parte está formada por los capítulos 6 y 7, y está centrada en diferentes aplicaciones del análisis de señales cardiorespiratorias en el campo de las ciencias del deporte. El capítulo 6 aborda la estimación del volumen tidal (TV) a partir del electrocardiograma (ECG). A pesar de que una correcta monitorización de la actividad respiratoria es de gran interés en ciertas enfermedades respiratorias y en ciencias del deporte, la mayor parte de la actividad investigadora se ha centrado en la estimación de la frecuencia respiratoria, con sólo unos pocos estudios centrados en el TV, la mayoría de los cuales se basan en técnicas no relacionadas con el ECG. En este capítulo se propone un marco de trabajo para la estimación del TV en reposo y durante una prueba de esfuerzo en tapiz rodante utilizando únicamente parámetros derivados del ECG. Errores de estimación del 14% en la mayoría de los casos y del 6% en algunos sugieren que el TV puede estimarse a partir del ECG, incluso en condiciones no estacionarias.

Por último, en el capítulo 7 se propone una metodología novedosa para la estimación del umbral anaeróbico (AT) a partir del análisis de las dinámicas de repolarización ventricular. El AT representa la frontera a partir de la cual el sistema cardiovascular limita la actividad física de resistencia, y aunque fue inicialmente concebido para la evaluación

de la capacidad física de pacientes con CVD, también resulta de gran interés en el campo de las ciencias del deporte, permitiendo diseñar mejores rutinas de entrenamiento o para prevenir el sobre-entrenamiento. Sin embargo, la evaluación del AT requiere de técnicas invasivas o de dispositivos incómodos. En este capítulo, el AT fue estimado a partir del análisis de las variaciones de las dinámicas de repolarización ventricular durante una prueba de esfuerzo en cicloergómetro. Errores de estimación de 25 W, correspondientes a 1 minuto en este estudio, en un 63% de los sujetos (y menores que 50 W en un 74% de ellos) sugieren que el AT puede estimarse de manera no invasiva, utilizando únicamente registros de ECG.

*If you don't build your dream,
someone else will hire you
to help them build theirs.*

- Dhirajlal H. Ambani

Contents

I	Introduction and methodology	1
1	Introduction	3
1.1	Motivation	3
1.2	Autonomic nervous system	4
1.3	Biological signals	5
1.3.1	Cardiac activity	6
1.3.2	Respiratory activity	8
1.4	Heart rate variability	12
1.4.1	Clinical relevance of HRV	14
1.4.2	Heart rhythm representations	14
1.4.3	HRV analysis	16
1.5	Target respiratory disorders	17
1.5.1	Asthma	17
1.5.2	Sleep apnea syndrome	23
1.6	Exercise physiology	26
1.6.1	Estimation of the tidal volume	27
1.6.2	Estimation of the anaerobic threshold	27
1.7	Structure of the thesis	28
1.8	Collaborations and research stays	32
2	Contextualized HRV analysis	35
2.1	Motivation	35
2.2	HRV assessment	36
2.3	Signal conditioning	38
2.4	Ectopic beats versus RSA	40

2.4.1	RSA detection algorithm	42
2.4.2	RSA correction in the presence of ectopic beats	46
2.4.3	Discussion	49
2.5	Peakness	51
2.5.1	Motivation	51
2.5.2	Definition	51
2.5.3	Parameter selection	53
2.5.4	Relationship with kurtosis	55
2.5.5	Relationship with HRV frequency domain analysis	59
2.5.6	Relationship with HRV nonlinear analysis	61
2.5.7	Discussion	61
2.6	Effect of the respiratory rate	63
2.6.1	Modified high-frequency bands	64
2.6.2	Removing respiratory influence from HRV	64
2.7	Cardiorespiratory coupling	67
2.8	Discussion and conclusions	69
II	HRV analysis in respiratory disorders	71
3	HRV analysis in children with asthmatic symptoms	73
3.1	Motivation	74
3.2	Materials and methods	75
3.2.1	Helsinki University Hospital dataset	75
3.2.2	Tampere University Hospital dataset	75
3.2.3	Preprocessing	77
3.2.4	HRV analysis	79
3.2.5	Peakness analysis	80
3.2.6	Time-frequency coherence analysis	80
3.2.7	Statistical methods	82
3.3	Results	82
3.3.1	Helsinki University Hospital dataset	82
3.3.2	Tampere University Hospital dataset	83
3.4	Discussion	86

3.4.1	Methodology	87
3.4.2	Helsinki University Hospital dataset	87
3.4.3	Tampere University Hospital dataset	93
3.4.4	Limitations	96
3.4.5	Physiological interpretation	96
3.5	Conclusion	97
4	HRV analysis in asthmatic adults	99
4.1	Motivation	99
4.2	Materials and methods	101
4.2.1	Study population	101
4.2.2	Preprocessing	101
4.2.3	HRV analysis	103
4.2.4	Respiration dynamics analysis	103
4.2.5	Statistical analysis	104
4.2.6	Automatic stratification	104
4.3	Results	106
4.4	Discussion	109
4.5	Conclusion	112
5	HRV analysis in sleep apnea syndrome with associated cardiovascular diseases	113
5.1	Motivation	113
5.2	Materials and methods	115
5.2.1	UZ Leuven dataset	115
5.2.2	Sleep Heart Health Study dataset	116
5.2.3	Preprocessing	117
5.2.4	HRV analysis	117
5.2.5	Effect of sleep stages on HRV	118
5.2.6	Effect of apneas, hypopneas and arousals on HRV	118
5.2.7	Effect of medication	119
5.2.8	Statistical methods	120
5.3	Results	120
5.3.1	UZ Leuven dataset	120

5.3.2	SHHS dataset	121
5.4	Discussion	123
5.4.1	UZ Leuven dataset	124
5.4.2	SHHS dataset	125
5.4.3	Limitations	125
5.5	Conclusion	126
III Cardiorespiratory signals analysis in sport sciences		127
6	Electrocardiogram-derived tidal volume estimation	129
6.1	Motivation	129
6.2	Materials and methods	130
6.2.1	Dataset	130
6.2.2	Preprocessing	131
6.2.3	Tidal volume estimation	132
6.2.4	Single-lead EDR	133
6.2.5	Multi-lead EDR	134
6.2.6	Instantaneous heart rate	135
6.2.7	Heart rate variability	135
6.2.8	Respiratory rate	136
6.2.9	Multi-parametric model	136
6.2.10	Subject-independent model	137
6.2.11	Performance measurement	137
6.3	Results	137
6.4	Discussion	141
6.5	Conclusion	144
7	Anaerobic threshold estimation through ventricular repolarization profile analysis	145
7.1	Motivation	145
7.2	Materials and methods	146
7.2.1	Dataset	146
7.2.2	Determination of the ventilatory threshold	147
7.2.3	Repolarization dynamics assessment	147

7.2.4	Anaerobic threshold estimation	149
7.2.5	Statistical analysis	150
7.3	Results	151
7.4	Discussion	152
7.5	Conclusion	154
IV	Conclusions	155
8	Conclusions and future work	157
8.1	Summary and conclusions	157
8.1.1	HRV analysis in asthma	158
8.1.2	HRV analysis in sleep apnea syndrome	159
8.1.3	Cardiorespiratory signals analysis in sport sciences applications ..	160
8.1.4	Conclusion	161
8.2	Future work	161
V	Appendix	163
	Awards and scientific contributions	165
	List of acronyms	169
	List of figures	172
	List of tables	183
	References	187

Part I

Introduction and methodology

1

Introduction

1.1 Motivation	1.5 Target respiratory disorders
1.2 Autonomic nervous system	1.5.1 Asthma
1.3 Biological signals	1.5.2 Sleep apnea syndrome
1.3.1 Cardiac activity	1.6 Exercise physiology
1.3.2 Respiratory activity	1.6.1 Estimation of the tidal volume
1.4 Heart rate variability	1.6.2 Estimation of the anaerobic threshold
1.4.1 Clinical relevance of HRV	1.7 Structure of the thesis
1.4.2 Heart rhythm representations	1.8 Collaborations and research stays
1.4.3 HRV analysis	

1.1 Motivation

The recent advances in data processing, analysis and acquisition systems have supported a rapid evolution transversal to a wide variety of fields, including that of medical and health sciences. The application of signal processing techniques to the analysis of human body functioning has enabled large research aiming to understand the human physiology and pathophysiology, which has resulted in new diagnostic approaches and monitoring devices. However, the relationship between technology and medicine is not unidirectional and the development of new analysis tools must be guided by a deep knowledge of

human anatomy and physiology, so that the results can be provided with a meaningful interpretation.

The possibility to manage large amounts of clinical data has facilitated a better phenotyping of the patients, which is rapidly evolving in what is known as personalized medicine, also complemented by the growing interest in the development of noninvasive approaches, aiming at increasing patients comfort. The noninvasive analysis of biological signals constitutes the core of the present dissertation. Concretely, the focus is on the assessment of autonomic nervous system (ANS) activity through the analysis of cardiorespiratory signals, applied to different clinical and non-clinical scenarios. The ANS is thought to be involved in the pathogenesis of several disorders of different nature, so that the assessment of ANS activity remains of great interest in order to shed some light on the underlying physiological mechanisms triggering them. Given the possibility to assess ANS noninvasively, the analysis of ANS activity has been regarded as an interesting approach for designing new diagnostic and monitoring methodologies. Since the analysis of heart rate variability is acknowledged as a convenient tool for the analysis of ANS, it occupies the majority of the research efforts summarized in this thesis, although several other biosignals such as the electrocardiogram, the respiratory effort or the tidal volume have been also considered. In order to better understand the nature of the different topics addressed in the following chapters, a physiological background of the implied human body systems, biological signals, and scenarios covered in this dissertation is provided below.

On the other hand, the analysis of biosignals has been also applied to the field of sport sciences. In this case, the largest interest is in the assessment of different markers of physical condition, such as the tidal volume or the anaerobic threshold, in a noninvasive way. The last part of this thesis is focused on the analysis of cardiorespiratory signals for sport sciences applications and, in the present chapter, an overview of exercise physiology and the considered applications is provided.

1.2 Autonomic nervous system

The ANS or involuntary nervous system is the division of the peripheral nervous system which controls the unconscious functioning of several organs and tissues in the body. It plays a crucial role in the maintenance of homeostasis through the monitoring and regulation of a series of physiological variables such as heart rate (HR), blood pressure, respiratory activity, body temperature or gastrointestinal peristalsis. In this way, the afferent fibers of different cranial nerves transmit sensory information to the brainstem and hypothalamus, where it is processed and integrated. Afterwards, these brain structures exert their control, which might be influenced by higher areas in the brain, by the transmission of nerve signals through the efferent fibers [173].

The ANS is divided in three branches: the sympathetic nervous system (SNS), the parasympathetic nervous system (PNS) and the enteric nervous system. The latter, which

governs the function of the gastrointestinal tract, will not be considered in this thesis. In the case of the SNS, it is usually associated with the so called “fight or flight” response, since its main function is to prepare the body for dealing with a threat. Hence, sympathetic activity is related with an increase in heart rate and force of contraction, respiratory rate, vasoconstriction, bronchodilation, skeletal muscle strengthen or pupil dilation. On the other hand, PNS activity is associated with the “rest and digest” state, i.e., with the relaxation of the body. Therefore, parasympathetic activity induces a decrease in heart and respiratory rates, vasodilation, bronchoconstriction and pupil constriction [112,242]. Since most of the tissues are innervated by both branches, exerting opposing effects, the ANS provides a rapid and effective control of organs function. Importantly, both systems have respective basal discharge rates, which are referred to as sympathetic and parasympathetic (or vagal) tones. In this way, SNS and PNS activity is modulated by changes in the efferent fibers discharge rate [112]. This mechanism also results in a similar effect of an increased sympathetic activity or a vagal withdrawal (and vice versa) on several homeostatic functions, thus yielding to an enhanced precision in their control.

Autonomic pathways are composed by two neurons: a preganglionic neuron, which originates in the central nervous system and projects to an autonomic ganglion outside it, and a postganglionic neuron, which projects from the ganglion to the target tissue [242]. According to the neurotransmitter that they release, these fibers can be divided in adrenergic, if they secrete noradrenaline (also called norepinephrine), or cholinergic, if they release acetylcholine, although there is growing evidence of the existence of non-adrenergic non-cholinergic autonomic pathways in the human body [242, 279]. All the preganglionic fibers are cholinergic, both in the SNS and the PNS. On the other hand, whereas almost all the postganglionic fibers in the PNS are cholinergic, most of the postganglionic sympathetic fibers are adrenergic, so that acetylcholine and noradrenaline are usually regarded as parasympathetic and sympathetic neurotransmitters respectively [112]. Nevertheless, sympathetic activity is also regulated by circulating catecholamines (adrenaline and noradrenaline), which are secreted by the suprarenal glands and exert almost the same effects that sympathetic nerve stimulation in the different tissues. Since adrenaline and noradrenaline are directly released into the blood flow, the effect of a sympathetic activation is more generalized than in the case of a parasympathetic activation, with a more local effect. A schematic of ANS anatomy is depicted in Fig. 1.1.

1.3 Biological signals

A biological signal or biosignal is any physical change that takes place in a living being and that is susceptible of being measured. They contain large information about the status of an organism and, in the case of human biosignals, their analysis and interpretation is of great interest in order to identify pathological conditions. In this dissertation, the focus is on several biosignals accounting for cardiac, respiratory and autonomic activity,

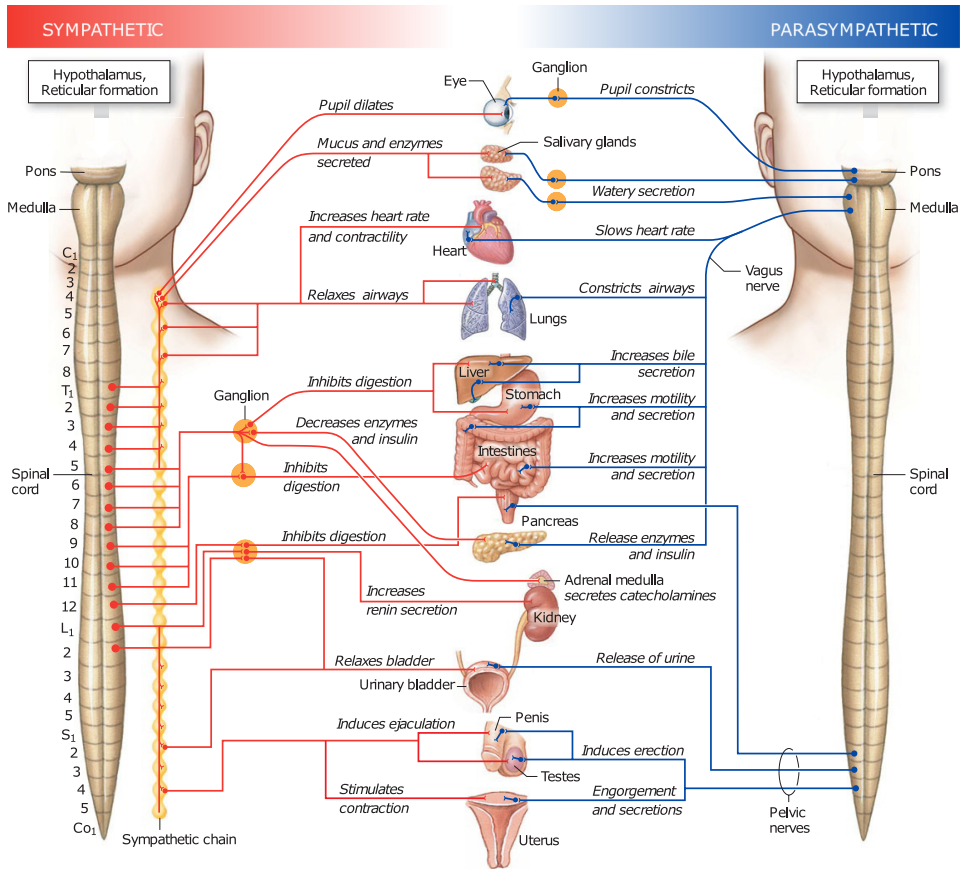


Figure 1.1: Anatomy of the sympathetic (left) and parasympathetic (right) branches of the autonomic nervous system. The effect exerted by each branch over the different organs that they innervate is indicated. Reproduced and modified from [242].

as detailed below. Note that, although heart rate variability is a biosignal, it is described in a different section, since its analysis remains the core of this thesis.

1.3.1 Cardiac activity

The electrocardiographic signal or electrocardiogram (ECG) describes the electrical activity of the cardiac muscle, as measured on the body surface through electrodes attached to the skin. It is composed of the spatio-temporal sum of the action potentials generated by all the cells in the cardiac tissue (see Fig. 1.2), which generates characteristic wave-forms whose morphology and timing contain information that is largely used in the diagnosis of cardiac pathologies. In this way, a cardiac cycle is reflected in the ECG as consecutive positive and negative deflections that are related with the depolarization and repolarization of the cardiomyocytes of the different regions of the heart. An example is displayed in Fig. 1.3, where the typical waves that compose the ECG are depicted. The cardiac cycle

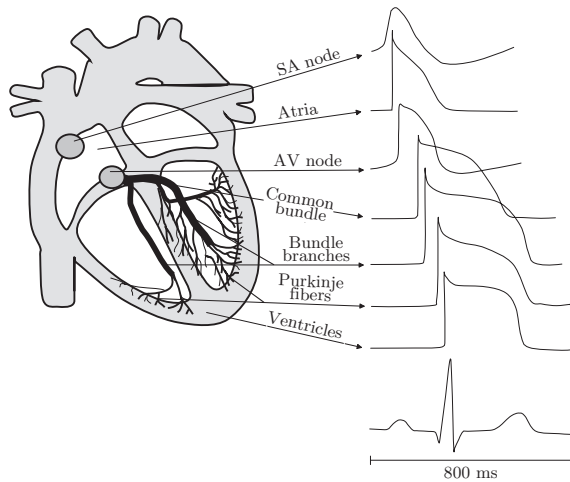


Figure 1.2: Cardiac electrical conduction system. The morphology and timing of the action potentials generated in different parts of the heart and the surface electrocardiogram resulting from their spatio-temporal combination are displayed. Reproduced from [246].

of a normal beat starts with the spontaneous depolarization of the cells in the sinoatrial (SA) node, located laterally to the entrance of the superior vena cava, in the right atrium. The electrical impulse first propagates through both atria, and the depolarization of the atrial cells is reflected in the ECG as the so-called P wave. Afterwards, it is transmitted to the ventricles through the atrioventricular (AV) node, located in the lower back section of the inter-atrial septum, which remains the only electrical pathway between the atria and the ventricles. The electrical impulse is conducted from the AV node to the bundle of His, from which it rapidly propagates towards the ventricular walls through the Purkinje fibers. The depolarization of the ventricles is reflected in the ECG as the QRS complex, usually composed by a negative deflection (Q wave), followed by a positive deflection (R wave) and another negative one (S wave), although it may be composed by less than three waves. The end of the S wave is referred to as the J point. To finish the cardiac cycle, ventricular repolarization, reflected in the ECG as the T wave, prepares the ventricles for the next beat.

There are also some important time intervals in the ECG. The PQ interval represents the time required for the transmission of the electrical impulse from the SA node to the ventricles. On the other hand, the QT interval represents the time that passes from the onset of ventricular depolarization until the offset of ventricular repolarization, whereas the ST segment accounts for the time during which the ventricles remain in a depolarized state. Finally, the time between two consecutive R waves is referred to as RR interval, and it is often considered as the time between consecutive beats and used for the characterization of arrhythmias and for the study of heart rate variability [246].

In an ECG recording, a lead is the voltage difference between two electrodes (bipolar lead) or between a single electrode and a reference electrode selected in order to have an almost constant voltage during the entire cardiac cycle (unipolar lead). The most em-

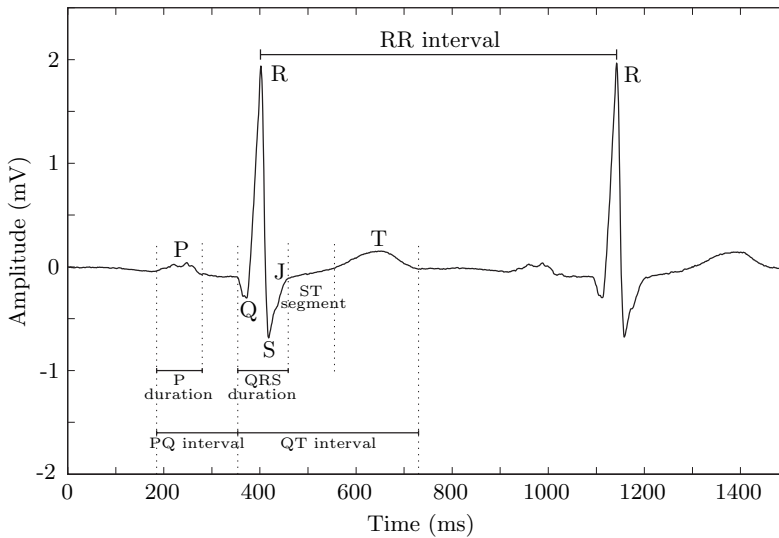


Figure 1.3: Characteristic waves and intervals in the electrocardiogram. Reproduced from [246].

ployed recording configuration in the clinical routine is the standard 12-lead ECG, in which the electrodes are placed as indicated in Fig. 1.4. This configuration accounts for the electrical activity in the frontal plane, through the standard bipolar limb leads (I , II and III) and the augmented unipolar limb leads (aVF , aVL and aVR), and in the horizontal plane, through the six unipolar precordial leads (V_1 to V_6), as depicted in Fig. 1.5. Another interesting recording scheme is the orthogonal leads (or Frank's leads) configuration, in which the electrical activity of the heart is captured through three pairs of electrodes positioned along mutually perpendicular lines, denoted as X , Y and Z . This configuration is very convenient for tracking the dominant direction of the electrical axis of the heart.

1.3.2 Respiratory activity

Breathing is the process through which the body meets its oxygen demands and eliminates the excess of CO_2 . It is divided in two stages: inspiration and expiration. During the inspiration stage, the thorax and the diaphragm expand, thus creating a negative intra-thoracic pressure that allows the entrance of oxygenated air into the lungs, where the gas exchange takes place. Afterwards, during expiration, the inspiratory muscles in the thorax and the diaphragm relax, so that the lungs are compressed, thus forcing the exhalation of air rich in CO_2 . The control of respiration is accomplished by various respiratory centers located in the brain stem. The nucleus tractus solitarius (NTS), located in the medulla, contains an area called dorsal respiratory group, which controls the inspiratory muscles. The NTS also receives input from chemoreceptors and mechanoreceptors, and transmits it to the pontine respiratory group (PRG) in the pons, where it is integrated. The PRG appears to help in the coordination of the respiratory rhythm.

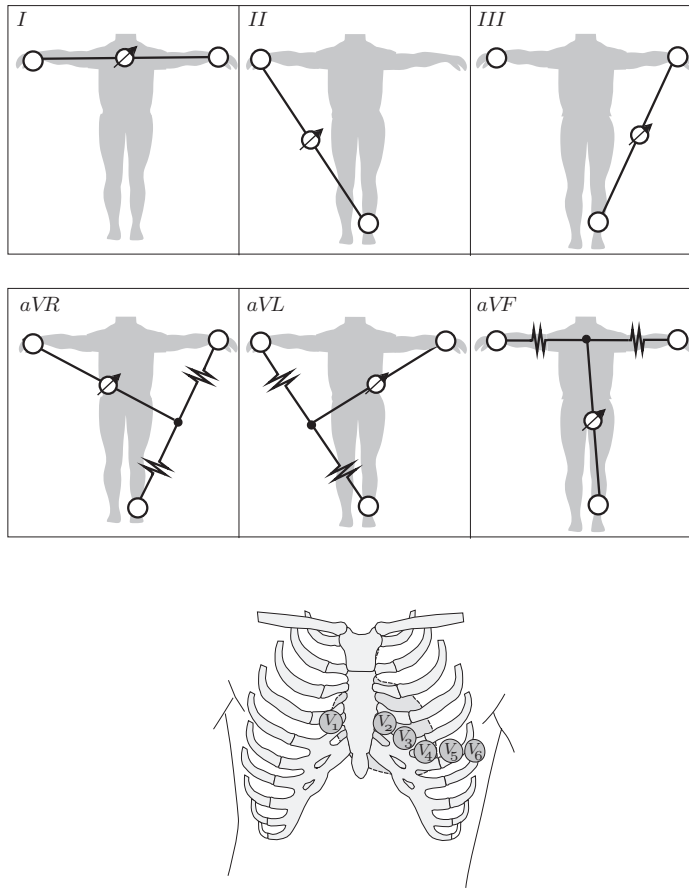


Figure 1.4: Electrodes placement in the standard 12-lead ECG. The dispositions for the acquisition of the bipolar limb leads (*I*, *II* and *III*), the augmented unipolar limb leads (*aVF*, *aVL* and *aVR*) and the unipolar precordial leads (V_1 to V_6) are displayed. Reproduced from [246].

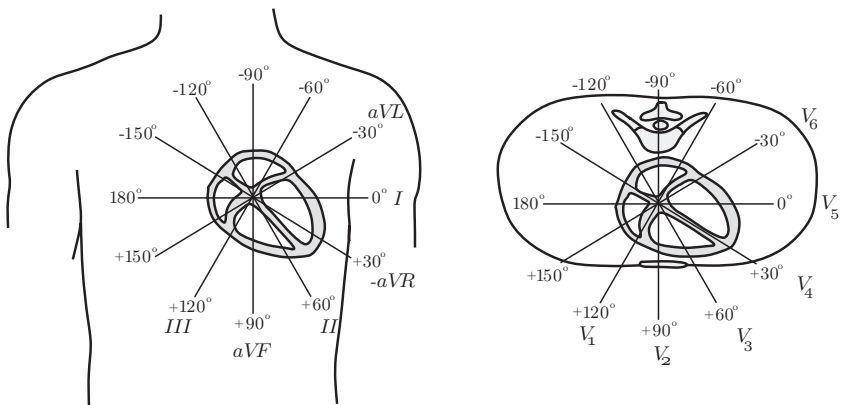


Figure 1.5: Angular directions covered in the frontal (left) and horizontal (right) planes with the limb and precordial leads, respectively. Reproduced from [246].

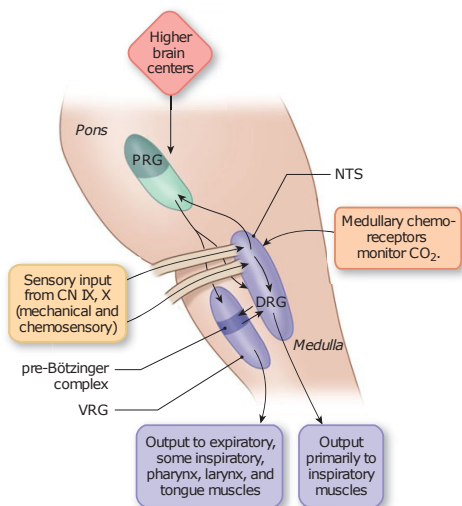


Figure 1.6: Anatomy of the respiratory centers (NTS: nucleus tractus solitarius, PRG: pontine respiratory group, DRG: dorsal respiratory group, VRG: ventral respiratory group, CN: cranial nerves). Reproduced and modified from [242].

On the other hand, the pre-Bötzinger complex, an area of the ventral respiratory group (VRG), contains spontaneously firing neurons, that may act as the respiratory rhythm pacemaker. Other areas in the VRG are in charge of the control of the expiratory muscles, and mainly activate during active expiration. A schematic of the respiratory centers anatomy is displayed in Fig. 1.6.

Apart from the inhaled and exhaled air composition, there are several respiratory parameters of great clinical interest, being the most important the following:

- **Respiratory rate:** it is the inverse of the time between consecutive breaths, and its clinical relevance has been proved in several respiratory disorders [51, 105, 142], as well as in cardiorespiratory arrest prediction [85]. It is also known to increase in response to physical [20] and psychological [121] stress, to increase during sleep [73], and to decrease rapidly during the first year of life [89].
- **Tidal volume:** it is the amount of air involved in each inspiration or expiration, and its value is drastically reduced in obstructive respiratory disorders, such as chronic obstructive pulmonary disease (COPD), or during asthma exacerbations.
- **Minute ventilation:** it is the amount of air inhaled or exhaled per minute, and it is controlled by both the respiratory rate and the tidal volume.
- **Lung function tests:** several parameters such as the peak expiratory flow or the forced expiratory volume in one second can be obtained from spirometric tests, being largely used in the assessment of respiratory disorders.

The respiratory activity can be captured in several manners and using different techniques. From the above-mentioned parameters, the monitoring of the respiratory rate has probably resulted in the widest variety of approaches, ranging from contact-based (acoustic methods, chest and abdominal movement detection, air temperature or humidity sensors, or transcutaneous CO₂ or O₂ monitoring) to noncontact-based (radar, optical or thermal sensors) methods [5, 170]. From all these options, the approaches used in this thesis for assessing the respiratory activity are limited to the use of impedance pneumography (IP) recordings, respiratory belts and facemasks.

The changes in air volume and composition inside the lungs, in addition to other effects such as the flow and composition of blood in the chest, lead to variations in thoracic impedance value and distribution that can be measured through IP. For this purpose, a known alternating current (composed by one or several frequency components, depending on the application) is led through the chest of a subject using electrodes, and the voltage drop is measured so that the thoracic impedance can be estimated following the Ohm's law. Despite the fact that its only current clinical application is the measurement of the respiratory rate, research efforts are being made in order to obtain absolute measurements of the air volume within the lungs [238]. Another possibility relies in the quantification of the thoracic expansion and contraction along the respiratory cycle, using respiratory belts. These belts can operate according to different technologies, such as respiratory inductance plethysmography or piezoelectric sensors. Finally, the respiratory flow can be directly acquired using facemasks and devices that are able to account for the air exchange through the mouth and nose. Whereas respiratory flow assessment using facemasks can result inconvenient and interfere with natural breathing, the measurements based on IP or respiratory belts are more non-invasive, but they may require from calibration and obtain relative rather than absolute volume measurements.

Respiratory modulation of the electrocardiogram

Despite the fact that ECG mainly represents the electrical cardiac activity measured on the surface of the skin, it is known to carry some respiratory information. Essentially, ECG is modulated by respiration through three different mechanisms: respiratory sinus arrhythmia (RSA), changes in the relative position of the recording electrodes, and changes in thoracic impedance. RSA is an extra-cardiac modulation of the HR which reflects as a tachycardia during inspiration followed by a bradycardia during expiration. The origin of RSA is not completely understood, and three main non-exclusive hypotheses have been proposed, suggesting a central [75], baroreflex-mediated [135] or mechanical [42] origin, as well as a combination of them [127]. Also other reflexes, such as those triggered by chemo- and stretch-receptors are thought to play a fundamental role in the regulation of RSA [71]. The fact that cardiac vagal preganglionic neurons are thought to be directly modulated by a central respiratory drive [117, 229] has led to establish a strong relationship between RSA and cardiac vagal activity, which has been reinforced by several studies assessing RSA and cardiac parasympathetic tone abolishment following atropine infusion [7, 176, 233]. Moreover, the extensive overlap between the brainstem

areas controlling HR and respiration, and the interactions at medullary level between the respiratory control neurons in the pre-Bötzinger complex and the cardiac control neurons in the nucleus ambiguus, reveal a close relationship in the neural control of respiration and HR [72, 93]. Since RSA has received widespread research interest, the effect of several confounding variables and scenarios has been addressed in the literature. In this way, RSA is increased in the supine position and with low respiratory rate or large tidal volume, whereas it decreases in the upright position, and with high respiratory rate or small tidal volume [50, 106, 107, 221]. It also decreases with age [87, 141] and during physical or psychological stress [13, 106, 107], it increases in relax situations [13, 225], and it is greater during non-rapid eye movement (NREM) than during rapid eye movement (REM) sleep [52].

Nevertheless, there is still controversy regarding the physiological role of RSA. Whilst some studies have regarded RSA as a mechanism for increasing gas exchange efficiency [96, 117, 118], evidence has been provided of a shift in the relative phases of respiratory and cardiac rhythms at different respiratory rates [259], which is inconsistent with the former hypothesis. RSA has been also proposed as an energy-saving mechanism, since the results of mathematical modeling might suggest that it reduces the cardiac workload for maintaining the blood partial pressure of CO_2 [31, 32].

On the other hand, variations in the relative position of the recording electrodes due to chest movement during respiration result in alterations of the electrical pathway between them. Moreover, changes in the amount and composition of air inside the lungs or in the flow or composition of blood in the chest lead to different thoracic impedance value and distribution. These impedance changes directly affect electrical propagation, which is reflected as a modulation of the ECG morphology.

In this way, changes in cardiac activity, as synchronized with respiration, have been exploited by several authors to extract respiratory information from ECG features such as R or R-to-S waves amplitude [169], the QRS-complex slopes [145] and QRS-complex area [182] variations, or vectocardiogram rotations [21]. This family of methods is usually referred to as ECG-derived respiration (EDR), as they allow to extract respiratory information only from the ECG, without need of additional sensors. In the literature, EDR has been widely employed for estimating the respiratory rate using only ECG signals. An example of the extra-cardiac respiratory-related modulation of an ECG signal is depicted in Fig. 1.7.

1.4 Heart rate variability

In normal conditions, HR is controlled by the SA node, whose depolarization periodicity depends on both SNS and PNS. Far from being constant, HR varies in a beat-to-beat basis, and this variation, known as heart rate variability (HRV), is subjected to the opposing effects of sympathetic and vagal activity, which are intended to meet the homeostatic demands of the body. Whereas increased sympathetic activity or parasympathetic with-

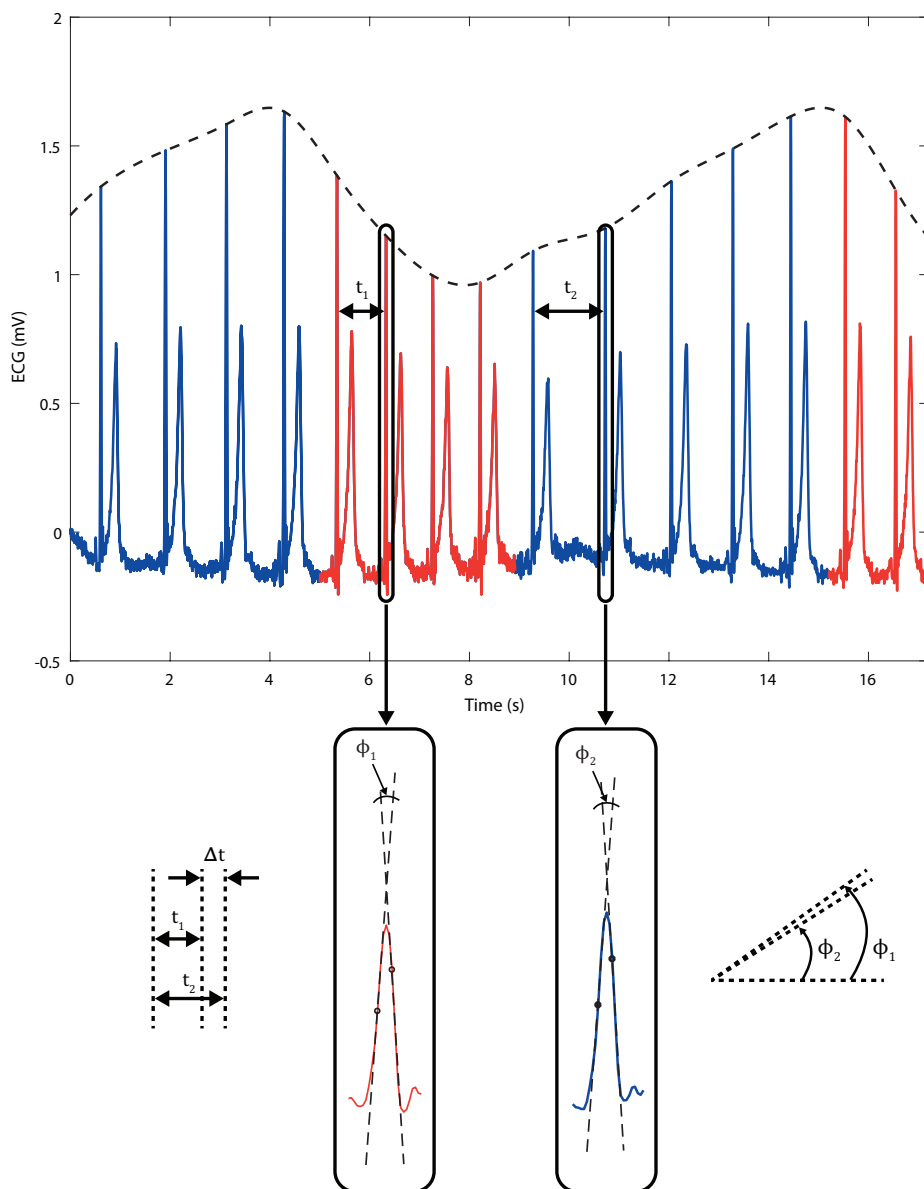


Figure 1.7: Example of the effect of respiratory activity on the ECG. Red and blue segments corresponds to inspiration and expiration respectively. Three different effects are displayed in the figure: amplitude changes (marked with a black dashed line), respiratory sinus arrhythmia (that manifests as decreasing inter-beat intervals during inspiration, t_1 , which increase again during expiration, t_2), and changes in QRS complex morphology (reflected, e.g., as variations in the R wave angle from inspiration, ϕ_1 , to expiration, ϕ_2).

drawal result in an increase in HR, a vagal surge or a reduction in sympathetic activity lead to a HR deceleration. Hence, HRV analysis has been proposed as a highly interesting tool for the non-invasive assessment of ANS [252].

1.4.1 Clinical relevance of HRV

HRV has been suggested to vary according to a wide range of demographic, physiological and psychological conditions. HRV reduces with age, and differs between males and females, and among races [12, 153, 268]. Moreover, it has been found to vary from wakefulness to sleep, and within the different sleep stages [52]. It modifies during physical activity [45], and also varies with mental stress [121], and according to the emotional state [187]. Whereas the described alterations of HRV remain physiological, HRV has been found to be altered in a large series of pathological conditions in which abnormal ANS behavior (or dysautonomia) is thought to be involved. E.g., altered HRV has been assessed in subjects suffering from several cardiovascular diseases, such as hypertension [126], coronary artery disease [275], late-stage congestive heart failure [57, 113] or at increased risk of death following a myocardial infarction [139]. Abnormal ANS function has been also assessed through HRV analysis in respiratory disorders, such as asthma [131, 240] or sleep apnea [111, 199], in subjects suffering from mental diseases like major depressive disorder [269] or Alzheimer's disease [289], and in overtrained athletes [45].

1.4.2 Heart rhythm representations

Heart rhythm representations are intended to accurately reflect the variations in HR, in order to apply different HRV analysis methodologies [246]. There are several possible heart rhythm representations, being the interval tachogram (Fig. 1.8 b)) the simplest one, as it consists in a RR interval series. The inverse interval tachogram (Fig. 1.8 c)) can be constructed as the inverse of the RR interval series, so that it reflects rate instead of time. There are also more informative representations, such as the interval function (Fig. 1.8 d)) and the inverse interval function (Fig. 1.8 e)), which are defined in a continuous time basis. Both of them consist in a train of unit impulses occurring at the times when a beat takes place and, whereas in the former each unit impulse is scaled by the length of the preceding RR interval, in the latter the impulses are scaled by the inverse of their corresponding RR intervals, thus representing rate [246]. It is important to note that the interval function and the inverse interval function are unevenly sampled by definition.

In this thesis a more complex approach, known as heart timing signal, was employed. The heart timing signal is defined as an unevenly sampled series that accounts for the deviation of each beat occurrence time from its expected occurrence time, calculated according to the time-varying integral pulse frequency modulation (TVIPFM) model [19]. The TVIPFM model assumes the existence of a modulating signal that alters the mean heart period due to the combined action of SNS and PNS, and has been widely used in the

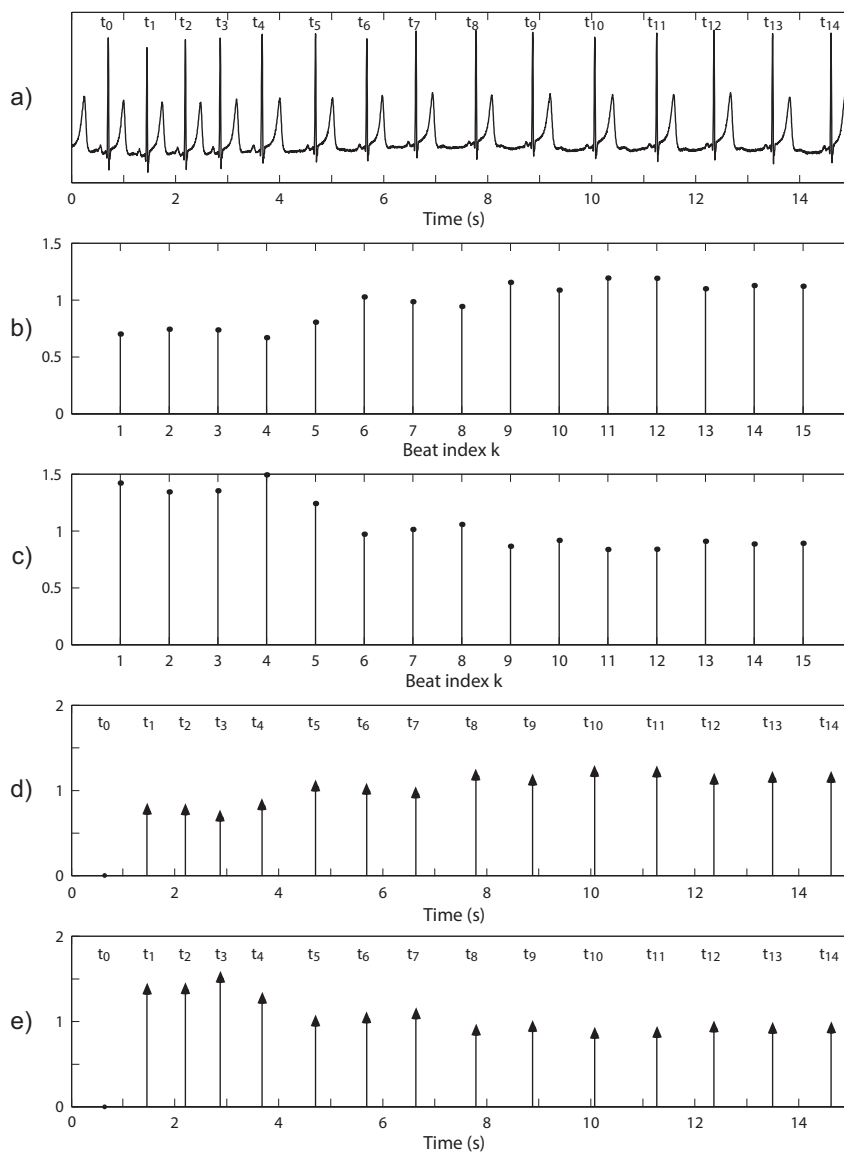


Figure 1.8: Different heart rhythm representations are displayed. In a), an ECG with the beat occurrence times is displayed. Below, the interval tachogram (b)), inverse interval tachogram (c)), interval function (d)) and inverse interval function (e)) representations are depicted. The units in the ordinate axes of a) are given in arbitrary units, whereas those in b) and d) are expressed in seconds, and those in c) and e) in hertz. Reproduced and modified from [246].

field of HRV analysis. It is this modulating signal which is thought to carry information of ANS activity [19, 27, 34, 171]. A more detailed description of the TVIPFM model is given in Ch. 2.2.

1.4.3 HRV analysis

The study of HRV can be conducted from different heart rhythm representations, and attending to several analysis strategies. The most extended approaches are those based on time and frequency domains, as well as nonlinear analysis. All of them have their own particularities, and result more appropriate for certain scenarios. A brief description of the three approaches and the commonly used parameters is provided below.

- Time-domain analysis:** it is focused on the first order moments or geometric properties of the normal-to-normal (NN) interval series. They are computationally simple, and the most employed indexes are the mean and standard deviation of the NN interval series (\overline{NN} and SDNN, respectively), the standard deviation and root mean square of the difference between adjacent NN intervals (SDSD and RMSSD, respectively), and the percentage of successive differences of NN intervals differing by more than 50 ms (pNN50). Whereas \overline{NN} and SDNN are related with the overall HRV; SDSD, RMSSD and pNN50 are associated with short-term variations [252]. There is also a subgroup of time-domain measurements which are referred to as geometric measures, since they are obtained from the RR interval histogram, which usually presents a triangular shape. In this way, the HRV triangular index is calculated as the integral of the density of the RR interval histogram divided by its height, whereas the triangular interpolation of the NN interval histogram is obtained as the width of the histogram baseline [239].
- Frequency-domain analysis:** it consists in the analysis of the power distribution in the different frequency components that are present in the HRV. In short-term analysis, three main frequency bands of interest have been defined: the very low frequency (VLF) band, ranging from 0 to 0.04 Hz, the low frequency (LF) band, which extends from 0.04 up to 0.15 Hz, and the high frequency (HF) band, which goes from 0.15 to 0.4 Hz [252]. Based on studies using pharmacological SNS and PNS inhibitors and to the application of external stressors, the power content in the HF (P_{HF}) band has been related with parasympathetic activity, being RSA the main contributor, whereas the content of the LF band (P_{LF}) has been suggested to represent both sympathetic and parasympathetic modulation, and is thought to be mainly influenced by baroreflex activity [164, 196]. On the other hand, the physiological interpretation of the power in the VLF band (P_{VLF}) is not that direct, although it has been related with thermoregulation and the rennin-angiotensin system [217]. Apart from these indexes, also the total spectral power (TP), calculated as the sum of P_{LF} and P_{HF} , the LF to HF power ratio ($R_{LF/HF} = P_{LF}/P_{HF}$) and the normalized LF power ($P_{LFn} = P_{LF}/(P_{LF} + P_{HF})$) are widely employed. Whereas TP is related with the total variation of SNS and PNS activity, $R_{LF/HF}$ and P_{LFn} are often interpreted as

measurements of the sympathovagal balance, and therefore as a quantitative representation of the interaction between both branches of the ANS [163,196]. Several different analysis approaches have been proposed in the literature, ranging from parametric to non-parametric or from time-variant to time-invariant methodologies [19, 161, 246, 252].

- **Nonlinear analysis:** the advances in the theory of nonlinear dynamics have motivated the extension of the developed techniques to the evaluation of biosignals. Nonlinear analysis is based on quantitative measurements of the complexity or regularity of HRV, which are represented by parameters such as the correlation dimension (D_2) [104], the approximate entropy (*ApEn*) [205] or the sample entropy (*SampEn*) [218]. Another well-known nonlinear approach is the Poincaré plot, consisting in reconstructing the phase space of the RR interval series, from where different parameters accounting for the short-term (SD1) or overall (SD2, S) HRV can be extracted [239].

Also strategies based on information dynamics are recently gaining attention [208]. Further information concerning the different HRV analysis approaches and parameters can be found elsewhere [1, 228, 239, 252].

1.5 Target respiratory disorders

The clinical focus of this thesis is on two concrete respiratory disorders: asthma and sleep apnea syndrome. A description of the particularities, diagnostic methods, treatment and relationship with autonomic control of each of them is provided below.

1.5.1 Asthma

Asthma is a complex and heterogeneous chronic respiratory disease, usually characterized by airway inflammation [97]. It produces a series of respiratory symptoms, such as bronchial hyper-responsiveness, spasmodic contraction of the bronchioles and increased mucus segregation, thus resulting in variable airway obstruction and expiratory limitation, cough, shortness of breath and chest tightness. Although asthma affects people of any age, it is prone to start during early childhood [168], with an earliest onset in the case of boys [166], and its recent increased prevalence [10, 47] has risen it as one of the most common chronic diseases of childhood [47, 53, 168]. Due to the intrinsic heterogeneity of asthma, an actual tendency is to group the asthmatic subjects in clusters or phenotypes attending to different clinical and pathophysiological characteristics. In this way, the Global Initiative for Asthma (GINA) [97] distinguishes between several phenotypes of asthma, such as allergic asthma, non-allergic asthma, late-onset asthma, asthma with fixed airflow limitation or asthma with obesity. The possibility that different pheno-

types have distinct underlying mechanisms could lead to more effective and personalized treatments [11].

Diagnosis

In the case of adults, diagnosis and later clustering of the patients in phenotypes is often based on the clinical history, assessment of inflammatory markers and single-time lung function measurements, being spirometry the most extended test. However, lung function tests remain inappropriate for young children, since they are very effort dependent and require cooperation [97]. Despite that some studies have suggested that children can perform acceptable flow-volume curves from an age of 3 years [40, 79], measurement criteria need to be standardized, since differences in the relative size of children airways and lungs with respect to adults make the most common measurements unsuitable for this population [40, 203]. Moreover, the training of those children for performing the maneuvers is time-consuming. Other lung function testing methods, such as rapid thoracoabdominal compression (RTC) and raised volume RTC, have been found to discriminate between health and disease [158, 285], although reference values are not yet available to be used in clinical settings [159].

For these reasons, diagnosis of asthma in young children is very dependent on the clinical history, which is retrospective in nature and could be even incomplete. This, together with the high percentage of children with recurrent viral-induced wheezing [166], result in a less strict diagnosis than in the case of adults. In this way, the common practice consists in the definition of a current asthma status, which is usually confined to a higher or lower risk of having/developing asthma in the future, or the presence or absence of asthma-like symptoms. In the literature, several clinical history-based indexes have been proposed for the assessment of the current asthma status in young children, e.g., the modified asthma predictive index (mAPI) [108]. Essentially, mAPI assigns a score according to several risk factors for asthma (such as parental asthma, atopy or peripheral eosinophilia) and if the resulting score is greater than zero the children are classified as high risk of developing asthma, whereas they are classified as low risk otherwise. Other studies (Isle of Wight [143], PIAMA [59]) have employed different criteria for risk of asthma stratification, and although they share a high specificity with mAPI, very low sensitivity is also a common feature [58], which might lead to a lot of missing diagnoses.

Treatment

Inhaled corticosteroids (ICS) remain the standard medication for the prevention of the symptoms of asthma. Depending on the severity degree, ICS therapy needs to be combined with long-acting β_2 -agonists (LABA) for a proper control of the symptoms. Despite the use of high-doses of ICS and LABA, the symptoms remain uncontrolled in certain subgroups of subjects, which has motivated the search of alternative treatments that target

concrete inflammatory mediators [82]. Nevertheless, these therapies are neither effective in all the cases.

In the case of young children, there is some controversy regarding the possible negative effects that ICS may exert during childhood. In this way, ICS have been pointed as the origin of growth reduction during the first weeks of treatment, as well as hypothalamic-pituitary-adrenal suppression [60, 69, 119]. This, together with the low perceived risk, have contributed to a low adherence to asthma treatment [46]. However, early intervention remains crucial, as lung function increases up to 20-fold during the first 10 years of life [248], so that absence of treatment when needed could lead to permanent airway remodeling [2]. In this way, a proper monitoring of the symptoms is needed in order to decide whether continuing or interrupting the ICS treatment.

The inflammatory response

A schematic of the inflammatory response in asthma, referred to as type 2 inflammation since it is triggered by type 2 helper (T_H2) cells, is depicted in Fig. 1.9. When an allergen is detected by the dendritic cells, they release cytokines that attract T_H2 cells. The T_H2 cells orchestrate the inflammatory response by secreting several interleukines (IL): IL-13 and IL-4 stimulate B cells growth and differentiation, as well as immunoglobulin E (IgE) synthesis, IL-5 stimulates eosinophils production and IL-9 stimulates mast cell growth. All of these cells are thought to play an important role in asthma. The B cells release allergen specific IgE which binds to IgE receptors in other inflammatory cells, inducing the release of pro-inflammatory substances such as major basic proteins and eosinophil cationic proteins in the case of eosinophils, or histamine and heparin in the case of mast cells. The combined action of these substances is known to produce local blood vessel dilation, increased capillary permeability, local smooth muscle contraction, increased mucus secretion and edema. All these factors produce airway obstruction in asthmatics subjects. However, the role of the different pro-inflammatory substances in the development of airway hyper-responsiveness is not that clear.

Histamine is a well known inflammatory mediator that produces contraction of local smooth muscle, and has been related with decreased spirometry performance in asthmatics [65]. Nevertheless, other studies have found no differences in the smooth muscle contraction of asthmatics and non-asthmatics when subjected to different histamine doses [101], as well as a limited bronchodilation after anti-histamine administration [261]. In the case of heparin, it is a powerful anti-coagulant, and inhaled heparin has been suggested to prevent from exercise-induced bronchoconstriction [3] and to act as a protective agent in asthma [33], so it does not represent a likely cause of bronchial hyper-responsiveness. Local eosinophilia has also been considered as a possible underlying cause of hyper-responsiveness, although no increase in the risk of asthma has been observed in eosinophilic subjects [140]. Moreover, in a recent cohort study which enrolled 995 asthmatics, a 57% of them were non-eosinophilic [174]. On the other hand, the results of using anti-interleukines for IL-4, IL-5, IL-9 and IL-13 for controlling asthma symptoms

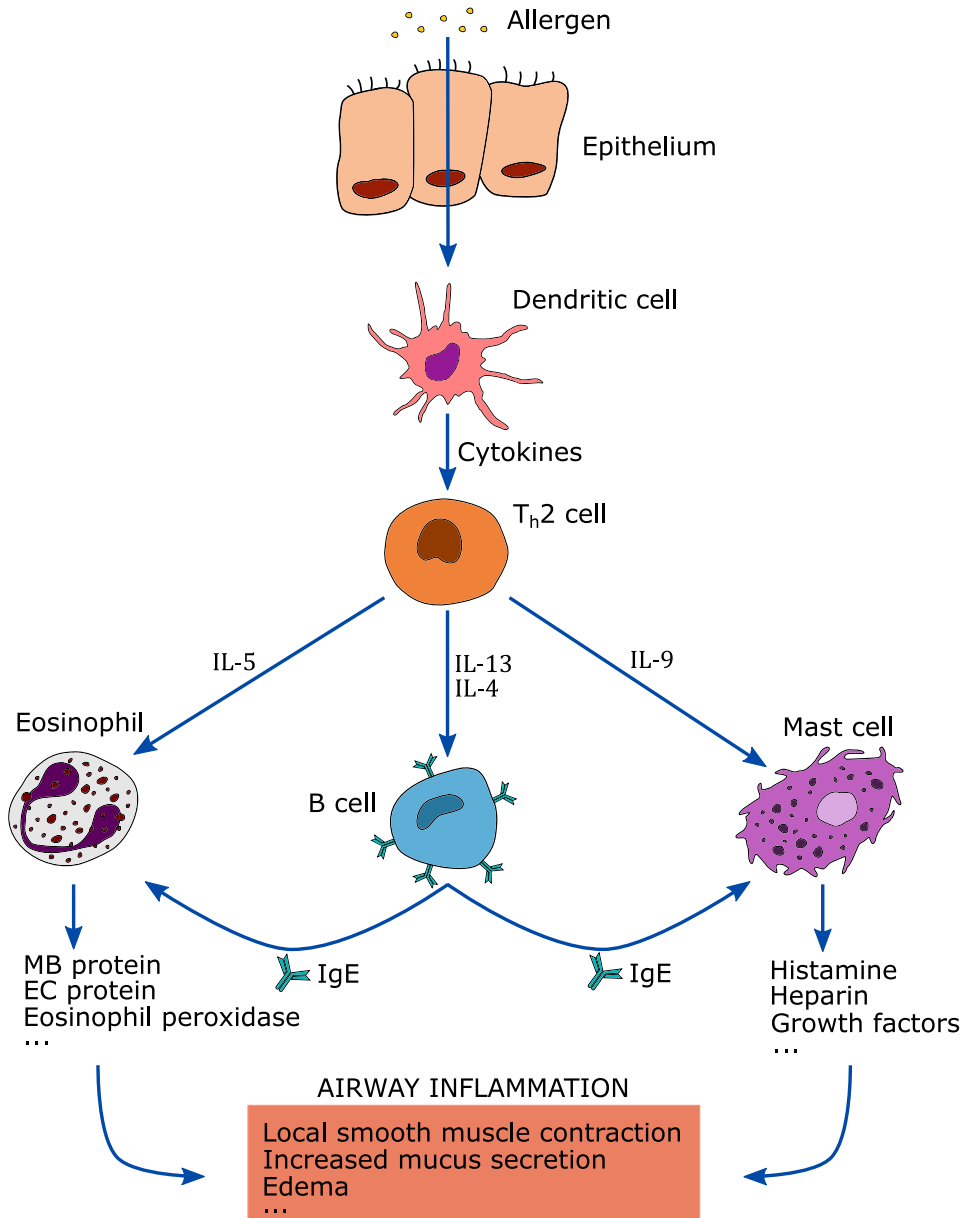


Figure 1.9: The inflammatory response in asthma. When the presence of an allergen in the airways is detected, the dendritic cells release cytokines to attract T_h2 cells, which triggers a complex inflammatory response. The T_h2 cells secrete several interleukins which stimulate B cells and mast cells growth, as well as eosinophils and IgE production. The binding of IgE to specific receptors in the eosinophils and mast cells cause the release of a series of pro-inflammatory substances, whose combined effects lead to airway inflammation.

are not consistent [92, 137, 193], and also other studies analyzing the effect of additional substances involved in the inflammatory response, such as IL-17 or inducible nitric oxide, are controversial [62, 154]. Finally, there is a large subgroup of asthmatics who do not respond to T_{H2} -targeted therapies [276]. All these facts suggest the existence of other underlying mechanisms in asthma, apart from the type 2 inflammatory response.

The role of ANS in asthma

The ANS controls the smooth muscle tone in the airways through three different pathways: adrenergic, cholinergic and non-adrenergic non-cholinergic (NANC). Adrenergic innervation is sparse or absent in human airways, although it is found in submucosal glands, bronchial blood vessels and airway ganglia. Nevertheless, there is a high density of β_2 -adrenoreceptors in airway smooth muscle that mediate bronchoconstriction through circulating catecholamines, which have been suggested to play a protective role in asthma [247]. However, adrenergic control is not the most likely source of airway hyper-reactivity, since non-asthmatics do not develop it after β -adrenergic blockade or adrenalectomy [185]. Regarding the cholinergic control, two types of acetylcholine (ACh) muscarinic receptors are present in the airways: M_2 , which do not play a role in smooth muscle contraction but limit the excess release of ACh from vagus nerves (see Fig. 1.10 a), c) and e)), and M_3 , which mediate smooth muscle contraction, although no evidence of changes in the number or functionality of M_3 receptors have been found in asthmatics with respect to non-asthmatics [84, 90]. Notwithstanding, the study of the role of M_2 receptors in asthmatics has revealed a consistent reduced functionality with respect to non-asthmatics [90, 179]. One possible explanation is the presence of eosinophils [90]. The rationale relies in the several proteins that eosinophils release during the inflammatory response, which are positively charged. Since M_2 receptors are particularly prone to blockade by positively charged proteins, the presence of eosinophilic proteins results in a dysfunction of the M_2 receptors, thus inhibiting the negative feedback that they provide after an ACh discharge, and resulting in an excessive and uncontrolled ACh release (see Fig. 1.10 b), d) and f)) [90]. In this way, M_2 receptors dysfunction appears to be a major component of airway hyper-responsiveness, although the fact that there is a large subgroup of asthmatics that are persistently non-eosinophilic [174] suggests the existence of other mechanisms that may contribute to the altered operation of M_2 receptors. Finally, the NANC pathway represents the dominant relaxant innervation in human airways, and vasoactive intestinal peptide and nitric oxide have been proposed as its possible neurotransmitters [23, 279], although the role of NANC control in the pathogenesis of asthma has not been yet elucidated.

The suspicion that the ANS plays an important role in the pathogenesis of asthma, and the difficulties for asthma diagnosis (especially in children) and continuous monitoring, have motivated large research aiming to assess ANS activity in asthmatics. Under the assumption that altered control in airway caliber may be reflected in parallel alterations in the regulation of HR, HRV analysis has been considered for the characterization of autonomic activity both in adults [94, 131, 240, 287] and in children [80, 257] suffering

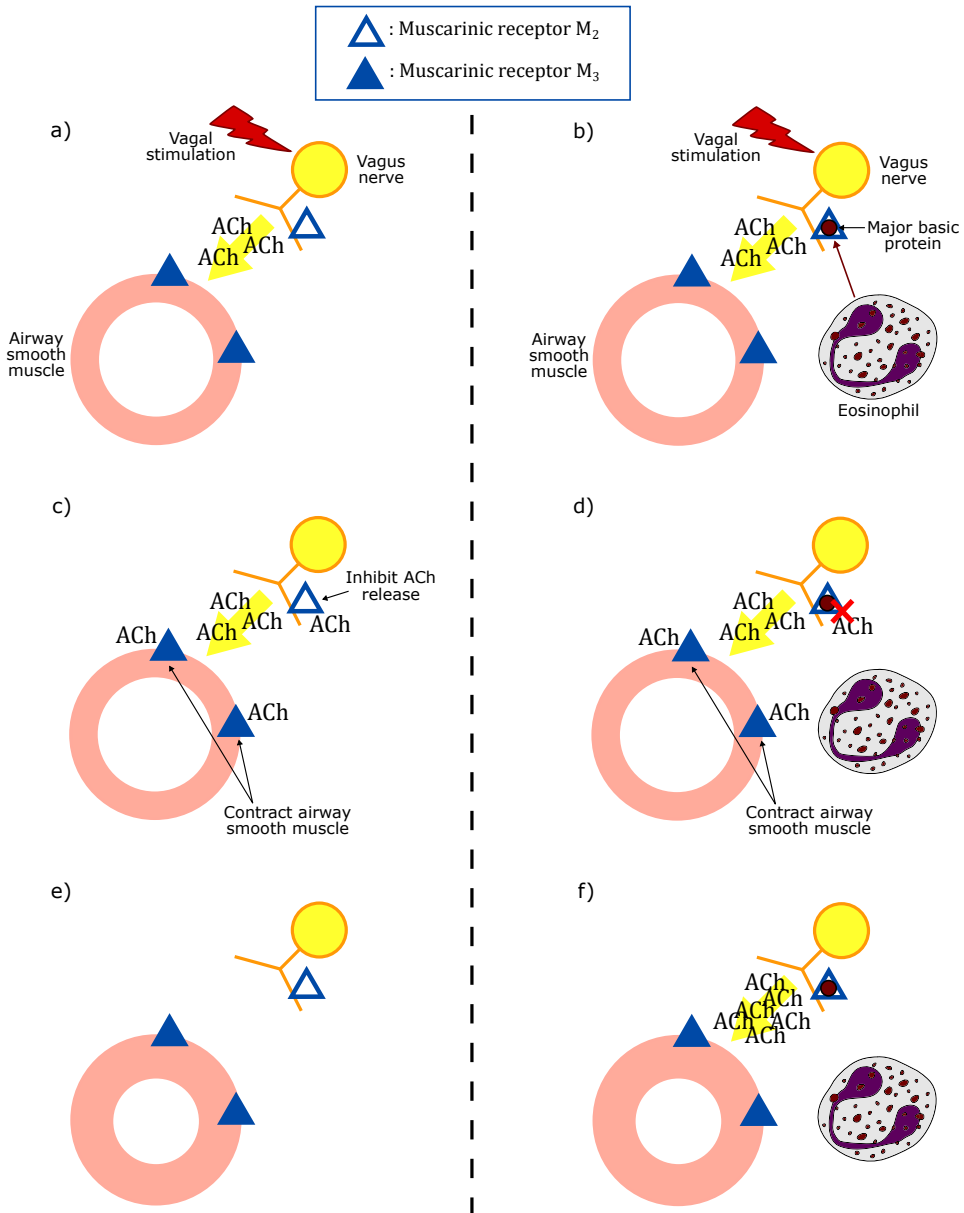


Figure 1.10: An example of the effect of M_2 receptors dysfunction in the presence of eosinophils is displayed. In a) and b), a vagal stimulus triggers the secretion of acetylcholine (ACh) from the vagus nerve. In c), the ACh binds to the M_2 and M_3 receptors, which inhibit the further release of ACh and contract the airway smooth muscle respectively, as in e). During an inflammatory response, the eosinophils release positively charged proteins, such as major basic proteins, which bind to the M_2 receptors (b)), thus blocking the binding of ACh, as in d). This leads to an uncontrolled ACh release (f)), which may result in excessive smooth muscle contraction. This figure has been adapted and modified from [90].

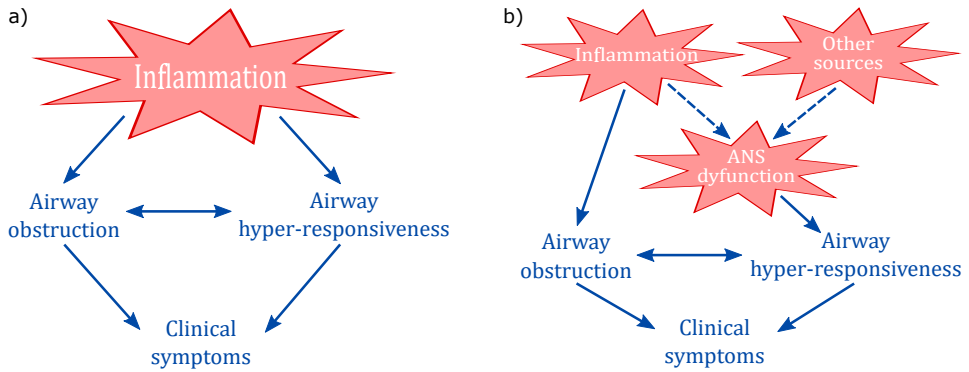


Figure 1.11: Two different interpretations of the pathogenesis of asthma. In a), inflammation is the direct cause of airway obstruction and hyper-responsiveness. However, this scheme is not enough to explain certain phenotypes of asthma in which inflammation is not a likely underlying cause of hyper-responsiveness. In b), ANS dysfunction (e.g., M_2 receptors dysfunction) is presented as the cause of airway hyper-responsiveness, and it can be originated either by inflammation or by any other cause, thus providing a more complete frame.

from asthma. Whereas some authors have reported increased vagal tone [257, 287] or an increased vagal dominance [94] in asthmatics than in controls, others report increased parasympathetic reactivity to autonomic control tests [80, 131, 240], such as HR response to deep breathing or Valsava maneuver. Moreover, the measured increased vagal activity presented a positive correlation with asthma severity in children [80]. Hence, as PNS is involved in bronchoconstriction [151] and bronchomotor tone control [184], an altered PNS activity has been pointed as a possible underlying factor in the pathogenesis of asthma, thus coinciding with the hypothesis of M_2 receptors dysfunction as the main cause of airway hyper-responsiveness. In this way, the traditional picture of inflammation as the main cause of airway hyper-responsiveness could evolve towards a more complete frame in which ANS dysfunction is presented as the main cause, whereas it can be a consequence of inflammation or of other mechanisms (see Fig. 1.11).

1.5.2 Sleep apnea syndrome

Sleep apnea syndrome (SAS) is a complex sleep-disordered breathing (SDB) that manifests as a repetitive partial (hypopnea) or total (apnea) cessation of airflow into the lungs, which is usually terminated with the arousal of the subject. Despite the fact that there is no consensus in the prevalence of SDB, with numbers varying from 24 to 49.7% in males and from 9 to 23.4% in females [120, 201, 286], it has experienced an increase during the last decades [201].

Apneas and hypopneas can originate due to an upper-airway collapse (obstructive sleep apnea, OSA), an absence of respiratory drive (central sleep apnea, CSA) or a combination of both (mixed sleep apnea). In the case of OSA, pharyngeal collapse occurs posterior to the tongue, soft palate or uvula, as displayed in Fig. 1.12. Since the intermediate portion of the pharynx has little rigid support, the diameter of its lumen largely

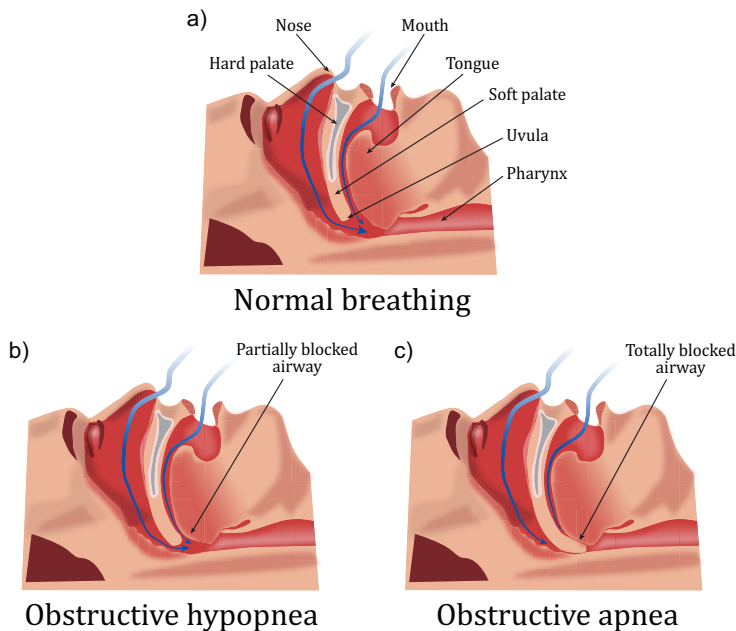


Figure 1.12: An example of obstructive sleep apnea and hypopnea is displayed. In a), the upper airways remain open, thus enabling normal breathing. When a partial (b)) or total (c)) obstruction of the respiratory flow takes place, the interruption of normal breathing is referred to as obstructive hypopnea or apnea, respectively.

depends on muscle activity. During wakefulness, pharyngeal patency is maintained by a reflex-driven activation of pharyngeal dilator muscles. However, this reflex activity is reduced during sleep. Hence, an anatomically small pharynx (e.g., due to genetic reasons or obesity), a dysfunction in pharyngeal muscles or nerves structure or activity, or an altered ventilatory control due to a misbehavior of the chemoreceptors feedback loop, result in increased risk of OSA [245,278]. Regarding CSA, altered ventilation control does not have a single cause, and so a series of syndromes have been identified. Some examples of CSA manifestations are the Cheyne-Stokes respiration, the idiopathic CSA or the congenital central hypoventilation syndrome. Whereas the two formers may have their origin in alterations of the chemoreceptors feedback loop gain, Cheyne-Stokes respiration can be also due to long systemic circulation delays, so it is generally seen in patients with congestive heart failure [76,278]. The congenital central hypoventilation syndrome, on the other hand, has a likely genetic origin, without a clear anatomic pathology [76].

Immediate effects of apneic episodes include recurrent hypoxia, fragmented sleep and large fluctuations in intrathoracic pressure, blood pressure and sympathetic activity. This acute effects might evolve in chronic sequels such as hypertension or other cardiovascular comorbidities associated with an increased risk of stroke or heart failure [202,245]. Moreover, SAS usually produces excessive daytime sleepiness, and has been linked to

decrements in cognitive function [138, 283], as well as to depression disorders [200]. SAS has been also independently related with increased risk of car accident [253, 258].

Diagnosis

Full night polysomnography (PSG) remains the current gold standard for the diagnosis of SAS. PSGs are usually conducted in sleep laboratories attended by sleep experts, and they consist in multi-parametric tests which involve the continuous recording of several biosignals, including electroencephalogram, electrooculogram, electromyogram, ECG, nasal and oral airflow, thoracic and abdominal respiratory effort, pulse oximetry and capnography. Afterwards, sleep stages and respiratory events are manually annotated in 30-second epochs. The scoring rules for ensuring homogeneity across different studies were established by the American Academy of Sleep Medicine (AASM) [9], and are subjected to constant revision [37–39]. In this way, a 90% decrease in airflow lasting more than 10 seconds should be identified as an apnea. In the case of hypopneas, a 30% decrease in airflow lasting more than 10 seconds is required, and it must be accompanied by either an oxygen desaturation $\geq 3\%$ or by an arousal (defined according to electroencephalographic and electromyographic activity). In the case that continuous or increasing inspiratory effort is observed during the period of reduced airflow, the event should be identified as obstructive, whereas the lack of inspiratory effort should be associated with a central event. If there is no inspiratory effort at the beginning of the event but it resumes along the event's duration, then the event should be labeled as mixed [38]. There is also an adapted version of these scoring rules for pediatric SDB assessment.

The severity of SAS is established according to the so called apnea-hypopnea index (AHI), which accounts for the total number of apneas and hypopneas divided by the total sleep time. The AASM defines the stratification of SAS severity in mild ($5 \leq \text{AHI} < 15$), moderate ($15 \leq \text{AHI} < 30$) or severe ($\text{AHI} \geq 30$) [9].

Treatment

The recommended treatment for SAS is usually dependent on the severity and nature of the disease. Positive airway pressure (PAP) has risen as the preferred treatment for both OSA and CSA, and should be offered as an option to all patients [14, 76, 81]. There are several modalities of PAP therapy, which essentially consist in different settings of mechanical ventilation. For those subjects who refuse PAP treatment, there are other recommended options, such as behavioral strategies (ranging from weight loss to positional therapy and the avoidance of alcohol and sedatives before bedtime), oral appliances intended to improve upper airway patency, and surgical upper airway remodeling or bypass [81]. As in many other diseases, there is a growing effort in understanding the different phenotypes of SAS, so that other important features apart from AHI are considered, thus leading to personalized and more effective treatment strategies [16, 77, 288].

SAS, ANS and cardiovascular disease

During an OSA episode, forced inspiration against an obstructed airway leads to exaggerated negative intrathoracic pressure and is accompanied by immediate hypoxia, which triggers a complicated autonomic response [245]. Previously to the apneic episode, an increase in vagal drive is observed, reflecting as a bradycardia. Given the impossibility to breathe, a sudden sympathetic activation is triggered, leading to the arousal of the subject and the consequent interruption of the apneic event. This adrenergic surge can be also noticed as an abrupt increase in HR and blood pressure [110, 262]. Although the physiological mechanisms underlying the autonomic-mediated response to apneic events have yet not been completely elucidated, the existence of non-invasive methods for ANS assessment, such as HRV analysis, has motivated several works studying autonomic activity in SAS patients, in comparison with controls. These studies have generally revealed an altered sympathovagal balance in subjects suffering from SAS, reflected in an increased sympathetic dominance both during sleep [111, 199] and in 24-hour holter recordings [15]. Despite the fact that PSG settings remain the gold standard for the diagnosis of SAS, the possibility of developing a noninvasive tool for its premature diagnosis and monitoring, based on ANS assessment, has received widespread attention.

Since apneic patients are subjected to recursive overnight alterations in intrathoracic and blood pressure, HR, and autonomic control, all of them having a direct effect on cardiovascular activity, SAS has been proposed as an independent risk factor for developing hypertension, heart failure, cardiac arrhythmias, myocardial ischemia and other cardiovascular diseases (CVD) [150, 198, 202, 245]. Actually, SAS has been related with a 5-fold increase in the risk of developing CVD, which could rise to 11-fold if not conveniently treated [198]. Nevertheless, only some of the diagnoses of SAS are associated to cardiac comorbidities. Given that altered HRV has been independently related with increased risk of CVD and mortality [57, 126, 139, 254], and since many physiological and psychosomatic conditions that constitute risk factors for CVD have been also related with ANS dysfunction [254], there is an increasing interest in understanding the relationship between SAS, CVD and autonomic control.

1.6 Exercise physiology

There is also a big portion of this thesis addressing the noninvasive analysis of cardiorespiratory signals in the context of sport sciences. It is well-known that the combined action of a sympathetic activation and a vagal withdrawal during exercise results in several alterations in the cardiovascular and respiratory physiology, aimed at meeting the enlarged metabolic demands of the body. In this way, larger tidal volume (facilitated by bronchodilation) and respiratory rate augment the gas exchange in the lungs, thus providing the blood with larger amounts of O₂. Regarding the cardiac system, increased HR, systolic blood pressure and stroke volume guarantee a continuous supply of oxygen to the muscles. During moderate exercise, the aerobic energy production system uses

this O_2 in combination with carbohydrates, fats and proteins stored in the muscle tissue to synthesize adenosine triphosphate (ATP), which is the molecule providing the muscles with energy. However, the rhythm at which ATP is produced through the aerobic pathways results insufficient to maintain muscle activity at higher exercise intensity. In this situation, ATP starts to be produced through the anaerobic pathways, which employ the glycogen stored in the muscles. Another characteristic of the anaerobic energy production is that it also releases lactate and H^+ ions as residuals, resulting in metabolic acidosis [112,207]. The O_2 consumption above which anaerobic mechanisms are needed to complement aerobic energy production, thus causing a sustained increase in lactate levels and metabolic acidosis, is referred to as anaerobic threshold [271]. The increase in H^+ ions production is associated with larger ventilation, aimed at reducing metabolic acidosis by a reduction in the CO_2 levels.

The anaerobic threshold represents an inflection point in the way the body is obtaining energy to maintain its work capacity. Moreover, it accounts for the limit in O_2 consumption beyond which metabolic acidosis occurs and beyond which the cardiovascular system limits the endurance work [270]. In this way, an accurate estimation of the anaerobic threshold remains of large interest in the field of sport sciences, as it can be used to design better training routines, quantify athletes performance or prevent from overtraining. Moreover, the estimation of the anaerobic threshold has some clinical applications and, actually, it was initially intended to assess the exercise capacity in cardiac patients [272]. Several methods for the estimation of the anaerobic threshold have been proposed in the literature, and some of the most relevant are described below.

1.6.1 Estimation of the tidal volume

As mentioned above, during exercise there is an increase in tidal volume and respiratory rate intended to meet the metabolic demands of the body. Since both of them are related with the physical condition, their assessment represents a useful tool in the development of training routines and in several fields of sport sciences. Moreover, they have a clinical value in the monitoring of a range of respiratory disorders. Whereas the estimation of the respiratory rate is a recurrent topic in the literature, tidal volume estimation has been only addressed by a few authors, which have proposed the use of image acquisition [216], tracheal sounds [215] and inductive [238] or opto-electronic plethysmography [213]. In a recent study, the estimation of tidal volume using electrocardiographic and intra-cardiac signals has been proposed using mechanically ventilated swines [230]. Nevertheless, more research effort is required in this field.

1.6.2 Estimation of the anaerobic threshold

Since there are different mechanisms involved in the anaerobic metabolism, there are several methods for estimating the anaerobic threshold based on each of them. One of them is its approximation by the lactate threshold, which is extensively used in the literature

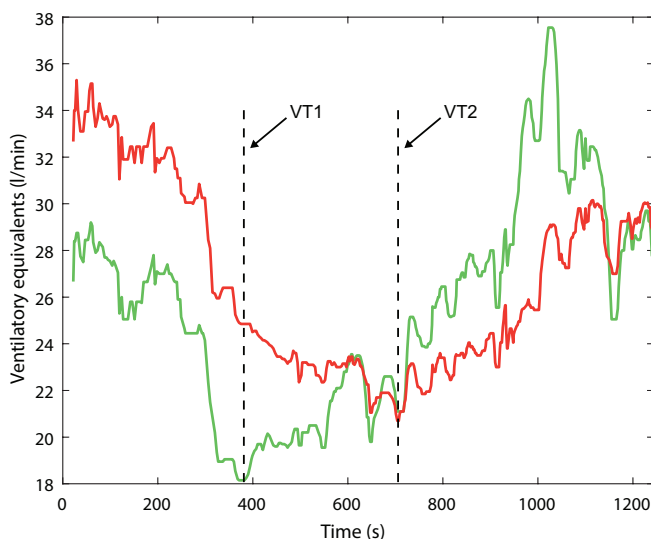


Figure 1.13: The ventilatory equivalents for O_2 (\dot{V}_E/\dot{V}_{O_2} , green) and CO_2 (\dot{V}_E/\dot{V}_{CO_2} , red) are displayed during an incremental effort test. The point at which \dot{V}_E/\dot{V}_{O_2} starts to increase without an increase in \dot{V}_E/\dot{V}_{CO_2} is identified as the aerobic threshold or VT1, whereas the point at which there is a simultaneous increase in \dot{V}_E/\dot{V}_{O_2} and \dot{V}_E/\dot{V}_{CO_2} is referred to as the anaerobic threshold or VT2.

and accounts for the exercise intensity above which there is a substantial increase in the levels of blood lactate during an incremental exercise test [251]. As ventilation pattern is also altered during anaerobic metabolism, another family of methods have focused on approximating the anaerobic threshold through the so called ventilatory thresholds. Given the minute ventilation (\dot{V}_E), and the O_2 and CO_2 consumption (\dot{V}_{O_2} and \dot{V}_{CO_2}), the method of the ventilatory equivalents [214] relies on the temporal evolution of the ventilatory equivalent for O_2 (\dot{V}_E/\dot{V}_{O_2}) and for CO_2 (\dot{V}_E/\dot{V}_{CO_2}), which represent the minute ventilation required to consume one liter of O_2 or produce one liter of CO_2 , respectively. The point at which \dot{V}_E/\dot{V}_{O_2} starts to increase without an increment in \dot{V}_E/\dot{V}_{CO_2} is referred to as VT1 or aerobic threshold, whilst that at which \dot{V}_E/\dot{V}_{CO_2} starts to grow simultaneously with \dot{V}_E/\dot{V}_{O_2} is referred to as VT2 or anaerobic threshold (see Fig. 1.13). Another example is the V-slope method [28], in which the anaerobic threshold is identified as the point at which there is an exponential increment of \dot{V}_{CO_2} as a function of \dot{V}_{O_2} (see Fig. 1.14). Finally, the change in the slope of the HR profile during an incremental effort test has been also proposed as a possible estimation methodology.

1.7 Structure of the thesis

This dissertation is structured in three main parts. In the first one (Ch. 1 and 2), an introduction to the physiology of the different scenarios covered in the thesis and to the framework for HRV analysis is provided. The second part (Ch. 3, 4 and 5) is focused on the

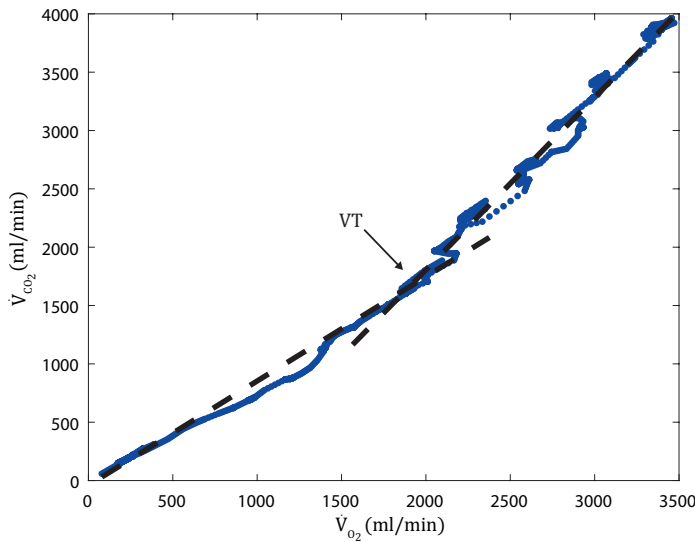


Figure 1.14: The \dot{V}_{CO_2} is displayed as a function of the \dot{V}_{O_2} . The point at which \dot{V}_{CO_2} increases exponentially with respect to \dot{V}_{O_2} is referred to as the ventilatory threshold (VT).

analysis of HRV applied to different respiratory disorders, concretely asthma and sleep apnea syndrome. The third part (Ch. 6 and 7) is dedicated to the noninvasive analysis of cardiorespiratory signals in the context of sport sciences, for the estimation of tidal volume and anaerobic threshold. Finally, Ch. 8 contains the main conclusions and future research lines. The organization of the different chapters is the following:

- **Chapter 1. Introduction:** In the present chapter, the ANS and the most relevant biological signals used in this thesis were introduced. Moreover, a physiological background of all the scenarios considered throughout the next chapters was provided.
- **Chapter 2. Contextualized HRV analysis:** In this chapter, a methodological framework for the analysis of HRV is presented. Apart from the mathematical model used for the estimation of the different HRV parameters, the effect of noise, ectopic beats, RSA and respiratory rate in the analysis and interpretation of the results is discussed in detail. Moreover, the concept of cardiorespiratory coupling is introduced, and the mathematical tools used for estimating it from the HRV and respiratory activity time-frequency coherence maps are presented. Finally, a frequency domain HRV index aimed at measuring the distribution of the HF components is introduced. This index, named peakness, is analyzed in detail in order to obtain the most adequate parameters setting, and to understand its relationship with the conventional frequency and nonlinear domain HRV indexes. The frame-

work described in this chapter will be used in all the chapters in the second part of this dissertation.

- **Chapter 3. HRV analysis in children with asthmatic symptoms:** Using the methodological framework introduced in Ch. 2, in this chapter ANS activity was assessed through HRV analysis in two independent datasets of preschool children classified attending to their asthmatic condition. The results suggest an increased vagal dominance and a peakier HF component in those children at higher risk of asthma. Moreover, vagal activity and cardiorespiratory coupling were reduced following an ICS treatment in the group of children with a good asthma outcome, whereas it kept unchanged in those with a worse prognosis. Since it is noninvasive in nature, HRV analysis could represent a feasible tool for the continuous monitoring of asthma in young children, providing an objective measurement of the evolution of the disease and aiding in the study of the underlying pathophysiology. The research described in this chapter generated the following publications:
 - **Milagro, J.**, Gil, E., Bolea, J., Seppä, V. P., Malmberg, L. P., Pelkonen, A. S., Kotaniemi-Syrjänen, A., Mäkelä, M. J., Viik, J. and Bailón, R. Nonlinear Dynamics of Heart Rate Variability in Children with Asthmatic Symptoms. *Joint conference of the European Medical and Biological Engineering Conference (EM-BEC) and the Nordic-Baltic Conference on Biomedical Engineering and Medical Physics (NBC)*, 2017, pp. 815-818. Springer, Singapore.
 - **Milagro, J.**, Gil, E., Lázaro, J., Seppä, V. P., Malmberg, L. P., Pelkonen, A. S., Kotaniemi-Syrjänen, A., Mäkelä, M. J., Viik, J. and Bailón, R. Nocturnal Heart Rate Variability Spectrum Characterization in Children with Asthmatic Symptoms. *IEEE J Biomed Health Inform*, 2017, vol. 22, n. 5, pp. 1332-1340.
 - **Milagro, J.**, Gracia, J., Seppä, V. P., Karjalainen, J., Paasilta, M., Orini, M., Bailón, R., Gil, E. and Viik, J. Noninvasive Cardiorespiratory Signals Analysis for Asthma Evolution Monitoring in Preschool Children. Major revision (*IEEE Trans Biomed Eng*).
 - **Milagro, J.**, Gracia, J., Seppä, V. P., Karjalainen, J., Paasilta, M., Orini, M., Gil, E., Bailón, R. and Viik, J. Cardiorespiratory coupling in asthmatic children. Accepted for publication (*Computing in Cardiology conference* 2019).
- **Chapter 4. HRV analysis in asthmatic adults:** The methodological framework introduced in Ch. 2 was employed for the assessment of HRV in a dataset composed by asthmatic adults, classified attending to their degree of symptoms control and also with respect to the disease severity. The HRV features were employed in combination with several respiratory-derived and clinical features for training different classification algorithms, aiming to stratify the patients. The inclusion of ANS-related features for clasifying the subjects attending to their asthma severity resulted in a similar performance than in the case of employing only clinical features, outperforming it in some cases, therefore suggesting that ANS assessment could represent a feasible complement for the diagnosis and monitoring of asthma in adults.

- **Chapter 5. HRV analysis in sleep apnea syndrome with associated cardiovascular diseases:** SAS has been related to an increased risk of suffering from CVD. However, and despite the characteristic autonomic response to an apneic episode shared by most of the patients, only some of them will develop CVD. Since altered HRV has been independently related to both conditions, in this chapter HRV analysis was performed in a group of patients with SAS, half of which also had cardiovascular comorbidities. Moreover, a subset of subjects who did not have any CVD at the moment of the recordings but who developed them afterwards was also considered. The results revealed a higher sympathetic dominance in those subjects with CVD or that will develop CVD in the future, therefore suggesting that altered autonomic activity could constitute a risk factor for the development of cardiac comorbidities in subjects with sleep apnea. The research described in this chapter generated the following publication:
 - **Milagro, J.**, Deviaene, M., Gil, E., Lázaro, J., Buyse, B., Testelmans, D., P. Borzée, R. Willems, S. Van Huffel, R. Bailón and Varon, C. Autonomic Dysfunction Increases Cardiovascular Risk in the Presence of Sleep Apnea. *Front Physiol*, 2019, vol. 10, n. 620, pp. 1-11.

- **Chapter 6. Electrocardiogram-derived tidal volume estimation:** In this chapter, a novel methodology for the noninvasive estimation of the tidal volume during a treadmill test is presented. Several parameters were derived only from the ECG in a group of athletes who underwent two treadmill tests in different days. The parameters obtained in the first recording were used to train a subject-oriented model that was tested in the second recording. Several approaches were compared, and fitting errors lower than 14% in most of the cases and lower than 6% in some of them suggest that the tidal volume can be estimated from the ECG in non-stationary conditions. The research described in this chapter generated the following publications:
 - **Milagro, J.**, Hernando, D., Lázaro, J., Casajús, J. A., Garatachea, N., Gil, E. and Bailón, R. On Deriving Tidal Volume From Electrocardiogram During Maximal Effort Test. *Proceedings of the XLV International Conference on Computing in Cardiology*, 2018, pp. 1-4, Maastricht, The Netherlands.
 - **Milagro, J.**, Hernando, D., Lázaro, J., Casajús, J. A., Garatachea, N., Gil, E., and Bailón, R. Electrocardiogram-Derived Tidal Volume During Treadmill Stress Test. *IEEE Trans Biomed Eng*, 2019. In early access.
DOI: 10.1109/TBME.2019.2911351.

- **Chapter 7. Anaerobic threshold estimation through ventricular repolarization profile analysis:** A novel methodology for the noninvasive estimation of the anaerobic threshold during a cycle ergometer test is presented in this chapter. Essentially, it is based on the analysis of the ventricular repolarization dynamics. The general increase in the repolarization instability observed in most of the subjects was used for the estimation of the anaerobic threshold. An estimation error

lower than 1 minute in a 63% of the subjects suggests that the anerobic threshold can be estimated noninvasively, using only ECG recordings.

- **Chapter 8. Conclusions and future work:** This last chapter contains the main conclusions of the research presented in this thesis, as well as a proposal of future research lines.

1.8 Collaborations and research stays

All the research presented in this dissertation was conducted within the Biomedical Signal Interpretation & Computational Simulation (BSICoS) group (University of Zaragoza, Zaragoza, Spain), under the supervision of Prof. Raquel Bailón and Prof. Eduardo Gil. Moreover, the vast majority of the studies were performed in collaboration with researchers belonging to other research groups, who actively collaborated with methodological, physiological and data collection support. The visible heads of these research groups are:

- *Jari Viik*
Faculty of Medicine and Health Technology, Tampere University, Tampere, Finland.
- *Ville-Pekka Seppä*
Revenio Research Ltd., Vantaa, Finland.
- *L. Pekka Malmberg, Anna S. Pelkonen, Anne Kotaniemi-Syränen and Mika J. Mäkelä*
Skin and Allergy Hospital, Helsinki University Hospital, Helsinki, Finland.
- *Jussi Karjalainen and Marita Paassilta*
Allergy Centre of the Tampere University Hospital, Tampere, Finland.
- *Carolina Varon and Sabine Van Huffel*
Department of Electrical Engineering-ESAT, STADIUS Center for Dynamical Systems, Signal Processing and Data Analytics, KU Leuven, Leuven, Belgium, and IMEC, Leuven, Belgium.
- *Bertien Buyse and Dries Testelmans*
Department of Pneumology, UZ Leuven, Leuven, Belgium.
- *Rik Willems*
Department of Cardiovascular Sciences, UZ Leuven, Leuven, Belgium.
- *Nuria Garatachea and José Antonio Casajús*
Growth, Exercise, Nutrition and Development (GENUD) group at the Faculty of Health and Sport Sciences, IIS Aragón, University of Zaragoza, Zaragoza, Spain.

- *Vicente Plaza, Lorena Soto and Jordi Giner*
Pneumology and Allergy Department, Santa Creu i Sant Pau Hospital, Barcelona, Spain.
- *Michele Orini*
Institute of Cardiovascular Science, University College of London, London, United Kingdom.
- *Jordi Aguiló*
Microelectronics and Electronic Systems Department, Autonomous University of Barcelona, Bellaterra, Spain.

Additionally, I had the opportunity of benefiting from two research stays in the context of my PhD, which are listed below:

- January 2016 - May 2016: *Tampere University of Technology, Tampere, Finland*. I worked with Prof. Jari Viik in order to set up the framework for the analysis of HRV in preschool asthmatic children. During the stay I got familiar with the dataset of asthmatic children acquired at the Helsinki University Hospital, which is described in Ch. 3, and we designed the analysis criteria and parameters to be considered.
- September 2017 - December 2017: *KU Leuven, Leuven, Belgium*. This stay was an opportunity to discuss closely with Prof. Carolina Varon and Prof. Sabine Van Huffel in the context of the analysis of HRV in patients with sleep apnea syndrome and cardiovascular comorbidities. Apart of getting familiar with the data to be analyzed, we sat up a proper framework for its analysis, with the collaboration of the doctors from the University Hospital of Leuven.

2

Contextualized HRV analysis

2.1 Motivation	2.5.4 Relationship with kurtosis
2.2 HRV assessment	2.5.5 Relationship with HRV frequency domain analysis
2.3 Signal conditioning	2.5.6 Relationship with HRV nonlinear analysis
2.4 Ectopic beats versus RSA	2.5.7 Discussion
2.4.1 RSA detection algorithm	2.6 Effect of the respiratory rate
2.4.2 RSA correction in the presence of ectopic beats	2.6.1 Modified high-frequency bands
2.4.3 Discussion	2.6.2 Removing respiratory influence from HRV
2.5 Peakness	2.7 Cardiorespiratory coupling
2.5.1 Motivation	2.8 Discussion and conclusions
2.5.2 Definition	
2.5.3 Parameter selection	

2.1 Motivation

As already mentioned, extra-cardiac modulations of HR differ with age, gender and race [12, 153, 268]. Even when considering a single subject, HRV is altered under different situations, such as physical [45] or psychological stress [121], or during sleep, being it also different across sleep stages [52]. Moreover, circadian rhythms can result in a dis-

tinct HRV at different times of the day [125]. As it is well-known, several pathologies of distinct nature result in alterations of ANS functioning, which are often reflected in HRV. Therefore, a deep knowledge of the physiological changes induced by them is required for a proper analysis.

Apart from demographic and pathophysiologic reasons, HRV analysis and interpretation could be affected by several other confounders. One of these factors is the presence of ectopic beats. This problem is frequently addressed, although some of the techniques developed for removing the effect of ectopic beats from the tachogram based on beat-to-beat interval constrains might also remove some strong RSA events misclassified as ectopics, and which contain valuable information about ANS functioning.

On the other hand, HRV frequency-domain analysis has been traditionally focused on the power content of predefined frequency bands, completely ignoring how the power is distributed within those bands, which might be relevant in the analysis of ANS activity alterations. In this chapter, a novel index for the quantification of HF power distribution is presented and discussed in relation to the traditional frequency-domain indexes.

Another factor to take into account is the well-known coupling between HRV and respiration which, in the presence of lower or higher than normal respiratory rates, can lead to a shift of power of the HRV respiratory-related components towards frequency bands where they are not expected to be, thus compromising traditional ANS activity interpretation. The effect of the respiratory rate on HRV analysis was considered, together with the assessment of cardiorespiratory coupling.

It is for all these reasons that HRV analysis should be always contextualized and guided by physiology, being adapted to each concrete situation and hence minimizing the possible factors leading to a wrong interpretation. In this chapter, the introduced sources of error are discussed, and a framework for dealing with them is provided.

2.2 HRV assessment

In this dissertation, HRV has been analyzed in time, frequency and nonlinear domains. Whereas time domain analysis was performed directly from the RR interval series constructed from beat occurrence times, spectral estimation was applied to the modulating signal obtained from the time-varying integral pulse frequency modulation (TVIPFM) model [19]. The TVIPFM model is used for representing the generation of an event series from a continuous-time signal, which can be provided with a physiological interpretation [246]. In the case of HRV representation, the beat occurrence times, t_k , are supposed to be generated by a modulating signal, $m(t)$, which has zero-mean and carries the information of ANS modulation. A schematic of the TVIPFM model is displayed in Fig. 2.1. The input signal, consisting in $m(t)$ superimposed to a DC level, is integrated until a threshold, $T(t)$, which accounts for the time-varying mean heart period. Once the threshold is reached, a heart beat occurs, and the integration process is reset. Under the

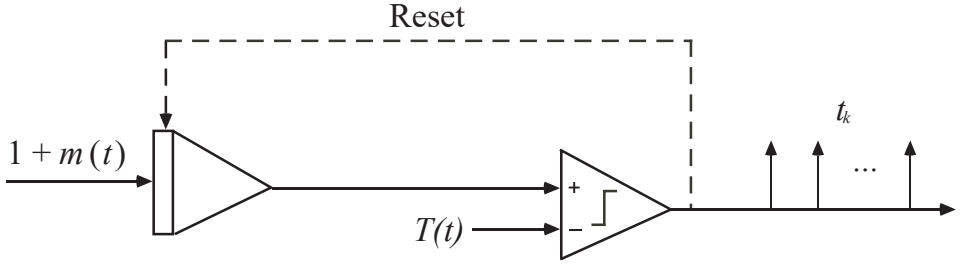


Figure 2.1: Schematic of the time-varying integral pulse frequency modulation (TVIPFM) model. Reproduced and modified from [19].

assumption that $m(t)$ is casual, band-limited and < 1 , and that the time occurrence of the first beat is at time $t_0 = 0$, the beat occurrence time series can be related with $m(t)$ as:

$$k = \int_0^{t_k} \frac{1 + m(t)}{T(t)} dt, \quad (2.1)$$

being k and t_k the index and occurrence time of the k -th beat, respectively. In Eq. 2.1, the term:

$$d_{\text{HR}}(t) = \frac{1 + m(t)}{T(t)} = \frac{1}{T(t)} + \frac{m(t)}{T(t)}, \quad (2.2)$$

accounts for the instantaneous HR, and is composed by two terms: the HRV signal, $m(t)/T(t)$, and the time-varying mean HR, $1/T(t)$. Under the assumption that the variations in mean HR are much slower than the variations in HRV, the latter term can be easily obtained by low-pass filtering $d_{\text{HR}}(t)$. Defining the resulting signal as $d_{\text{HRM}}(t) = 1/T(t)$, $m(t)$ can be calculated as:

$$m(t) = \frac{d_{\text{HR}}(t) - d_{\text{HRM}}(t)}{d_{\text{HRM}}(t)}. \quad (2.3)$$

Afterwards, an evenly-sampled discrete-time version of the modulating signal, $m(n)$, can be obtained by resampling $m(t)$, typically at 4 Hz. It is this $m(n)$ which was used for frequency domain HRV analysis in this thesis. All the frequency domain indexes computed in the following chapters were obtained from 5-minute segments of $m(n)$ following the Task Force recommendations [252], whose spectra, $\hat{S}_{\text{HRV}}(F)$, were estimated by the Welch's periodogram method [273], using 50-second Hamming windows with 50% overlap. The different frequency-domain indexes, i.e., P_{VLF} , P_{LF} , P_{HF} , $R_{\text{LF/HF}}$ and P_{LFn} (see Ch. 1.4.3), were then calculated from $\hat{S}_{\text{HRV}}(F)$.

Regarding the nonlinear-domain analysis, D_2 , $ApEn$ and $SampEn$ were considered in Ch. 3, being computed from the interpolated RR interval series. The computation of D_2 corresponds to that of $\hat{D}_{2(\text{max})}$ proposed by *Bolea et al.* [43], since it is computationally efficient.

2.3 Signal conditioning

Noise can be understood as any information contained in a given signal that does not contribute to (or interfere with) the purpose for which the signal is being analyzed. In this way, what is considered as noise will depend on the application: e.g., in the analysis of an ECG signal, the electromyographic activity will be a source of noise that will contaminate the target signal. However, if the interest is in the electrical response of the muscles in the thorax, then the ECG will become a primary source of noise.

The presence of noise in the ECG signal may blur the exact position of the R wave fiducial points, thus compromising HRV analysis for which accurate R peak detection remains crucial. For this reason, a proper conditioning of the signals is required prior to fiducial points detection. Some common interferences in the ECG signals are the baseline wander, consisting in a low frequency modulation of the ECG occasioned by body movement (respiration, postural changes or exercise) or poor electrode contact, the power line interference and high-frequency noise, with its main source in electromyographic activity [246]. The removal of the baseline wander can be accomplished in several ways, from a simple high-pass filtering to polynomial fitting. The approach used in this thesis consists in extracting the baseline with a forward-backward low-pass filter (3rd order Butterworth filter with 0.5 Hz cut-off frequency), so that it can be further subtracted from the original ECG:

$$x_{\text{ECG}}(t) = x_{\text{ECG}}^{\text{bl}}(t) - x_{\text{bl}}(t), \quad (2.4)$$

where $x_{\text{ECG}}(t)$ is the clean ECG signal after baseline wander removal, $x_{\text{ECG}}^{\text{bl}}(t)$ is the original ECG signal and $x_{\text{bl}}(t)$ is the baseline signal as obtained from low-pass filtering. In the case of power line interference and high-frequency noise, different filtering techniques can be applied, being the most extended the notch filtering (at 50 or 60 Hz) and low-pass filtering respectively.

On the other hand, there are some sources of noise that can not be avoided by simple filtering. This is the case of technical artifacts, such as poor electrode attachment or electrode detachment, as well as some fast postural changes that can induce high-amplitude noise in the ECG signal, completely masking it. In this situations, the R peak detection algorithms might not be accurate and could compromise the further physiological interpretation, which is especially hampering in ambulatory scenarios. Hence, signal segments affected by this kind of artifacts should be conveniently identified and discarded from the analysis. One possible solution relies in estimating the signal-to-noise ratio (SNR) of the ECG signal in a continuous-time basis, so that those periods for which SNR falls below a predefined threshold are discarded. *Bailón et al.* used a method for beat-to-beat SNR estimation [21], where the SNR is computed as:

$$\hat{x}_{\text{SNR}}(i) = \frac{A(i)}{1 + P_N(i)}, \quad (2.5)$$

where $\hat{x}_{\text{SNR}}(i)$, $A(i)$ and $P_{\text{N}}(i)$ are the SNR, peak-to-peak amplitude and level of high-frequency noise of beat i , respectively. $A(i)$ was obtained as the difference between the maximum and the minimum value of the QRS-complex corresponding to beat i , whereas $P_{\text{N}}(i)$ was calculated as:

$$P_{\text{N}}(i) = \sqrt{\frac{1}{t_2(i) - t_1(i)} \int_{t_1(i)}^{t_2(i)} x_{\text{HF}}^2(t) dt} \quad (2.6)$$

where $x_{\text{HF}}(t)$ is a high-pass filtered version of the ECG signal (2nd order, 20 Hz cut-off frequency Butterworth filter) and $t_1(i)$ is set 150 ms after the QRS-complex corresponding to beat i , whereas $t_2(i)$ is dependent of the instantaneous HR and is calculated as $t_1(i) + \text{RR}(i)/2$, being $\text{RR}(i)$ the RR interval (in ms) between beat i and beat $i + 1$. Therefore, beat-to-beat signal quality can be assessed by comparing $\hat{x}_{\text{SNR}}(i)$ with a threshold, so that those beats for which the SNR do not exceed it are discarded from the analysis.

Nevertheless, not only noise but also physiology itself can compromise ECG and HRV analysis, since different physiological statuses may affect biosignals distinctly. One well known example is the effect of sleep stages on HRV analysis, with decreased sympathetic dominance during NREM sleep which is increased towards awake-like levels in REM sleep [52]. This variability in HR control should be considered in the analysis, and the absence of polysomnographic recordings will unavoidably constitute a limitation of any HRV analysis performed during night. Some other examples of the importance of subjecting the analysis to physiological conditions can be found in the behavior of different biosignals to emotional or physical stress [45,121], or according to demographics (age, gender or race) [12, 153, 268]. For these reasons, HRV analysis is usually performed during rest, or in order to compare resting conditions with physiological changes of different nature, and taking demographics into account. For those situations when no resting conditions are available, the averaging of the analyzed parameters over long time windows can be used to mitigate the effect of time-varying physiological conditions (e.g., in the case of sleep, averaging over a complete sleep cycle).

Moreover, there are also pathological conditions that can lead to misinterpretation of HRV analysis, such as some heart rhythms distinct from sinus rhythm (e.g., atrial fibrillation). Since HRV analysis is aimed to assess ANS activity, it is not suitable for those conditions where the beats are not originated at the sinus node, since HR is not modulated by autonomic activity in these cases. Also exacerbations in some pathologies such as COPD, apneic episodes in SAS and other similar events are accompanied by complex autonomic responses which should be taken into account in the analysis. Nonetheless, several other pathologies and medications might also compromise HRV analysis interpretation, since they may have a direct effect on autonomic activity or modulation of HR. In such situations, physiological interpretation must be addressed carefully.

2.4 Ectopic beats versus RSA

Since the SA node is not the only auto-excitabile group of cells within the heart, it may occur that a beat originated in a region different from the SA node interrupts the normal sinus rhythm. These kind of beats are known as ectopic beats, and can have either a supra-ventricular or a ventricular origin which is unrelated to ANS modulation (an example showing a ventricular ectopic beat is displayed in Fig. 2.2 a)). They are often premature beats, and induce a characteristic disturbance in the tachogram, consisting in a reduced beat-to-beat interval followed by a compensatory pause which reflects as a long beat-to-beat interval [132], as depicted in Fig. 2.2 d). The presence of ectopic beats may distort HRV analysis, especially in the frequency domain, since the spike-like artifacts that they introduce in the tachogram are reflected as a wide-band noise in the frequency domain (Fig. 2.2 e)), thus altering the spectra and leading to erroneous frequency domain indexes estimation [41, 156]. In Fig. 2.2, the effect of adding a different number of ectopic beats to the same 5-minute tachogram is displayed.

In this way, it is evident that a proper ectopic beat management remains essential in every HRV analysis, and several authors have proposed a variety of methods based on direct removal or interpolation of the ectopic RR intervals [156], different filtering techniques such as impulse rejection [175] or threshold-based filtering [147], or either variations in the instantaneous HR [157, 172], among others. In this dissertation, the heart timing signal-based method proposed by *Mateo and Laguna* [172] was employed. Essentially, those beats exceeding a threshold for the allowed HR variation, U , are labeled as ectopics. In [172], the threshold U was varied according to a parameter ξ , which in this thesis will be referred to as θ_{HR} , so that lower values of θ_{HR} are more restrictive to rhythm changes.

On the other hand, RSA is the principal short-term modulator of HR, and so it represents the main contribution to the HF power of HRV [4, 6]. However, the use of an ectopic beat correction methodology which is only based on rhythm changes (and not in ECG morphology) may cause the identification of some RSA episodes as ectopic beats, so that they would be corrected to follow what is considered as “normal rhythm” by the algorithm (see Fig. 2.3). Despite the fact that there might be no difference in the effect produced by an ectopic or by a strong and isolated RSA episode, the latter has an ANS-mediated origin, and hence should be considered for a proper physiological interpretation. The identification of RSA episodes with ectopic beats may particularly affect HRV analysis in young children, who usually present a stronger RSA [87, 141] and are less prone to the occurrence of ectopic beats [186, 192]. As the different study cases included in this thesis largely involve young children, an algorithm for the appropriate detection of RSA episodes based both on ECG morphology and on HR dynamics has been proposed.

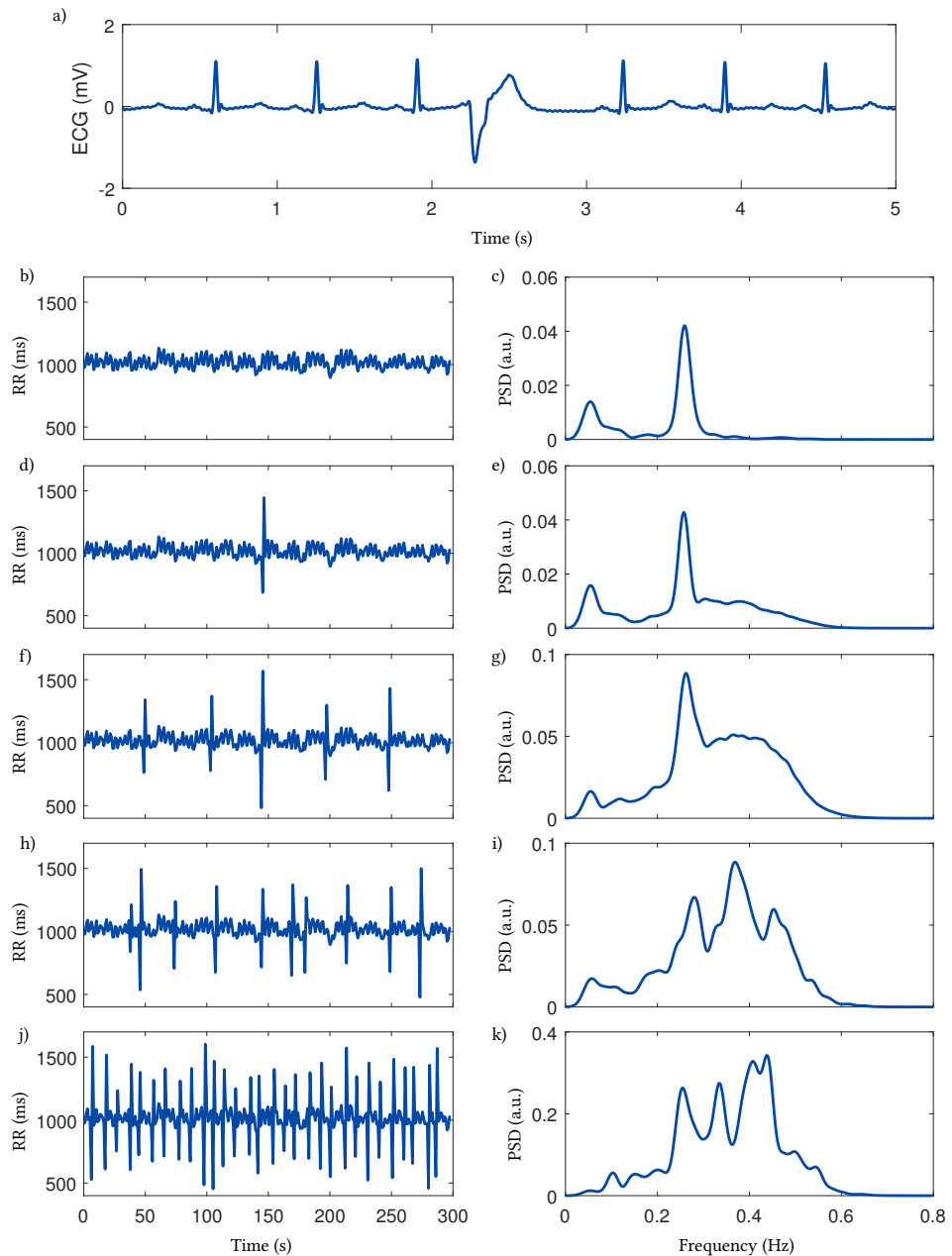


Figure 2.2: A real premature ventricular contraction (a) and some examples showing the effect that ectopic beats exert on HRV spectrum is displayed. The spectra on the right column correspond to the tachograms on their left. In b) and c), the original tachogram and its spectra is shown, whereas in the other examples 1 (d) and e)), 5 (f) and g)), 10 (h) and i)) and 30 (j) and k)) ectopic beats were added. It can be noticed how an increasing number of ectopic beats distort the power distribution of the HRV spectra, thus compromising HRV analysis.

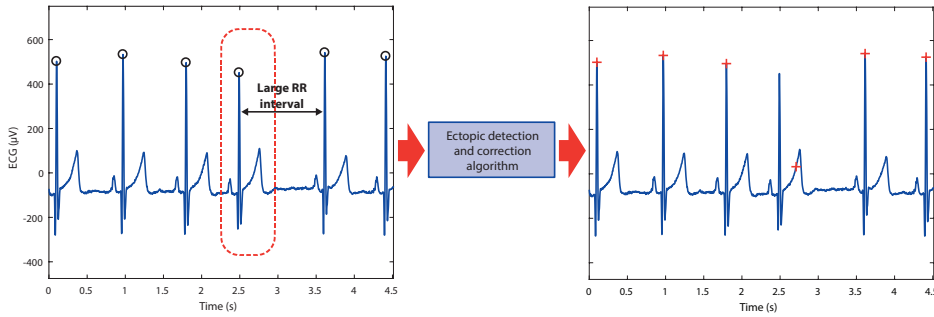


Figure 2.3: Example of a failure in ectopic beat correction. Original R peaks detections are marked with black circles, whereas red crosses indicate the corrected positions after applying the ectopic correction algorithm. The large RR interval in the figure on the left is interpreted as abnormal, so that the beat highlighted with a red dashed line is considered as ectopic and its R peak location is modified.

2.4.1 RSA detection algorithm

The algorithm consists in a two-stage analysis that departs from the ectopic beat identification and correction generated by the method of *Mateo and Laguna* [172], which essentially consists in the position of those beats labeled as ectopics and the corrected beat positions. A complete schematic of the algorithm is displayed at Fig. 2.4.

Each time that a beat is labeled as a possible ectopic, it undergoes a morphology analysis stage, which follows the outline below:

1. The beat labeled as ectopic, as well as the previous and the next beats, are segmented using a fixed window going from 200 ms before the R peak location to 400 ms after it. The three ECG segments are then normalized to the maximum amplitude found in any of them, and aligned using the maximum of their covariance, as exemplified in Fig. 2.4 a.1) to d.1). A maximum shift of ± 150 ms is allowed in order to prevent from aligning with waves that do not correspond to the target beats. The resulting normalized and aligned waveforms corresponding to the ectopic beat, its previous beat, and the following one are referred to as $w_{ec}(t)$, $w_{pre}(t)$ and $w_{post}(t)$, respectively.
2. Considering each of the three waveforms as a vector in a K -dimensional euclidean space, the euclidean distance between pairs of waveforms was considered as a metric of their morphological similarity. In this way, three distance measurements were obtained:

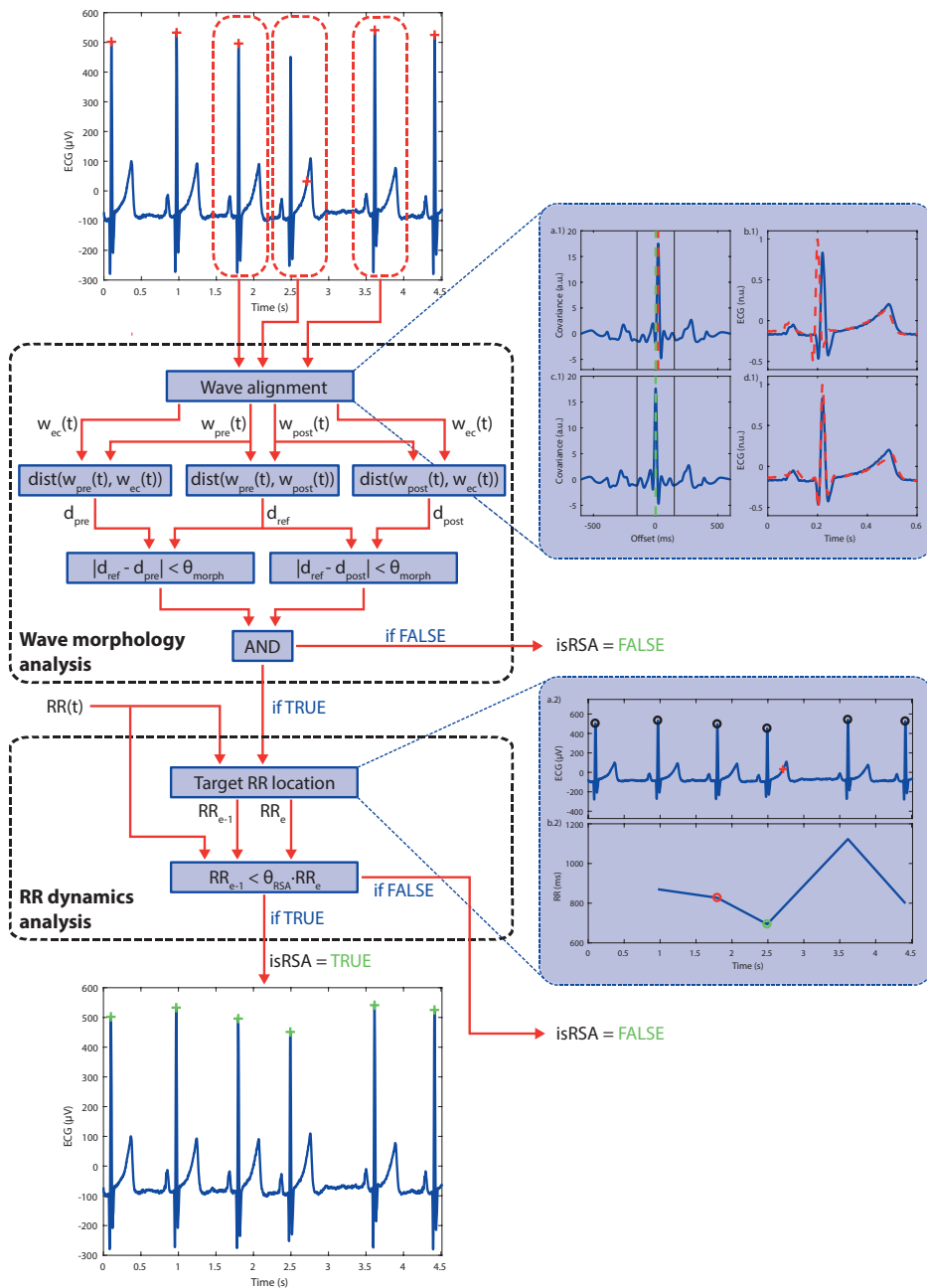


Figure 2.4: A schematic of the algorithm for RSA episodes detection and correction is displayed. First, the beat labeled as ectopic comes through a morphology analysis, and if it is considered similar to its surrounding beats, the RR interval dynamics are taken into account. If the pattern followed by the tachogram is identified as a RSA episode, beat positions are updated. Otherwise, beat positions obtained from the ectopic correction algorithm are kept unchanged (see text for a detailed description of the algorithm).

$$\begin{aligned}
d_{\text{ref}} &= \sqrt{\int (w_{\text{pre}}(t) - w_{\text{post}}(t))^2 dt}, \\
d_{\text{pre}} &= \sqrt{\int (w_{\text{ec}}(t) - w_{\text{pre}}(t))^2 dt}, \\
d_{\text{post}} &= \sqrt{\int (w_{\text{ec}}(t) - w_{\text{post}}(t))^2 dt},
\end{aligned} \tag{2.7}$$

where d_{ref} accounts for the morphological difference between $w_{\text{pre}}(t)$ and $w_{\text{post}}(t)$ and it is considered as a reference, whereas d_{pre} and d_{post} account for the morphological distance between $w_{\text{ec}}(t)$ and either $w_{\text{pre}}(t)$ or $w_{\text{post}}(t)$.

3. Finally, the absolute values of the differences between d_{pre} and d_{ref} and between d_{post} and d_{ref} are computed independently. If the result is in both cases lower than a predefined morphological threshold, θ_{morph} , $w_{\text{ec}}(t)$ is considered morphologically similar to its adjacent beats, and the next stage of the algorithm is applied. Otherwise, $w_{\text{ec}}(t)$ is considered as an ectopic and not as a RSA episode, so that the original beat position detection is replaced by the output of the ectopic correction method.

If the possible ectopic is considered morphologically similar to its adjacent beats, a HR analysis is performed. Essentially, the pattern of the tachogram in the vicinity of the considered event is analyzed to determine whether there is a RSA episode or not. For this purpose, the RR interval between the ectopic and the previous one, RR_e , and the RR interval previous to it, RR_{e-1} , are located (Fig. 2.4 a.2) and b.2)), as they define a pattern that can be used to interpret if the episode corresponds with RSA. Given a predefined variation threshold, θ_{RSA} , four different patterns have been identified:

1. If $RR_{e-1} < RR_e$ the event is considered as the start of the HR deceleration posterior to the acceleration in a RSA episode (Fig. 2.5 a) and b)).
2. If $RR_{e-1} < \theta_{\text{RSA}}RR_e$ and the RR interval following RR_e is larger than it, then the event is considered as the end of the HR acceleration previous to the deceleration in an RSA episode (Fig. 2.5 c) and d)).
3. If $RR_{e-1} < \theta_{\text{RSA}}RR_e$ and the RR interval following RR_e is shorter than it, then the event is considered as the beginning of the HR acceleration of an RSA episode (Fig. 2.5 e) and f)).
4. Otherwise, the beats is considered as an ectopic.

In any of the first three cases, the original detections are left uncorrected, whereas if the beat is labeled as an ectopic, the original beat position detection is replaced by the output of the ectopic correction method. Some graphical examples of the resulting tachograms after applying only the ectopic correction method or the ectopic correction

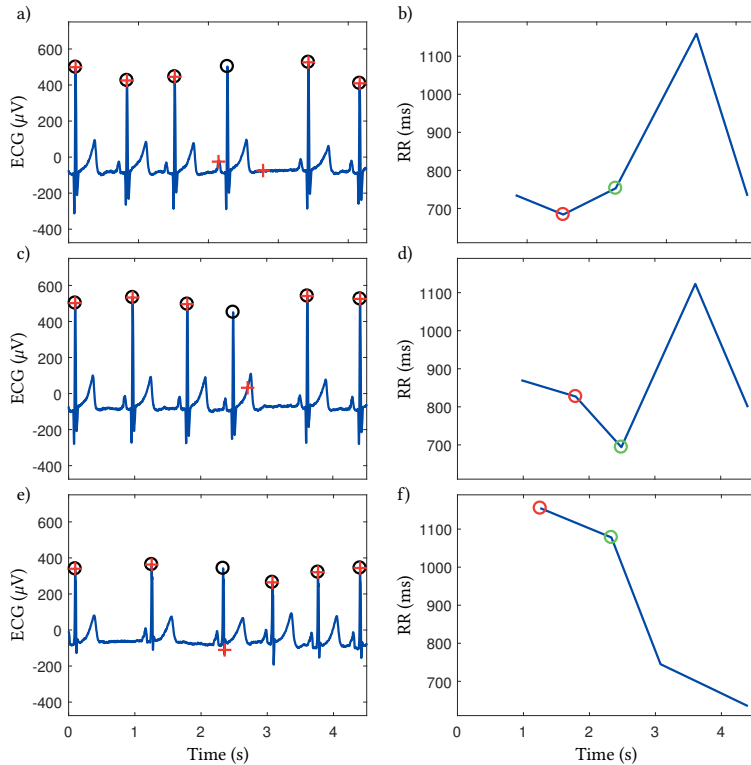


Figure 2.5: Three different RSA patterns are displayed. Each RR interval series correspond to the ECG segment displayed at its left. In a) and b), a decelerating pattern is shown, whereas the end and the beginning of two acceleration patterns are displayed at c) and d) and at e) and f) respectively. In the ECG segments, the black circles and the red crosses indicate the original detections and the detections after applying the ectopic correction respectively. The red circles in the RR interval series indicate the RR interval previous to the possible ectopic (RR_{e-1}), and the green ones indicate the RR interval occasioned by it (RR_e).

plus a subsequent RSA detection and correction using different threshold combinations are displayed in Figs. 2.6 and 2.7. In these figures, the effect of the accurate detection of the RSA episodes in the resulting HRV spectra is also shown (note that the HF component exceeds 0.4 Hz, since the employed ECGs belong to young children, with higher respiratory rates than the adults).

Although at this point one might think that increasing θ_{HR} would have been enough to consider all the beats as non-ectopics, the analysis of Figs. 2.6 and 2.7 reveals the existence of some advantages of applying the RSA algorithm after ectopics correction. First, ectopic correction is limited in the amount of HR variation than can be admitted, as it can be noticed in Fig. 2.7, where not every RSA episode is captured in spite of the increase in the threshold. This bound is needed in order to be able to detect an absence of beats, e.g., in a compensatory pause, as allowing larger variations would lead to interpret this pause as normal, without labeling and correcting it. Once the beats that are suspicious of being ectopics have been detected, the RSA algorithm allows to consider wider variations in HR as normal if desired, only taking into account the variation in HR with respect to

the previous beat, and not to the average HR. On the other hand, the ectopic correction algorithm does not consider any kind of morphological information. By performing a wave morphology analysis, the RSA correction method can better identify whether a beat has a normal morphology or either the detected event is a real ectopic beat or a noisy segment.

2.4.2 RSA correction in the presence of ectopic beats

In order to better analyze the effect of using different thresholds and to assess the performance of the RSA detection and correction algorithm in the presence of ectopic beats, it was applied to the MIT-BIH arrhythmia database [181], freely available at PhysioNet [100]. This dataset contains 48 half-an-hour ECG segments which were annotated by two or more cardiologists, who established the beat time occurrences, the nature of each beat, and changes in the type of rhythm. Beat labels identify each beat either as normal or as a given class of abnormal beat, which range from atrial premature beats to premature ventricular contraction or bundle branch block beats. Also rhythm changes can belong to a large variety apart from normal sinus rhythm, e.g., atrial fibrillation, ventricular bigeminy or ventricular tachycardia. All the signals were recorded at a sampling rate of 360 Hz, and a complete description of the dataset and all the possible annotations can be found at PhysioNet and in [181]. The total number of normal and ectopic beats considered here was 57285 and 3852, respectively.

After ECG segments baseline wander removal and interpolation to 1000 Hz, R peaks positions were detected using the wavelet-based method proposed by *Matínez et al.* [167]. For simplicity, only those beats occurring during normal sinus rhythm and labeled as normal beat, atrial premature beat, aberrated atrial premature beat, supraventricular premature beat or premature ventricular contraction were considered. The ectopic and RSA detection and correction algorithms were applied sequentially to all the recordings, using different sets of thresholds. In the case of the ectopic detection and correction, θ_{HR} ranged from 0 to 3 in steps of 0.5. Regarding the RSA algorithm, θ_{morph} was varied between 0 and 5 in steps of 0.5, whereas two values of θ_{RSA} , 1.15 and 1.5, were tested (these values were selected since they were later applied in Ch. 3). The performance evaluation was accomplished by calculating the sensitivity and specificity of the beats classification in normal or ectopics after applying either the ectopic correction alone or followed by the RSA correction algorithm, for the different proposed sets of parameters. The results are summarized in Figs. 2.8 and 2.9, and numerical values for some threshold combinations are displayed in Table 2.1.

As expected, increasing the value of θ_{HR} (i.e., allowing higher deviations from the mean HR) results in a reduction of the sensitivity in the detection of ectopic beats, whereas small increases in θ_{morph} when the value of θ_{HR} is kept low results in an increase of the sensitivity and specificity of the detection of normal and ectopic beats, respectively, as displayed in Fig. 2.8 and Table 2.1. Although the specificity in the case of normal beats and the sensitivity in the case of ectopics are reduced, this reduction is much smaller than the

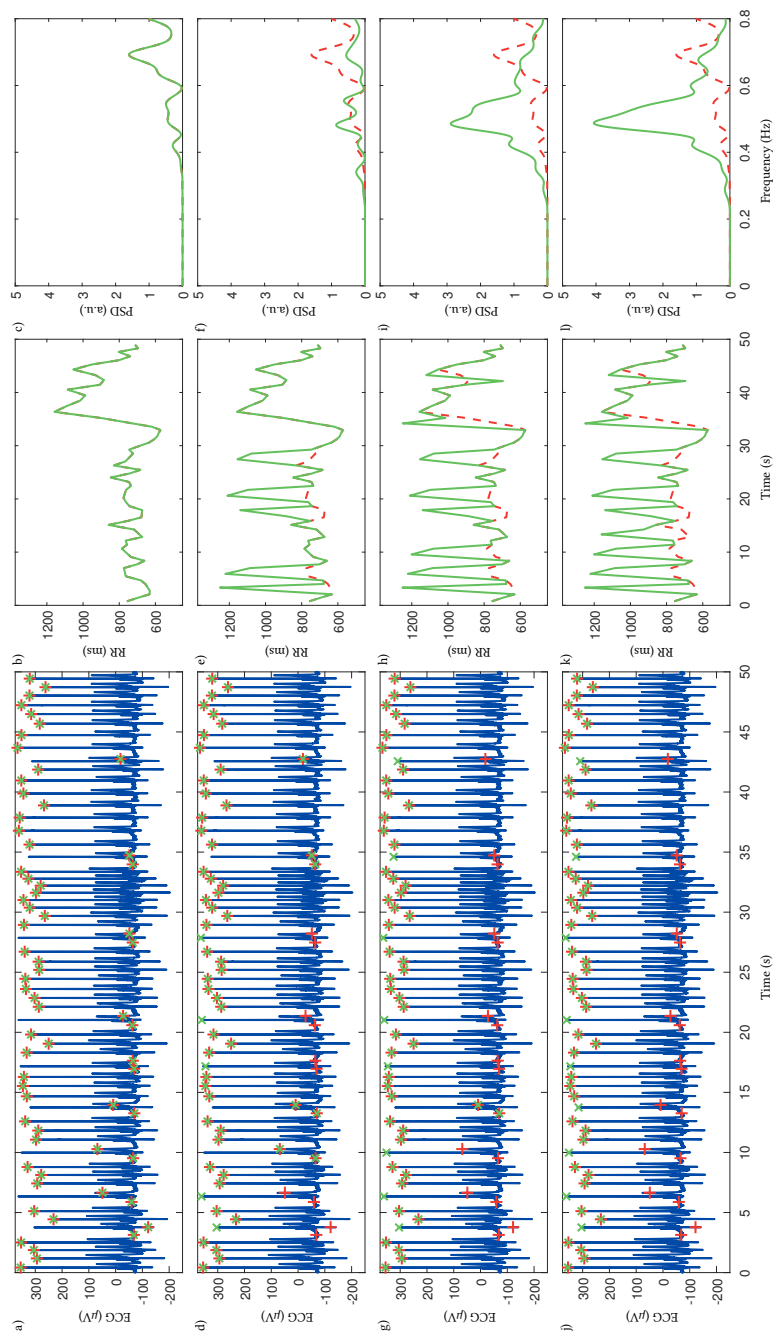


Figure 2.6: Differences in the tachograms obtained when varying ectopic and RSA detection and correction thresholds. The same ECG segment is represented in a), d), g) and j), and the tachograms on the right of each ECG representation were obtained from the detection of its R peaks, whereas in c), f), i) and l) the spectrum of each tachogram is shown. Red crosses and dashed lines represent the detections after applying the ectopic correction algorithm and the tachogram obtained from them, respectively, whereas the green crosses and solid lines represent the detections after applying the RSA detection and correction, and the resulting tachograms. In this example, θ_{HR} and θ_{RSA} were fixed at 1 and 1.5 respectively, whereas θ_{morph} was selected as 0 in a), b) and c), 0.5 in d), e) and f), 1 in g), h) and i), and 1.5 in j), k) and l).

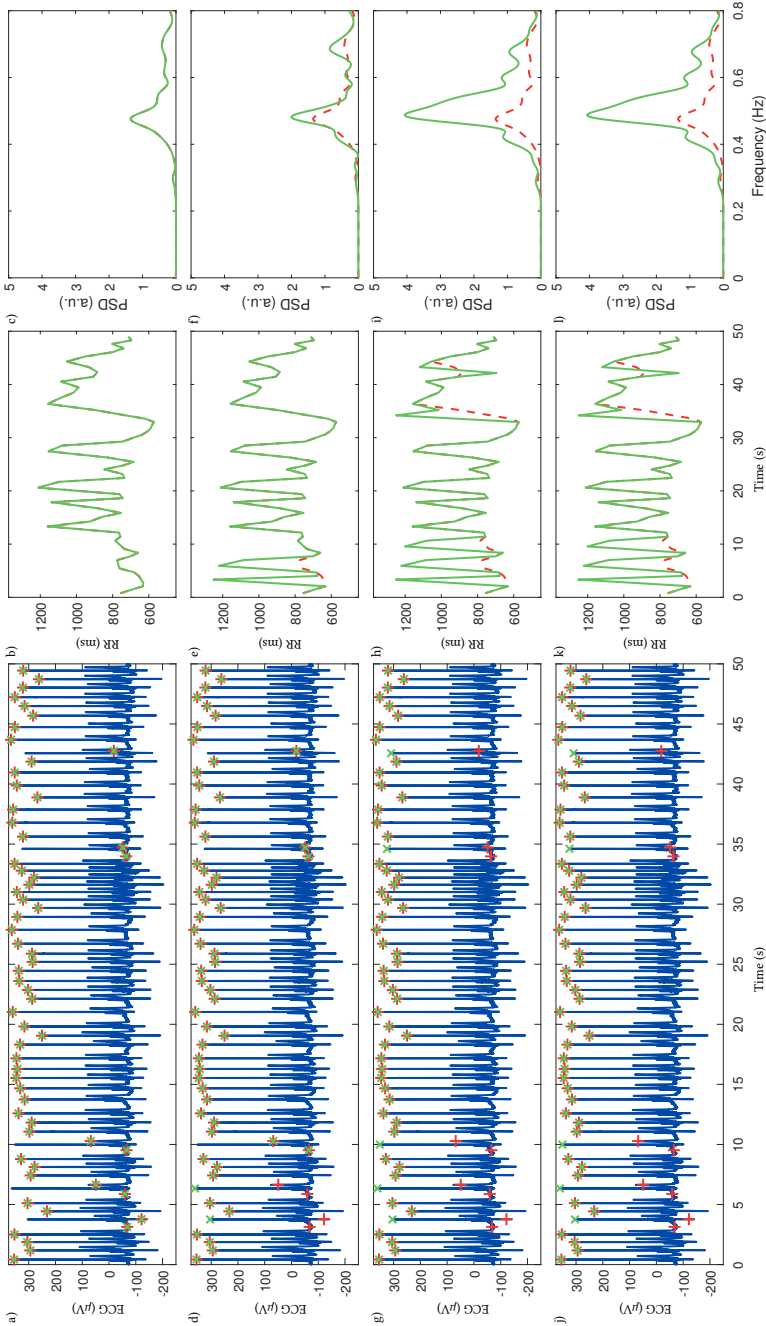


Figure 2.7: Differences in the tachograms obtained when varying ectopic and RSA detection and correction thresholds. The same ECG segment is represented in a), d), g) and j), and the tachograms on the right of each ECG representation were obtained from the detection of its R peaks, whereas in c), f), i) and l) the spectrum of each tachogram is shown. Red crosses and dashed lines represent the detections after applying the ectopic correction algorithm and the tachogram obtained from them, respectively, whereas the green crosses and solid lines represent the detections after applying the RSA detection and correction, and the resulting tachograms. In this example, θ_{HR} and θ_{RSA} were fixed at 2 and 1.5 respectively, whereas θ_{morph} was selected as 0 in a), b) and c), 0.5 in d), e) and f), 1 in g), h) and i), and 1.5 in j), k) and l).

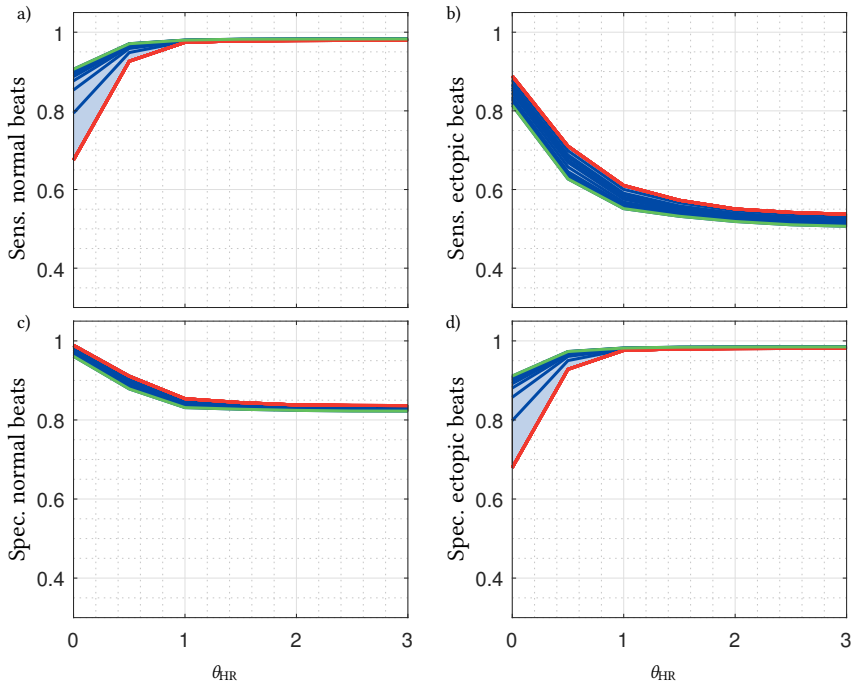


Figure 2.8: Sensitivity and specificity of the beat classification in normal (a) and c)) or ectopics (b) and d)), for the different proposed thresholds. The red lines indicate the results obtained when only ectopic correction is applied, whereas the blue lines indicate the results obtained after applying both ectopic and RSA detection and correction (the results for growing values of θ_{morph} are further from the red line and closer to the green line, the latter indicating the results obtained for the largest value of θ_{morph}). $\theta_{RSA} = 1.15$ was employed.

increase in the other parameters. This behavior is maintained when increasing the value of θ_{RSA} (see Fig. 2.9 and 2.1). However, the choice of high values for θ_{morph} results in a faster decrease of the performance in the later case. Depending on the application, a different set of parameters should be chosen, although considering the results of the simulation, it can be concluded that the inclusion of the RSA detection and correction approach can complement and even increase the performance of the ectopic beats correction alone.

2.4.3 Discussion

The main limitation of the previous simulation is that the mean age of the population in the MIT-BIH arrhythmia dataset is much higher than the two children populations described in Ch. 3, for which the RSA correction methodology was developed. Hence, much less frequent strong RSA episodes were present in the MIT-BIH arrhythmia dataset, so that this simulation should be only considered as a concrete example of the methodology performance, and cannot be used for establishing the thresholds for the datasets employed in Ch. 3, for which less restrictive thresholds were employed. Since ectopic beats are not frequent in young children, there is no reason for thinking that relaxing the al-

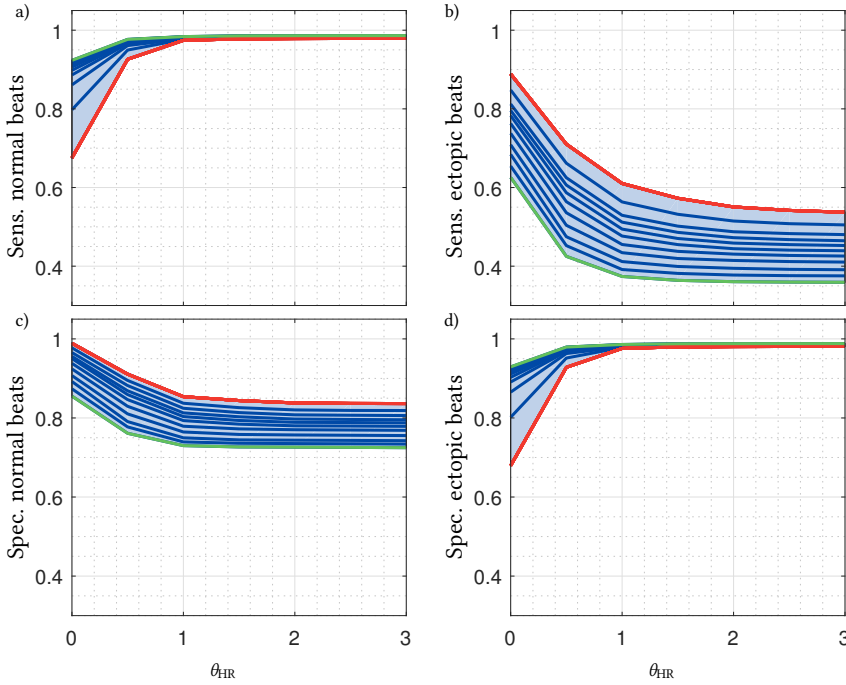


Figure 2.9: Sensitivity and specificity of the beat classification in normal (a) and c)) or ectopics (b) and d)), for the different proposed thresholds. The red lines indicate the results obtained when only ectopic correction is applied, whereas the blue lines indicate the results obtained after applying both ectopic and RSA detection and correction (the results for growing values of θ_{morph} are further from the red line and closer to the green line, the latter indicating the results obtained for the largest value of θ_{morph}). $\theta_{\text{RSA}} = 1.5$ was employed.

lowed RR variation could result in an increased number of false detections. As described in Ch. 3, the employed thresholds were adjusted to each dataset by visual inspection of the detections. Another limitation is the highly unbalanced number of normal and ectopic beats, which might have an effect in the results of the simulation.

There is still not a unified explanation for the increased HR respiratory-related modulation in young children when compared with adults, although several hypotheses have been proposed in the literature. On one hand, the smaller size of a child's heart might make it more responsive to fluctuations caused by respiration [87]. On the other hand, and under the assumption that RSA could play a role in minimizing the workload of the heart [31, 32], it is possible that the increased cardiac activity of young children is accompanied by a greater energy saving. Finally, maturation of the ANS may be also an important factor.

Table 2.1: Sensitivity and specificity of the detection of normal and ectopic beats in the MIT-BIH arrhythmia dataset (see test for details) with the proposed methodology. The results obtained for different combinations of thresholds are displayed.

		$\theta_{\text{morph}} = 0$		$\theta_{\text{morph}} = 2.5$		$\theta_{\text{morph}} = 5$	
		$\theta_{\text{HR}} = 0$	$\theta_{\text{HR}} = 0.5$	$\theta_{\text{HR}} = 0$	$\theta_{\text{HR}} = 0.5$	$\theta_{\text{HR}} = 0$	$\theta_{\text{HR}} = 0.5$
$\theta_{\text{RSA}} = 1.15$	Sens. Normal (%)	67.54	92.61	89.41	96.75	90.59	97.07
	Spec. Normal (%)	98.93	91.15	98.31	90.16	96.10	87.85
	Sens. Ectopic (%)	88.80	71.03	85.45	66.87	81.42	62.69
	Spec. Ectopic (%)	67.94	92.81	89.89	96.97	91.11	97.31
$\theta_{\text{RSA}} = 1.50$	Sens. Normal (%)	67.54	92.61	90.61	97.17	92.33	97.67
	Spec. Normal (%)	98.93	91.15	93.81	84.63	85.52	76.12
	Sens. Ectopic (%)	88.80	71.03	76.27	56.39	62.58	42.50
	Spec. Ectopic (%)	67.94	92.81	91.12	97.40	92.92	97.93

2.5 Peakness

2.5.1 Motivation

Short-term frequency domain HRV analysis is performed under the assumption that autonomic modulation-induced changes in HR are stationary during the analyzed period, typically of 5 minutes. Despite that recordings of approximately 1 and 2 minutes would be enough for the estimation of the HF and LF components respectively [252], the standard has been set to 5 minutes for two reasons: first, it results in better estimations of the LF component. Second, it provides a common framework for different studies considering short-term HRV. But the use of this rather long analysis window size has its counterpart, especially in what concerns HF components, with faster oscillations. Since HRV is not truly stationary, measurements performed in 5 minute windows account for the average autonomic modulation, but do not provide any information regarding how this modulation varies. In this way, non-stationarity of the vagal contribution could result in a widening of the HF component of the HRV spectrum which, eventually, might even present a multi-modal behavior. However, this information is not accounted for by any of the traditional frequency domain parameters, which are based on the measurement of the power content in the different frequency bands (see Fig. 2.10). Since changes in the vagal modulation pattern could provide additional information about PNS activity and might be reflected as variations in the shape of HF spectra, a novel parameter which accounts for how the power is distributed within the HF band is proposed below.

2.5.2 Definition

The concept of peakness was first introduced by *Bailón et al.* [21] in the context of robust respiratory rate estimation, and it was later exploited by *Lázaro et al.* [146] and *Hernando et al.* [121] for PPG-based respiratory rate estimation and stress assessment, respectively.

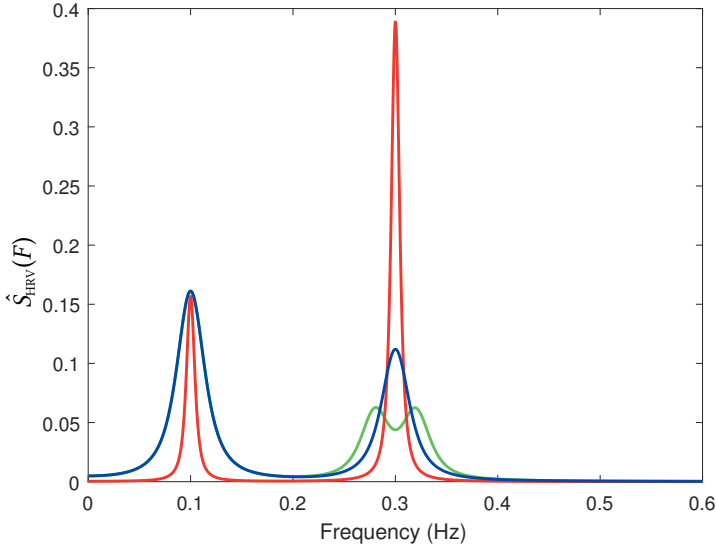


Figure 2.10: Three different simulated HRV spectra with the same P_{HF} but different shapes are displayed.

Essentially, it represents a measurement of how the power of a given frequency band is concentrated around a frequency of interest, and it can be expressed mathematically as:

$$\wp = \frac{\int_{\Omega_1} S(F) dF}{\int_{\Omega_2} S(F) dF}, \quad (2.8)$$

where Ω_1 is a frequency band centered in the frequency of interest, Ω_2 is the considered frequency range and $S(F)$ is the spectrum to be analyzed. According to Eq. 2.8, \wp will range from 0 to 1, being 0 when there is no power in Ω_1 and 1 when all the power in Ω_2 is also contained in Ω_1 . At this point, it is clear that the main challenge in the definition of peakness is the selection of appropriate frequency bands, which should be guided by physiology and application.

In difference with previous studies where \wp was employed to decide whether a dominant component was present in the analyzed spectra, in this dissertation it is proposed as a measurement of the spectral distribution of the HF components of HRV, and hence some methodological differences arise. The first one consists in the resolution of $S(F)$, as it must be high enough to distinguish between near components. Here, the same resolution used in the frequency domain analysis of HRV was employed, so that $S(F)$ was estimated from 5-minute length segments (since in this case $S(F)$ represents the estimation of the HRV spectrum, it will be referred to as $\hat{S}_{HRV}(F)$), using the Welch's periodogram method (50 second windows, with 50% overlap), with Hamming windows. Hence, the spectral resolution will be that of the Hamming window: $\Delta H = 1.3 \frac{F_s}{N} = 0.026$ Hz (since $F_s = 4$ Hz, $N = 50 \text{ secs} \times F_s = 200$ samples). In previous works using \wp for estimating the respiratory rate, spectral resolution was not that critic, and therefore the spectra were estimated from

smaller segments of 60 [21], 42 [121] and 40 [146] seconds (instead of the 5-minute windows considered here). Another difference with previous works relies in the integration bounds delimited by Ω_1 and Ω_2 . Both frequency bands were centered in the respiratory rate, so they were calculated in a time-variant basis. Whereas the bandwidth (BW) of Ω_1 was set to Δf (the appropriate selection of this parameter is discussed below), in the case of Ω_2 it was set to $\Delta F = 0.15$ Hz, so that only frequency components which are close to the respiratory rate are considered. Moreover, both frequency bands were bounded below by 0.15 Hz (which remains the lower limit for classical HF band) and above by $\overline{\text{HR}}/2$ (given in Hz, HR remains the intrinsic sampling frequency of HRV [144]). In this way, Eq. 2.8 can be rewritten as:

$$\wp(k) = \frac{\int_{\max(\overline{F}_r(k)-\Delta f/2, 0.15)}^{\min(\overline{F}_r(k)+\Delta f/2, \overline{\text{HR}}(k)/2)} \hat{S}_{\text{HRV}}(k, F) dF}{\int_{\max(\overline{F}_r(k)-\Delta F/2, 0.15)}^{\min(\overline{F}_r(k)+\Delta F/2, \overline{\text{HR}}(k)/2)} \hat{S}_{\text{HRV}}(k, F) dF}, \quad (2.9)$$

where k represents the k -th 5-minute segment of the analyzed signal, and $\overline{F}_r(k)$ accounts for the mean respiratory rate in the k -th segment. In the following sections, the adequate selection of Δf and the relationship of \wp with several other indexes are detailedly discussed.

2.5.3 Parameter selection

In order to evaluate the behavior of \wp attending to the selection of Δf , a simulation study consisting in the generation of synthetic HRV spectra was proposed. Since the main concern relied in measuring how \wp is able to account for the distribution of power around a peak of interest, it was of great importance that the selected simulation model allowed to vary the BW of the peaks in the generated spectra.

Synthetic HRV signals were generated as sums of sinusoids with custom frequencies and amplitudes, so that:

$$x_{\text{HRV}}(n) = A_{\text{LF}} e^{j2\pi F_{\text{LF}} n} + A_{\text{HF}_1} e^{j2\pi F_{\text{HF}_1} n} + A_{\text{HF}_2} e^{j2\pi F_{\text{HF}_2} n} + \dots + A_{\text{HF}_L} e^{j2\pi F_{\text{HF}_L} n} + w(n), \quad (2.10)$$

where A_{LF} and F_{LF} represent the amplitude and frequency of the LF component respectively, and A_{HF_i} and F_{HF_i} symbolize the amplitudes and frequencies of up to L different components in the HF band. Finally, $w(n)$ is a white gaussian noise that accounts for model inaccuracies and for the existence of jitter in the R wave detection. Signals of 5-minute length were generated at a sampling rate of 4 Hz. Afterwards, the HRV spectrum was estimated with the method proposed in [195], which allows to control the degree of frequency smoothing through the parameter τ_0 , so that a larger τ_0 results in wider spectral components. This simulation configuration allows to represent the effect of the widening of the HF component, as well as a multimodal HF spectrum.

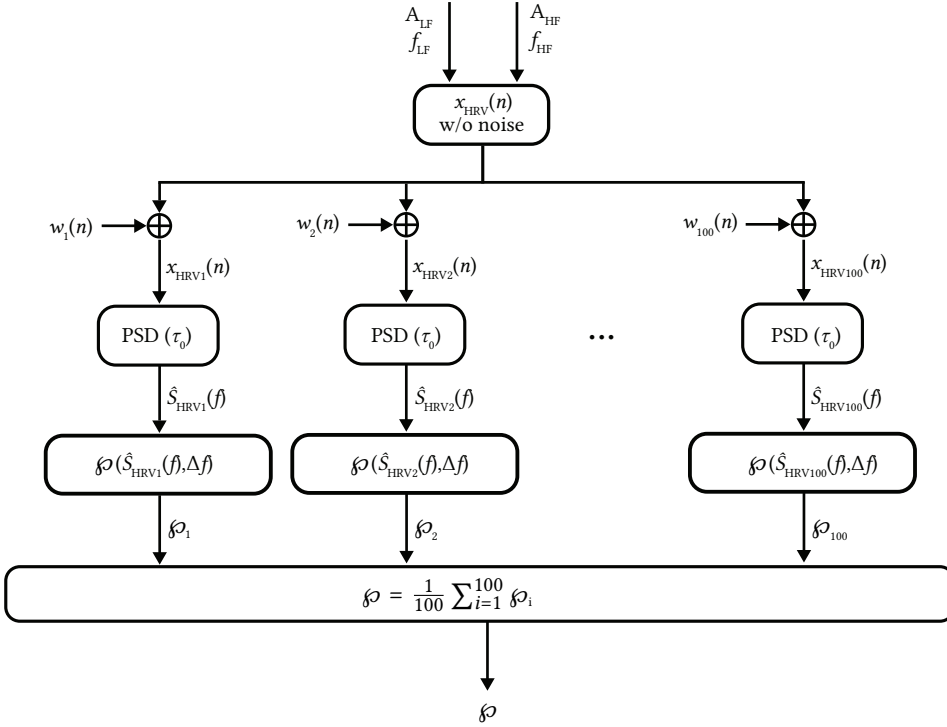


Figure 2.11: Scheme followed for studying the relationship of \wp with different parameters (see text for details).

The simulations were performed according to the following scheme, which is depicted in Fig. 2.11:

1. Provided the desired frequency components and their amplitudes, a 5-minute length HRV analytic signal ($x_{HRV}(n)$), sampled at 4 Hz, was generated as in Eq. 2.10, without adding the noise term.
2. One hundred realizations of $x_{HRV}(n)$ were generated by adding different realizations of additive white gaussian noise (AWGN), $w_i(n)$.
3. The spectrum of each realization ($\hat{S}_{HRV_i}(F)$) was estimated, provided τ_0 .
4. The peakness of each $\hat{S}_{HRV_i}(F)$, \wp_i , was computed with a given Δf . An example of this process is shown in Fig. 2.12.
5. The estimation of \wp was obtained as the mean of all the \wp_i .

In order to study the behavior of \wp against different BW, several simulations were conducted, considering one LF component ($A_{LF} = 0.12$ a.u., $F_{LF} = 0.1$ Hz) and one HF component ($A_{HF} = 0.1$ a.u., $F_{HF} = 0.3$ Hz). Fixed $v_0 = 0.01$ and $\lambda = 0.3$ were selected for the spectral estimation (see [195]), whereas τ_0 was varied from 0.01 to 0.25, and Δf ranged from $0.25\Delta H$ to $4\Delta H$ Hz. The power of the different realizations of AWGN was set to

0.01 a.u.², which is approximately the power of the error introduced by a jitter of one sample in the fiducial points detection when the sampling frequency of the ECG is 250 Hz [20]. The value of \wp was computed for each possible combination of τ_0 and Δf , and the results are displayed in Fig. 2.13, where also the relationship between peakness and the HF component BW (measured at -3 dB) for different values of Δf is shown.

According to the simulation results, the behavior of \wp is similar independently of the selected Δf , with low values when the BW is large and most of the power lays outside Δf , and tending to saturate with small BW, when most of the power is contained within the band delimited by Δf . However, not all the options for Δf are equally adequate for the purpose of this thesis. E.g., values lower than $0.5\Delta H$ present a more linear behavior, not tending to saturate with a reasonably small BW. On the other hand, values larger than $2\Delta H$ saturate very fast, thus providing a small dynamic range. From the remaining options, the most interesting one is $\Delta f = \Delta H$ because of two desirable properties: it will account for all the power of a perfect sinusoid (since it shares the spectral resolution of the spectral estimation method) and, in the presence of two sinusoids with the same amplitude, one of which lays within the band delimited by Δf , the value of \wp will be 0.5. The latter property can be extended to the case when N sinusoids with equal amplitudes are present in the spectra and only one of them lays within the band delimited by Δf , for which $\wp = (\text{total power})/N$. For these reasons, and when not indicated, $\Delta f = \Delta H$ will be considered.

2.5.4 Relationship with kurtosis

In probability theory and statistics, the kurtosis of a random variable is a measurement of the propensity of its probability distribution function to produce outliers. In other words, kurtosis accounts for the tailedness of a given random variable. Mathematically, kurtosis is defined as:

$$\kappa = \text{Kurt}(x) = \text{E} \left[\left(\frac{x - \mu}{\sigma} \right)^4 \right] = \frac{\text{E}[(x - \mu)^4]}{(\text{E}[(x - \mu)^2])^2} = \frac{\mu_4}{\sigma^4}, \quad (2.11)$$

where x is a random variable, μ and σ are respectively the mean and standard deviation of x , and E is the expectation operator. It can be demonstrated that the kurtosis of a normally distributed random variable is equal to 3, and this fact was considered by *Pearson* [197] to define κ as:

$$\kappa = \frac{\mu_4}{\sigma^4} - 3, \quad (2.12)$$

so that its value is relative to that of the normal distribution. Although the definition in Eq. 2.12 is known as excess kurtosis, it has been also referred to simply as kurtosis, which can lead to confusion if the definition is not provided. Here, correction with respect to normal distribution was not considered, so the definition in Eq. 2.11 was employed.

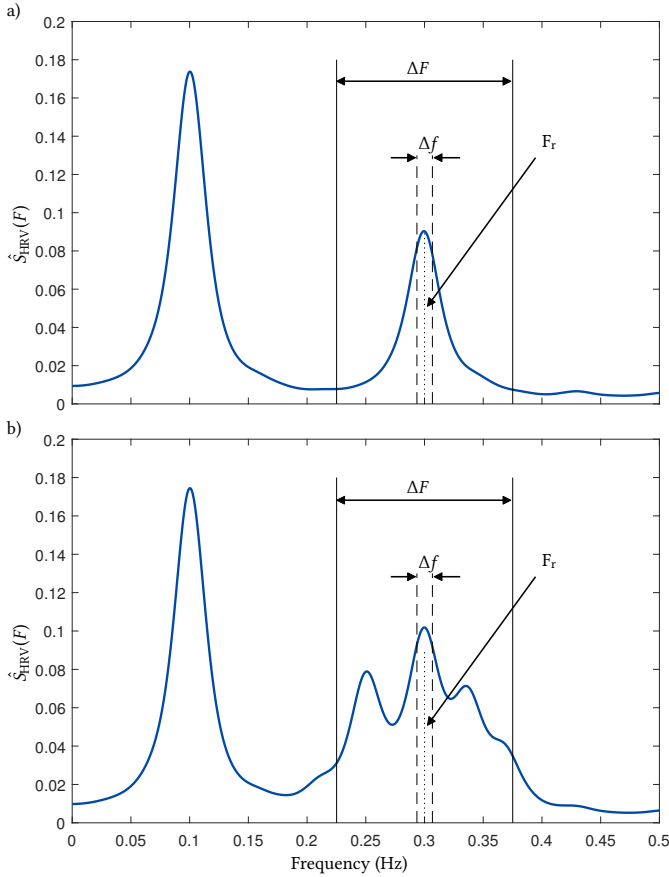


Figure 2.12: Synthetic HRV spectral with one (a)) or several (b)) peaks in the HF band. The frequency bands used for the computation of peakness and the frequency of the component of interest (F_r) are displayed. In the case of the unimodal signal, $\varphi = 0.44$, whereas in the multi-modal signal $\varphi = 0.24$.

Pearson regarded kurtosis as “a degree of flat-toppedness which is greater or less than that of the normal curve” [197]. He also introduced the terms platykurtic, leptokurtic and mesokurtic to refer to a distribution which is respectively more flat-topped, less flat-topped or equally flat-topped than the normal curve. Although the concept of kurtosis has been widely considered as a measurement of flat-toppedness or peakness, as proposed by *Pearson*, for more than a century, *Westfall* provided strong evidence that kurtosis reflects negligible information about the peak of a distribution, being it rather related with its tails [277].

Thinking of φ from *Westfall*'s interpretation, it could occur that the total frequency content of ΔF contributed much more than the content of Δf to the value of φ . In this way, it results interesting to compare φ and κ in order to comprehend whether they are measuring different phenomena or can be used interchangeably.

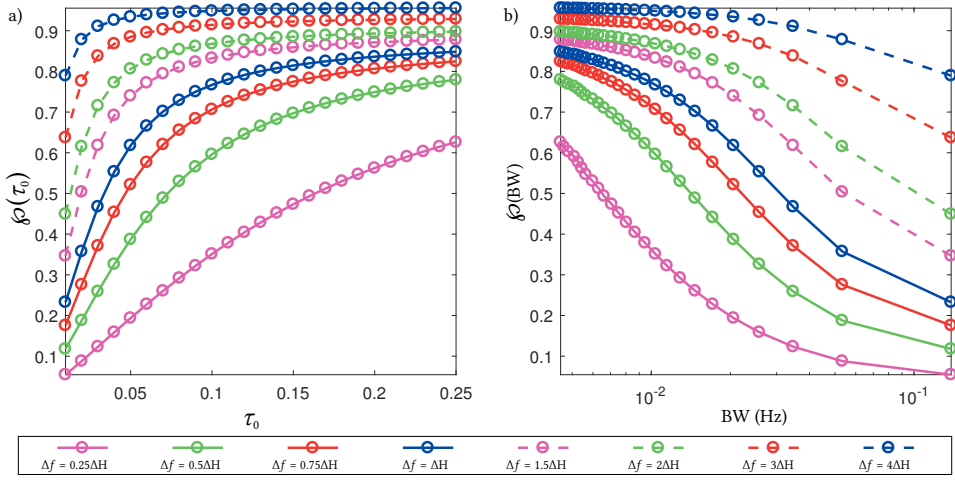


Figure 2.13: Evolution of \wp in function of τ_0 (a) and BW (b). \wp is shown for several different values of Δf selected as multiples of the resolution of the Hamming window. Note that in b) the axis of abscissas is represented in logarithmic scale.

The first difference between \wp and κ resides in their upper bound: whereas \wp saturates at 1, when all the power in ΔF is also contained in Δf , κ is unbounded above, thus complicating the definition of what low and high κ values are. Another important difference arises when considering the scenarios that would lead to an increase in each magnitude. In the case of \wp , its value can only get higher if a greater percentage of the total power in ΔF lays within Δf . In contrast and according to *Moors'* interpretation [183], there are two circumstances that lead to increased κ :

- (a) if most of the samples are concentrated around the mean of the distribution, and
- (b) if most of the samples lay in the tails of the distribution.

Hence, it is possible that \wp and κ might share a common meaning in the case of (a), but it follows that they will not account for the same information in scenario (b). In order to study similarities between both measurements given a distribution which is concentrated around its mean value, the simulation proposed above was reproduced. Thus, synthetic HRV spectra with different BW were generated, and \wp and κ were calculated with respect to them (see Fig. 2.14). It is important to note that κ was only calculated in the frequency band delimited by $[\bar{F}_i - \Delta F/2, \bar{F}_i + \Delta F/2]$, so that the same frequency components were considered for κ and \wp .

As it can be noticed in Fig. 2.14, whereas \wp resembles an inverted sigmoid function, κ presents a negative exponential-like behavior. Hence, assuming that:

$$\wp(x) \sim \frac{1}{1 + e^x}, \quad (2.13)$$

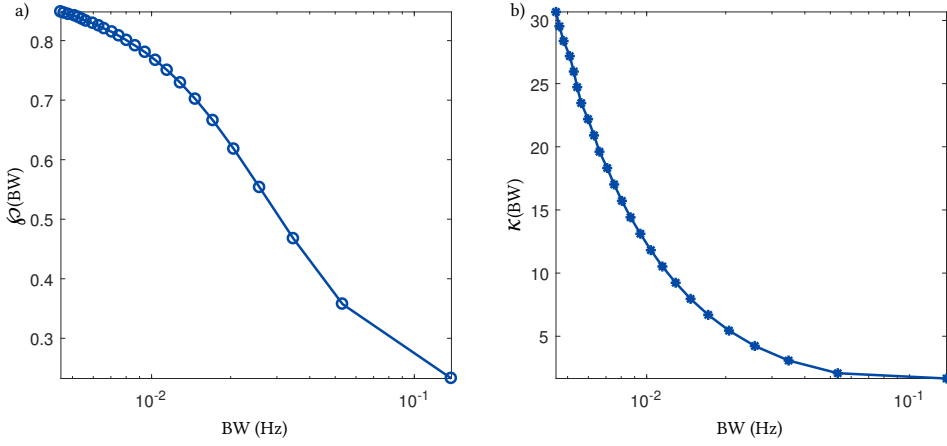


Figure 2.14: Evolution of \wp (a) and κ (b) in function of BW. For the computation of \wp , $\Delta f = \Delta H$ was selected. Note that the axes of abscissas are represented in logarithmic scale.

and

$$\kappa(x) \sim e^{-x}, \quad (2.14)$$

a relationship between \wp and κ can be established as:

$$\wp \sim \frac{1}{1 + 1/\kappa}. \quad (2.15)$$

In order to provide the inverse sigmoidal model with more degrees of freedom, a modified Boltzmann sigmoidal model (used by *Navarro et al.* for modeling the phase transition of smart gels [189] and by *Bolea et al.* for fitting *log-log* curves for correlation dimension calculations [43]) was employed, so that \wp and κ were related as:

$$\hat{\wp}(\kappa) = A_2 - \frac{A_2 - A_1}{B + e^{\frac{(\ln(\kappa) - \kappa_0)}{\alpha}}}, \quad (2.16)$$

being A_1 , A_2 , B , κ_0 and α the design parameters, which were obtained by fitting the model in a least squares sense. Since the behavior of \wp depends on the selected Δf , also the model will show this dependence, as displayed in Fig. 2.15.

Given the relationship displayed in Eq. 2.15 it is clear that, in the presence of a unimodal distribution with the probability mass concentrated around its mean, both measurements can be considered as equivalent. However, this equivalence should vanish in the case of multi-modal distributions, where the ratio of the power in the different modes should affect \wp and κ distinctly. Hence, a new simulation with two peaks in the HF band, placed at 0.25 and 0.3 Hz, and fixed $\tau_0 = 0.03$ was conducted. The peak in 0.3 Hz was

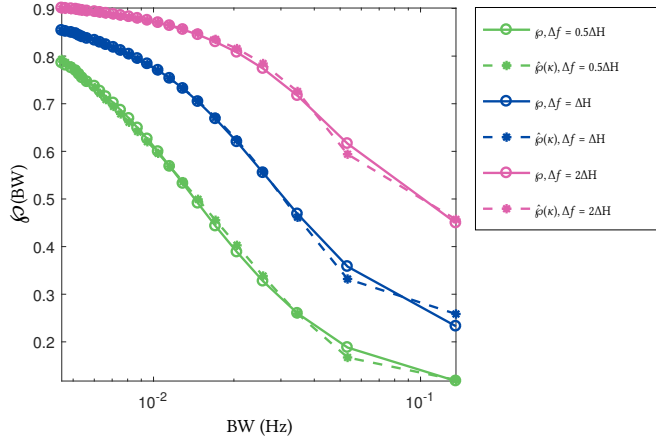


Figure 2.15: Evolution of φ (solid line) and $\hat{\varphi}(\kappa)$ (dashed line) in function of BW. Both parameters are shown for several different values of Δf selected as multiples of the resolution of the Hamming window. Note that the axis of abscissas is represented in logarithmic scale.

selected as the peak of interest, and the ratio between the amplitudes of both peaks was modified in order to evaluate the effect of a shift of power from the peak of interest towards the other frequency component. The results of this simulation are reflected in Fig. 2.16, where it can be noticed how the value of φ increases as the power is concentrated in the peak of interest independently of the selected Δf , as expected. In contrast, and according to *Moors* [183], κ presents a local minimum when both peaks have the same amplitude, and its value increases either if the power tends to concentrate near to the peak of interest or away from it. In view of this behavior, it can be concluded that kurtosis can not be employed as a synonym of peakness in the presence of a multi-modal distribution, since it may reflect either the amount of power contained in the component of interest, or the shift of power towards other frequency components, thus having an ambiguous interpretation. Since the HF band of HRV can present a multi-modal behavior, peakness might be regarded as a more adequate mathematical tool for characterizing the power distribution.

2.5.5 Relationship with HRV frequency domain analysis

Since φ is proposed as a new parameter for the characterization of HRV spectra, it is important to study its relationship with the classical frequency domain HRV indexes. In this way, two new simulations were proposed, in which the power within the HF band was varied according to two different strategies: augmenting the power of a single peak or of several peaks contained within the HF band. In both cases, the simulation scheme proposed in Fig. 2.11 was used. Whereas in the former the amplitude of the HF component ($F_{\text{HF}} = 0.3$ Hz) was varied between 0.025 and 0.5 a.u., in the latter the ratio between the amplitude of the component of interest ($F_{\text{HF}} = 0.3$ Hz) and the sum of the amplitudes of four other components located at 0.22, 0.35, 0.33 and 0.37 Hz was varied

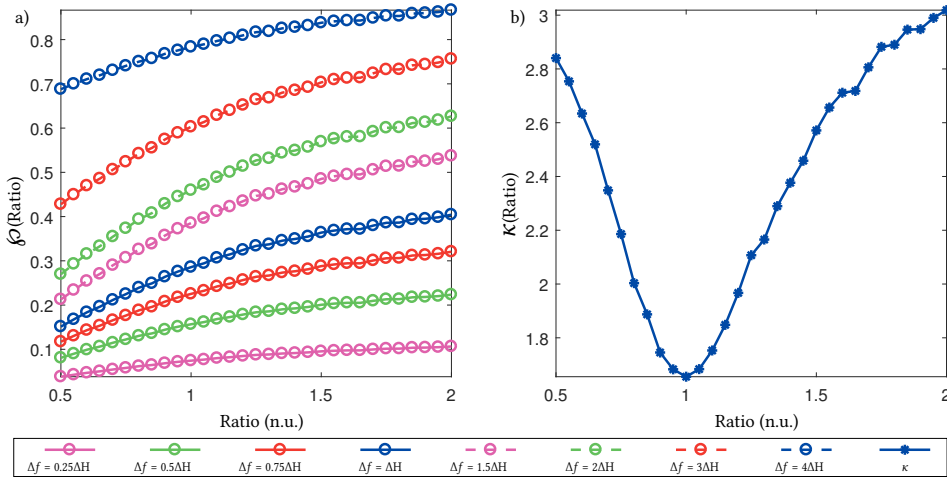


Figure 2.16: Evolution of ϕ and κ in function of the ratio of the amplitudes of two peaks placed within the HF band of HRV spectra. ϕ is shown for several different values of Δf selected as multiples of the resolution of the Hamming window.

from 0.1 to 1.5. Fixed $\tau_0 = 0.03$ was employed, and classical P_{LF} and P_{HF} were computed as the power within the $[0.04, 0.15]$ Hz and the $[0.15, 0.4]$ Hz bands, respectively, as proposed by the *Task Force* [252]. Results of these simulations are displayed in Figs. 2.17 (a) and b)) and 2.18 (a) and b)).

In Fig. 2.17 (a) and b)) it can be noticed how ϕ is scarcely affected by changes in the power of the measured peak, and that this behavior is the same independently of the selected Δf . However, Spearman correlation of $\rho = 1$ for all the considered Δf indicates a monotonous behavior, so that the value of ϕ always increase with increasing P_{HF} . Nevertheless, and as displayed in Fig. 2.18 (a) and b)), this is not true in the presence of a multi-modal HF spectrum. In this case, $\rho = -1$ for all the analyzed Δf indicated a total negative correlation between ϕ and P_{HF} , thus enhancing the fact that not only HF power but also how this power is distributed in the spectra might contribute with additional information to the traditional HRV analysis. Regarding P_{LF} , its relationship with ϕ remains more difficult to establish, since it will only have an effect on it when the LF components are very close to the LF upper bound, thus leading to a shift of power towards the HF band that could directly affect the computation of ϕ , and, in this case, the physiological interpretation would be compromised.

Nevertheless, it is crucial to keep in mind that simulation is not enough for modeling the complex interactions between the two main branches of ANS, and hence between P_{LF} and P_{HF} . The fact that SNS and PNS often present an opposing effect, and taking into account that a withdrawal in sympathetic tone is reflected similarly to an increase in vagal tone and vice versa, it follows than the relationship between P_{LF} , P_{HF} and ϕ may be much more complex than that suggested by simulations. In this way, the relationship between measurements of the sympathovagal balance such as $R_{LF/HF}$ and P_{LFn} with ϕ might be of

great interest in order to elucidate whether \wp could contribute to the classical frequency domain HRV analysis. This analysis is performed in Ch. 3, using real HRV signals.

2.5.6 Relationship with HRV nonlinear analysis

From Figs. 2.17 (a) and b)) and 2.18 (a) and b)), it can be inferred that \wp and P_{HF} are not measuring the same phenomena. Since \wp is related with how the power in the HF band is distributed, it could be also associated with how complex a spectrum is, understanding complexity as the number of frequency components present in the spectrum. In this way, the least complex spectrum would be that of a perfect sinusoid (with only one spectral component), whereas the most complex one would be that of a white gaussian noise (with all the possible spectral components).

In order to evaluate how \wp might be related with nonlinear HRV analysis, D_2 was computed from the same two simulations proposed in the section above, where one and five HF components were considered. Importantly, a high-pass filtering (5th order Butterworth filter) was applied so that the contribution of the LF components to D_2 was not considered. D_2 was calculated as proposed by *Bolea et al.* [43] ($D_{2(\text{max})}$), and the results are displayed in Figs. 2.17 (c)) and 2.18 (c)). When considering only one peak, D_2 does not present a dependence with P_{HF} , and the deviations from its constant-like behavior are more likely due to the effect of noise (see Fig. 2.17 (c)). In this case, a clear relationship with \wp can not be established, since they present a very low Spearman correlation ($\rho = 0.37$), although since \wp tends to saturate they both resemble a similar behavior. When adding more peaks, as in Fig. 2.18 (c), D_2 presents a monotonous decreasing behavior when the dominance of one single component increases, which is highly inversely correlated with \wp ($\rho = -0.99$). Hence, lower values of \wp are apparently related with more complex spectra, understood as spectra with more variety of non-negligible frequency components. However, it is important to highlight that this simulation analysis is not enough to establish a relationship between \wp and nonlinear HRV analysis, since two signals with the same spectra can present very different nonlinear dynamics [133], which can not be assessed from frequency-domain analysis.

2.5.7 Discussion

Traditional frequency domain HRV analysis relies on the assumption that signals are stationary during the analyzed period. However, biological signals are far from being stationary, even in segments of only some minutes. The effect of non-stationarity reflects in the spectrum as a widening of the main components, which might even result in the appearance of several peaks with very close central frequencies. This phenomenon particularly affects HF components, with faster fluctuations, but is not assessed through traditional indexes based on in-band power quantification. For this reason, an index to account for the power distribution within the HF band, \wp , has been presented. Despite being conceptually similar to the kurtosis of a distribution, it has been proven to provide

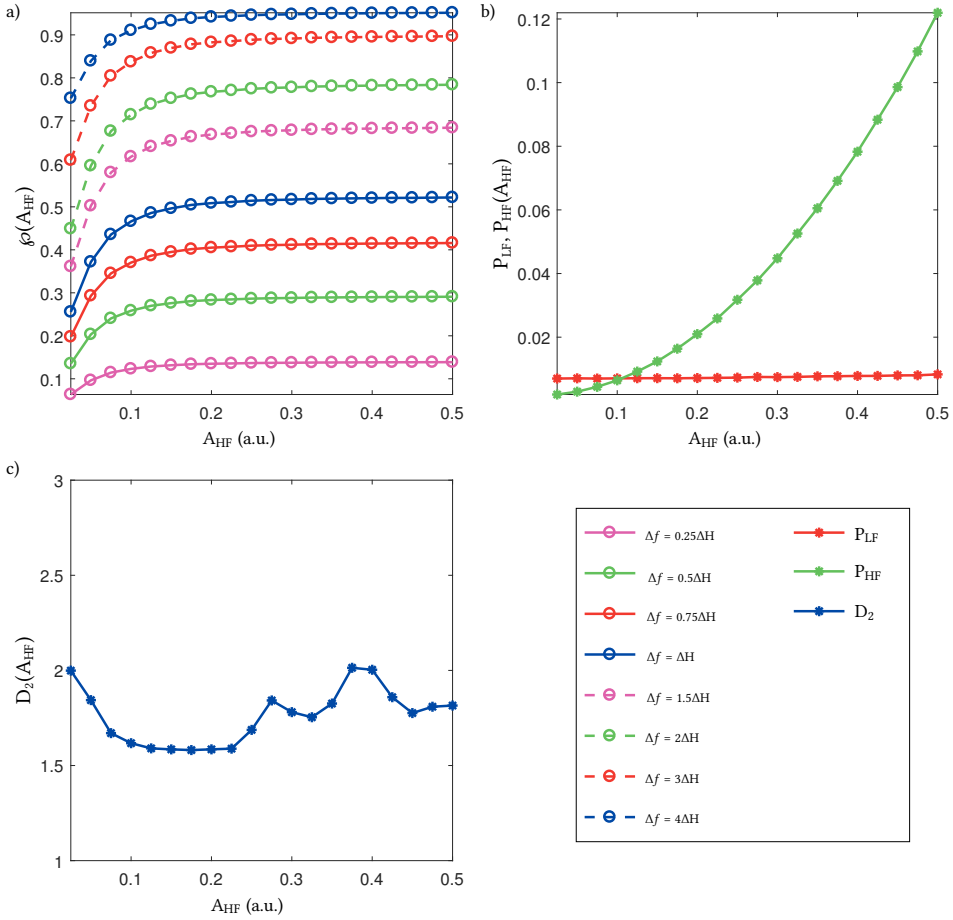


Figure 2.17: Evolution of ϕ , P_{LF} , P_{HF} and D_2 in function of A_{HF} when only one HF peak is considered. ϕ is shown for several different values of Δf selected as multiples of the resolution of the Hamming window.

different information. In this way, ϕ is monotonically increasing with increasing concentration of power near the frequency of interest, whereas kurtosis can increment its value with increasing power concentration either around a frequency component or far from it. Moreover, an analysis of the appropriate parameters for ϕ calculation and a comparison with traditional frequency and nonlinear domain analysis was performed, revealing the potential value that it could add to HRV analysis, since it is not necessarily related with any of the considered parameters. Considering that ϕ accounts for the distribution of power around a frequency component of interest, its physiological interpretation could be related with the stationarity of that frequency component. Given that the frequency of interest is that of the mean respiratory rate, which is known to represent the main contribution to the HF band, lower values of ϕ might reflect an increased variability of the respiratory rate during the analysis period, or either an increased adaptability of vagal modulation, which is in constant change to meet the homeostatic demands of the body.

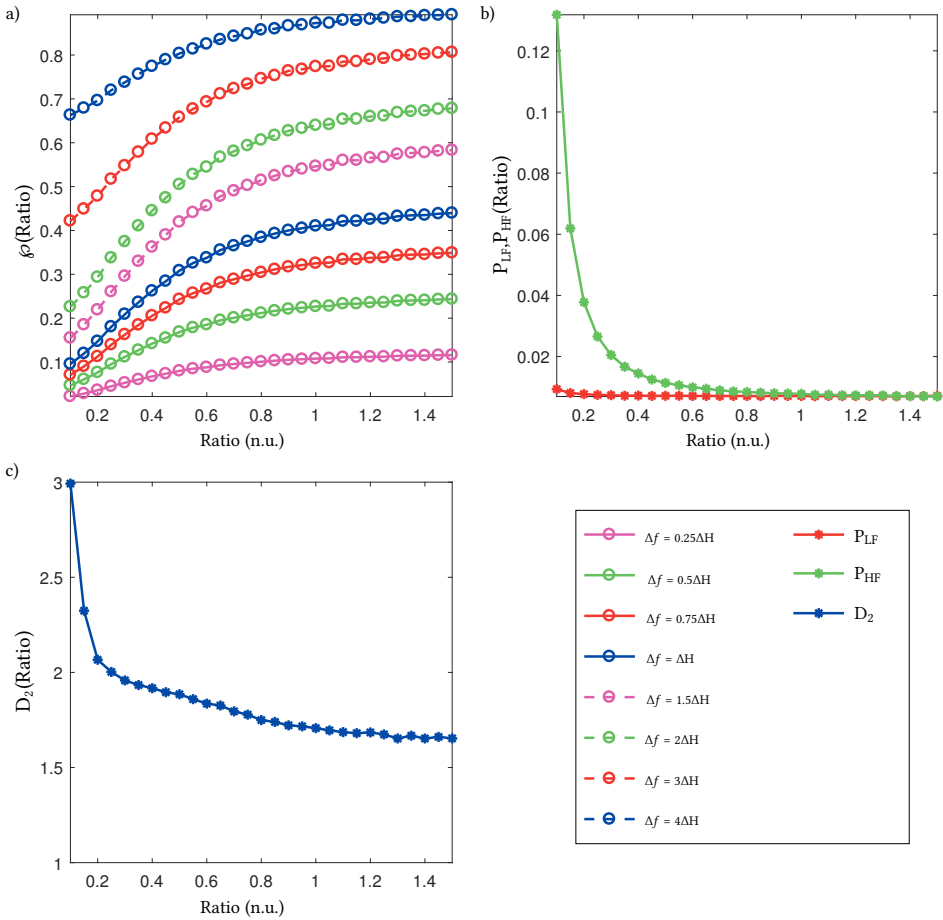


Figure 2.18: Evolution of ϕ , P_{LF} , P_{HF} and D_2 in function of the ratio of the amplitude of the peak of interest and the sum of the amplitudes of four additional peaks. ϕ is shown for several different values of Δf selected as multiples of the resolution of the Hamming window.

2.6 Effect of the respiratory rate

Despite RSA represents the main contribution to the HF power of HRV [4,6], there are scenarios in which the respiratory rate is not contained in the [0.15, 0.4] Hz HF band, so that the respiratory-related modulation of the HR is shifted towards higher or lower frequencies, thus compromising the classical frequency domain HRV analysis [36]. Hence, it is of paramount importance to simultaneously consider respiration when analyzing HRV [50]. When the respiratory rate is above 0.4 Hz, e.g. during sport [20, 122] or in infants and children [89], the HF band has to be redefined so that it contains the respiratory-related components. On the other hand, when it is lower than 0.15 Hz, as it occurs, e.g. in relax situations [121], a redefinition of the HF band is not enough, since it would overlap with the LF band, thus resulting in a lack of differentiation between the HRV compo-

nents related or unrelated with respiration. In this case, some authors opt for discarding those segments for which respiratory-rate lays within the LF band [121]. However, some mathematical tools for removing respiratory influence from HRV have been proposed in recent years [149,280], thus enabling the further analysis of periods with low respiratory rates.

2.6.1 Modified high-frequency bands

When respiratory rate is close to or above 0.4 Hz, a shift of power towards higher frequency components results in an unreliable HF power measurement (as displayed in Fig. 2.19 a)). In order to account for the respiratory-related power, the HF band must be re-defined. There are various options, which range from extending the bandwidth of the classical HF band to the definition of a new band which is guided by respiration, and the selection of the approach to implement should be guided by physiology and application. Some possibilities are:

1. *Extended HF band*: the upper bound of the HF band is changed to $\overline{\text{HR}}/2$ (see Fig. 2.19 b)). This approach is independent on the respiratory rate, but since it is very wide, it could include some components with uncertain origin. Additionally, HR variations affect the window length and therefore the power estimation. The time-varying extended HF band is mathematically defined as:

$$\Omega_{\text{HF}}^e(k) = [0.15, \overline{\text{HR}}(k)/2]\text{Hz}. \quad (2.17)$$

2. *HF band centered in respiration*: the HF band is determined as a fixed frequency window (ΔF) centered in the mean respiratory rate of the analyzed period, $\overline{F}_r(k)$ (see Fig. 2.19 c)). It avoids the inclusion of frequency components with uncertain origin, such as mid-frequency components [4, 103], although it requires a continuous estimation of the respiratory rate, and an appropriate selection of ΔF . The time-varying HF band centered in respiration is then defined as:

$$\Omega_{\text{HF}}^{c,fb}(k) = [\max(0.15, \overline{F}_r(k) - \Delta F/2), \min(\overline{F}_r(k) + \Delta F/2, \overline{\text{HR}}(k)/2)]\text{Hz}. \quad (2.18)$$

In 5, both options were considered, so that, in order to distinguish between them, when the extended HF band is used, the HF-related HRV variability parameters will be referred to as P_{HF}^e , $R_{\text{LF/HF}}^e$ and P_{LFn}^e . On the other hand, when the centered HF band is employed, they will be referred to as P_{HF}^c , $R_{\text{LF/HF}}^c$ and P_{LFn}^c . In Ch. 3 and 6, only the HF band centered in respiration is employed and, for simplicity, the power within it will be referred to as P_{HF} .

2.6.2 Removing respiratory influence from HRV

There are also scenarios in which the respiratory rate is very low, as it happens during relax situations [121], or in certain applications related with the control of respiration,

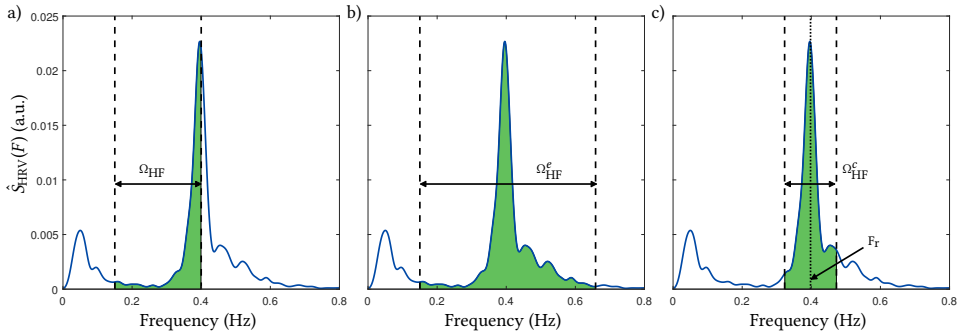


Figure 2.19: The definition of different HF bands for the same HRV spectrum are displayed: the classical HF band (a), the extended HF band (b) and a HF band centered in respiration (c). The green area in each case represents the part of the spectrum that is considered for the calculation of the HF power.

e.g., meditation [148]. In those cases, the RSA-related components might lie within the LF band or close to its upper bound, as displayed in Fig. 2.20 (c) and d)). Under such a condition, classical HRV analysis would lead to an underestimation of the HF power and an overestimation of the LF power, thus resembling either a sympathetic activation or a vagal withdrawal, and resulting in a misinterpretation of the real ANS state [36].

If HRV is to be analyzed in the presence of low respiratory rates, there are several methodologies that can be followed. The most simple and straightforward option would be to discard from the analysis those samples for which respiratory rate lays within the LF band. However, if an important percentage of data is discarded, this could have a direct effect on the obtained results. Moreover, in short recordings or in certain applications, it can occur that there are no samples for which respiratory rate is above 0.15 Hz, thus impeding classical HRV analysis. Another alternative relies in avoiding the use of frequency domain HRV analysis, considering other approaches such as time domain or nonlinear analyses. Although it may be sufficient in some cases, this would difficult the differentiation between the activity of the sympathetic and the parasympathetic branches of the ANS, thus hampering the physiological interpretation. Nevertheless, several authors have considered a more interesting approach consisting in removing the respiratory influence from HRV, so that frequency-domain HRV analysis can be still applied.

A series of methodologies have been proposed for removing respiratory influence from HRV: Granger's causality [149], adaptive filtering, ARMAX modeling, multi-scale principal component analysis or orthogonal subspace projection (OSP) [280]. From all this possibilities, OSP was considered in this work, due to its simplicity and its performance in different applications, such as emotional stress assessment [264, 281] and automatic sleep apnea detection [263].

Orthogonal subspace projection

Given a matrix \mathbf{X} of size $(K \times L)$, formed by L column vectors $x_i = \{x_i(1), x_i(2), \dots, x_i(K)\}^T$, an orthogonal projection matrix, \mathbf{P} , that maps any vector in a subspace defined by the column space of \mathbf{X} , $\mathcal{S}(\mathbf{X})$, can be constructed as:

$$\mathbf{P} = \mathbf{X}(\mathbf{X}^T \mathbf{X})^{-1} \mathbf{X}^T, \quad (2.19)$$

and the projection of a vector $\mathbf{y} \in \mathbb{R}^K$ in $\mathcal{S}(\mathbf{X})$ can be calculated as:

$$\mathbf{y}_{\mathcal{S}(\mathbf{X})} = \mathbf{P}\mathbf{y}. \quad (2.20)$$

In this way, the information in the HRV signal which is linearly related to respiration can be removed by projecting the original modulating signal (which, for simplicity, will be referred to in vector notation, \mathbf{m} , in this section), into a subspace defined by respiration. Hence, \mathbf{X} is constructed using delayed versions of a given respiratory signal [264], \mathbf{x}_{resp} , up to 2 seconds. Then, the respiratory and residual (non-respiratory related) components of \mathbf{m} (\mathbf{m}_{resp} and $\mathbf{m}_{\text{resid}}$ respectively) can be obtained as:

$$\begin{aligned} \mathbf{m}_{\text{resp}} &= \mathbf{P}\mathbf{m}, \\ \mathbf{m}_{\text{resid}} &= (\mathbf{I} - \mathbf{P})\mathbf{m} = \mathbf{m} - \mathbf{m}_{\text{resp}}. \end{aligned} \quad (2.21)$$

As displayed in Eq. 2.21, $\mathbf{m}_{\text{resid}}$ will not contain information linearly related with respiration and therefore it can be employed for HRV analysis in the classical HF band. Nevertheless, the interpretation of the HF band content in the absence of RSA contribution remains uncertain. In order to keep on distinguishing between sympathetic and parasympathetic activity, \mathbf{m}_{resp} can be considered, as far as its frequency content is related with respiration and hence it should have a vagal origin (there are some situations, such as during exercise or when a person is speaking, in which the power content in the HF band may not be related with PNS activity). In this way, new LF and HF power measurements can be defined as:

$$\begin{aligned} P_{\text{LF}}^{\text{OSP}} &= \int_{0.04}^{0.15} \hat{S}_{\text{resid}}(F) dF, \\ P_{\text{HF}}^{\text{OSP}} &= \int_{0.04}^{\overline{\text{HR}}/2} \hat{S}_{\text{resp}}(F) dF, \end{aligned} \quad (2.22)$$

where $\hat{S}_{\text{resid}}(F)$ and $\hat{S}_{\text{resp}}(F)$ are the spectra of $\mathbf{m}_{\text{resid}}$ and \mathbf{m}_{resp} respectively. In the case of $P_{\text{HF}}^{\text{OSP}}$, the onset of the frequency band of interest is set at 0.04 Hz, since the initial assumption was that the respiratory rate laid within the LF band. Once that a definition of $P_{\text{LF}}^{\text{OSP}}$ and

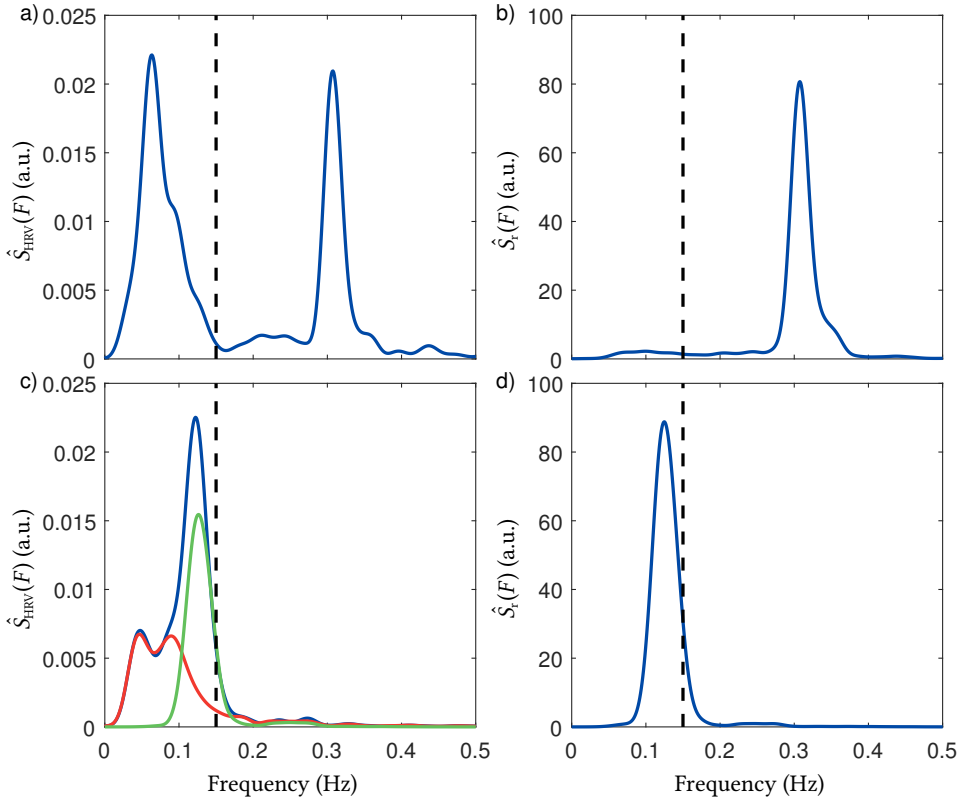


Figure 2.20: Two examples of HRV spectra (a) and c)) and their correspondent respiration spectra (b) and d), respectively) are displayed. Whereas in a) and b) the respiratory rate is above 0.15 Hz (marked with black dashed lines), in c) and d) it lays within the LF band, thus compromising HRV analysis. Orthogonal subspace projection decomposition was applied to the spectra in c) and d), and the respiration (green) and residual (red) components are displayed.

P_{HF}^{OSP} is available, an unconstrained measurement of the sympathovagal balance can be defined as $SB_u = P_{LF}^{OSP} / P_{HF}^{OSP}$ [264]. An example of the OSP decomposition is displayed in Fig. 2.20.

2.7 Cardiorespiratory coupling

As aforementioned, HRV and respiration are intrinsically linked, being RSA the main contribution to rapid HR variations. In this way, the interpretation of HRV analysis should be always driven by its relationship with respiratory activity. However, including respiratory information in HRV analysis is not the only way to account for the effect of respiration on HRV, and there is a growing interest in studying the so called cardiorespiratory coupling (CRC), which represents the association between neural control of respiration and HR. Actually, *Schäfer et al.* suggested that RSA and cardiorespiratory syn-

chronization are two different phenomena representing distinct aspects of the interaction between cardiac and respiratory rhythms [231]. Some authors have reported the appearance of periods of CRC during rest [231], controlled breathing [68] or anesthesia [91], and whereas the general belief is that it is lost in some respiratory disorders [93, 129] or during mental stress [191], *Riedl et al.* suggested an increased CRC in sleep apnea, maybe linked to the high autonomic stress induced by the disease [219].

Nevertheless, there is no consensus in the most appropriate way of measuring CRC, and several approaches have been proposed in the literature. Some examples include the use of Granger causality, entropy measurements or phase synchronization analysis, as well as nonlinear prediction approaches [235]. In this dissertation, we analyzed CRC through the time-frequency (TF) coherence (TFC) maps of HRV and respiration. Therefore, the TF cross-spectrum of the HRV and the respiratory signals, $\hat{S}_{\text{HRV,resp}}(t, f)$, was estimated using a TF distribution belonging to Cohen's class, defined as in [195]:

$$\hat{S}_{\text{HRV,resp}}(t, f) = \iint_{-\infty}^{\infty} A_{\text{HRV,resp}}(\nu, \tau) \Phi(\nu, \tau) e^{j2\pi(t\nu - f\tau)} d\nu d\tau, \quad (2.23)$$

where $A_{\text{HRV,resp}}(\nu, \tau)$ is the ambiguity function [88] of the analytical signal representation of the modulating and the respiratory signals, $x_{\text{HRV}}(t)$ and $x_{\text{resp}}(t)$ (which were obtained using the Hilbert transform). On the other hand, $\Phi(\nu, \tau)$ is a smoothing function in the ambiguity domain for the reduction of the cross terms in a quadratic distribution (in this thesis it was selected as an elliptic exponential kernel). They are respectively defined as:

$$\begin{aligned} A_{\text{HRV,resp}}(\nu, \tau) &= \int_{-\infty}^{\infty} x_{\text{HRV}}\left(t + \frac{\tau}{2}\right) x_{\text{resp}}^*\left(t - \frac{\tau}{2}\right) e^{-j2\pi\nu t} dt, \\ \Phi(\nu, \tau) &= e^{-\pi \left[\left(\frac{\nu}{\nu_0}\right)^2 + \left(\frac{\tau}{\tau_0}\right)^2 \right]^{2\lambda}}. \end{aligned} \quad (2.24)$$

The time and frequency resolution of $\hat{S}_{\text{HRV,resp}}(t, f)$ can be adjusted by modifying the shape of the smoothing kernel in Eq. 2.24 through the parameters ν_0 and τ_0 , respectively. Also the roll-off factor of the kernel can be controlled with λ . Afterwards, the TFC distribution was obtained as:

$$\hat{\gamma}^2(t, f) = \frac{|\hat{S}_{\text{HRV,resp}}(t, f)|^2}{\hat{S}_{\text{HRV}}(t, f) \hat{S}_{\text{resp}}(t, f)}, \quad (2.25)$$

where $\hat{S}_{\text{HRV}}(t, f)$ and $\hat{S}_{\text{resp}}(t, f)$ represent the TF spectra of the modulating and the respiratory signals respectively, estimated as in Eq. 2.23. From the TFC distribution it is possible to obtain different measurements that are expected to reflect the degree of CRC, such as the bandwidth in which $\hat{\gamma}^2(t, f)$ is higher than a predefined threshold or its mean value in a given bandwidth. These two CRC measurements are proposed and discussed in Ch. 3.

2.8 Discussion and conclusions

In this chapter, a framework for contextualized HRV analysis has been presented. First, the methodology followed in this dissertation for HRV assessment, based on the TVIPFM model, was introduced. Afterwards, some of the most relevant aspects that should be addressed in HRV analysis were described, including the effect of noise, physiology and pathophysiology, presence of ectopic beats and strong RSA, and the effect of respiratory rate. Also, an index for quantifying the distribution of the HF components of HRV was described and compared with traditional frequency and nonlinear domain analyses. Nonetheless, two different parameters for the quantification of CRC were introduced.

The use of the TVIPFM model presents some advantages that make it appealing for HRV estimation. On one hand, it assumes the existence of a modulating signal that carries the information concerning SNS and PNS activity, so that it can be provided with a physiological background which remains crucial for results interpretation. Moreover, the TVIPFM model formulation allows to account for the presence of ectopic beats, and provides a time-varying correction to remove the influence of mean HR, which make it suitable for a large set of scenarios. Nevertheless, it is important to keep in mind that the TVIPFM model is only a simplification of the enormously complex HR control system, and it was not specifically developed for heart beat occurrence time series representation, although it is highly related with the SA node behavior.

Regarding the presence of noise, the different preprocessing techniques for dealing with the most common sources of artifacts are well know. Beyond technical noise, it is important to pay attention to the different sources of physiological information that may be present in the analysis, since HRV is widely altered according to the physiological status. The same is true for a wide range of pathological conditions or the use of medication, since they might alter HRV and hence compromise the further interpretation. In this way, HRV analysis should be guided by physiology, so that the possible physiological confounders are taken into account.

Also the effect of ectopic beats and strong RSA episodes were considered. Despite the fact that they could exert a similar effect on HRV spectrum in certain cases, ectopic beats do not have their origin in the sinus node and thus they are not governed by ANS modulation. Therefore, ectopic beats do not reflect ANS activity and their effect should be corrected. On the other hand, strong RSA episodes may provide valuable physiological information, specially in the case of young children. However, most of the techniques employed for ectopic beats detection are only based on thresholding the RR interval series, or either in the deviation of a given RR interval from its expected value, which could lead to the misclassification of RSA episodes as ectopic beats. Here, a methodology for distinguishing between both events has been introduced. Although the algorithm performance quantification presented in this chapter is limited to the concrete dataset in which it was applied, its dependency with respect to the different parameters was analyzed. The strength of this algorithm is better exploited in Ch. 3, where children populations were analyzed.

Furthermore, \wp was introduced as a complement to frequency domain HRV analysis, allowing to quantify the power distribution of the HF components of HRV. A careful analysis of the behavior of \wp in function of different parameters as well as of their appropriate ranges of values for HRV analysis has been conducted through a simulation study. Moreover, the relationship between \wp and traditional frequency and nonlinear domain HRV analyses was considered, concluding that \wp could provide an added value, which might be related to the stationarity or adaptability of vagal activity.

Respiratory rate is another well-known confounder in HRV analysis. In this way, classical definition of the LF and HF bands may derive in misleading in-band power measurements when respiratory rate is either too high or too low. In the former case, the most common approaches rely on the redefinition of the HF band, which can be extended towards higher frequencies or shifted to be centered in the respiratory rate, so that respiratory-related components are well captured. When the respiratory rate is too low, redefining the frequency bands is not an option, since vagal and sympathetic influence on HRV are mixed within the LF band. In order to deal with this situation, several authors have proposed different methods aiming to remove respiratory information from HRV [149, 280], so that respiratory-related and -unrelated components can be analyzed separately. In this dissertation, the OSP methodology was employed due to its reduced computational complexity and its promising performance in previous works [263, 264, 281]. Nevertheless, the use of techniques for dealing with the effect of high or low respiratory rates is crucial in HRV analysis, since the nature of the frequency components in the HF band when respiratory modulation is not contained within it remains an open debate.

Although the interactions among respiration and HRV are usually quantified through RSA, there is evidence that synchronization between them represents a different phenomenon [231], which can be assessed through various CRC measurements. Despite the fact that CRC is known to be altered in several disorders and conditions, there is still controversy regarding the direction and nature of these changes, and the same is true for the most appropriate way of accounting for them. In addition, whereas CRC measurements are aimed at assessing neural control of cardiorespiratory activity, it is important to take into account that respiration also modulates HR by mechanical effects [42], which could compromise the physiological interpretation. Hence, large research is still to be conducted in the potential of CRC for ANS assessment.

Summarizing, HRV analysis should be performed carefully and subjected to physiology, since otherwise wide intra- and inter-individual variations might compromise the interpretation of the results. Under the proper framework, HRV analysis could raise as a convenient noninvasive tool for aiding in the increasingly expanding field of personalized diagnosis and treatment of several pathologic conditions.

Part II

HRV analysis in respiratory disorders

3

HRV analysis in children with asthmatic symptoms

3.1 Motivation		3.3.1 Helsinki University Hospital dataset
3.2 Materials and methods		3.3.2 Tampere University Hospital dataset
3.2.1 Helsinki University Hospital dataset		
3.2.2 Tampere University Hospital dataset	3.4 Discussion	
3.2.3 Preprocessing	3.4.1 Methodology	
3.2.4 HRV analysis	3.4.2 Helsinki University Hospital dataset	
3.2.5 Peakness analysis	3.4.3 Tampere University Hospital dataset	
3.2.6 Time-frequency coherence analysis	3.4.4 Limitations	
3.2.7 Statistical methods	3.4.5 Physiological interpretation	
3.3 Results	3.5 Conclusion	

3.1 Motivation

Lung function assessment remains essential for the diagnosis and monitoring of several respiratory affections such as chronic obstructive pulmonary disease or asthma. Whereas in the former pulmonary function is permanently reduced, asthma is characterized by a variable and irregular respiratory tract obstruction, and therefore a continuous monitoring of airway function would be desirable in asthmatics. Yet, the diagnosis of asthma is performed through the evaluation of the clinical history, assessment of inflammatory markers and single-time airway function measurements, being spirometry the most extended test. However, since young children are not able to perform repeatable expiratory maneuvers, there is still not a feasible means for the objective diagnosis of asthma in this population [97]. In this way, the diagnosis of asthma in young children is very dependent on the clinical history, and usually based on prediction indexes, such as the modified asthma predictive index (mAPI), which have employed different criteria like parental asthma, atopy or the presence peripheral eosinophilia for risk of asthma stratification. Whereas these methodologies share a high specificity, very low sensitivity is also a common feature [58], which might lead to a lot of missing diagnoses.

Treatment of asthma during childhood is equally challenging, and although ICS remain the standard medication for the prevention of symptoms, there is some controversy regarding the possible negative effects that ICS may have during childhood, since their use has been related with growth reduction and hypothalamic-pituitary-adrenal suppression [60, 69, 119].

These difficulties in the diagnosis, monitoring and treatment of asthma during childhood have motivated several studies aiming at developing a noninvasive tool that can be used for patient state assessment in a time-continuous manner. Most of them have focused on ANS monitoring, since abnormal ANS activity has been related with the pathogenesis of asthma [80, 130]. Particularly, the parasympathetic branch of the ANS is involved in bronchoconstriction [151] and bronchomotor tone control [184], and the fact that sympathetic innervation is sparse in the small airways [151] has pointed to PNS as strongly related with altered airway tone in asthmatics. Since ANS, also modulates cardiac activity, HRV analysis has been employed for its characterization in asthma, both in adults [131, 287] and children [80]. Nevertheless, and to the best of our knowledge, preschool children have not been considered. Hence, in this chapter we aimed at assessing the possible clinical value of HRV analysis for the characterization of a group of preschool children classified attending to their risk of developing asthma. Furthermore, we considered the possibility of using the proposed indexes for the monitoring of the asthma condition in children under and after ICS treatment. Under the hypothesis that PNS activity is altered in asthma, it is expectable that it will turn normal after treatment in subjects without or with low risk of asthma, but it should remain unchanged in children with or at high risk of asthma.

3.2 Materials and methods

Two independent databases were analyzed in this chapter, namely the Helsinki University Hospital and Tampere University Hospital datasets. The former was employed for characterizing the HRV spectra of children classified according to their risk of asthma. In the latter, the same characterization was used for monitoring the asthma condition of a group of children who underwent a three month ICS treatment. Both datasets are described below.

3.2.1 Helsinki University Hospital dataset

The first dataset analyzed in this chapter consists of ECG holter and IP recordings of 44 children who were referred to the Pediatric Allergy Unit of Helsinki University Hospital due to persistent or recurrent lower respiratory tract symptoms, such as wheezing (a whistling sound when expiring air from the lungs), shortness of breath or coughing. From this 44 recordings, 10 were discarded due to electrode detachment, patient turning off the device or forgetting to turn on the device. The recording devices and the ECG and IP acquisition were custom designed at Tampere University of Technology (Tampere, Finland) [236], and signals were acquired with a sampling frequency of 256 Hz. The mean length of the recordings is about 14 hours (± 3.5 hours).

Patients were classified into three groups according to their mAPI [108]. Children with a positive mAPI were classified as a high risk (HiR) group for developing persistent asthma, whereas children with negative mAPI were classified as low risk (LoR). Furthermore, another group was formed with children with a confirmed history of wheeze but that were under ICS treatment at the time of the recording. In the case of the HiR and LoR groups, none of the subjects was under regular asthma treatment, nor were they supplied bronchodilators during the recordings. Table 3.1 contains a summary of patient information. Data acquisition was approved by an institutional pediatric ethics review board and informed written consent was received from guardians of all patients. Also informed written parental consent was received before data acquisition. For simplicity, this dataset will be referred to as HUH dataset hereon.

3.2.2 Tampere University Hospital dataset

The second dataset is composed by 68 children (45 boys and 23 girls) with a median age of 2.5 years (range [0.9, 5.7]), who visited the Tampere University Hospital (Tampereen Yliopistollinen Sairaala, TAYS) emergency room due to recurrent obstructive bronchitis. All of them were prescribed ICS treatment during three months. ECG and IP were acquired at a sampling rate of 256 Hz with the same custom designed recording device used for the previous dataset [236]. Three different recordings were scheduled for each subject:

Table 3.1: Characteristics of the children in the HUH dataset. (Whereas continuous variables are expressed as median (min-max), integer variables are displayed as n (%). BMI: Body Mass Index, SPT: Skin Prick Test.)

	LoR	HiR	ICS	Total
n	14	13	7	34
Sex (male)	6 (43%)	5 (39%)	4 (57%)	15 (44%)
Age (years)	5.0 (3.4-6.6)	4.6 (3.4-6.8)	5.1 (3.8-6.7)	4.9 (3.4-6.8)
Height (cm)	111 (96-121)	110 (94-126)	108 (104-127)	109 (94-127)
Birth weight (kg)	3.6 (2.1-5.2)	3.6 (2.8-4.6)	3.5 (3.0-4.1)	3.5 (2.1-5.2)
BMI	16.5 (13.5-18.3)	15.9 (14.8-18.0)	16.1 (14.5-18.0)	16.1 (13.5-18.3)
Wheeze	5 (36%)	13 (100%)	7 (100%)	26 (77%)
Allergic rhinitis	2 (14%)	3 (23%)	2 (29%)	7 (21%)
Atopic dermatitis	7 (50%)	7 (54%)	3 (43%)	17 (50%)
SPT positivity	3 (21%)	9 (69%)	5 (71%)	17 (50%)
Parental asthma	4 (28%)	6 (46%)	4 (57%)	14 (41%)

- Recording 1 (R1): it was scheduled 1 week before the end of the ICS treatment. It started at the clinic, where the parents were instructed how to place the electrodes and start and pause the biosignals acquisition, and lasted until the next morning, when parents stopped the measurement.
- Recording 2 (R2): the second recording was conducted 1-2 weeks after the end of the treatment and was performed at home, solely by the parents. In order to ensure the validity of the recordings, the parents were requested to take pictures of the electrodes placement. The recording started along the evening, and lasted until the children woke up in the morning.
- Recording 3 (R3): it was scheduled 3-4 weeks after the end of the treatment and, as in R2, it was conducted by the parents, who were asked to take pictures of the electrodes position and to start the recording during the evening and to finish it in the next morning.

Additionally, parents were requested to annotate the times when children fall asleep and woke up in the morning.

Patients were followed up during a period of 6 months after R3 by a pediatric pulmonologist, in order to determine their current asthma (CA) status. They were labeled as having current asthma (CA-Y) if they had been prescribed medication for the control of asthma in that period because of wheezing evidence, or reported nocturnal or exercise-induced shortness of breath or cough which were reversible with bronchodilator medication. Patients who did not meet the previous criteria but were intermittently prescribed with medication because of symptoms of asthma were labeled as possible current asthma (CA-P), whereas all the remaining patients were labeled as absence of current asthma (CA-N). Patients were also classified attending to their atopic status, measured through a skin prick test (SPT). The responses to the SPT were considered positive when at least

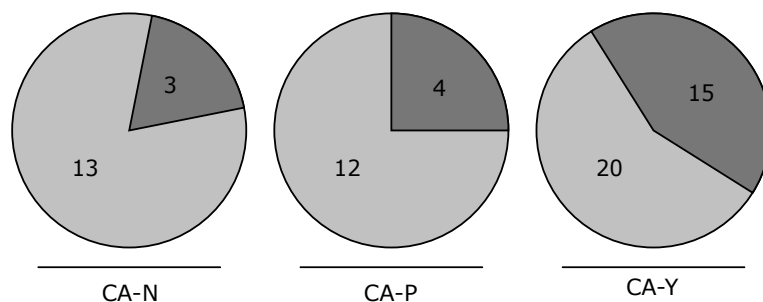


Figure 3.1: Distribution of the subjects in the TAYS dataset attending to their current asthma status (CA-N: no current asthma, CA-P: possible current asthma, CA-Y: current asthma) and their risk of developing asthma as derived from the mAPI (light gray: low risk, dark gray: high risk). This information was not available for 1 of the 68 subjects.

one of the assessed allergens (egg, cat, dog, birch and timothy) caused a wheal with a diameter greater than or equal to 3 mm without showing reaction to a negative control substance. Patients were classified as atopics or non-atopics attending to a positive or negative response to the SPT, respectively. Furthermore, they were classified attending to their response to ICS treatment as effective, partially effective or not effective. Also the classification as low or high risk of asthma attending to mAPI was available. The classification of the subjects attending to the different criteria is summarized in Figs. 3.1 and 3.2. Classification criterion was absent for one subject. Additionally, atopic condition was not available for one subject.

All the subjects had not previous history of laryngeal disease, tracheobronchial malacia, parenchymal lung disease or bronchopulmonary dysplasia. Since these conditions might be accompanied by an asynchrony of the chest wall motion or changes in the venous return and blood volume during a breathing cycle, they could lead to a loss of linearity between the flow signal and the acquired IP signal due to changes in the electrical conductivity of the thorax, and hence to lower quality IP recordings [165]. Written informed consent was received from the parents of all the children. For simplicity, this dataset will be referred to as TAYS dataset hereon.

3.2.3 Preprocessing

Only night time was considered in the analysis, since vagal modulation of cardiac activity [52] and broncho-constriction [24] are increased during night, together with a reduction in airway function which is especially noticeable in asthmatics [22, 24]. Moreover, children activity during day time is usually higher than in the case of adults (and also unknown in the analyzed database), compromising the analysis and interpretation of the results in this period. For these reasons, signals were segmented according to parents annotations of when children fall asleep and woke up in the case of the TAYS dataset. However, no annotations were available in the case of the HUH dataset, so the analysis

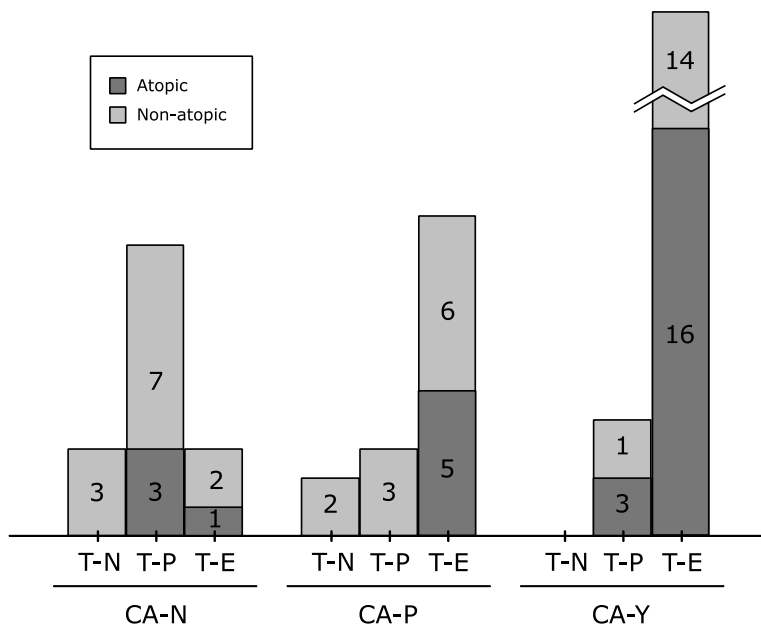


Figure 3.2: Distribution of the subjects in the TAYS dataset attending to the three different classifications. In the figure, CA-N, CA-P and CA-Y refer to the current asthma status (CA-N: no current asthma, CA-P: possible current asthma, CA-Y: current asthma), whereas T-N, T-P and T-E refer to the response to ICS treatment (T-N: not effective, T-P: partially effective, T-E: effective). Dark gray represents the atopic subjects, whilst light gray is used for non-atopics. This information was not available for 2 of the 68 subjects.

period was set between 23:00 and 05:00 in this case, according to a consistent reduction in mean HR at this time interval, indicating a resting/sleeping state of the subjects.

The acquired signals of both datasets underwent a similar preprocessing. First, ECG signals were resampled at 1000 Hz with linear interpolation, so that the effect of sampling frequency on HRV analysis was reduced [177]. Afterwards, baseline wander was corrected by subtracting the ECG baseline (extracted with low-pass filtering with 0.5 Hz cut-off frequency) from the interpolated signals. For R peak detection, the wavelet-based approach described by *Martínez et al.* [167] was employed, and the method proposed by *Mateo and Laguna* [172] was used for ectopic beats detection and correction. However, ectopic beats are not very frequent in young children [186, 192], so it is important to distinguish their effect from the effect of RSA episodes, which are stronger for children than for adults [87]. In this way, RSA episodes were distinguished from ectopic beats using the approach presented in Ch. 2.4. The RR variation threshold (θ_{RSA} in Ch. 2.4) was selected as 1.15 in the HUH dataset and as 1.5 in the TAYS dataset. These values were selected by visual inspection, and they only needed to be adjusted manually for 6 subjects.

In order to avoid noisy signal segments (probably movement artifacts) that could compromise the analysis, signal-to-noise ratio (SNR) was evaluated beat by beat, as described by *Bailón et al.* [21], and in Ch. 2.3. Beats with a SNR more than 20 dB below the median SNR of the whole night recording were labeled as “low quality”. If “low quality” beats

were found during more than 3 consecutive seconds, this segment was considered noisy and discarded from the analysis.

On the other hand, IP recordings were downsampled at 4 Hz, and band-pass filtered (cut-off frequencies of 0.05 and 0.5 Hz) so that the baseline and other components unrelated with respiration were discarded. Respiratory rate, F_r , was estimated from the IP signals in a time-continuous basis, according to the method proposed by *Lázaro et al.* [145].

3.2.4 HRV analysis

Time, frequency and nonlinear domain HRV analyses were considered, and they were performed in five-minute windows, with four-minute overlap. For the time domain analysis, \overline{NN} , SDNN, SDSD, RMSSD and pNN50 were derived from the RR interval series after ectopic correction, as suggested by the *Task Force* [252].

Regarding the frequency domain analysis, the modulating signal $m(t)$ was estimated using the TVIPFM model [19], and P_{LF} , P_{HF} , $R_{LF/HF}$ and P_{LFn} , were then derived from its spectrum, $\hat{S}_{HRV}(F)$, as described in Ch. 2.2. With respect to the LF and HF frequency bands, the traditional [0.04, 0.15] Hz band [252] was considered. However, the increased F_r observed in children, with values close to the upper limit of the classical HF band that could lead to an underestimation of P_{HF} due to a shift of power towards frequencies higher than 0.4 Hz, motivated a redefinition of the HF band. In this way, instead of the classical [0.15, 0.4] Hz HF band, a 0.15 Hz bandwidth centered in the mean respiratory rate of each segment was employed.

For the nonlinear analysis, correlation dimension (D_2), approximate entropy ($ApEn$) and sample entropy ($SampEn$) were considered. The calculation of the three indexes was performed as in [43] (in the case of D_2 , it was calculated as $\hat{D}_{2(max)}$), and all of them are dependent on two parameters: the embedding dimension, and the threshold. D_2 was computed by varying the embedding dimension from 1 to 16 in steps of 1, and the threshold from 0.01 to 3 in steps of 0.01. Regarding the $SampEn$ and $ApEn$, an embedding dimension of 2 was selected, and whereas the threshold was fixed to 0.15 in the former, in the case of $ApEn$ it was selected for maximizing it ($ApEn_{max}$). Since the asthmatic condition has been mainly related with an altered vagal activity, we proposed to estimate the nonlinear HRV indexes after minimizing the sympathetic influence present in the analyzed series. In this way, the RR interval series were filtered (10th order band-pass Butterworth filter) to preserve only those components that are thought to be related with parasympathetic activity. Two different filters were applied, defining the unfiltered band as either the extended HF band or the HF band centered in respiration, as proposed in Ch. 2.6.1. Then, the nonlinear indexes were calculated from the original RR series and from its two filtered versions.

3.2.5 Peakness analysis

The HRV spectra was also characterized using peakness (\wp), as defined in Ch. 2.5. The bandwidths employed for \wp calculation, Δf and ΔF , were selected as 0.026 (resolution of the Hamming window) and 0.15 Hz (bandwidth of the HF band), respectively. Since \wp was calculated from the HRV spectrum and using the respiratory rate derived from the IP signals, it will be referred to as $\wp_{\text{HRV}}^{\text{IP}}$. In order to assess if the respiratory signal can be excluded from the analysis, thus only considering ECG, another approach was proposed. In this case, the respiratory rate was estimated from the QRS slopes and R wave angles ECG-derived respiration (EDR) approach proposed by *Lázaro et al.* [145]. Hence, the new definition of \wp is:

$$\wp_{\text{HRV}}^{\text{EDR}} = \frac{\int_{\max(\bar{F}_{\text{EDR}} - \Delta f/2, 0.15)}^{\min(\bar{F}_{\text{EDR}} + \Delta f/2, \overline{\text{HR}}/2)} \hat{S}_{\text{HRV}}(F) dF}{\int_{\max(\bar{F}_{\text{EDR}} - \Delta F/2, 0.15)}^{\min(\bar{F}_{\text{EDR}} + \Delta F/2, \overline{\text{HR}}/2)} \hat{S}_{\text{HRV}}(F) dF}, \quad (3.1)$$

where the subindex HRV and the superindex EDR indicate that $\wp_{\text{HRV}}^{\text{EDR}}$ is calculated from the HRV spectrum and estimating the respiratory rate from the EDR.

Finally, the complementary case of using only the IP signal was considered. Hence, \wp was derived directly from the PSD of the IP signals as:

$$\wp_{\text{IP}}^{\text{IP}} = \frac{\int_{\max(\bar{F}_r - \Delta f/2, 0.15)}^{\min(\bar{F}_r + \Delta f/2, \overline{\text{HR}}/2)} \hat{S}_{\text{IP}}(F) dF}{\int_{\max(\bar{F}_r - \Delta F/2, 0.15)}^{\min(\bar{F}_r + \Delta F/2, \overline{\text{HR}}/2)} \hat{S}_{\text{IP}}(F) dF}, \quad (3.2)$$

where $\hat{S}_{\text{IP}}(F)$ is the PSD of the IP signal and the subindex IP and the superindex IP indicate that $\wp_{\text{IP}}^{\text{IP}}$ is calculated from the IP PSD and estimating the respiratory rate from the IP signal. These two alternative definitions of \wp were only tested in the HUH dataset.

3.2.6 Time-frequency coherence analysis

Given the close existing relationship between HRV and respiration control, cardiorespiratory coupling (CRC) has also been suggested to be altered in some respiratory disorders [93], although to the best of our knowledge it has not been studied in asthma. Hence, we also considered the possibility that CRC might be modified in asthmatics and contribute to the monitoring of the asthmatic condition, so we analyzed it in the TAYS dataset. For this purpose, the time-frequency (TF) cross-spectrum of the HRV and the IP signals was estimated using the methodology presented in Ch. 2.7, setting ν_0 , τ_0 and λ to 0.045, 0.05 and 0.3, as in [194]. Afterwards, two different parameters were proposed as

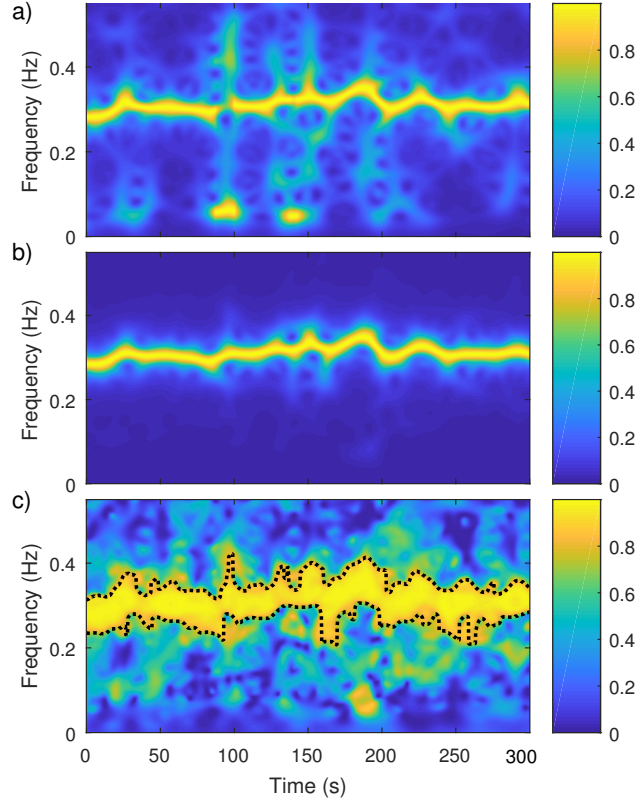


Figure 3.3: A five-minute segment of the normalized time-frequency distribution of the heart rate modulating signal (a) and the impedance pneumography signal (b) are displayed. In c), the time-frequency coherence distribution is depicted. The black dotted lines represent the limits between which $\hat{\gamma}^2(t, f) \geq \gamma_{\text{TH}}(t, f; \alpha)$, defining $\Omega(t)$ (see text for details).

CRC measurements. The first one consists in the bandwidth, $\Omega(t)$, in which both spectra are considered coherent for each time instant t , i.e., the bandwidth for which the TF coherence, $\hat{\gamma}^2(t, f)$, satisfies the condition $\hat{\gamma}^2(t, f) \geq \gamma_{\text{TH}}(t, f; \alpha)$, being $\gamma_{\text{TH}}(t, f; \alpha)$ the signal-independent threshold defined in [195], with $\alpha = 0.01$. An example of the calculation of Ω is displayed in Fig. 3.3. Moreover, the mean coherence in $\Omega(t)$, $\hat{\gamma}_{\Omega}^2(t)$, was obtained as:

$$\hat{\gamma}_{\Omega}^2(t) = \frac{1}{\Omega(t)} \int_{\Omega_1(t)}^{\Omega_2(t)} \hat{\gamma}^2(t, f) df, \quad (3.3)$$

being $\Omega_1(t)$ and $\Omega_2(t)$ the lower and upper limits of the frequency band for which $\hat{\gamma}^2(t, f) \geq \gamma_{\text{TH}}(t, f; \alpha)$ at the time instant t .

3.2.7 Statistical methods

Median of each parameter was obtained from two-hour windows, so that at least one complete sleep cycle is covered [70] and the effect of sleep stages is hence minimized. In this way, several two-hour medians were obtained per each parameter and subject (and in the case of the TAYS dataset, per recording day). In the HUH dataset, differences among LoR, HiR and ICS were assessed using a two-sided Wilcoxon rank-sum test. Also Spearman correlation coefficient (ρ) and Bland-Altman plot [8] were calculated for assessing the relationship between parameters. Moreover, the mean absolute error in the estimation of F_{EDR} was computed.

On the other hand, in the case of the TAYS dataset the differences in the groups classified attending to the CA status, atopy and response to treatment were assessed by comparing each two-hour median of each subject along the three recording days, using a paired Wilcoxon signed-rank test. In order to evaluate whether HRV parameters were related to the CA status rather than to the mAPI (since in the HUH dataset there was not an a posteriori evaluation of the asthma status available), differences among children classified as low risk of developing asthma attending to mAPI but with distinct CA outcomes were evaluated in each measurement day, using also a paired Wilcoxon signed-rank test. Additionally, in order to assess if the presence of atopy or the response to medication had an effect in the results obtained for the classification according to the CA status, differences among these subgroups within the CA-N group were assessed using a Wilcoxon rank-sum test.

In all the tests, $p < 0.05$ was set as the significance level to consider statistical differences. Normality of the data was rejected using a Kolmogorov-Smirnov test, and when the classification was in more than two groups, Bonferroni correction was applied.

3.3 Results

3.3.1 Helsinki University Hospital dataset

The highest number of significant differences between groups was found for the two-hour period going from 02 to 04 a.m. Results obtained for this period are displayed in Table 3.2, where it can be noticed that the three \wp , $R_{\text{LF/HF}}$ and P_{LFn} presented statistically significant differences between LoR and HiR. On the other hand, mean P_{HF} , $R_{\text{LF/HF}}$, P_{LFn} , $\wp_{\text{HRV}}^{\text{IP}}$ and $\wp_{\text{HRV}}^{\text{EDR}}$ were able to distinguish between LoR and ICS.

In order to check the accuracy of the respiratory frequency estimation obtained from the EDR method, the mean absolute error between F_{IP} and F_{EDR} was calculated, being it 0.0038 ± 0.0044 Hz.

Comparing the results obtained for each of the groups, increased values of the three different \wp and also decreased values of $R_{\text{LF/HF}}$ and P_{LFn} were obtained for HiR and ICS

with respect to LoR. The median values of the three different versions of \wp are consistent within each group, being them slightly reduced for $\wp_{\text{HRV}}^{\text{EDR}}$ and slightly increased for $\wp_{\text{IP}}^{\text{IP}}$ with respect to $\wp_{\text{HRV}}^{\text{IP}}$.

Since P_{HF} mainly reflects parasympathetic activity and $\wp_{\text{HRV}}^{\text{IP}}$ aims to measure the spectral distribution in HF band, it would be interesting to analyze if there exist a monotonic relationship between P_{HF} and $\wp_{\text{HRV}}^{\text{IP}}$, as an increased mean P_{HF} could be related with increased $\wp_{\text{HRV}}^{\text{IP}}$. Spearman correlation coefficient was calculated between both parameters, being it $\rho = 0.38$, thus discarding monotony between them, consistently with the simulation results obtained in Ch. 2.5.5. On the other hand, a possible relationship with sympathovagal balance was considered (lower P_{LFn} was observed for HiR than for LoR), so correlation between P_{LFn} and $\wp_{\text{HRV}}^{\text{IP}}$ was calculated. In this case, $\rho = -0.72$ was obtained, thus revealing a negative correlation between the indexes. This might indicate that higher values of $\wp_{\text{HRV}}^{\text{IP}}$ would be associated with parasympathetic dominance. Regarding $\wp_{\text{HRV}}^{\text{IP}}$ and $\wp_{\text{IP}}^{\text{IP}}$, $\rho = 0.94$ was obtained, reflecting a strong correlation. However, Bland-Altman plot displayed in Fig. 3.4 suggests that both methods are not equivalent since the range of the confidence intervals is larger than the difference of the medians between groups (Table 3.2). The negative bias indicates that $\wp_{\text{IP}}^{\text{IP}}$ usually presents higher values (as can be also noticed in their median values displayed in Table 3.2).

In addition, in Fig. 3.5, boxplots of mean $\wp_{\text{HRV}}^{\text{IP}}$ and P_{LFn} for the three groups are shown for each two-hour interval, in order to evaluate the robustness of each of the parameters to discriminate between them along the whole night. According to this figure, $\wp_{\text{HRV}}^{\text{IP}}$ is a much more robust index, since it is able to discriminate between LoR and HiR at almost every interval. The performance of the other measurements of \wp , although similar to that of $\wp_{\text{HRV}}^{\text{IP}}$, was lower.

Regarding the nonlinear domain analysis, the D_2 obtained when the RR series were filtered with a band-pass filter centered in the respiratory rate was decreased in HiR with respect to LoR during almost all the analysis period, but no differences were observed in the *ApEn* or the *SampEn*. Also decreased D_2 was observed in ICS with respect to LoR from 01 to 04 a.m. (see Table 3.2).

3.3.2 Tampere University Hospital dataset

Since the children were labeled attending to their CA statuts, atopy and response to ICS treatment, the results of the analysis were evaluated considering each of these classifications independently. The greatest amount of significant differences was obtained for the HRV indexes accounting for parasympathetic activity and the CRC parameters so, for simplicity, only they were considered below. From all the available subjects, there were 3 with the 3 recordings absent or discarded due to bad quality, and also 10 for which 2 out of 3 recordings were not considered for the same reasons. Since inter-day behavior of the different parameters followed a similar tendency along the night, results obtained at the hour with the greatest amount of significant differences, i.e., at 04 a.m., are summarized in Tables 3.3, 3.4 and 3.5. Additionally, boxplots of the two-hours median of some of the

Table 3.2: Median value between 02 and 04 a.m. of the presented parameters for each of the groups of the HUH dataset (median [25th, 75th percentiles]). * and ** indicate differences with LoR ($p < 0.05$ and $p < 0.017$ respectively). Since P_{LF} , P_{HF} and TP are calculated from $m(n)$ and not directly from RR interval series, they are adimensional (ad). Nonlinear indexes were calculated from a filtered version of the RR intervals (band-pass filter centered in the respiratory rate).

	LoR (n=14)	HiR (n=13)	ICS (n=7)
F_{IP} (Hz)	0.30 [0.27, 0.31]	0.29 [0.27, 0.30]	0.29 [0.23, 0.33]
F_{EDR} (Hz)	0.30 [0.26, 0.31]	0.29 [0.27, 0.30]	0.29 [0.24, 0.33]
\overline{NN} (ms)	751.04 [692.84, 843.38]	772.26 [722.13, 850.99]	804.03 [740.32, 826.13]
SDNN (ms)	73.20 [56.90, 82.85]	74.19 [36.12, 99.00]	92.46 [28.84, 94.12]
SDSD (ms)	83.33 [57.64, 91.30]	74.96 [38.40, 103.48]	108.47 [44.50, 113.25]
RMSSD (ms)	83.22 [57.57, 91.21]	74.87 [38.35, 103.35]	108.33 [44.45, 113.11]
pNN50 (%)	46.08 [20.88, 50.23]	37.39 [15.22, 51.60]	51.10 [31.61, 64.25]
P_{LF} (ad $\times 10^{-3}$)	2.10 [1.20, 2.71]	2.05 [0.45, 2.79]	2.34 [0.77, 3.14]
P_{HF} (ad $\times 10^{-3}$)	3.37 [1.98, 3.57]	2.89 [1.04, 6.34]	5.77 [1.39, 6.89]*
TP (ad $\times 10^{-3}$)	5.87 [4.25, 6.59]	4.91 [1.66, 9.17]	9.21 [1.43, 9.74]
$R_{LF/HF}$ (n.u.)	0.77 [0.51, 1.00]	0.43 [0.29, 0.51]*	0.26 [0.04, 0.34]**
P_{LFn} (n.u.)	0.44 [0.34, 0.50]	0.30 [0.23, 0.34]*	0.20 [0.04, 0.25]**
ρ_{HRV}^{IP} (n.u.)	0.38 [0.31, 0.41]	0.45 [0.40, 0.46]*	0.47 [0.38, 0.48]*
ρ_{HRV}^{EDR} (n.u.)	0.35 [0.30, 0.38]	0.39 [0.37, 0.40]*	0.42 [0.34, 0.43]*
ρ_{IP}^{IP} (n.u.)	0.44 [0.41, 0.45]	0.49 [0.46, 0.55]**	0.50 [0.41, 0.52]
D_2	2.68 [2.44, 2.75]	2.42 [2.34, 2.49]*	2.38 [2.27, 2.39]*
<i>ApEn</i>	0.57 [0.55, 0.57]	0.56 [0.54, 0.56]	0.57 [0.49, 0.57]
<i>SampEn</i>	0.50 [0.46, 0.51]	0.50 [0.47, 0.50]	0.49 [0.47, 0.52]

considered parameters and an example of the time course of the HF power are displayed in Figs. 3.6 and 3.7, respectively.

Attending to current asthma status: A clear tendency towards increased P_{LFn} and decreased RMSSD, P_{HF} and ρ_{HRV}^{IP} was found in R3 with respect to R1 and R2 in CA-N. This behavior was consistent along several parameters and two-hour windows, as displayed in Fig. 3.6. These differences were especially noticeable at 03 and 04 a.m. in the frequency-domain HRV indexes. A similar behavior was assessed in the CRC parameters (see Fig. 3.6). On the other hand, only scarce differences between the three recording days were found in CA-Y and CA-P.

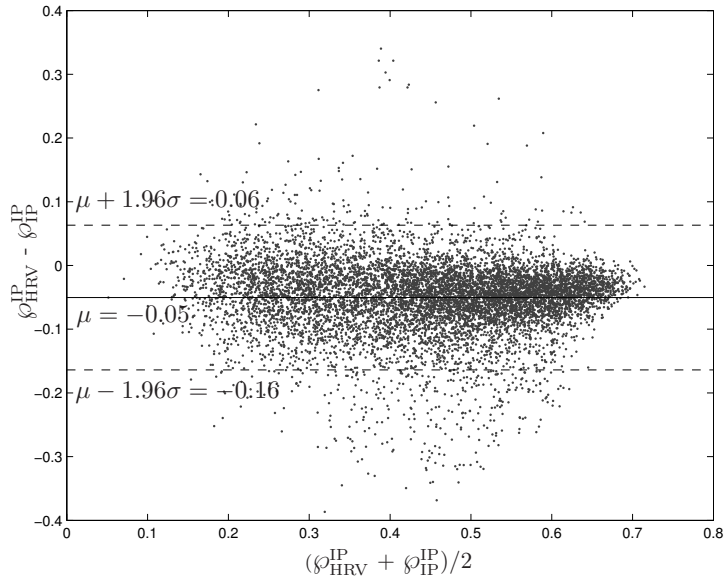


Figure 3.4: Bland-Altman plot for agreement evaluation between $\phi_{\text{HRV}}^{\text{IP}}$ and $\phi_{\text{IP}}^{\text{IP}}$. In the figure, μ is the mean of $\phi_{\text{HRV}}^{\text{IP}} - \phi_{\text{IP}}^{\text{IP}}$, whereas σ is the standard deviation of these differences.

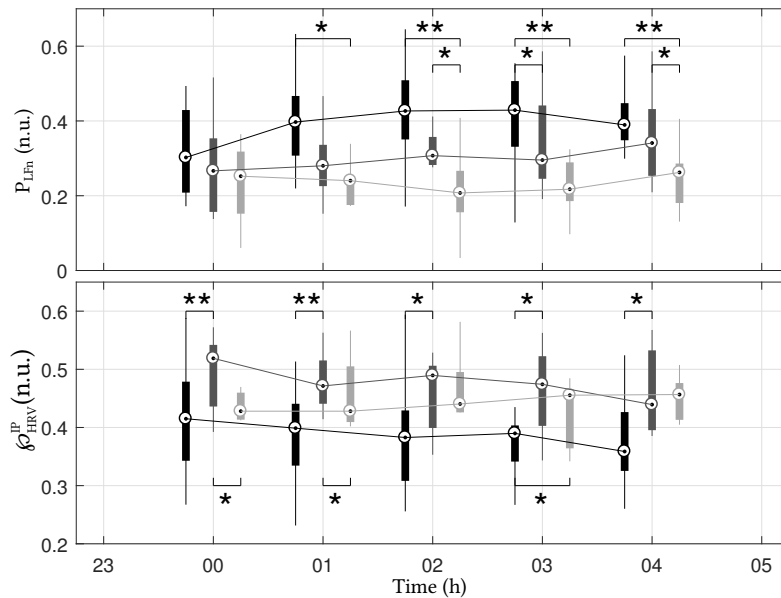


Figure 3.5: Temporal evolution of the mean values of $\phi_{\text{HRV}}^{\text{IP}}$ and P_{LFn} is shown for the LoR (black), HiR (dark gray) and ICS (light gray) groups of the HUH dataset. Boxplots are centered in the intermediate hour of the two-hour interval considered (boxplots for different groups, although plotted separately for interpretation purposes, are calculated with the same time references). * and ** indicate significant differences ($p < 0.05$ and $p < 0.017$ respectively) among groups in the given two-hour interval.

Attending to atopic status: Patients classified as atopic presented significantly decreased $\wp_{\text{HRV}}^{\text{IP}}$ in R3 with respect to R2 from 02 to 03 a.m. In the case of non-atopic subjects, they presented decreased $\wp_{\text{HRV}}^{\text{IP}}$ in R3 when compared with R1 at 01 and from 05 to 06 a.m., and in R2 with respect to R1 at 05 a.m, and increased P_{LFn} in R3 with respect to R1 at 05 a.m. Finally, a tendency towards decreased Ω and $\hat{\gamma}_{\Omega}^2$ was assessed in R3 with respect to R2 and R1, turning statistically significant for Ω from 23 to 01 a.m.

Attending to the response to treatment: Statistically significant differences were only found in the group with partial response to ICS treatment, being only noticeable in P_{LFn} , which was increased in R3 when compared with R1 at 05, and at 03 a.m. when compared with R2. Regarding the CRC indexes, decreased Ω and $\hat{\gamma}_{\Omega}^2$ were assessed in the group with partial response to treatment from 01 to 03 and 02 a.m. respectively. The same behavior was found at 00 a.m. in the group which responded effectively to treatment.

Since several subjects classified as low risk attending to the mAPI were actually labeled as CA-Y (Fig. 3.1), we also analyzed the behavior of the different indexes attending to the classification as CA-Y or CA-N, but only considering those subjects labeled as low risk. In this case, significant differences were only present in CA-N (apart from isolated differences in RMSSD and Ω in CA-Y, at 05 and 00 a.m. respectively). Regarding CA-N, decreased P_{HF} in R3 with respect to R2 was assessed at 04 a.m. Also increased P_{LFn} and decreased $\wp_{\text{HRV}}^{\text{IP}}$ were found in R3 with respect to R2 from 03 to 04 and from 02 to 04 a.m. respectively. With respect to the CRC indexes, their behavior was the same as when considering only the CA status, with lower values in R3 in those children classified as CA-N. These results are displayed in Fig. 3.8.

Regarding the nonlinear domain analysis, there were no consistent differences among the two-hour windows medians for any of the considered parameters, groups or recording days.

Finally, when comparing the different atopy or response to treatment groups within the CA-N group, no differences were assessed for any tow-hours window or recording day.

3.4 Discussion

Several studies have pointed out to the parasympathetic branch of ANS as the main responsible of broncho-constriction mechanisms [151, 185] and bronchomotor tone control [184], which are closely related to asthma. The increased vagal activity and altered autonomic airway control observed in asthmatic patients may be also reflected in cardiac vagal activity [80, 131] and hence HRV could be a suitable tool for evaluating those changes. In this chapter, we hypothesized that not only increased vagal tone but also a distinct behaviour of vagal activity could be related with asthma, and that these differences could be characterized through HRV spectral analysis. For this purpose, we defined \wp as an index to evaluate the spectral distribution of the HF components of HRV spectra,

and we used it in the characterization of a dataset of preschool children classified attending to their risk of developing asthma (HUH dataset). Afterwards, we extended the study to a second dataset (TAYS dataset), with a more precise classification and a larger number of subjects. Moreover, the TAYS dataset allowed to study the evolution of the different HRV parameters following ICS treatment.

3.4.1 Methodology

\wp was analyzed together with classical time and frequency domain HRV indexes. Previously, HRV signals were conveniently preprocessed. Although it is well known that an accurate ectopic beats detection and correction is crucial in HRV analysis, the problem in this case is different: if we considered a strong RSA episode as ectopic (overcorrection), we would be losing fundamental information, since RSA is essentially what we pretend to characterize through \wp . The RSA episodes detector proposed here aims to minimize the number of false ectopic detections, which would lead to a smoother spectrum, therefore introducing a bias in the computation of \wp . The fact that the respiratory rate is higher in children than in adults could also compromise the traditional HRV analysis, given that the upper bound of the HF band results insufficient for an accurate measurement of the HF power. In this way, the HF band was redefined adaptively in function of the respiratory rate, as proposed in Ch. 2.6.1.

Whereas $\wp_{\text{HRV}}^{\text{IP}}$ requires from respiratory information for its computation, the possibility of using only the ECG was addressed. In this way, a respiratory rate estimation obtained from an EDR signal as proposed by *Lázaro et al.* [145] was used for computing $\wp_{\text{HRV}}^{\text{EDR}}$. On the other hand, the analogous case of using only respiratory information was also considered, so that $\wp_{\text{IP}}^{\text{IP}}$ was defined. Although the performance of the three indexes was similar, some differences arise. In the case of $\wp_{\text{HRV}}^{\text{EDR}}$, median values were slightly lower than in $\wp_{\text{HRV}}^{\text{IP}}$, thus revealing that $\wp_{\text{HRV}}^{\text{IP}}$ is sensitive to the accuracy of the respiratory rate estimation. Regarding $\wp_{\text{IP}}^{\text{IP}}$, it overestimated $\wp_{\text{HRV}}^{\text{IP}}$. In order to understand whether $\wp_{\text{HRV}}^{\text{IP}}$ does reflect a measurement of the respiratory activity or either it accounts for another mechanism, correlation and Bland-Altman plot were analyzed. High correlation between both definitions ($\rho = 0.94$) suggests strong relationship. However, the Bland-Altman plot displayed in Fig. 3.4 suggests that both measurements are not equivalent, since the range of the confidence intervals is larger than the difference of the medians between groups. In this way and despite the fact that both indexes are thought to measure a similar phenomenon, they cannot be used interchangeably due to the existence of different spectral components in respiration and HRV. For these reasons, in the case of the TAYS dataset, only $\wp_{\text{HRV}}^{\text{IP}}$ was employed.

3.4.2 Helsinki University Hospital dataset

Results in Table 3.2 suggest a peakier component in the HF band accompanied by a reduced sympathovagal balance in the group classified as HiR when compared with LoR.

Table 3.3: Median and [25th, 75th percentiles] of the most relevant time domain HRV parameters obtained from a two-hour window centered at 04 a.m. in the TAYS dataset. Results for each recording day attending to their current asthma status, atopy and response to treatment are displayed. Statistical significant differences with R1 are indicated with * ($p \leq 0.05$), whereas differences with R2 are labeled with † ($p \leq 0.05$). Statistical differences after Bonferroni correction ($p \leq 0.017$) are labeled as ** or ‡.

	NN (ms)			RMSSD (ms)		
	R1	R2	R3	R1	R2	R3
<i>Attending to asthma:</i>						
• CAN	743.9 [663.0, 786.7]	695.5 [628.0, 777.1]	671.5 [639.4, 733.7]†	67.41 [33.89, 134.2]	58.96 [31.68, 124.82]	42.39 [23.94, 106.59]†*
• CA-P	731.8 [702.0, 835.1]	696.5 [672.9, 779.1]	686.4 [683.4, 792.7]	86.26 [48.59, 122.67]	62.33 [41.24, 100.83]	74.56 [37.12, 129.01]
• CA-Y	703.7 [636.5, 803.3]	748.0 [623.6, 767.6]	714.4 [662.0, 772.8]	79.43 [44.94, 108.5]	87.41 [47.43, 130.64]	64.33 [42.64, 123.81]
<i>Attending to SPT:</i>						
• Non-atopic	715.9 [637.1, 742.7]	696.5 [612.2, 757.2]	684.0 [648.5, 733.7]	69.01 [38.68, 93.27]	58.96 [37.56, 103.66]	59.74 [28.86, 93.26]
• Atopic	796.0 [665.2, 838.0]	748.0 [656.8, 827.6]	714.4 [670.1, 850.6]	96.80 [55.74, 144.44]	94.39 [41.45, 125.59]	83.88 [43.98, 126.36]
<i>Attending to treatment:</i>						
• No effective	744.9 [695.1, 812.4]	695.5 [645.6, 715.7]	684.0 [623.9, 733.85]	86.26 [46.75, 139.44]	58.20 [34.69, 117.66]	58.39 [28.17, 83.29]
• Partially effective	709.2 [634.5, 764.8]	670.5 [620.7, 777.1]	670.1 [623.5, 710.6]	51.30 [31.33, 85.46]	45.07 [29.42, 120.87]	34.80 [23.45, 68.34]
• Effective	722.0 [638.4, 807.4]	731.3 [649.3, 792.2]	711.3 [665.7, 786.2]	81.59 [48.51, 122.16]	79.82 [47.12, 123.58]	78.77 [45.78, 126.91]

Table 3.4: Median and [25th, 75th percentiles] of the most relevant frequency domain HRV parameters obtained from a two-hour window centered at 04 a.m. in the TAYS dataset. Results for each recording day attending to their current asthma status, atopy and response to treatment are displayed. Statistical significant differences with R1 are indicated with * ($p \leq 0.05$), whereas differences with R2 are labeled with † ($p \leq 0.05$). Statistical differences after Bonferroni correction ($p \leq 0.017$) are labeled as ** or ‡.

	$P_{\text{HF}} (\text{ad} \times 10^{-3})$			$P_{\text{HF}} (\text{ad} \times 10^{-3})$			$\rho_{\text{HF}}^{\text{IP}} (\text{n.u.})$		
	R1	R2	R3	R1	R2	R3	R1	R2	R3
<i>Attending to asthma:</i>									
• CA-N	2.86 [1.08, 7.32]	2.85 [1.08, 7.91]	1.53 [0.43, 3.92] ^{†,‡}	0.35 [0.25, 0.49]	0.39 [0.29, 0.47]	0.45 [0.40, 0.53] [‡]	0.39 [0.32, 0.42]	0.40 [0.33, 0.44]	0.34 [0.30, 0.40] [‡]
• CA-P	4.20 [1.64, 7.59]	2.86 [1.17, 6.06]	2.53 [1.24, 9.26]	0.39 [0.27, 0.44]	0.42 [0.27, 0.50]	0.44 [0.29, 0.50]	0.38 [0.32, 0.42]	0.37 [0.34, 0.43]	0.40 [0.32, 0.43]
• CA-Y	3.05 [1.58, 6.57]	4.64 [1.67, 8.89]	2.97 [1.30, 8.27]	0.34 [0.25, 0.51]	0.33 [0.24, 0.44]	0.35 [0.27, 0.51]	0.38 [0.31, 0.44]	0.39 [0.31, 0.47]	0.40 [0.31, 0.48]
<i>Attending to SPT:</i>									
• Non-atopic	2.96 [1.44, 5.64]	2.48 [1.28, 6.59]	2.14 [0.67, 4.23]	0.43 [0.27, 0.52]	0.40 [0.28, 0.50]	0.44 [0.32, 0.54]	0.36 [0.32, 0.42]	0.40 [0.31, 0.44]	0.38 [0.30, 0.46]
• Atopic	5.14 [2.21, 8.79]	5.64 [1.69, 7.80]	4.46 [1.39, 9.37]	0.30 [0.22, 0.41]	0.32 [0.24, 0.41]	0.34 [0.27, 0.46]	0.38 [0.32, 0.44]	0.38 [0.34, 0.47]	0.39 [0.32, 0.44]
<i>Attending to treatment:</i>									
• No effective	4.34 [1.87, 6.88]	2.83 [1.15, 6.09]	2.26 [0.70, 3.47]	0.42 [0.31, 0.44]	0.39 [0.36, 0.44]	0.47 [0.44, 0.53]	0.35 [0.30, 0.41]	0.36 [0.33, 0.45]	0.33 [0.29, 0.36]
• Partially effective	2.22 [0.77, 5.00]	1.66 [0.92, 8.83]	0.98 [0.37, 2.97]	0.32 [0.25, 0.48]	0.42 [0.21, 0.47]	0.43 [0.35, 0.54]	0.39 [0.33, 0.45]	0.41 [0.35, 0.47]	0.40 [0.33, 0.49]
• Effective	3.54 [1.67, 7.41]	4.52 [1.65, 7.53]	3.09 [1.33, 8.97]	0.35 [0.26, 0.49]	0.33 [0.26, 0.46]	0.36 [0.28, 0.48]	0.38 [0.30, 0.43]	0.38 [0.31, 0.43]	0.38 [0.31, 0.44]

Table 3.5: Median and [25th, 75th percentiles] of the proposed cardiorespiratory coupling parameters obtained from a two-hour window centered at 04 a.m. in the TAYS dataset. Results for each recording day attending to their current asthma status, atopy and response to treatment are displayed. Statistical significant differences with R2 are indicated with † ($p \leq 0.05$) or ‡ (after Bonferroni correction, $p \leq 0.017$).

	Ω (Hz)			μ_n^2 (n.u)		
	R1	R2	R3	R1	R2	R3
<i>Attending to asthma:</i>						
• CA-N	0.087 [0.068, 0.099]	0.089 [0.078, 0.105]	0.082 [0.068, 0.097]‡	0.909 [0.899, 0.915]	0.911 [0.906, 0.915]	0.907 [0.901, 0.915]
• CA-P	0.088 [0.073, 0.102]	0.087 [0.075, 0.104]	0.086 [0.074, 0.101]	0.912 [0.904, 0.915]	0.911 [0.902, 0.916]	0.910 [0.900, 0.916]
• CA-Y	0.088 [0.075, 0.109]	0.091 [0.080, 0.107]	0.086 [0.076, 0.102]	0.912 [0.908, 0.916]	0.913 [0.907, 0.917]	0.911 [0.904, 0.917]
<i>Attending to SPT:</i>						
• Non-atopic	0.087 [0.073, 0.102]	0.089 [0.075, 0.105]	0.082 [0.070, 0.101]	0.911 [0.905, 0.916]	0.911 [0.904, 0.917]	0.910 [0.901, 0.915]
• Atopic	0.087 [0.074, 0.102]	0.088 [0.082, 0.102]	0.090 [0.073, 0.101]	0.910 [0.904, 0.916]	0.913 [0.907, 0.916]	0.912 [0.905, 0.917]
<i>Attending to treatment:</i>						
• No effective	0.076 [0.072, 0.102]	0.080 [0.064, 0.108]	0.082 [0.071, 0.091]	0.906 [0.901, 0.915]	0.905 [0.895, 0.919]	0.907 [0.900, 0.911]
• Partially effective	0.087 [0.070, 0.103]	0.089 [0.078, 0.108]	0.082 [0.068, 0.104]†	0.910 [0.904, 0.915]	0.911 [0.909, 0.917]	0.912 [0.901, 0.917]
• Effective	0.088 [0.075, 0.103]	0.089 [0.079, 0.104]	0.087 [0.073, 0.101]	0.912 [0.906, 0.916]	0.912 [0.906, 0.915]	0.911 [0.903, 0.915]

Also a similar behavior was observed in ICS, together with an increased P_{HF} with respect to LoR. Similar results obtained for HiR and ICS could be due to the fact that children under medication are symptomatic. Nevertheless, the limited size of the ICS group compromises the further physiological interpretation. Since \wp is a measurement of how the power is concentrated around the respiratory rate, a peakier HF component seems to be a common feature of children with enhanced risk of asthma. A possible explanation of the increased \wp_{HRV}^{IP} would be a strong relationship with P_{HF} . However, correlation between both variables has been discarded in the simulation study of Ch. 2.5.5, and also in this study, where moreover the P_{HF} was similar for LoR and HiR. On the other hand, negative correlation between \wp_{HRV}^{IP} and P_{LFn} suggests that the spectral distribution of the HF components may be closely related with changes in the sympathovagal balance, whose altered behavior has been proposed to be responsible of the increased broncho-constriction and bronchomotor tone observed in asthmatics [151, 184, 185]. Despite, the nature of these changes is not easy to analyze, since an increase in SNS activity often produces a similar effect than a decrease in PNS activity and vice versa. Even though correlation between \wp_{HRV}^{IP} and P_{LFn} has been assessed, the former has been presented as a more robust index against inter- and intra-subject variability for distinguishing between HiR and LoR, as displayed in Fig. 3.5.

In a previous study, *Emin et al.* [80] reported increased PNS activity in response to autonomic tests in older children (7-12 years) with a clinical diagnosis of asthma, as well as the possibility to stratify asthma severity attending to HRV analysis. Here, increased parasympathetic dominance assessed in HiR and ICS by lower $R_{LF/HF}$ and P_{LFn} is consistent with the results in [80]. However, in difference with [80], mean P_{HF} was similar in LoR and HiR, which might be due to several reasons. First, distinct definitions of the HF band were employed, since in [80] it was defined as [0.15, 0.5] Hz, thus impeding direct comparison of the results. Moreover, the aim of this study was not to perform a classification of children with diagnosed asthma, but a characterization of groups that were formed attending to the predicted asthma risk. Also age difference between the populations of both studies is probably accompanied by differences in the ANS functioning. Finally, the recordings in *Emin et al.* were performed under predefined conditions of stimulated PNS activity (deep breathing, Valsalva maneuver) [80], whereas in our study ECGs were acquired without a controlled environment.

Regarding the nonlinear analysis, D_2 was different among groups only when the RR intervals were filtered to preserve the respiration-related components. The fact that D_2 was lower for the HiR group might suggest a reduction in the number of degrees of freedom in the case of HiR, i.e., a reduction in the adaptability of vagal activity. Although this result is coherent with a reduced \wp_{HRV}^{IP} in this group, both parameters remain difficult to relate, since two different HRV signals of distinct complexity could share similar spectra [133]. On the other hand, no differences were found in *ApEn* and *SampEn*, which may suggest that some of the features of the analyzed signals remained hidden in a low-dimensional analysis (in the case of D_2 , the embedding dimension was varied from 1 to 16).

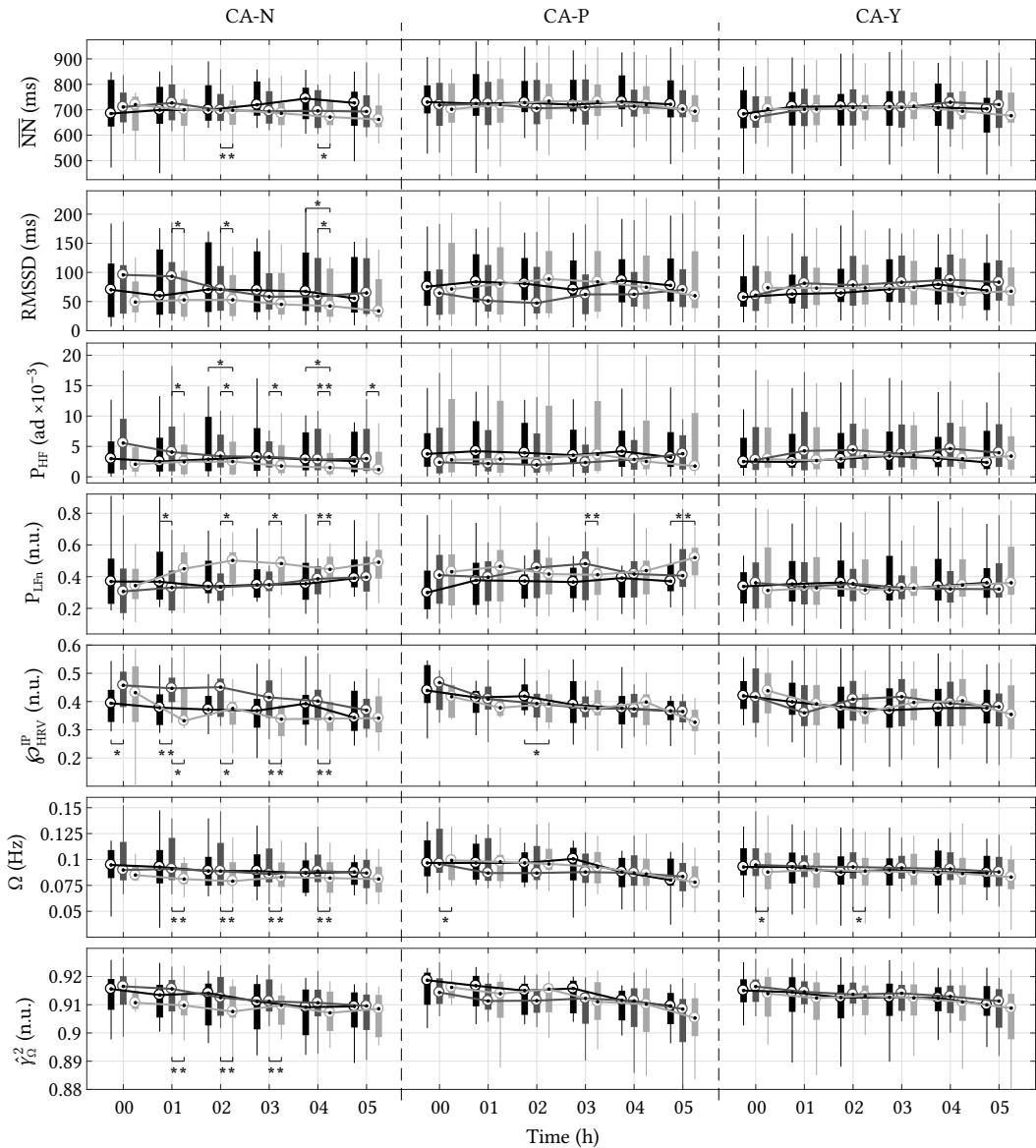


Figure 3.6: Boxplots corresponding to some of the analyzed parameters in R1 (black), R2 (dark gray) and R3 (light gray) in the TAYS dataset, attending to the current asthma status. Each box corresponds to a two-hour window centered in the hour depicted in the figure (although boxes with the same time reference are depicted separately for clarity, same central hour was considered in the analysis). Medians of the boxes corresponding to the same measurement day are connected with solid lines, and statistical significant differences are labeled with * ($p \leq 0.05$). Statistical differences after Bonferroni correction ($p \leq 0.017$) are labeled as **. P_{HF} , as obtained from $m(n)$, is adimensional (ad). In order to improve the readability of the figure, only the interval 00 to 05 a.m. is displayed.

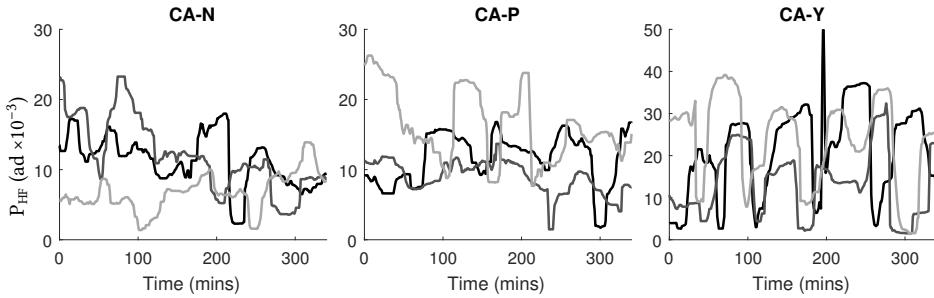


Figure 3.7: Time course of P_{HF} for R1 (black), R2 (dark gray) and R3 (light gray) of three subjects belonging to the different current asthma groups. P_{HF} , as obtained from $m(n)$, is adimensional (ad).

3.4.3 Tampere University Hospital dataset

All the children underwent the same ICS treatment during three months. However, whereas ANS activity (as measured from HRV) remained unchanged after treatment completion in those children classified as CA-Y, a decrease in parasympathetic activity and an increase in sympathetic dominance was observed in the CA-N group. Since previous studies have assessed an augmented vagal activity in asthmatics [80, 131, 287], the lowered PNS activity in CA-N following treatment could be reflecting recovery from illness, so that vagal over-activity is gradually diminished towards homeostatic levels. Also a reduction in ϕ_{HRV}^{IP} and CRC (as measured from Ω and \hat{y}_{Ω}^2) were assessed in this group. Since CRC is related to how the respiratory activity modulates the HR, a reduction in CRC measurements and ϕ_{HRV}^{IP} could be reflecting a less synchronous vagal modulation of respiratory and cardiac rhythms or a less regular PNS activity, respectively. In this case, the interpretation might be linked to the concept of illness as a state of reduced complexity [99, 212], suggesting that HRV might be more dependent on the respiratory activity in asthma or in subjects at an increased risk of developing asthma in the future. The fact that both Ω and \hat{y}_{Ω}^2 were lowered in R3 in the CA-N group suggests a reduction in the frequency span in which HRV is governed by respiration, but also in the strength of the interdependence of cardiac and respiratory control in those subjects that have overcome the disease. This hypothesis is supported by previous studies suggesting lowered chaoticity and regularity of impedance pneumography [237] and airflow pattern [267] in subjects with a worse asthma outcome. It is noteworthy that, in concordance with the results obtained for the HUH dataset, most significant differences were obtained between 02 and 04 a.m., thus when airway function is lowest [24, 30]. Regarding the CA-P group, only scarce differences in ANS activity were assessed, which could reflect an intermediate behavior between those of CA-N and CA-P.

Despite not being specific for asthma, the presence of atopy enhances the probability that a patient with respiratory symptoms presents allergic asthma [97], and it has been included as a factor for the prediction of asthma in, e.g., the Isle of Wight study [143]. For these reasons, we analyzed the results regarding the atopic status of the patients. Although a reduced CRC was assessed in R3 in the non-atopic group, the fact that not

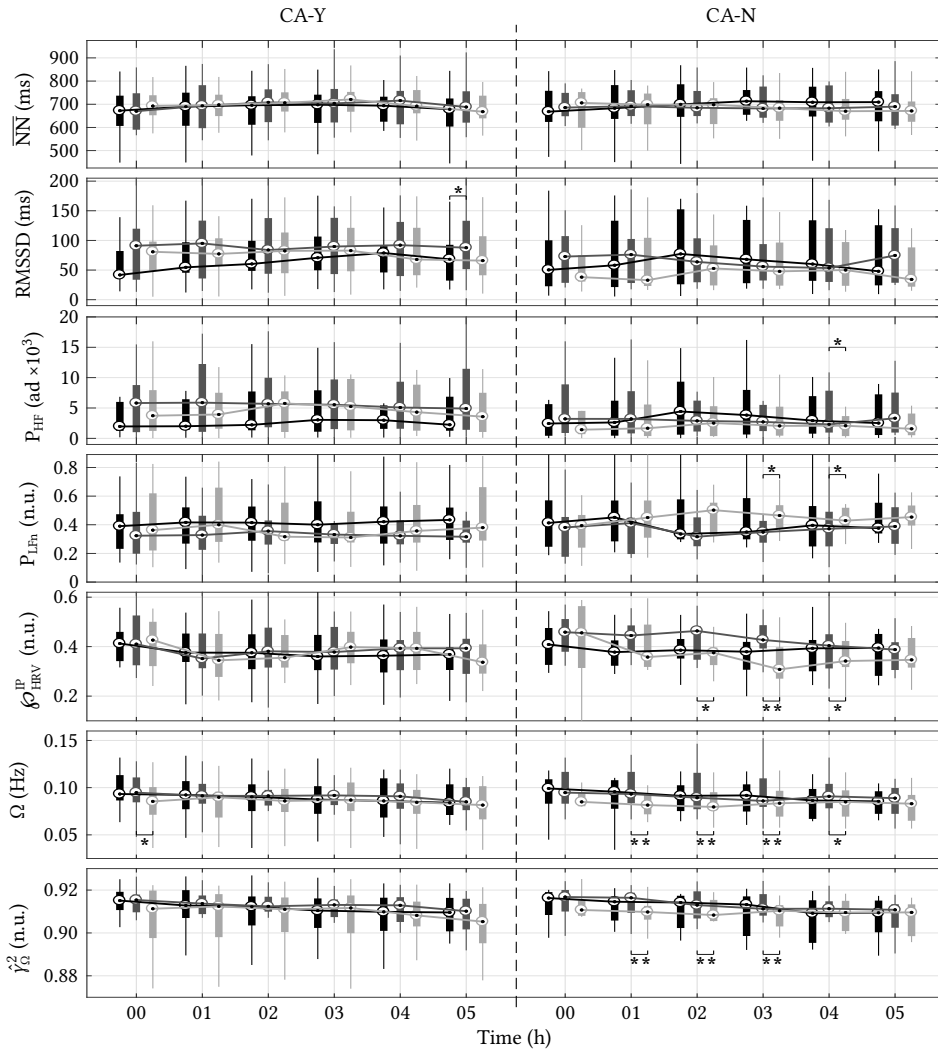


Figure 3.8: Boxplots corresponding to some of the analyzed parameters in R1 (black), R2 (dark gray) and R3 (light gray) in the TAYS dataset. Only the subjects classified as low risk and CA-Y/CA-N are depicted. Each box corresponds to a two hours window centered in the hour depicted in the figure (although boxes with the same time reference are depicted separately for clarity, same central hour was considered in the analysis). Medians of the boxes corresponding to the same measurement day are connected with solid lines, and statistical significant differences are labeled with * ($p \leq 0.05$). Statistical differences after Bonferroni correction ($p \leq 0.017$) are labeled as **. P_{HF} , as obtained from $m(n)$, is adimensional (ad). In order to improve the readability of the figure, only the interval 00 to 05 a.m. is displayed.

consistent differences were found in the other considered indexes suggests that atopy is not closely related with the apparent altered ANS activity in CA-Y.

On the other hand, whereas changes in ANS function were expected to be produced by a proper response to ICS treatment, no differences were found in the HRV parameters of the group for which treatment resulted effective (which constitutes the majority of the dataset). However, some scarce differences were found in the group with partial response to treatment, specially in the CRC. The most likely explanation for this outcome is that most of the children for which the treatment was effective were classified as CA-Y or CA-P, whereas the group with partial response to ICS is mainly formed by subjects classified as CA-N (Fig. 3.2), thus suggesting that the observed differences may not be related with the treatment but with the evolution of the illness itself. This result is particularly interesting, as it could indicate that, despite ICS treatment which is aimed to reduce airway inflammation, altered ANS behavior might be still present in the groups with a worse asthma prognosis.

Nevertheless, the fact that children with different atopic or response to treatment status are classified as CA-N could have a direct influence in the observed results. In this way, we studied the differences between atopics and non-atopics classified as CA-N, as well as between the subgroups attending to the response to treatment. The absence of significant differences suggests that the observed results attending to the CA status are not likely due to the atopic condition or the response to treatment of the different subjects.

In the case of the HUH dataset, subjects classified as LoR attending to mAPI presented a similar behavior than the CA-N group, with a reduced vagal dominance and ϕ_{HRV}^{IP} with respect to the HiR group. However, similarities between the classification based on mAPI and the CA status should be regarded carefully. If we analyze the subject distribution in Fig. 3.1, we can observe that 57% of the children that were classified as LoR attending to mAPI were labeled as CA-Y after the 6-month follow up, thus revealing the low sensitivity of this method and highlighting the need of robust alternatives. In this way, we evaluated the temporal evolution of those subjects labeled as CA-Y and CA-N, with the additional restriction that they were labeled as LoR attending to the mAPI. As depicted in Fig. 3.8, no differences were found in the CA-Y group (except from isolated differences in RMSSD and Ω) regardless of their classification as LoR, whereas the expected differences appeared in the CA-N group, being Ω the best performing index. Hence, it is possible that changes in HRV might be better related with the CA status than with mAPI in this dataset.

Finally, nonlinear analysis did not reveal any difference among groups, in contrast with the results obtained in the HUH dataset. Therefore, it is possible that the results in the HUH dataset are more related to some of the clinical parameters involved in the calculation of the mAPI than to the real asthmatic condition.

3.4.4 Limitations

The main limitation of this study resides in the absence of polysomnographic recordings, so that it was not possible to look for differences in HRV along the various sleep stages. In order to deal with this restriction, we proposed to calculate two-hour medians of the analyzed indexes to cover at least one complete sleep cycle [70]. Furthermore, we checked that the overnight variation was not higher than the interday variation for any of the considered parameters, being \overline{NN} , RMSSD and P_{HF} those that showed a larger inter-day variability. Another limitation relies in the possibility of a coexistence of additional confounders apart from the risk of asthma, such as obstructive sleep apnea syndrome (OSAS) or COPD, which are also obstructive diseases causing dyspnea and that have been related with altered HRV [95, 111]. In the case of OSAS, visual analysis of the IP signals of the different patients revealed the absence of generalized amplitude decreases that could indicate apneic episodes, and no differences between changes in IP amplitude were noticed in the different groups. To the authors knowledge, no COPD diagnosis was made for any of the subjects in the database, although the diagnosis of COPD remains compromised in so young children.

3.4.5 Physiological interpretation

In spite of the many studies stating the important role of PNS as a source of the airway hyper-responsiveness characteristic of asthma, the underlying mechanisms causing an abnormal vagal activity have not yet been elucidated. The presence of immune cells which are involved in the inflammatory response has been considered as one likely explanation, as they release inflammatory mediators that could alter local PNS activity and trigger bronchial hyper-reactivity. However, several counterpoints can be highlighted. First, preventive treatment with anti-inflammatory corticosteroids has been shown to be insufficient for avoiding the development of asthma in young children [109]. Second, the presence of different phenotypes of asthma with distinct manifestations and responses to treatment, together with an apparent absence of relationship between inflammation and airway remodeling in children [152] suggest the existence of other factors. Moreover, the fact that altered PNS activity in asthmatics can be also noticed in HRV opposes to the idea of a local effect. *Fryer et al.* suggested that excessive vagal stimulation could be caused by a dysfunction of the M_2 muscarinic receptors [90], which are largely present in the post-ganglionic nerves innervating the airways and provide negative feedback in response to acetylcholine (ACh) withdrawal, thus inhibiting the further release of ACh. Although the lowered control over ACh release might explain the increased vagal dominance observed through HRV in the presence of asthma, as well as the more regular PNS activity suggested by increased ϕ , if cardiac vagal fibers also presented M_2 receptors dysfunction, the simultaneous reduction in the adaptability of cardiac and respiratory vagal control due to excessive ACh release could resemble an increased CRC. In this way, further research is needed to completely understand the neural control in asthmatics.

3.5 Conclusion

HRV analysis has been presented as a suitable non-invasive tool for the assessment of abnormal ANS activity in children at risk of asthma. In the HUH dataset, HRV analysis was used for the characterization of ANS activity in a dataset of pre-school children divided in three groups based on the risk of asthma development and on medication intake. Consistently with previous studies, a decreased symphahtovagal balance was assessed in those children at higher risk of developing asthma, who also presented a peakier HF component, as measured through peakness.

Regarding the TAYS dataset, the main outcome is that vagal activity and cardiorespiratory coupling, measured in a group of children with obstructive bronchitis, were reduced after ICS treatment in the subgroup at lower risk of asthma, whereas it kept unchanged in those who presented a worse prognosis. This result is in concordance with our initial hypothesis that altered PNS activity would turn normal after treatment in children without or with low risk of asthma, but not in those with or at high risk of asthma. The difficulties of young children to perform repeatable spirometric tests together with the lack of collaboration and the low adherence to ICS treatment emphasize the interest in a continuous monitoring of asthma in order to detect or predict exacerbations, thus providing an objective measurement of the evolution of the disease.

Both studies reflected coherent results, which were in concordance with previous works assessing HRV in asthmatic children. In this way, since HRV analysis is non-invasive in nature, it stands out as a feasible option for aiding in the study of the neural mechanisms underlying asthma. In addition, the possibility of a continuous monitoring of ANS activity in asthmatics could shed some light on the nature of this disease, and hence be useful for patient phenotyping, which constitutes the first step towards personalized treatment.

4

HRV analysis in asthmatic adults

4.1 Motivation	4.2.5 Statistical analysis
4.2 Materials and methods	4.2.6 Automatic stratification
4.2.1 Study population	4.3 Results
4.2.2 Preprocessing	4.4 Discussion
4.2.3 HRV analysis	4.5 Conclusion
4.2.4 Respiration dynamics analysis	

4.1 Motivation

The diagnosis of asthma in adults is performed following a well-established clinical routine, and it is based on the assessment of lung function via spirometric tests and in the quantification of different inflammatory biomarkers, such as the inflammatory cells count in the induced sputum, the amount of serum immunoglobulin E (IgE) or the levels of exhaled nitric oxide (FeNO) [97, 206]. Apart from the severity of the disease, there is a high clinical interest in stratifying the level of control of the symptomatology, since a poor symptoms control has been related with an increased risk of suffering exacerbations [232], and might require from additional treatment. However, asthma is a very heterogeneous disorder, presenting itself with a variety of symptoms that also vary over time, therefore hindering its accurate diagnosis and the clustering of patients in the different

phenotypes. In this way, there is a high inter-subject variability which reflects in several aspects of the disease. E.g., although asthma is usually accompanied by chronic airway inflammation, studies in large populations have revealed that a 40% of the asthmatics do not present bronchial inflammation (as measured from induced sputum) [234], whereas a 57% are persistent non-eosinophilics [174]. Hence, the role of inflammatory cells and pro-inflammatory substances in the characteristic bronchial hyper-responsiveness observed in asthmatics is yet a debate topic. On the other hand, there is also controversy regarding the reliability of the self-applied questionnaires in the diagnosis of asthma [35, 243].

Since broncho-constriction and bronchomotor tone control are mainly mediated by the vagal pathways of the ANS [151, 184], and given the role of the neural control as a modulator of airway inflammation [26], the suspicion that an altered ANS functioning could be an important factor in the pathogenesis of asthma has received widespread research attention for decades. Therefore, several authors have focused on the development of noninvasive approaches for the study of ANS activity in asthmatics. In this context, HRV analysis has raised as a feasible option, and has been employed for the characterization of ANS activity in asthmatic children [80, 178] and adults [131, 287], revealing an increased vagal dominance in response to autonomic tests [80, 131] or during sleep [178, 287]. Moreover, the study of asthmatic subjects classified based on their asthma control suggests a decreased HRV in subjects with uncontrolled asthma [160]. Other works have focused on the respiratory activity, which is also highly influenced by neural control. In this way, a more rapid decay in the inspiratory muscle activity has been reported in subjects with airway obstruction than in healthy controls [64], suggesting that the analysis of the inspiration dynamics may also shed some light on the underlying ANS status in asthmatics. On the contrary, the expiratory activity is more related with the mechanical properties of the respiratory system, and a reduced compliance has been reported in subjects with obstructed airways [241]. Furthermore, respiratory dynamics have been suggested to be altered in asthmatic subjects in response to stress [220] which, together with the aforementioned vagal dominance in response to autonomic tests [80, 131], could be an indicator of an imbalanced autonomic response against demanding scenarios.

Nevertheless, and in spite of the growing evidence of the important role of ANS in asthma, no ANS information is employed in its diagnosis and monitoring. If noninvasive ANS assessment resulted useful for this application, it could complement the clinical routine, so that the evaluation of the asthmatic status of a patient could be performed faster and with less specific equipment, and eventually without a hospital visit. For this reason, the aim of this chapter is twofold. First, to investigate the capability of several cardiorespiratory-derived indexes, which are thought to be related with the ANS and the respiratory system status, to distinguish between subjects classified based on their asthma severity and on their degree of control of the disease, during basal conditions. Second, to evaluate the potential of the considered features for the automatic classification of the subjects.

4.2 Materials and methods

4.2.1 Study population

We recruited 30 adults with diagnosed asthma (the diagnosis was performed attending to the criteria established in the Spanish guidelines for the management of asthma [206]). They belonged to three different asthma severity groups, namely mild asthma (10 subjects), severe asthma with controlled symptoms (9 subjects) and severe asthma with uncontrolled symptoms (11 subjects). The patients were also classified attending to their degree of symptomatology control in controlled asthma (19 subjects) and uncontrolled asthma (11 subjects), attending to the results of a self-applied asthma control test (ACT, controlled asthma if the score of the test was ≥ 20 and uncontrolled asthma otherwise) [266]. All the subjects were requested to remain seated and without talking for a period of 10 minutes, during which multi-lead ECG and respiratory effort (using a respiratory band) were acquired at 1000 and 250 Hz, respectively. Afterwards, they underwent spirometric, skin prick and induced sputum tests, in order to assess airway obstruction, their atopic status and the existence of airway inflammation (when the count of either eosinophils or neutrophils was higher than the reference levels established by *Pin et al.* [204]). Airway obstruction was assessed through the forced expiratory volume in one second (FEV_1), the percentage of FEV_1 with respect to a normalized population ($FEV_{1,\%}$) and the FEV_1 with respect to the forced vital capacity (FEV_1/FVC). Moreover, the fraction of FeNO was assessed, and saliva and blood tests were performed to account for the levels of cortisol and IgE respectively, as well as the existence of peripheral eosinophilia (considered as positive when the blood eosinophils count was higher than 300 per mm^3). Finally, they filled a questionnaire aiming to assess their perceived quality of life (mini asthma quality of life questionnaire, MiniAQLQ [128]). The demographics and clinical parameters of the subjects in the different groups are displayed in Table 4.1. The data acquisition was performed in accordance with the Declaration of Helsinki, being approved by the Ethic Committee of Clinical Investigation of the Santa Creu i San Pau Hospital (Barcelona, Spain). All the subjects provided a signed written informed consent prior to their inclusion in the study, and none of them presented cardiac, neurological or endocrine disease, nor other obstructive disease different from asthma at the time of the study.

4.2.2 Preprocessing

Baseline wanders were extracted from the ECG signals using a low-pass filter (3rd order Butterworth filter with 0.5 Hz cut-off frequency), and they were further subtracted from the original signals. Afterwards, the wavelet-based approach described by *Martínez et al.* [167] was applied for the R peaks detection, and ectopic beat detection and correction was performed according to the method proposed by *Mateo and Laguna* [172] (the number of detected ectopic beats represented a 0.13% of the total number of beats). Regarding the respiratory effort signals, they were band-pass filtered (3rd order Butterworth filter with

Table 4.1: Demographics and clinical parameters of the subjects classified based on their asthma severity and control. The values are displayed as median [25th, 75th percentiles] for the continuous variables (* and † indicate $p < 0.05$ with respect to the mild and severe controlled groups respectively, whereas ** and ‡ indicate $p < 0.017$. On the other hand, # indicates $p < 0.05$ between the controlled and the severe uncontrolled groups. BMI: body mass index, Eos: eosinophilia, Inflam: upper airway inflammation.)

	Controlled		Severe uncontrolled
	Mild	Severe controlled	
N (#)	19		11
	10	9	
Age (years)	50.00 [39.50, 58.50]		49.00 [42.75, 63.25]
	50.00 [41.00, 51.00]	53.00 [38.50, 61.00]	
Sex (Male/Female)	11 / 8		2 / 9 [#]
	6 / 4	5 / 4	
BMI (kg/m ²)	26.40 [23.85, 27.75]		30.00 [25.25, 33.50] [†]
	26.85 [23.30, 28.90]	24.00 [23.50, 26.93]	
Atopy (Yes/No)	16 / 3		8 / 3
	9 / 1	7 / 2	
FEV ₁ (liters)	3.20 [2.40, 3.63]		2.00 [1.72, 2.29] ^{**‡, #}
	3.40 [2.40, 3.63]	3.19 [2.15, 3.64]	
FEV _{1,5%} (%)	91.00 [84.25, 96.50]		87.00 [57.50, 91.25] ^{*, #}
	96.00 [87.00, 100.00]	89.00 [83.75, 92.50]	
FEV ₁ /FVC (%)	73.00 [65.50, 76.00]		56.00 [50.75, 74.00] [*]
	75.00 [73.00, 78.00]	67.00 [56.00, 73.00] [*]	
FeNO (ppb)	27.00 [20.75, 34.50]		41.00 [22.25, 87.88]
	24.65 [18.00, 32.00]	28.00 [22.25, 35.25]	
ACT	24.00 [21.00, 25.00]		18.00 [14.50, 19.00] ^{**‡, #}
	23.50 [22.00, 25.00]	24.00 [23.00, 25.00]	
MiniAQLQ	6.60 [6.40, 6.80]		5.20 [3.43, 5.45] ^{**‡, #}
	6.65 [6.40, 6.80]	6.50 [5.10, 6.80]	
Peripheral Eos (Yes/No)	7 / 12		6 / 5
	4 / 6	3 / 6	
IgE (UI/ml)	131.00 [59.50, 209.00]		204.00 [28.83, 478.75]
	109.00 [64.00, 287.00]	131.00 [51.30, 203.00]	
Inflam (Yes/No)	4 / 15		3 / 8
	2 / 8	2 / 7	
Cortisol (pg/ml)	860.00 [522.50, 1212.50]		655.00 [491.30, 1670.00]
	577.50 [530.00, 1190.00]	925.00 [475.00, 1357.50]	

0.05-1 Hz cut-off frequencies) in order to discard the baseline and those components that are not expected to be related with respiration, and they were downsampled at 4 Hz. In all the cases, forward-backward filtering was applied for preserving the morphology of the signal.

4.2.3 HRV analysis

\overline{NN} , SDNN, SDDSD, RMSSD and pNN50 were computed from the RR interval series following ectopic correction, according to the *Task Force* [252]. The analysis was performed in five-minute windows, with four-minute overlap, and each subject was characterized by the median value of each parameter in the different time windows.

Regarding the frequency-domain HRV analysis, the modulating signal, $m(n)$, was estimated using the TVIPFM model [19] and resampled at 4 Hz (see Ch. 2.2). An *a priori* analysis of the respiratory rate revealed that it was lower than or slightly above 0.15 Hz in a 13 % of the subjects. Since 0.15 Hz represents the lower limit of the HF band traditionally employed in the frequency-domain HRV analysis [252], when the main components of the respiratory modulation of the HR fall below this limit there is an overestimation of the LF and an underestimation of the HF contributions of HRV. Moreover, the power content in the HF band is assumed to be originated by the respiratory modulation of the HR, so that the interpretation of the frequency components within this band, when the respiratory contribution lays outside it, remains an open debate [36]. Therefore, the respiratory-related and residual components of $m(n)$ were obtained using the orthogonal subspace decomposition (OSP) approach [264] described in Ch. 2.6.2. The spectra of both components, $\hat{S}_{\text{resp}}(F)$ and $\hat{S}_{\text{resid}}(F)$, were estimated in five-minute windows with four-minute overlap, using the Welch's periodogram (50 s windows, 50% overlap). An example of an spectrum before and after the OSP decomposition is displayed in Fig. 4.1. Afterwards, the non-respiratory related HRV power, $P_{\text{resid}}^{\text{LF}}$, was obtained as the power content of $\hat{S}_{\text{resid}}(F)$ within the LF band, whereas the respiratory-related power, P_{respir} , was computed as the power of $\hat{S}_{\text{resp}}(F)$ within the $[0.04, \overline{\text{HR}}/2]$ Hz band, where $\overline{\text{HR}}$ represents the mean HR expressed in Hz. Finally, the ratio $\text{SB}_u = P_{\text{resid}}^{\text{LF}}/P_{\text{respir}}$ was calculated as an unconstrained measurement of the sympathovagal balance [264]. All the described indexes were calculated from the spectra corresponding to each five-minute window.

4.2.4 Respiration dynamics analysis

The respiratory effort signals were analyzed in the time domain as follows. First, the peak, nadir and the points with the maximum upslope and downslope within each breath were detected (see Fig. 4.2). Afterwards, the breaths were delineated, and the onset and offset of each breath were detected as the time instants at which the derivative of each breath has reached a 20% of its maximum or minimum value respectively. The time difference between the peaks of two consecutive breaths (breath-to-breath interval, BB), between the onset of each breath and its peak (duration of inspiration, T_{insp}), between the peak of each breath and its offset (duration of expiration, T_{exp}) and between the offset of each breath and its nadir (T_{idle} , accounting for the time that passes from the end of an expiration to the beginning of the next inspiration) were used as features for characterizing the morphology of the respiratory effort signals. Also the ratio between T_{insp} , T_{exp} and T_{idle} with respect to BB, the ratio between T_{insp} and T_{exp} , and the time (Δt_s) and amplitude (ΔA_s) difference between the points with maximum upslope and downslope were considered.

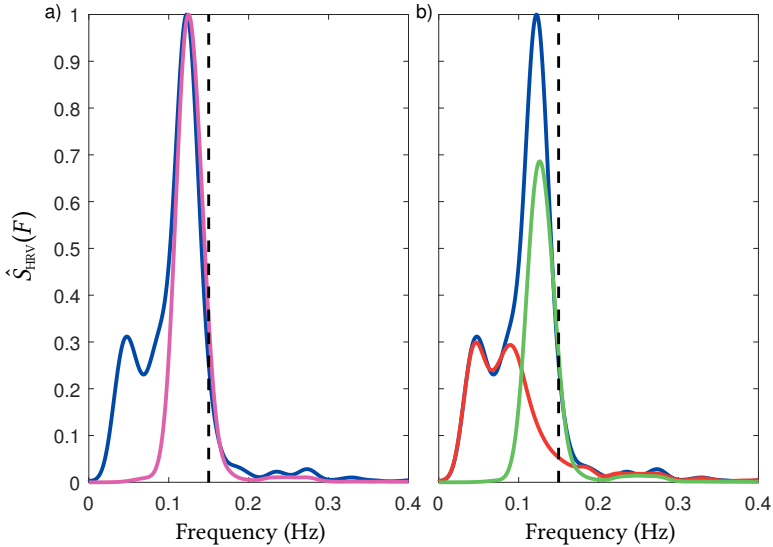


Figure 4.1: a) Normalized power spectral density of the modulating signal (blue) and the respiratory effort (pink) in a five-minute segment. Note that the respiratory activity lays below 0.15 Hz (black dashed line). b) Orthogonal subspace projection was applied to separate the respiratory-related (green) and -unrelated (red) components of the modulating signal.

A schematic exemplifying the definition of the aforementioned features is depicted in Fig. 4.2.

4.2.5 Statistical analysis

The temporal median of all the time and frequency domain HRV parameters, as well as from the time-domain respiratory indexes, was obtained for each subject. Normality of the data was rejected using a Kolmogorov-Smirnov test, so that a Wilcoxon rank-sum test was applied in order to assess the differences between groups. The statistical significance threshold was set to $p = 0.05$ and when the comparison was between more than 2 groups, Bonferroni correction was applied.

Additionally to the univariate analysis, several machine learning algorithms were applied, in order to explore the potential of the described features to classify the asthmatic patients in the different groups. The feature selection and classification approaches used for this purpose are described below.

4.2.6 Automatic stratification

First, feature importance was computed using the out-of-bag permuted predictor importance algorithm [48], using a random forest with 400 decision trees. After training each tree using a random subset of patients (bagging), their accuracy was computed on

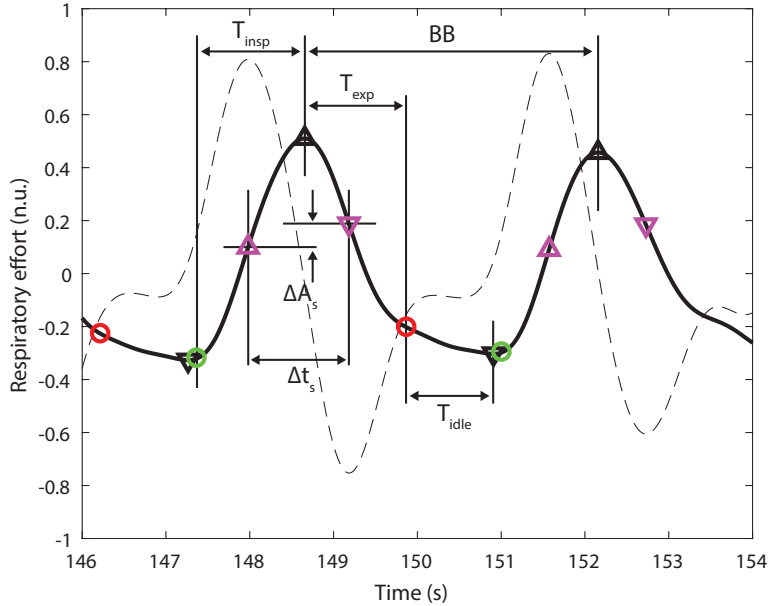


Figure 4.2: A segment of a respiratory effort signal (solid line) and its derivative (dashed line) are displayed, together with the definition of the parameters used for the characterization of the respiratory dynamics. The delineation of a given breath is shown, so that the black facing-up and -down triangles represent its peak and nadir, the pink facing-up and -down triangles mark the points of maximum up and downslope and the green and red circles indicate its onset and offset, respectively.

the remaining data (out-of-bag examples). Then, the importance of a given feature was quantified by comparing the resulting accuracy of each tree with the accuracy achieved when the values of the feature under evaluation were randomly permuted. This process was repeated for all the trees where this feature was employed, and the feature importance was computed as the mean of the differences between the accuracies before and after the random permutation divided by its standard deviation.

Those features with an almost negligible importance (< 0.05) were discarded, and the remaining were considered as candidates for building a classification model. When two features were highly correlated (Pearson correlation coefficient higher than 0.75) the one with lower feature importance was discarded. A different model was constructed for classifying the subjects based on their degree of asthma control or to their asthma severity, and six different approaches were tested, namely logistic regression (LR), k nearest neighbors (kNN) and support vector machines (SVM). For the SVMs, linear, quadratic, cubic and radial basis function (RBF) kernels were considered. For each type of classifier, feature selection was addressed using a greedy forward algorithm, maximizing the F1 score of the minority class in the case that the classification is performed according to the level of asthma control, and maximizing the total accuracy when asthma severity was considered. In order to avoid overfitting, leave-one-patient-out cross-validation was combined with bootstrapping [78], following the methodology in [44], as depicted in Fig. 4.3 ($K_{train} = 10000$ was employed, being K_{train} the number of folds used in the

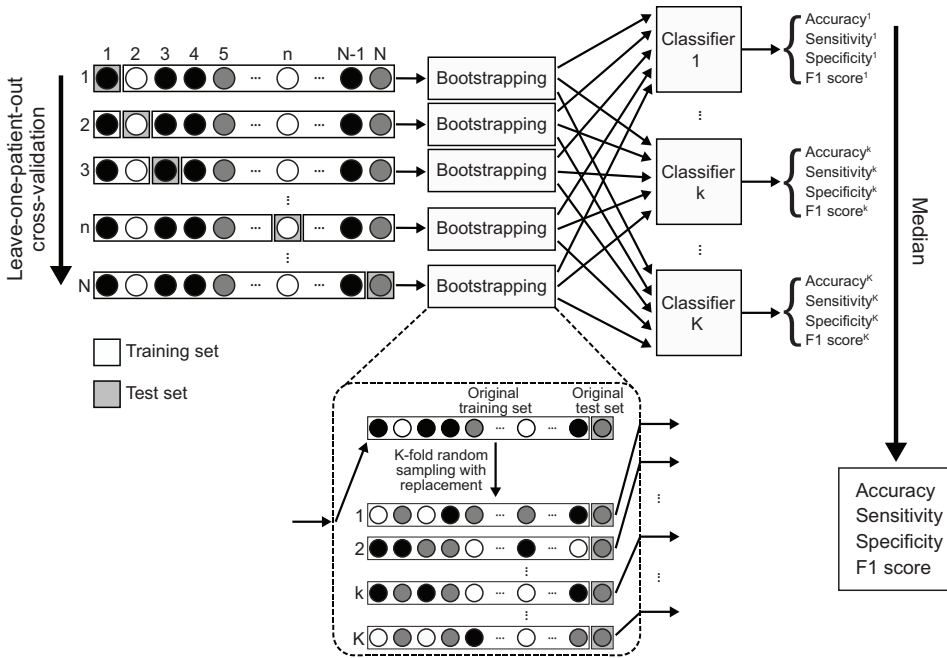


Figure 4.3: A schematic of the combination of the leave-one-patient-out cross-validation with bootstrapping is displayed. The circles represent the subjects in the dataset (N subjects) whereas their color represent that they belong to different groups. After defining a training (white rectangle) and a test (gray square) set, bootstrapping is applied K times to obtain K different training sets. Then, the median of the performance of the K classifiers is used as a robust measure of the performance of the tested classification model.

bootstrapping, which is different from the number of folds of the leave-one-patient-out cross-validation), and the maximum number of features was restricted to the square root of the number of subjects in the minority group (i.e., to 3). Afterwards, the leave-one-patient-out cross-validation and bootstrapping were repeated for constructing a model and testing the performance of the features selected for each classifier (with $K_{\text{test}} = 100$ in this case). The number of neighbors in the k NN algorithm was set to 7.

This process was repeated considering only the clinical variables, the cardiorespiratory-derived features, and both of them simultaneously, so that the performance of the three approaches can be compared.

4.3 Results

The indexes that yielded to statistically significant differences among groups are displayed in Table 4.2. Those parameters were able to distinguish between controlled and uncontrolled asthma, and also between mild and severe uncontrolled asthma. Additionally, $p\text{NN}50$ and P_{resid} also differed between severe controlled and severe uncontrolled asthma.

Table 4.2: Median [25th, 75th percentiles] of the parameters that were significantly different among groups. (* and † indicate $p < 0.05$ with respect to the mild and severe controlled groups respectively, whereas ** and ‡ indicate $p < 0.017$. On the other hand, # indicates $p < 0.05$ between the controlled and the severe uncontrolled groups.)

	Controlled		Severe uncontrolled
	Mild	Severe controlled	
SDNN (ms)	37.51 [29.41, 46.15]		23.46 [20.92, 27.41]**,#
	40.06 [34.63, 42.60]	29.88 [24.74, 56.44]	
SDSD (ms)	18.10 [16.15, 32.53]		13.94 [10.29, 15.64]*,#
	18.10 [16.09, 22.40]	18.85 [14.03, 32.66]	
RMSSD (ms)	18.08 [16.13, 32.48]		13.92 [10.28, 15.61]*,#
	18.08 [16.07, 22.38]	18.83 [14.01, 32.61]	
pNN50 (%)	0.84 [0.45, 10.84]		0.00 [0.00, 0.55]**,†,#
	0.84 [0.45, 5.24]	0.65 [0.35, 12.16]	
TP (a.u. $\times 10^{-3}$)	13.65 [6.49, 16.65]		4.85 [2.61, 5.73]*,#
	7.80 [6.49, 15.56]	15.60 [6.27, 16.96]	
P _{resid} (a.u. $\times 10^{-3}$)	5.67 [3.78, 9.94]		2.02 [1.55, 3.22]*,†,#
	4.17 [3.78, 6.85]	8.07 [3.60, 9.94]	
P _{resp} (a.u. $\times 10^{-3}$)	2.66 [1.37, 5.26]		0.85 [0.27, 1.70]**,#
	2.66 [2.02, 5.36]	3.48 [0.86, 5.74]	

In Table 4.3, the results of the classification attending to the degree of asthma control are displayed. The best performance, as measured by the F1 score, was achieved when using the LR classifier in the case of considering all the available features, and with the k NN classifier when using only the cardiorespiratory ones (although in the latter case best accuracy was also obtained with the LR classifier). The use of all the available parameters resulted in an increased performance than employing only the cardiorespiratory ones, with an increase in the accuracy ranging from a 5 to a 16%. Nevertheless, in some of the classifiers, the inclusion of cardiorespiratory features outperformed the use of only clinical features (see Table 4.3), reaching an accuracy of almost a 77% in the case of the SVM with cubic kernel. With respect to the classification performance based on asthma severity, in Fig. 4.4 it can be noticed that the combination of the cardiorespiratory and clinical features resulted in a similar performance than when using any of them separately, except for the SVM with cubic and RBF kernels, when the feature combination outperformed the other options. Whereas the F1 score was similar for the groups with mild and severe controlled asthma, it was much higher for the uncontrolled asthma group in all the tested classifiers.

Regarding the feature selection, FEV₁, FEV_{1,%} and IgE were the most frequently selected clinical features (IgE was closely followed by FeNO), whilst SDNN, P_{resid} and P_{resp} were the most relevant cardiorespiratory features (see Table 4.4). None of the parameters

Table 4.3: Median [25th, 75th percentiles] of the accuracy, sensitivity, specificity and F1 score obtained with the different classification algorithms when the subjects were classified based on their degree of asthma control. The sensitivity, specificity and F1 score were computed considering the uncontrolled asthma group as the positive class. The results correspond to the case of combining cardiorespiratory and clinical features, or using any of them separately.

		Acc. (%)	Sens. (%)	Spec. (%)	F1
LR	All	80.00 [76.67, 83.33]	72.73 [72.73, 81.82]	84.21 [78.95, 89.47]	0.75 [0.70, 0.78]
	Clin	80.00 [76.67, 83.33]	72.73 [72.73, 81.82]	84.21 [78.95, 89.47]	0.75 [0.70, 0.78]
	HRV	70.00 [63.33, 73.33]	54.55 [54.55, 63.64]	73.68 [68.42, 78.95]	0.57 [0.52, 0.64]
kNN	All	73.33 [70.00, 76.67]	72.73 [63.64, 81.82]	73.68 [68.42, 78.95]	0.67 [0.61, 0.72]
	Clin	70.00 [66.67, 73.33]	54.55 [54.55, 63.64]	78.95 [73.68, 84.21]	0.60 [0.52, 0.67]
	HRV	68.33 [63.33, 73.33]	63.64 [54.55, 72.73]	68.42 [68.42, 73.68]	0.61 [0.55, 0.67]
SVM (linear kernel)	All	80.00 [76.67, 83.33]	63.64 [63.64, 72.73]	89.47 [84.21, 94.74]	0.70 [0.67, 0.74]
	Clin	80.00 [76.67, 83.33]	63.64 [63.64, 72.73]	89.47 [84.21, 94.74]	0.70 [0.67, 0.74]
	HRV	65.00 [60.00, 70.00]	54.55 [45.45, 63.64]	73.68 [68.42, 78.95]	0.52 [0.43, 0.61]
SVM (quadratic kernel)	All	80.00 [76.67, 83.33]	63.64 [54.55, 63.64]	89.47 [89.47, 94.74]	0.70 [0.63, 0.74]
	Clin	80.00 [76.67, 83.33]	63.64 [54.55, 63.64]	89.47 [89.47, 94.74]	0.70 [0.63, 0.74]
	HRV	63.33 [60.00, 70.00]	54.55 [45.45, 63.64]	68.42 [63.16, 73.68]	0.55 [0.48, 0.61]
SVM (cubic kernel)	All	76.67 [73.33, 80.00]	63.64 [54.55, 72.73]	89.47 [84.21, 89.47]	0.67 [0.60, 0.73]
	Clin	66.67 [63.33, 73.33]	54.55 [45.45, 63.64]	78.95 [73.68, 78.95]	0.55 [0.45, 0.64]
	HRV	63.33 [60.00, 70.00]	54.55 [45.45, 63.64]	68.42 [68.42, 73.68]	0.51 [0.48, 0.60]
SVM (RBF kernel)	All	80.00 [73.33, 83.33]	54.55 [54.55, 63.64]	89.47 [84.21, 94.74]	0.67 [0.60, 0.71]
	Clin	80.00 [73.33, 83.33]	54.55 [54.55, 63.64]	89.47 [84.21, 94.74]	0.67 [0.60, 0.71]
	HRV	66.67 [63.33, 73.33]	54.55 [45.45, 63.64]	78.95 [73.68, 78.95]	0.55 [0.45, 0.64]

Table 4.4: Features selected for each of the classification approaches and methodologies, when considering all the features or only the clinical or cardiorespiratory ones separately. When the classification was performed attending to the asthma control, the criteria for the feature selection algorithm was to maximize the F1 score of the uncontrolled group. When the classification was based on the asthma severity, the total accuracy was maximized.

		Asthma Control	Asthma Severity
LR	All	{FEV ₁ , FeNO, IgE}	{FEV ₁ }
	Clinical	{FEV ₁ , FeNO, IgE}	{FEV ₁ }
	HRV	{SDNN, P _{resid} }	{SDNN, P _{resid} }
kNN	All	{SDSD, P _{resp} , FEV ₁ }	{SDNN, P _{resid} }
	Clinical	{FEV ₁ , FEV _{1.5} }	{FEV _{1.5} , FEV ₁ /FVC, FeNO}
	HRV	{SDNN, P _{resid} }	{SDNN, P _{resid} }
SVM (linear kernel)	All	{FEV ₁ , FEV _{1.5} , IgE}	{FEV ₁ }
	Clinical	{FEV ₁ , FEV _{1.5} , IgE}	{FEV ₁ }
	HRV	{SDNN, P _{resid} , P _{resp} }	{SDNN, P _{resp} }
SVM (quadratic kernel)	All	{FEV ₁ , FEV _{1.5} , IgE}	{pNN50, FEV ₁ }
	Clinical	{FEV ₁ , FEV _{1.5} , IgE}	{FEV _{1.5} , FEV ₁ /FVC}
	HRV	{SDNN, P _{resid} }	{SDNN, P _{resid} }
SVM (cubic kernel)	All	{SDNN, FEV _{1.5} , FeNO}	{SDNN, FEV _{1.5} , FeNO}
	Clinical	{FEV _{1.5} }	{FEV _{1.5} }
	HRV	{SDNN, P _{resid} }	{SDNN, P _{resid} }
SVM (RBF kernel)	All	{FEV ₁ , FEV _{1.5} , IgE}	{SDNN, P _{resid} , FEV _{1.5} }
	Clinical	{FEV ₁ , FEV _{1.5} , IgE}	{FEV _{1.5} , FEV ₁ /FVC, FeNO}
	HRV	{SDNN, P _{resid} }	{SDNN, P _{resid} }

extracted from the respiration dynamics analysis was able to distinguish among groups, nor were they selected as features for any of the classification models.

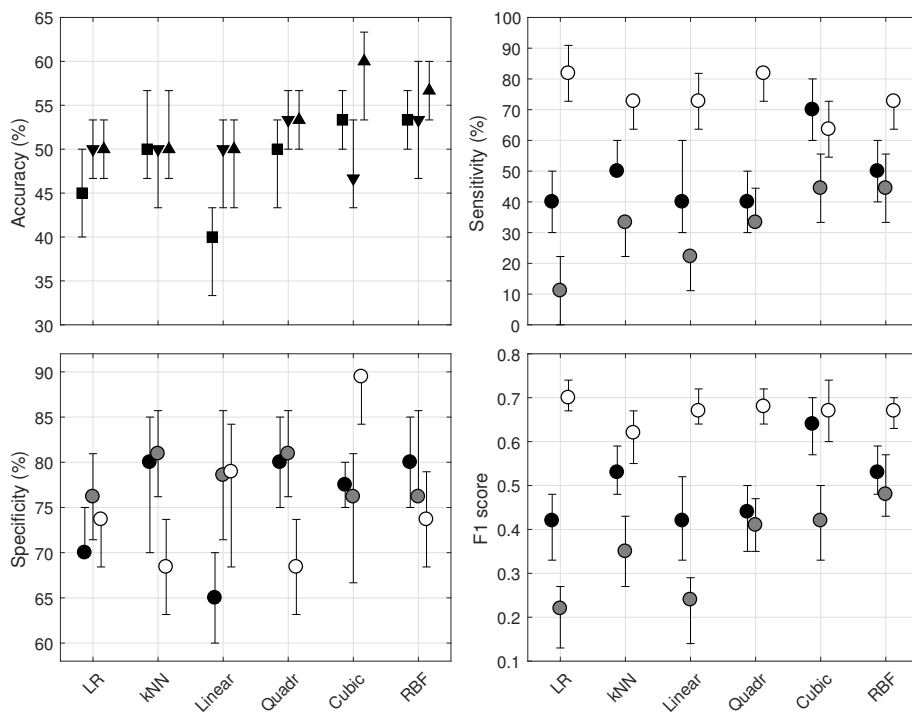


Figure 4.4: The accuracy, sensitivity, specificity and F1 score obtained with the different classifiers when the patients were classified based on their asthma severity are displayed. In the case of the accuracy, the squares represent the values obtained when only the cardiorespiratory features were consider in the model, whereas the down-facing triangles account for the results when only the clinical parameters were used and the up-facing triangles represent the performance when all the features were used together. In the other cases, the black, gray and white circles represent the values obtained for the mild, severe controlled and severe uncontrolled groups respectively, when all the features were employed. Linear, quadr, cubic and RBF refer to the kernels employed in the SVM classifier (see text for details).

4.4 Discussion

ANS is acknowledged as a modulator of lower airway inflammation [26] and control [151, 184]. Therefore, the altered autonomic activity [80, 131, 178, 287] and respiratory dynamics [64, 220, 241] observed in asthmatics and subjects with lower airway obstruction suggest an important relationship between ANS and the pathogenesis of asthma. In this chapter, we aimed at evaluating the capability and added value of ANS assessment in the stratification of asthmatic subjects. ANS was assessed from time- and frequency-domain HRV analyses, as well as from respiratory effort dynamics. However, a preliminary analysis of the respiratory rate revealed that it was lower than or very close to 0.15 Hz in some subjects, which remains the lower limit of the HF band traditionally employed in frequency-domain HRV analysis [252]. For this reason, the HRV signals were decomposed in their respiratory-related and -unrelated components, so that they can be still analyzed. The OSP algorithm was used for the decomposition, given its performance

in previous works [264]. Although it is a linear method which does not consider some nonlinearities that may be relevant [264], it shows to be sufficient for the proposed task.

Regarding the results displayed in Table 4.2, a reduction in the sympathetic (P_{resid}) and vagal (SDSD, RMSSD, pNN50 and P_{resp}) components of HRV, as well as in the total HRV (SDNN, TP), was obtained in the uncontrolled asthma with respect to the controlled asthma group, in concordance with previous studies [160], and also in the severe uncontrolled asthma compared with the mild asthma group. In the case of severe controlled asthma, higher values of all the indexes than in the other two groups were obtained, except for SDNN and pNN50, which showed a decreasing tendency with increasing asthma severity. Although these results appear to be contradictory with previous works reporting increased vagal activity in asthmatics [80,131,178,287], in these studies they evaluated the autonomic activity in response to autonomic tests or during sleep (which represents a state of increased vagal dominance), whilst in the present study the signal acquisition was performed during basal conditions. In this way, it is possible that asthmatic subjects present a decreased autonomic control during rest, but their vagal pathways respond exaggeratedly to certain stimuli, yielding to the hyper-responsiveness characteristic of asthma [90]. The fact that larger values were generally obtained for the severe controlled group could be related with the higher intra-class variability observed in the features of this group, although provided the existing differences between mild and severe uncontrolled, and between controlled and uncontrolled asthmatics, it is possible that the selected features are more representative of the degree of symptoms control than of the severity of the disease itself. Nevertheless, a lower relative number of males and an increased median body mass index (BMI) were assessed in the uncontrolled asthma group (see Table 4.1). Whereas males usually present increased sympathetic and decreased vagal tone than females [12], a high BMI has been related with decreased HRV [254], which could compromise the interpretation of the HRV analysis in this group. However, P_{resp} was lower instead of higher in the uncontrolled asthma group, and the BMI was uncorrelated with all the HRV measurements, suggesting that the differences in ANS activity between controlled and uncontrolled asthmatics may be due to other causes than gender or obesity. Since the age range was very similar among groups, the reductions in the cardiorespiratory interactions due to aging were not considered here.

Interestingly, and in spite of a consistent decrease in FEV_1/FVC and an increase in FeNO and IgE with asthma severity or poor symptoms control, the only clinical parameters that were able to distinguish between the degree of symptomatology control were the FEV_1 and $FEV_{1,\%}$ (and the ACT and the MiniAQLQ questionnaires, which remain the gold standards in this classification criterion). On the other hand, and despite the different airway condition of the various groups (as measured from FEV_1 , $FEV_{1,\%}$ and FEV_1/FVC), the analysis of the respiratory effort dynamics did not succeed in distinguishing between any pair of groups. It is possible that these features do not reliably represent the airway status during resting conditions so that spirometric maneuvers are required. Nevertheless, and although previous studies suggest that the respiratory dynamics of asthmatic subjects are altered in response to stress [220] and that inspiratory muscle activity differs in the presence of airway obstruction [64], the proposed respiration dynamics features

were not able to distinguish between groups. Therefore, it is possible that these differences are not that clear among asthma categories than when comparing asthmatic and healthy subjects, although the possibility that the underlying respiration control is not accurately reflected by the proposed indexes should be considered.

Additionally, we tested the capability of several classifiers to correctly classify the patients based on their asthma control or severity. The feature selection process described above was repeated three times: once using only the clinical features, another using only cardiorespiratory-derived ANS features, and a third time combining both. Whereas the clinical features appeared to be more important in the classification regarding asthma control (although the cardiorespiratory features were also considered in some classifiers), in the case of the classification attending to asthma severity the cardiorespiratory features were included in 4 out of the 6 tested classifiers (see Table 4.4). In the latter case, the use of the ANS-related features resulted in an increased or similar performance than when only clinical features were employed (see Fig. 4.4). The best performance was achieved when using the LR classifier when the classification was based on the asthma control, whereas best results were obtained with the SVM with cubic or RBF kernels when it was based on asthma severity. It is possible that, given the more complex classification scheme when attending to asthma severity, and provided that the HRV features had a higher added value than in the case of asthma control, nonlinear classifiers are required to better exploit the complex interaction among the clinical and the HRV features. The most selected HRV features independently of the target classes or the classifier were SDNN, P_{resid} and P_{resp} , thus suggesting that not only the total HRV, but also the independent contribution of the sympathetic and the vagal branches of the ANS are important for patient stratification. Regarding the clinical features, FEV_1 , $FEV_{1,\%}$ and IgE were the most selected. It is important to highlight that, when the classification was based on asthma severity, the best results were achieved for the severe uncontrolled asthma group (as displayed in Fig. 4.4), which remains the group with a worse prognosis. Also the generally reduced sensitivity achieved in the classification of the severe controlled asthma group (see Fig. 4.4) is worth noticing. As aforementioned, the decreased performance of the selected features in this group could indicate that they are reflecting differences in the degree of asthma control, rather than in the disease severity. However, a careful analysis of the confusion matrices obtained for the different classifiers did not reveal a particular bias in the misclassification of the severe controlled asthmatics towards any of the other groups.

The use of ANS-derived information has some desirable properties. First, it is very noninvasive in nature, and can be acquired in a continuous manner, without requiring a visit to the hospital. Moreover, it is important to take into account that the clinical parameters were used for stratifying the subjects initially [206], which might result in an over-fitting for those features, whereas ANS assessment provides new information that could complement the current clinical practice.

There are also some limitations that should be considered when interpreting the results of this chapter. First, the dataset is composed by a small number of subjects, and it

is imbalanced regarding the classification based on the control of the symptoms. In order to reduce the impact of the low amount of data, we adopted the classification approach presented in [44], consisting of a combination of leave-one-patient-out cross-validation and bootstrapping. With this methodology, the performance for each subject was tested in several different classifiers that had been trained with different subsets of the original dataset, and the median performance of all the classifiers can be regarded as a much more robust measurement than if only leave-one-patient-out cross-validation was applied. The reduced number of subjects in the minority class also limited the maximum number of features to be considered in the classifiers, so that over-fitting is minimized. Additionally, the cardiorespiratory-derived features were extracted from only 10 minutes of ECG and respiratory effort recordings, so that they represent the instantaneous ANS status of each subject, and not an average ANS condition, which could be responsible of the increased intra-class variability observed in the features of the severe controlled asthma group (see Table 4.2). However, the subjects were requested to remain seated and without talking for some minutes prior to the biosignals acquisition, so that the most possible basal state was considered. On the contrary, the use of 10-minute recordings also constitutes a strength of this study, since it represents a low time-consuming test which, given its noninvasive nature, could eventually be realized without needing to attend to the clinic. Nonetheless, evaluation in larger datasets is required, and the assessment of the autonomic response of the subjects to different autonomic tests would probably contribute to improve the classification performance.

4.5 Conclusion

Noninvasive ANS assessment has been presented as a potential tool for asthma control and severity stratification. On one hand, the univariate analysis of the cardiorespiratory-derived features revealed a reduced HRV in uncontrolled with respect to controlled asthmatics, and in severe uncontrolled with respect to mild asthmatics. On the other hand, the inclusion of ANS information in the classification of the subjects attending to their asthma severity resulted in a similar performance than using only clinical features, outperforming them in some cases. In this way, ANS assessment through noninvasive cardiorespiratory signals analysis could represent a useful complement in the monitoring and diagnosis of asthma.

5

HRV analysis in sleep apnea syndrome with associated cardiovascular diseases

5.1 Motivation	5.2.8 Statistical methods
5.2 Materials and methods	5.3 Results
5.2.1 UZ Leuven dataset	5.3.1 UZ Leuven dataset
5.2.2 Sleep Heart Health Study dataset	5.3.2 SHHS dataset
5.2.3 Preprocessing	5.4 Discussion
5.2.4 HRV analysis	5.4.1 UZ Leuven dataset
5.2.5 Effect of sleep stages on HRV	5.4.2 SHHS dataset
5.2.6 Effect of apneas, hypopneas and arousals on HRV	5.4.3 Limitations
5.2.7 Effect of medication	5.5 Conclusion

5.1 Motivation

Sleep apnea syndrome (SAS) is a complex sleep-related breathing disorder characterized by a repetitive total (apnea) or partial (hypopnea) upper-airway collapse (obstructive sleep apnea, OSA), an absence of respiratory drive (central sleep apnea, CSA) or a combination of both (mixed sleep apnea). During an OSA episode, forced inspiration against an obstructed upper airway leads to exaggerated negative intrathoracic pressure

and is accompanied by immediate hypoxia, which triggers a complicated autonomic response [245] and large fluctuations in blood pressure [202] and HR [54, 150]. The apneic episode is often stopped by the arousal of the subject, thus resulting in a fragmented sleep. Combination of all these effects has been closely related with excessive daytime sleepiness, chronic hypertension and increased mortality [245]. Moreover, SAS has been related with a 5-fold increase in the risk for developing cardiovascular diseases (CVD), which could rise to 11-fold if not conveniently treated [198]. In this way, SAS represents a well known cause of secondary systemic and pulmonary hypertension, and a significant risk factor for coronary artery disease, cardiac arrhythmias and heart failure [255, 282]. Analogously, some CVD such as heart failure, atrial fibrillation or stroke may exert a negative effect in SAS, as a deficient blood conduction could lead to a dysregulation of PaCO₂ and hence trigger CSA episodes [136].

Notwithstanding the characteristic physiological response to an apneic episode shared by most of the patients, only some of them will develop CVD. Since altered HRV has been independently related to both conditions, HRV analysis has attracted widespread interest in the field of SAS (almost 200 publications in PubMed search including the key words heart rate variability and apnea, considering only the last 5 years). In this context, HRV analysis has revealed altered sympathovagal balance during sleep in subjects suffering from moderate or severe SAS when compared with healthy controls [111, 199]. Also 24-hour monitoring suggests altered autonomic control in SAS patients [15], which reflects in an increased sympathetic dominance. Moreover, many physiological (e.g.: hypertension, diabetes) and psychosomatic (e.g.: stress, depression) conditions that constitute risk factors for CVD development, have also been related with altered HRV and sympathovagal balance [254]. Hence, HRV analysis could shed some light on the role of ANS in the interaction between SAS and CVD.

Whereas polysomnographic (PSG) recordings remain the gold standard for the diagnosis of SAS, it would be interesting to dispose of a simple tool for the early identification of patients at cardiovascular risk, thus improving their screening and prioritizing their treatment. If there was a relationship between ANS activity, SAS and CVD, HRV could represent such a tool. Nevertheless, previous works aiming to characterize ANS activity in SAS patients using HRV analysis usually include the apneic episodes [15, 111, 199], so that the increased sympathetic dominance observed in SAS could be biased by the sympathetic activation taking place in response to an apnea, and might not reflect the baseline state of the ANS in these subjects.

For these reasons, the aim of the present chapter is twofold: first, to evaluate whether imbalanced autonomic activity could be related with CVD in SAS. Second, to investigate whether HRV analysis could be a useful tool for the early stage identification and screening of SAS patients at cardiovascular risk.

5.2 Materials and methods

Two independent databases were analyzed in this chapter, namely the UZ Leuven and the Sleep Heart Health Study datasets. The former was employed for assessing differences in ANS activity between patients suffering from SAS or SAS plus additional cardiac comorbidities. The latter was used to verify if altered ANS control can be assessed in subjects with SAS who will be latter diagnosed with cardiovascular comorbidities. Both datasets are described below.

5.2.1 UZ Leuven dataset

It is composed of 100 subjects (78 male, 22 female) who were referred to the sleep laboratory of the University Hospital Leuven (UZ Leuven, Leuven, Belgium) because of suspicion of SAS. PSGs were acquired, revised and annotated by sleep specialists according to the AASM 2012 scoring rules [39]. Sleep annotations included a classification of the recording period in rapid eye movement (REM) sleep and three non-REM stages (NREM1-NREM3), as well as the time occurrence and duration of each apneic/hypopneic episode and arousal. Sleep stage annotations were available for each 30-second epoch during the whole recording. In this study no difference was made between light and deep NREM sleep, so that the sleep stage classification was reduced to REM and NREM sleep. Only subjects with an apnea/hypopnea index (AHI) greater or equal than 15 were included. Bipolar ECG (lead II) and thoracic respiratory effort (recorded through respiratory inductive plethysmography) signals were acquired with a sampling frequency of 500 Hz.

The database consists of:

- 50 control patients without cardiac comorbidities (previous myocardial infarction, objective coronary disease, revascularization or stroke) and without cardiovascular risk factors (hypertension, hyperlipidemia, diabetes), and
- 50 patients with cardiac comorbidities or cardiovascular risk factors.

Subjects in both groups were matched in age (47.8 ± 10.9 years), gender (78 males, 22 females), body mass index (BMI, 30.0 ± 4.5 kg/m²) and smoking habits (24 habitual smokers at the time of the recordings). The average AHI was 41.3 ± 22.0 , and the average recording duration was 09:02:33 (hh:mm:ss). Demographics of each group are summarized in Table 5.1, where also the different medications used by the cardiac comorbidity group are indicated. Data acquisition was carried out in accordance with the recommendations of the Commissie Medische Ethiek UZ KU Leuven, and the protocol was approved by it (ML 7962). All subjects gave written informed consent in accordance with the Declaration of Helsinki.

Table 5.1: Anthropometric data of the UZ Leuven dataset. In the cardiac comorbidity group, subjects under medication intake can be treated with various distinct drugs simultaneously. (BMI: Body Mass Index, AHI: Apnea Hypopnea Index, ACE: Angiotensin Converting Enzyme.)

	Control	Cardiac comorbidity	Total
Number of patients	50	50	100
Age (years)	47.3 ± 10.5	48.2 ± 11.4	47.8 ± 10.9
Gender (male/female)	39 / 11	39 / 11	78 / 22
BMI (kg/m²)	29.9 ± 4.6	29.8 ± 4.4	30.0 ± 4.5
AHI	39.8 ± 23.3	42.7 ± 21.1	41.3 ± 22.0
Active smokers	12	12	24
Medication intake	0	33	33
• <i>β-blockers</i>	0	22	22
• <i>Ca channels inhibitors</i>	0	8	8
• <i>ACE inhibitors</i>	0	12	12
• <i>Diuretics</i>	0	4	4
• <i>Antidepressants</i>	0	1	1

5.2.2 Sleep Heart Health Study dataset

The Sleep Heart Health Study (SHHS) was conducted by the National Heart Lung & Blood Institute in order to assess the negative cardiovascular effects induced by sleep-disordered breathing in general population [211]. Acquisition was performed in two different sessions: a baseline session and a follow up session, performed 3 to 8 years after the baseline session. Despite the database is very extensive, we only considered a subset of individuals who were appropriate for the purpose of this study. Specifically, we were interested in those subjects who did not present any cardiac comorbidity or cardiovascular risk factor (the same ones than in the UZ Leuven dataset) at the baseline recording, but developed any of them afterwards. Conditions for inclusion were: baseline and follow up recordings available, no cardiac comorbidities or cardiovascular risk factors at baseline and subjects younger than 65 years, so that both databases were as similar as possible.

Thirty-three subjects satisfied the above mentioned criteria and suffered from a cardiac event at any point after the baseline session, so they were labeled as cardiovascular event group. Cardiac events considered for inclusion in this group were any of the following: myocardial infarction, stroke, revascularization, congestive heart failure, coronary artery disease and procedures related with any of the previous conditions. Afterwards, one control subject without cardiac comorbidities or cardiovascular risk factors (control group) and one subject who developed cardiovascular risk factors (hypertension, hyperlipidemia or/and diabetes) at any point after the baseline session (cardiovascular risk group) were matched to each subject in the cardiovascular event group, so that a final subset of 99 subjects was obtained. Matches were based on age (56.9 ± 4.4 years), gender (63 males, 36 females), BMI (28.1 ± 4.4 kg/m²), smoking habits (57 smokers at the time of the baseline session) and AHI (13.4 ± 10.9). The average recording duration was

Table 5.2: Anthropometric data of the SHHS dataset. (BMI: Body Mass Index, AHI: Apnea Hypopnea Index.)

	Control	Cardiovascular risk	Cardiovascular event	Total
Number of patients	33	33	33	99
Age (years)	55.8 ± 4.35	57.2 ± 4.2	57.8 ± 4.6	56.9 ± 4.4
Gender (male/female)	21 / 12	21 / 12	21 / 12	63 / 36
BMI (kg/m²)	28.3 ± 5.0	28.1 ± 4.5	27.9 ± 3.8	28.1 ± 4.4
AHI	13.8 ± 11.3	13.1 ± 10.1	13.3 ± 11.4	13.4 ± 10.9
Active smokers	19	19	19	57

08:27:38 (hh:mm:ss). Demographics of each group are summarized in Table 5.2. Since some subjects presented a low AHI, only those with $\text{AHI} \geq 5$ were considered in the further analysis (AHI = 5 remains the lower limit for the diagnosis of moderate SAS). None of the subjects in the two datasets suffered from atrial fibrillation.

As in the UZ Leuven database, PSGs were annotated by sleep experts, and sleep stage classification (REM and NREM) was available for each 30-second interval, together with the time of occurrence and duration of each apneic/hypopneic episodes and arousal. Since SHHS has several AHI measurements available, we selected the one that best resembled the AASM 2012 scoring (containing hypopneas with arousal/desaturation >3%). Bipolar ECG (modified lead II) and thoracic respiratory effort (recorded through respiratory inductive plethysmography) were acquired at 125 and 10 Hz, respectively.

5.2.3 Preprocessing

Same preprocessing was applied to the databases described above. First, bipolar ECG signals were resampled at 1000 Hz with cubic splines so that HRV analysis was not compromised by the effect of the sampling frequency [177]. Baseline wander removal was accomplished by extracting the baseline with a low-pass filter (0.5 Hz cut-off frequency). Afterwards, the baseline was subtracted from the ECG signal.

Subsequently, QRS-complexes were detected by the wavelet-based method proposed by *Martínez et al* [167]. Ectopic beat detection and correction was performed with the method described by *Mateo and Laguna* [172]. Then, ectopic beat positions and mis-detections were corrected by using the heart timing signal [172].

On the other hand, respiratory effort signals were resampled at 4 Hz and the respiratory rate, F_r , was estimated from them using the method proposed by *Lázaro et al* [145].

5.2.4 HRV analysis

HRV analysis was performed from the modulating signal, $m(n)$, which was estimated according to the TVIPFM model as described in Ch. 2.2. $m(n)$ was resampled at 4 Hz, and HRV power spectral density, $\hat{S}_{\text{HRV}}(k, F)$, was estimated from the k -th segment of length 5

minutes of $m(n)$ by the Welch's periodogram, with 4 minute overlap. 50-second Hamming windows with 50% overlap were employed. Subsequently, the spectral indexes were computed from $\hat{S}_{\text{HRV}}(k, F)$.

P_{LF} was defined as the power in the classical LF band [252]. However, a preliminary analysis of the respiratory rate revealed some values close to 0.4 Hz, which remains the upper limit of the classical HF band and could lead to an underestimation of P_{HF} [18]. For this reason, the two different alternative definitions of the HF band presented in Ch. 2.6.1 were used. In this way, P_{HF}^c , $R_{\text{LF/HF}}^c$ and P_{LFn}^c were obtained from the HF band centered in the respiratory rate, Ω_{HF}^c , whereas P_{HF}^e , $R_{\text{LF/HF}}^e$ and P_{LFn}^e were derived from the extended HF band, Ω_{HF}^e .

Also P_{VLF} was considered, being it defined as the power of the time-varying mean HR in order to account for the slower variations of $m(n)$. Finally, $\overline{\text{NN}}$ was also calculated from each five-minute window [252].

5.2.5 Effect of sleep stages on HRV

Sleep stages are known to exert an important effect on HRV, which is mainly reflected as an increased parasympathetic activity during NREM sleep and an awake-like sympathetic activity during REM sleep [52,244]. These large inter-stage fluctuations make it advisable to consider sleep stages in the analysis. In this way, HRV analysis was performed for NREM and REM sleep separately, by considering PSG-based sleep stage scoring.

5.2.6 Effect of apneas, hypopneas and arousals on HRV

The complex physiological response to an apnea or hypopnea usually finishes with an increase in sympathetic activity that may trigger an arousal, thus biasing any possible measurement in that period towards high sympathetic activity. Despite this well-known effect, apneic episodes are usually included in the analysis. A major innovation in this chapter is that the episodes of apneas, hypopneas and arousals (for simplicity summarized as apneic episodes hereon) were removed from the analysis, so that ANS activity can be assessed in a more basal state.

In order to minimize the effects of the recovery after an apneic episode, the minute after the offset of each event was also removed, since the tachycardia following an apnea or arousal often lasts about 20 to 30 seconds [249]. Some subjects presented an extremely high number of events, and hence only a few five-minute apneic episodes-free segments were usable (especially during REM sleep, which is a shorter stage and with higher incidence and duration of apneic episodes [61, 86]). Thus, and to guarantee a minimum sample size, subjects with less than 10 five-minute segments were discarded.

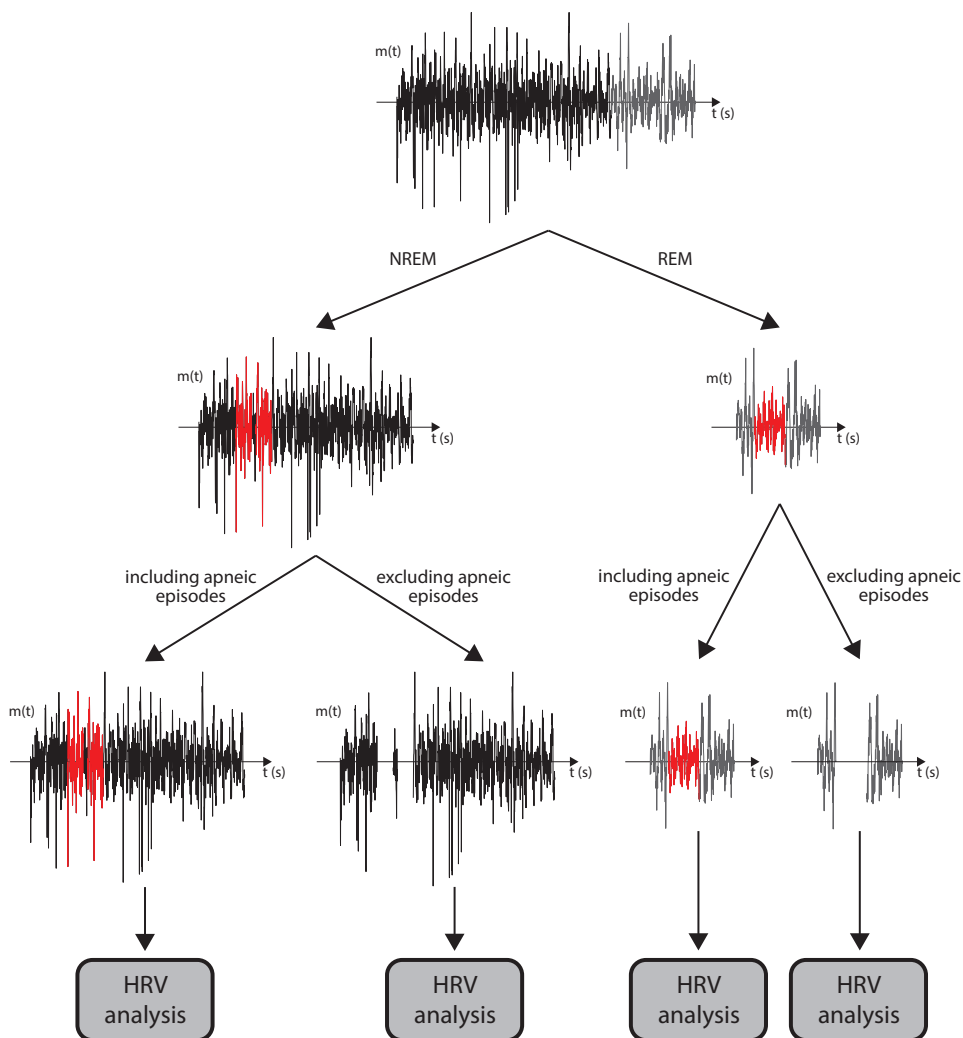


Figure 5.1: A flowchart of the data analysis performed for each subject is displayed. First, the modulating signal was divided in periods corresponding to NREM (black) and REM (gray) sleep. Afterwards, two different HRV analyses were performed in each of the sleep stages: one including the apneic episodes (red) and one excluding them (the one-minute period after the apneic episodes are included in the segments highlighted in red). The HRV analyses were performed over five-minute windows of available signal.

Nevertheless, the analysis was repeated including the apneic episodes, so that the results were comparable with previous studies. A schematic of the different proposed analyses is depicted in Fig. 5.1.

5.2.7 Effect of medication

Patients in the cardiac comorbidity group of the UZ Leuven dataset suffering from hypertension (33 out of 50) were under anti-hypertensive medication at the time of the

study. Each patient was administered a different drug or combination of drugs such as β -blockers, calcium channels inhibitors or blockers, angiotensin converting enzyme inhibitors, and diuretics, which are summarized in Table 5.1. Since anti-hypertensives could directly alter HRV measurements [29,114], we considered medication intake as a possible confounder in the analysis.

The effect of medication was analyzed in the following manner. First, patients with cardiac comorbidities were divided in two subgroups: under and not under anti-hypertensive drugs intake. Afterwards, the differences in \overline{NN} and P_{LFn}^e between each subject and his/her matched control were computed, and the distributions obtained for the two subgroups were compared.

5.2.8 Statistical methods

The mean value of each parameter for the different sleep stages was obtained for each subject. Normality of the data was rejected using a Kolmogorov-Smirnov test ($p < 0.05$) and so a paired Wilcoxon signed-rank test was applied in order to assess differences between the matched groups. This test was applied twice: once considering apneas, hypopneas and arousals, and another time excluding them from the analysis. When the comparison was between not matched groups, a two-sided Wilcoxon rank-sum test was applied instead. Significance level for considering statistical differences between groups was set to 0.05.

5.3 Results

In both datasets, results of the HRV analysis were similar when defining the HF band as Ω_{HF}^e or Ω_{HF}^c so, for simplicity, only those concerning the former are presented. The results obtained for each of the two datasets are summarized below.

5.3.1 UZ Leuven dataset

The results of the HRV analysis including and excluding apneic episodes are presented in Table 5.3. A tendency towards lower values of $R_{LF/HF}^e$ and P_{LFn}^e in the cardiac comorbidity group than in the control group was assessed when excluding apneic episodes from the analysis. These differences were statistically significant during NREM sleep. An example of the mean overnight spectra of a control subject and his/her comorbidity match during NREM sleep is displayed in Fig. 5.2. Similar results were obtained when including apneic episodes, although significant differences were only assessed during REM sleep in this case. Regarding the differences between sleep stages, decreased \overline{NN} and P_{HF}^e and increased $R_{LF/HF}^e$ and P_{LFn}^e were assessed during REM sleep. When excluding apneic episodes from the analysis, also F_i was increased during REM sleep.

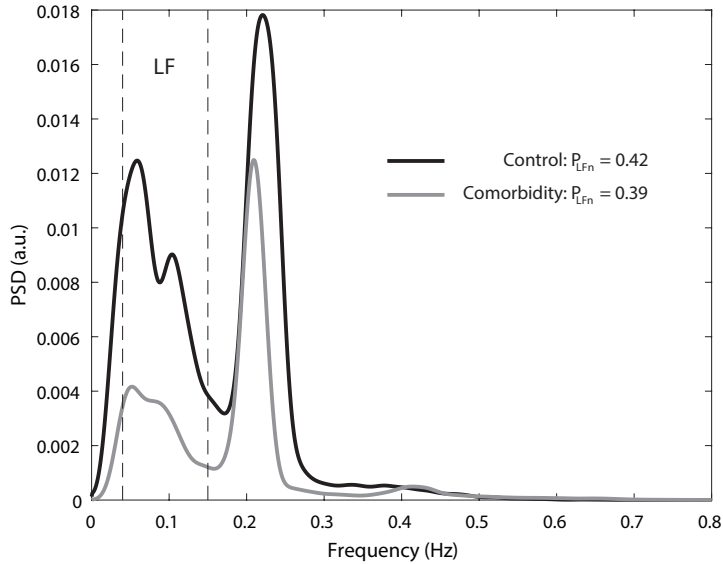


Figure 5.2: Average spectra for all the NREM segments (excluding those with apneic episodes) of a control subject of the UZ Leuven dataset (black) and his match (gray) are displayed. An increased sympathetic dominance can be noticed in the control subject, as reflected by the relative higher low frequency power content. The dashed black lines indicate the boundaries of the low frequency band. The number of averaged 5 minute segments was 50 and 36 for the control and the match respectively. As estimated from the modulating signal, the power spectral density is given in arbitrary units (a.u.).

The results obtained for the subgroups under and not under medication intake are displayed in Fig. 5.3. Whereas a higher \overline{NN} was assessed in the subgroup with medication, no differences were found regarding P_{LFn}^e (although in Fig. 5.3 only the analysis during NREM sleep and excluding apneic episodes is represented, no differences in P_{LFn}^e were found for REM sleep nor when including apneic episodes).

5.3.2 SHHS dataset

The results of the HRV analysis are summarized in Table 5.4. An increased P_{HF}^e and decreased $R_{LF/HF}^e$ and P_{LFn}^e were observed in the cardiovascular risk and cardiovascular event groups in comparison with controls when excluding the apneic episodes. In the cardiovascular event group, those differences turned statistically significant for P_{LFn}^e during NREM sleep. Similar results were obtained when including apneic episodes in the analysis. In general, differences between sleep stages were noticed as decreased \overline{NN} and P_{HF}^e and increased $R_{LF/HF}^e$ and P_{LFn}^e during REM sleep. However, higher \overline{NN} and lower P_{VLF} were assessed during REM than during NREM sleep in some cases (Tables 5.3 and 5.4), but this is most likely due to the reduced number of segments at REM sleep available for the analysis.

Table 5.3: Results of HRV analysis for the UZ Leuven dataset. Results are displayed as median (IQR), except for the number of subjects. Significant differences with the same sleep stage of the control group are marked with † ($p < 0.05$). Significant differences between NREM and REM sleep within each group are marked with * ($p < 0.05$).

	Control		Cardiac comorbidity	
	NREM	REM	NREM	REM
<i>Excluding apneic episodes:</i>				
F_r (Hz)	0.23 (0.06)	0.25 (0.06)*	0.23 (0.07)	0.25 (0.08)*
\overline{NN} (ms)	920.13 (184.89)	939.09 (178.61)*	951.08 (173.29)	911.34 (177.57)*
P_{VLF} (a.u.)	1.16 (0.40)	1.12 (0.40)*	1.09 (0.42)	1.20 (0.41)*
P_{LF} (a.u. $\times 10^{-3}$)	5.00 (6.11)	5.72 (14.68)	4.97 (6.71)	7.90 (12.68)
P_{HF}^e (a.u. $\times 10^{-3}$)	4.89 (9.70)	2.72 (4.54)*	6.19 (16.37)	4.54 (11.81)*
$R_{LF/HF}^e$ (n.u.)	0.96 (1.12)	2.43 (3.14)*	0.69 (0.94)†	1.52 (1.77)*
P_{LFn}^e (n.u.)	0.47 (0.24)	0.68 (0.22)*	0.38 (0.23)†	0.60 (0.19)*
N (subjects)	43	29	42	25
<i>Including apneic episodes:</i>				
F_r (Hz)	0.23 (0.05)	0.23 (0.07)	0.23 (0.06)	0.24 (0.07)
\overline{NN} (ms)	938.53 (200.44)	936.66 (198.97)*	950.39 (155.86)	900.00 (125.60)*
P_{VLF} (a.u.)	1.13 (0.42)	1.12 (0.48)*	1.10 (0.37)	1.23 (0.32)*
P_{LF} (a.u. $\times 10^{-3}$)	11.47 (12.57)	12.10 (19.98)	9.73 (14.73)	8.93 (13.77)†
P_{HF}^e (a.u. $\times 10^{-3}$)	6.42 (11.70)	4.33 (6.33)*	8.27 (16.05)	4.83 (9.09)*
$R_{LF/HF}^e$ (n.u.)	1.79 (2.56)	3.16 (3.41)*	1.42 (1.50)	1.72 (2.32)†,*
P_{LFn}^e (n.u.)	0.59 (0.28)	0.72 (0.20)*	0.52 (0.21)	0.60 (0.22)†,*
N (subjects)	46	50	49	46

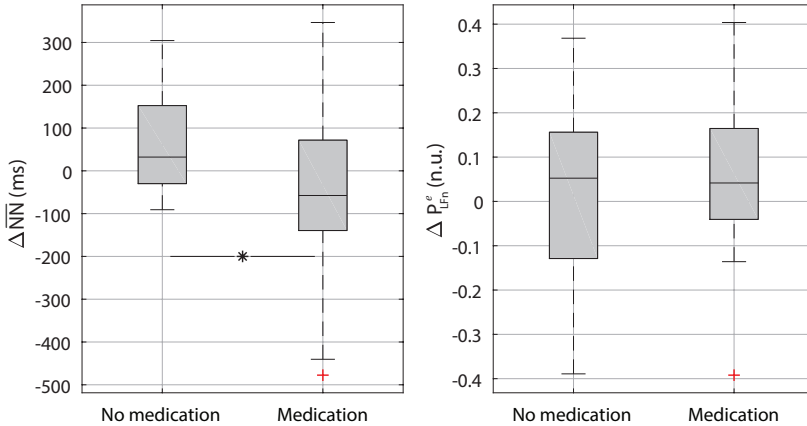


Figure 5.3: Boxplots of the differences in \overline{NN} ($\Delta \overline{NN}$) and P_{LFn}^e (ΔP_{LFn}^e) between the control subjects of the UZ Leuven dataset and their matches under or not under medication intake (during NREM sleep and excluding apneic episodes). Whereas $\Delta \overline{NN}$ was decreased in the group under medication intake when compared with the group without medication ($p < 0.05$, indicated with *), no differences in ΔP_{LFn}^e were assessed.

Table 5.4: Results of HRV analysis for the SHHS dataset. Results are displayed as median (IQR), except for the number of subjects. Significant differences with the same sleep stage of the control group are marked with † ($p < 0.05$). Significant differences between NREM and REM sleep within each group are marked with * ($p < 0.05$).

	Control		Cardiovascular risk		Cardiovascular event	
	NREM	REM	NREM	REM	NREM	REM
<i>Excluding apneic episodes:</i>						
F_r (Hz)	0.25 (0.05)	0.24 (0.03)	0.24 (0.04)	0.25 (0.03)	0.25 (0.05)	0.24 (0.07)
\overline{NN} (ms)	925.95 (150.24)	924.58 (123.65)	980.00 (168.87)	959.41 (266.71)	914.59 (201.34)	919.62 (186.39)*
P_{VLF} (a.u.)	1.16 (0.35)	1.15 (0.33)	1.03 (0.34)	1.07 (0.60)	1.18 (0.47)	1.17 (0.51)*
P_{LF} (a.u. $\times 10^{-3}$)	3.53 (4.10)	5.16 (8.73)	4.24 (4.68)	4.06 (25.65)	2.77 (2.46)	2.57 (3.00)
P_{HF}^e (a.u. $\times 10^{-3}$)	2.24 (2.53)	0.93 (1.53)	4.47 (5.34)	6.03 (7.25)	3.35 (5.29)	1.23 (0.95)*
$R_{VLF/HF}^e$ (n.u.)	1.13 (1.01)	3.99 (2.62)*	0.94 (1.21)	2.01 (2.38)	0.97 (0.99)	1.65 (4.06)
P_{Ln}^e (n.u.)	0.49 (0.17)	0.79 (0.11)*	0.45 (0.28)	0.67 (0.30)*	0.43 (0.28)†	0.59 (0.36)
N (subjects)	23	6	24	7	22	6
<i>Including apneic episodes:</i>						
F_r (Hz)	0.26 (0.05)	0.25 (0.04)	0.24 (0.04)	0.26 (0.04)	0.25 (0.05)	0.25 (0.04)
\overline{NN} (ms)	922.36 (158.63)	929.32 (154.77)	992.65 (144.38)	1016.15 (134.91)*	929.90 (217.02)	897.97 (154.08)
P_{VLF} (a.u.)	1.16 (0.39)	1.15 (0.36)	1.01 (0.30)	0.96 (0.26)*	1.16 (0.52)	1.22 (0.42)
P_{LF} (a.u. $\times 10^{-3}$)	5.30 (6.23)	5.13 (6.18)	5.62 (7.58)	6.50 (10.01)	3.86 (5.45)	5.18 (7.30)
P_{HF}^e (a.u. $\times 10^{-3}$)	2.60 (3.04)	1.71 (1.40)*	4.62 (4.60)	3.77 (3.52)†	3.88 (5.39)	1.93 (1.34)*
$R_{VLF/HF}^e$ (n.u.)	1.74 (1.08)	3.19 (2.94)*	1.39 (1.26)	2.09 (2.22)*	1.09 (1.27)†	2.86 (2.25)*
P_{Ln}^e (n.u.)	0.55 (0.13)	0.74 (0.18)*	0.53 (0.24)	0.66 (0.22)*	0.46 (0.24)†	0.67 (0.26)*
N (subjects)	25	23	26	25	25	22

5.4 Discussion

The main purpose of the present chapter was to assess whether imbalanced autonomic activity could be related to CVD in patients with SAS, as well as to investigate the potential use of ANS activity analysis in the early stage identification of patients at higher cardiovascular risk. ANS evaluation was achieved by HRV analysis, since it has been largely supported as a noninvasive tool for ANS activity assessment [252]. However, HRV should be addressed carefully in nocturnal recordings, since several studies have reported differences in HRV among the different sleep stages [52, 244]. Also differences in HRV when comparing subjects with and without apneas have been described in the literature [111, 199]. Nevertheless, whereas the effect of sleep stages is often considered in overnight HRV analysis, the effect of apneic episodes has been largely ignored. In this way, increased sympathetic dominance assessed in SAS patients might be reflecting the adrenergic surge following apneas and not a chronic SNS dominance during rest. For this reason, in this work we proposed to discard apneic episodes from the analysis, so that ANS evaluation is performed during the most basal condition.

The effect of excluding apneic episodes from the analysis can be noticed in both datasets (Tables 5.3 and 5.4), with large significant differences in P_{LF} and sympathovagal balance measurements. The apparent reduction observed in sympathetic activity when not considering the periods of apnea suggests that apneic episodes do alter ANS assessment by HRV and hence should be removed from the analysis, since changes in sympathetic activity unrelated to apneas might be masked otherwise. Moreover, this effect

was more evident for the patients in the UZ Leuven dataset, with larger AHI than in the SHHS.

With respect to the different definitions of the HF band employed in HRV analysis, Ω_{HF}^e resulted to be the most discriminative between groups, especially when apneic episodes were excluded from the analysis (although similar results were achieved with Ω_{HF}^c). The motivation for considering modified HF bands was that a preliminary analysis of F_r revealed the existence of some high values, which could yield to a power shift outside the band and hence result in underestimations of the real power. In this way, one possible solution is to center the band into the estimated respiratory rate, so that respiratory-related power lays inside the band. Besides, the fact that better results were obtained when considering Ω_{HF}^e could be related with differences in HR (as the higher limit of the extended band was selected as $\overline{\text{HR}}/2$ Hz, since HR remains the intrinsic sampling rate of HRV [144]), although the absence of significant differences in the $\overline{\text{NN}}$ of the distinct groups in both datasets suggests that this is not a likely explanation for the obtained results. Alternatively, the nonlinear interaction between HR and respiration during sleep [265] may result in meaningful frequency components that lie outside the classic and the centered bands.

5.4.1 UZ Leuven dataset

In order to study the relationship between ANS, SAS and CVD, we considered the UZ Leuven database described in Ch. 5.2.1, since it is composed by SAS patients with and without cardiac comorbidities that were matched based on age, gender, BMI and smoking habits. When comparing the patients with cardiac comorbidities with their matched controls a decreased sympathovagal balance, as assessed by lower values of $R_{\text{LF/HF}}^e$ and P_{LFn}^e , was observed in the former (Table 5.3). This decreased sympathetic dominance, exemplified in Fig. 5.2, could reflect a lack of adaptability of ANS and hence incapability to restore homeostasis after an apneic episode. If this was the case, an inefficient response to oxygen deprivation could directly affect the cardiovascular system, leading to inflammation [245], oxidative stress [250] or tonic chemoreceptor activation [188] among others, which are intrinsically related with the development of CVDs [245]. The fact that statistically significant differences were observed in NREM when excluding apneic episodes from the analysis but not when including them might suggest that the sympathetic activations following apneas could be masking the lowered sympathetic dominance in the comorbidity group. On the other hand, the increased incidence of apneic episodes during REM sleep [224] results in a reduction in the number of subjects considered in the analysis when excluding them, which could explain the absence of significant differences during this sleep stage. Similarly to previous studies [52,244], a higher sympathetic tone was assessed during REM than during NREM sleep, as reflected in increased P_{LF} , $R_{\text{LF/HF}}^e$ and P_{LFn}^e and decreased $\overline{\text{NN}}$ and P_{HF}^e in the former.

Nevertheless, altered sympathovagal balance should be regarded carefully, as 33 out of 50 patients in the cardiac comorbidity group were under anti-hypertensive medica-

tion at the time of the recordings. Since anti-hypertensives could contribute to reduced cardiac sympathetic activity [29, 114], a more detailed analysis was performed in order to check whether the observed differences could be explained by medication intake. In this way, the differences in mean \overline{NN} and P_{LFn}^e of the patients under medication and their matched controls were compared with those of the patients without medication (Fig. 5.3). The results revealed a higher \overline{NN} , i.e., a lower HR, in those patients under anti-hypertensives, as expected, although no differences were found in P_{LFn}^e . The higher \overline{NN} in the medication group would be reflected as a decrease in the mean HR which is corrected in the TVIPFM model (see Eq. 2.3) and hence is not expected to have a big influence in the analysis. On the other hand, P_{LFn}^e was apparently independent on the use of medication, possibly due to the aforementioned correction by mean HR intrinsic to the TVIPFM model.

5.4.2 SHHS dataset

Moreover, in order to evaluate if altered ANS activity may be prior to cardiovascular disorders in subjects with SAS, a second dataset consisting of a subset of the SHHS and described in Ch. 5.2.2 was considered. Again, HRV analysis revealed a decreased sympathetic dominance in the cardiovascular risk and cardiovascular event groups (Table 5.4), which turned statistically significant in the case of the cardiovascular event group (during NREM sleep). Given that subjects in the cardiovascular event group presented an altered sympathovagal balance when compared with their matched controls, despite the fact that they did not suffer from any CVD at the time of the recording, it is possible that individuals with SAS and altered sympathovagal balance are at augmented risk for developing CVDs. This unbalanced sympathovagal activity may be an indicator of either a lowered SNS activity, a dysfunction in the response to SNS stimuli or a combination of both. Although decreased LF variability has been assessed in severe chronic heart failure [260], this effect appears to be visible only in the most advanced stages of the disease. Nonetheless, the desensitization of β -adrenergic receptors when subjected to a recurrent stimuli [25] could point to SAS as a possible precursor of CVD, as heart damage has been associated with decreased β -adrenergic receptors density and decreased sensitivity to adrenergic stimulation [49]. Regarding the differences between sleep stages, increased sympathetic dominance was generally observed during REM sleep as expected.

5.4.3 Limitations

There are some limitations in this study that must be mentioned. The first and most important one is the use of anti-hypertensive medication by a large subset of subjects in the UZ Leuven database, which might compromise the physiological interpretation. Although the differences that may be induced by medication intake were analyzed carefully, it is not possible to ensure that it does not have an effect on the results. Moreover, there is controversy in the literature, with some studies reporting absence of changes in the

sympathovagal balance in subjects under β -blockers [102, 162], and some others suggesting altered sympathetic dominance [155, 227]. Another limitation is that the proposed analysis for ANS assessment is only valid during sinus rhythm and it is not applicable to other scenarios. This limitation takes special relevance in the case of atrial fibrillation, since it is known to be associated with SAS [255]. Regarding sleep stages, no distinction was made between light and deep NREM sleep due to the extremely low number of deep sleep epochs (less than 5% of the recording duration in most of the subjects in the UZ Leuven dataset, prior to apneic epochs deletion). In the SHHS dataset, the low number of analyzed subjects during REM sleep after removing apneic episodes compromises the further physiological interpretation. On the other hand, whereas the results obtained for both datasets are coherent, the datasets are not comparable, due to differences in mean age and AHI, and to the fact that cardiac comorbidity subjects in the UZ Leuven dataset had already developed CVDs. It is also important to highlight that subjects in the UZ Leuven dataset attended to the sleep laboratory because of complains and/or symptoms related to SAS, whereas volunteers in SHHS did not report any interference with their daily life, regardless of their scored AHI. Finally, and although several cardiac conditions with different origin and effects were considered simultaneously, the scope of this chapter was limited to the risk of developing CVDs as a whole.

5.5 Conclusion

The combination of all the underlying mechanisms that act in response to an apneic episode, together with the functional alterations caused by the different CVD, result in a very complex frame that obscures the physiological interpretation. Despite, decreased sympathetic dominance was assessed in SAS patients suffering from cardiac comorbidities. Furthermore, retrospective analysis of the subjects with SAS that will develop cardiovascular events in the future also revealed a reduced sympathetic dominance. Notwithstanding that further work is needed in the field of SAS phenotyping, HRV analysis could represent a useful tool for improving the screening and diagnosis of SAS patients with increased cardiovascular risk. Moreover, the importance of considering the effect of the apneic episodes in the interpretation of HRV analysis was addressed.

Part III

Cardiorespiratory signals analysis in sport sciences

6

Electrocardiogram-derived tidal volume estimation

6.1 Motivation	6.2.7 Heart rate variability
6.2 Materials and methods	6.2.8 Respiratory rate
6.2.1 Dataset	6.2.9 Multi-parametric model
6.2.2 Preprocessing	6.2.10 Subject-independent model
6.2.3 Tidal volume estimation	6.2.11 Performance measurement
6.2.4 Single-lead EDR	6.3 Results
6.2.5 Multi-lead EDR	6.4 Discussion
6.2.6 Instantaneous heart rate	6.5 Conclusion

6.1 Motivation

Monitoring respiratory activity is very important in several applications, e.g., respiratory rate is a sensitive clinical parameter in a multitude of pulmonary diseases [142]. Another important respiratory parameter is the tidal volume (TV), which is defined as the volume of air inhaled or exhaled during a respiratory cycle. TV is useful for monitoring some respiratory diseases, such as Cheyne-Stokes respiration and sleep apnea. Both respiratory rate and TV have been studied as indicators of the anaerobic threshold [56, 180],

which is related to the physical condition. The assessment of the physical condition results interesting for heart failure patients [284] and for athletes. Respiration monitoring techniques are usually based on plethysmography, pneumography or spirometry. These techniques require cumbersome devices which remain inconvenient for some applications, and which may interfere with natural breathing. Therefore, some alternatives have been presented in the literature.

As described in Ch. 1.3.2, ECG is known to carry some respiratory information. Essentially, it is modulated by respiration through at least three different mechanisms: RSA, variations in the relative position of the recording electrodes and changes in thoracic impedance. These mechanisms alter ECG morphology in synchrony with respiration, which has been exploited by several authors to develop different ECG-derived respiration (EDR) methods, consisting in extracting respiratory information from ECG features such as R or R-to-S waves amplitude [169], the QRS-complex slopes [145] and QRS-complex area [182] variations, or vectocardiogram rotations [21], without needing additional sensors. Despite the interest in EDR, research efforts have focused in estimating respiratory rate, with very few publications concerning TV estimation. Moreover and to the best of our knowledge, most of the studies aiming to estimate TV are based on ECG-unrelated techniques such as image acquisition [216], tracheal sounds [215] and inductive [238] or opto-electronic plethysmography [213].

Moody et al. already reported proportionality between TV and EDR [182]. Almost 30 years later, *Sayadi et al.* conducted a conceptual study aiming to derive TV using only ECG or different intra-cardiac signals in a controlled environment [230]. For this purpose, they employed mechanically ventilated swines, varying both TV and respiratory rate ranging from 0 to 750 ml and from 7 to 14 breaths/min (0.12 to 0.23 Hz) respectively. Each configuration was maintained for a minimum of 90 seconds, hence allowing stable measurement periods. In this chapter, we addressed TV estimation from ECG in rest and during a treadmill test, which constitutes a highly non-stationary scenario. Subject-specific models for TV based on ECG derived features were proposed and calibrated during a maximal effort test. These models were then validated for TV estimation in a submaximal treadmill test, conducted in a different day.

6.2 Materials and methods

6.2.1 Dataset

25 male volunteers aged 33.4 ± 5.2 years were recruited. All of them were apparently healthy and active, practicing aerobic training at least 3 times per week. None of the subjects were active smokers or reported any respiratory disorder by the time of the study, and only one of them was under medication intake (fluoxetine) during the recordings. They performed a maximal and a submaximal treadmill (Quasar MED LT h/p Cosmos, Nussdorf-Traunstein, Germany) test in different days, denoted as MaxT and SubT re-

Table 6.1: Demographics of the subjects in the presented dataset. All the values are given as mean \pm standard deviation, except from the number of subjects (N) and the maximum heart rate (the latter is provided as median [25th, 75th percentiles] since it was not normally distributed). (BMI: Body Mass Index).

N	Age (years)	Height (cm)	Weight (kg)	BMI (kg/m ²)	Max. HR (bpm)
25	33.4 \pm 5.2	178.0 \pm 5.5	74.8 \pm 7.0	23.6 \pm 2.1	180 [172, 186]

spectively. Both tests were divided in 3 stages: a 5-minute resting stage, during which the subjects remained seated and without talking, an exercise stage and a recovery stage. The resting stage was common to both tests, whereas different protocols were followed in the exercise stage. During MaxT, the volunteers started to run at an initial speed of 8 km·h⁻¹ which was increased 1 km·h⁻¹ per minute until they stopped due to volitional exhaustion. At this point, maximum HR was annotated for each subject. On the contrary, during SubT the procedure was similar to MaxT, but the speed was kept constant once the subjects reached the 90% of their maximum HR, and they were asked to keep running for 2 more minutes at the reached speed. Finally, the recovery stage was similar in both tests and lasted between 3 and 5 minutes during which the subjects were required to remain running at a comfortable speed of 8 km·h⁻¹.

Multi-lead ECG was acquired with a high-resolution holter (Mortara 48-hour H12+, Mortara Instrument, Milwaukee, Wisconsin). Leads *I*, *II*, *III*, *aVL*, *aVR*, *aVF*, *V4*, *V5* and *V6* were recorded at a sampling rate of 1000 Hz, whilst an Oxycon Pro device (Jaeger/Viasys, Germany) was used for recording breath-by-breath minute ventilation (\dot{V}_E) and respiratory rate (F_r). A breath-by-breath HR signal was also acquired with the latter device. Recordings were performed at University of Zaragoza (Spain), and the protocol was approved by the institutional ethics committee following the ethical principles of the Declaration of Helsinki. Written informed consent was received from all the volunteers, and the demographics are summarized in Table 6.1.

6.2.2 Preprocessing

Beat detection and delineation was accomplished in each ECG lead using the wavelet-based approach proposed in [167]. Instantaneous HR, $x_{\text{HR}}(n)$, was derived from beat time occurrence series as $60/d_{\text{F}}^u(n)$, where $d_{\text{F}}^u(n)$ represents the unevenly sampled interval function [223] (see Ch. 1.4.2). The reference for TV was obtained as $V_{\text{T}}(k) = \dot{V}_E(k)/F_r(k)$, where index k represents the k -th breath, and $x_{\text{HR}}(n)$ was synchronized with $V_{\text{T}}(k)$. Synchronization was performed by employing the derivatives of $x_{\text{HR}}(n)$ and the HR signal provided by the Oxycon Pro device, synchronized with $V_{\text{T}}(k)$. First, both HR signals were resampled at 4 Hz by linear interpolation. Afterwards, correlation between the derivatives of the interpolated signals was calculated, and the time difference was obtained as the maximum of this correlation. Finally, the interpolated and synchronized version of $x_{\text{HR}}(n)$ was resampled at the time instants k by linear interpolation, and $x_{\text{HR}}(k)$ and $V_{\text{T}}(k)$ were smoothed using a 10-sample median filter.

The described preprocessing was applied in MaxT and SubT. In order to distinguish the notation between the signals corresponding to each test, superindexes were employed so that $x_{\text{HR}}^m(k)$ and $V_{\text{T}}^m(k)$ refer to MaxT whereas $x_{\text{HR}}^s(k)$ and $V_{\text{T}}^s(k)$ allude to SubT.

Both stress tests were segmented into 5 different stages: a rest stage, three exercise stages, and a recovery stage. I_{rest} corresponds to the initial resting stage during which volunteers remained seated, and it lasts from the beginning of the recording until 30 seconds before exercise onset, so that transition from seated to the treadmill was discarded. I_{recoV} refers to the recovery stage, and it expands from 30 seconds after maximum HR was reached until the end of the acquisition. The initial time offset of 30 seconds was included to avoid transition from exercise to recovery stage, since subjects did not behave in the same way after reaching maximum HR: whereas some of them remained running, some others jumped from the treadmill and then started running again. The segmentation of the three exercise stages was performed automatically from $x_{\text{HR}}^m(k)$ as percentages of the range of variations of the HR: 0-60% (I_{0-60}), 60-80% (I_{60-80}) and 80-100% (I_{80-100}), considering the mean HR at I_{rest} as 0% and the maximum HR as 100%. Whereas the definition of I_{rest} and I_{recoV} was similar for MaxT and SubT, the percentages of maximum HR used for defining the other 3 stages were only calculated from $x_{\text{HR}}^m(k)$, and these values were employed in both tests. An example of this segmentation process is displayed in Fig. 6.1.

6.2.3 Tidal volume estimation

The proposed TV estimation approach consists in a linear model which was calibrated using the data in MaxT (training set) and evaluated using the data in SubT (test set). Both calibration and estimation were performed for each subject and stage. For the calibration process of each stage all the data samples in the current stage were used. Therefore, for stage I_i , the offset and slope (α_i and β_i respectively) of a linear model were estimated in a least squares sense by fitting $V_{\text{T},i}^m(k)$ with a determined feature of MaxT, $\theta_i^m(k)$. The selection of appropriate features remains essential for a proper TV estimation, and several options are described below. Afterwards, TV was estimated in SubT as:

$$\hat{V}_{\text{T},i}^s(k) = \alpha_i + \theta_i^s(k)\beta_i, \quad (6.1)$$

where θ_i^s represents the employed feature in stage I_i and in SubT.

Several features were tested as possible TV predictors: the amplitude of different EDR series (in a single-lead and a multi-lead approach), the instantaneous HR, the P_{HF} of the HRV signal and the respiratory rate. Moreover, a multi-parametric model including two or more of these features was also considered. The different methodologies followed for feature extraction are described below and, when not indicated, the same procedure was applied for feature extraction in MaxT and SubT. It is important to note that all the features were normalized with respect to MaxT in order to minimize inter-day changes in measurements (different electrode position, different basal state, etc), so that:

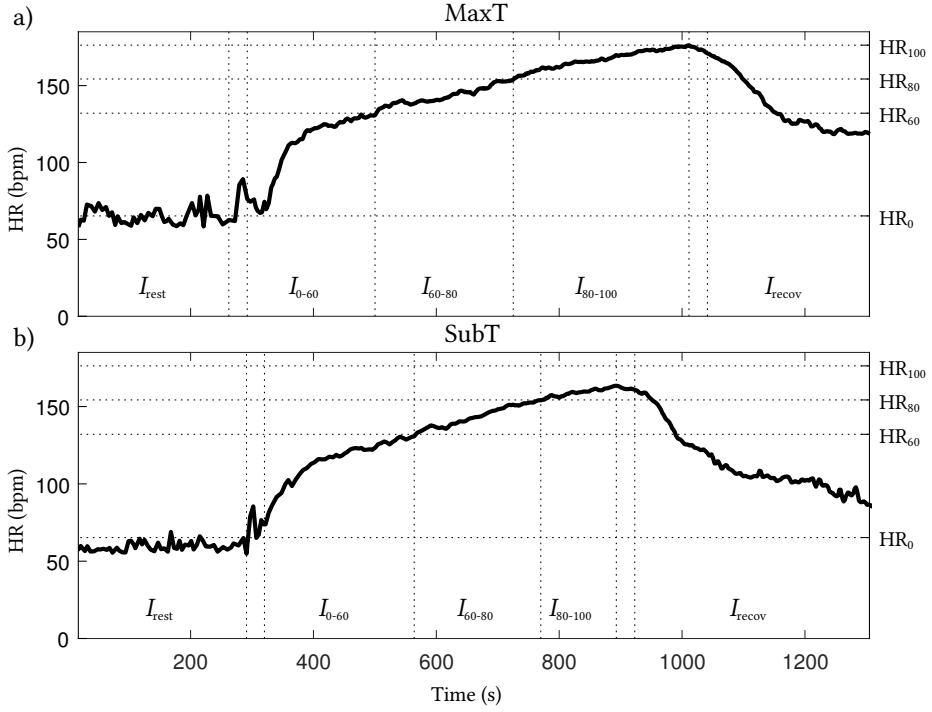


Figure 6.1: Stage segmentation for MaxT, a), and SubT, b), of one subject is shown. Vertical lines indicate onset and offset of the different stages for each test, whereas horizontal lines mark the different percentages of maximum HR used for segmentation. In both cases, there is a 30-second interval between I_{rest} and I_{0-60} , and between I_{80-100} and I_{recov} , in order to exclude the transition from rest to exercise and from exercise to recovery respectively.

$$\begin{aligned}\tilde{\theta}_i^m(k) &= \frac{\theta_i^m(k) - \mu_{\theta_i^m}}{\sigma_{\theta_i^m}}, \\ \tilde{\theta}_i^s(k) &= \frac{\theta_i^s(k) - \mu_{\theta_i^s}}{\sigma_{\theta_i^s}},\end{aligned}\quad (6.2)$$

being $\mu_{\theta_i^m}$ and $\sigma_{\theta_i^m}$ the mean and standard deviation of $\theta^m(k)$ during interval I_i respectively. $\tilde{\theta}_i^m$ and $\tilde{\theta}_i^s$ represent the normalized versions of $\theta^m(k)$ and $\theta^s(k)$ during interval I_i respectively, although they will be referred to as $\theta^m(k)$ and $\theta^s(k)$ for simplicity.

6.2.4 Single-lead EDR

Amplitude difference between peaks and nadirs of the EDR series obtained from each lead were used as features for TV estimation. For this purpose, several EDR signals were considered: R-S amplitudes [169], QRS upslopes and downslopes, and R wave angles

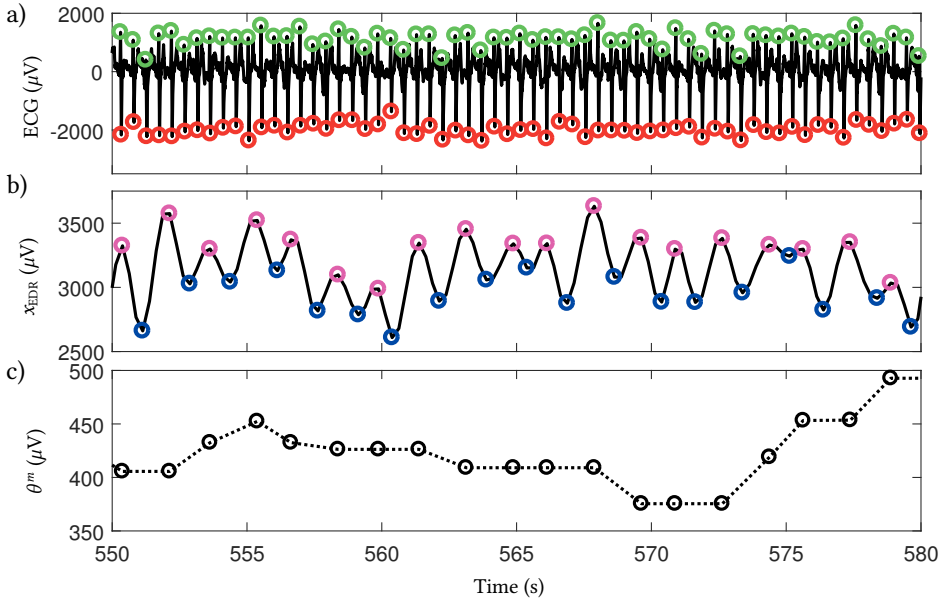


Figure 6.2: Derivation of the amplitude difference series using R-S amplitude as EDR. In a), R (green circles) and S (red circles) waves were detected in the ECG signal, and the difference between them was calculated for each beat to obtain an R-S amplitude series. $x_{\text{EDR}}(t)$ is a low-pass filtered version of this series (b)). Finally, the peaks and nadirs in $x_{\text{EDR}}(t)$ were detected (pink and blue circles respectively), and the series generated from the difference between them was resampled at the times when breaths occur and smoothed with a 10-sample median filter. The result, $\theta^m(k)$ (c)), was used as a feature for our linear model.

[145]. The resulting series were evenly sampled at 4 Hz and low-pass filtered at 1.5 Hz in order to discard HF components that are unrelated with respiration, and they were referred to as $x_{\text{EDR}}(t)$. As local maxima/minima in the EDR signal amplitude should be related with the end of expiration/inspiration, thus when electrodes are closer to/farther from the heart, peaks and nadirs in $x_{\text{EDR}}(t)$ were detected, and the difference between the amplitude of each peak and its corresponding nadir was calculated. The amplitude difference series were linearly interpolated at the time instants when expirations occur and smoothed with a 10-sample median filter, and the outputs of this process, $\theta^m(k)$, were used as features for estimating the TV. An example of this procedure using the R-S amplitude as EDR signal is displayed in Fig. 6.2.

6.2.5 Multi-lead EDR

During inspiration and expiration processes thorax expands or contract differently in the three spatial dimensions, and hence the use of spatial information could result in a better TV estimation. In this way, a multi-lead approach consisting in the combination of EDR signals extracted from different leads is proposed. The procedure is similar to the single-lead approach, and only differs in the definition of $x_{\text{EDR}}(t)$. In order to account for this three-dimensional behavior, in the multi-lead approach the EDR signals of three

different leads were combined using a principal component analysis (PCA), and $x_{\text{EDR}}(t)$ was obtained as the first component of this PCA. The employed leads were selected as those forming the most orthogonal combination possible, so that spatial information was maximized. In this case, leads $V4$, $V6$ and aVF were selected. Also the possibility of combining all the available leads was contemplated in the analysis.

As in the single-lead approach, R-S amplitudes, QRS upslopes and downslopes, and R wave angles were used as EDR signals.

6.2.6 Instantaneous heart rate

When body metabolic demands increase, TV and HR increase in order to enlarge gas exchange. In this way, it is expectable that TV and HR present some correlation, so HR was considered as a possible TV estimator. $x_{\text{HR}}^m(k)$ and $x_{\text{HR}}^s(k)$ were used as features for the linear model in MaxT and SubT respectively:

$$\begin{aligned}\theta^m(k) &= x_{\text{HR}}^m(k), \\ \theta^s(k) &= x_{\text{HR}}^s(k).\end{aligned}\tag{6.3}$$

6.2.7 Heart rate variability

Relationship between HRV and TV has been a recurrent topic in the literature [50,74,123], where association of an increased TV with a higher P_{HF} has been reported. For this reason, we considered P_{HF} as a potential feature for estimating TV. Although HRV is drastically reduced during moderate exercise [17, 67], the mechanical effect that breathing exerts over the SA node appears to be responsible of increased P_{HF} during high intensity exercise [66]. However, P_{HF} calculation should be addressed carefully during physical activity, since the increased F_r during exercise could yield to a shift of power towards higher frequency components [18]. In this way, we adopted the methodology proposed in [122] for the calculation of P_{HF} , where it was determined in a time-frequency basis ($P_{\text{HF}}(t)$), using an adaptive band centered in F_r . Moreover, the presence of non-respiratory-related frequency components that might lay within the HF band [17] was taken into account (see [122] for details). The obtained $P_{\text{HF}}(t)$ was resampled at the time instants when breaths occur, and the resulting discrete series ($P_{\text{HF}}^m(k)$ and $P_{\text{HF}}^s(k)$ for MaxT and SubT respectively) were used as features for TV estimation:

$$\begin{aligned}\theta^m(k) &= P_{\text{HF}}^m(k), \\ \theta^s(k) &= P_{\text{HF}}^s(k).\end{aligned}\tag{6.4}$$

Prior to HRV analysis, ectopic beats and misdetections were identified and corrected using the method described in [172] (less than a 0.1% of the beats were labeled as ectopics or misdetections).

6.2.8 Respiratory rate

Minute ventilation is defined as the volume of air inhaled or exhaled per minute. In this way, it is proportional to both TV and F_r . When an increase of gas exchange is required, the request can be satisfied by increasing either TV or/and F_r . However, in a very demanding situation such as a maximal effort test, the role of both magnitudes is closely related [256], so F_r was also considered as a possible TV estimator. Respiratory rate was estimated from the ECG as proposed by *Lázaro et al.* [145]. The EDR series calculated from the upslopes, downslopes and angles of the R waves of all the available leads were employed. Same parameters than in [145] were used for F_r estimation in I_{rest} , whereas they were modified in the exercise stages. Concretely, the Welch's periodogram parameters were set to $T_s = 12$ s, $T_m = 4$ s and $t_s = 1$ s. Also the peakness threshold for averaging was reduced to 50% ($\xi = 0.5$), and faster changes in F_r were allowed by increasing δ from 0.1 to 0.2 (see [145] for details). Finally, the upper limit of the EDR signals filtering was set to 1.5 instead of 1 Hz in order to adapt it to the studied scenario, where F_r can exceed 60 breaths/minute.

Afterwards, the estimated F_r for MaxT and SubT, \hat{F}_r^m and \hat{F}_r^s , were used as features for TV estimation:

$$\begin{aligned}\theta^m(k) &= \hat{F}_r^m(k), \\ \theta^s(k) &= \hat{F}_r^s(k).\end{aligned}\tag{6.5}$$

6.2.9 Multi-parametric model

Since in the literature TV has been related with all the previously described parameters independently, it might occur that combining the TV information obtained from different sources yields to a better estimation, so we considered the possibility of merging information from all the presented parameters using a multi-linear model, so that the final TV estimation was obtained as:

$$\hat{V}_{T,i}^s(k) = \alpha_i + \theta_i^{s,1}(k)\beta_i^1 + \theta_i^{s,2}(k)\beta_i^2 + \dots + \theta_i^{s,L}(k)\beta_i^L,\tag{6.6}$$

where $\theta_i^{s,l}(k)$ represents the different proposed features, i.e., parameters extracted from the single-lead and multi-lead EDR approaches, instantaneous HR, HRV and F_r . α_i and β_i^l represent the parameters of the multi-linear model estimated from MaxT, and L is

the number of parameters considered in the model. All the possible combinations of the proposed features were tested in order to obtain the best performing feature combination.

6.2.10 Subject-independent model

The possibility of having a single model which can be applied in a subject-independent basis was also addressed. For this purpose, the median of each of the coefficients of all the subject-specific multi-parametric models described above was calculated:

$$\begin{aligned}\bar{\alpha}_i &= \text{median}([\alpha_i(1), \alpha_i(2), \dots, \alpha_i(N)]), \\ \bar{\beta}_i^l &= \text{median}([\beta_i^l(1), \beta_i^l(2), \dots, \beta_i^l(N)]), \\ &\forall l \in [1, \dots, L],\end{aligned}\tag{6.7}$$

being $\bar{\alpha}_i$ and $\bar{\beta}_i^l$ the coefficients of the subject-independent multi-parametric model, $\alpha_i(n)$ and $\beta_i^l(n)$ the coefficients of the multi-parametric model for subject n , and N and L the total number of subjects and parameters considered in the model respectively.

6.2.11 Performance measurement

Median and IQR of the absolute (ϵ_a) and relative error (ϵ_r) were calculated for each methodology, stage and subject in order to quantify the accuracy of the estimation. Medians of medians and IQRs were computed among subjects for each methodology and stage. Moreover, accuracy in the estimation of F_r was quantified as the inter-subject median of the median absolute error in each stage.

6.3 Results

Median TV estimation errors obtained for each stage and approach are displayed in Tables 6.2 and 6.3. Also graphical examples of the different methodologies are depicted in Figure 6.3. From the 25 volunteers recruited for this study, a total of 11 subjects had to be discarded due to missing TV signal or ECG, or bad quality signals either in MaxT or SubT.

The estimation errors obtained with the single-lead approach are summarized in Table 6.2, where the results obtained for the different EDR methods can be compared. Although similar results were obtained for all the leads, lead *II* was the best performing independently of the considered EDR. The use of the downslopes of the R waves led to the lowest estimation errors in I_{rest} , I_{60-80} and I_{80-100} , with median relative errors of 11.68, 7.40 and 5.81%, respectively. On the other hand, the upslopes led to the best results in I_{0-60} , whereas the R-S amplitude was the best performing EDR in I_{recov} , with median relative

Table 6.2: Inter-subject medians of median and IQR of the fitting errors obtained with the single-lead EDR approach. Best results were achieved for lead II , so results obtained in lead II with each of the considered EDRs are displayed. The median and IQR of the absolute and relative error corresponding to the lowest relative error in each stage are highlighted in bold type.

		II_{R-S}		$II_{upslope}$		$II_{downslope}$		II_{angle}	
		Median	IQR	Median	IQR	Median	IQR	Median	IQR
I_{rest}	ϵ_a (liters)	0.11	0.11	0.10	0.11	0.11	0.12	0.09	0.09
	ϵ_r (%)	13.06	11.36	13.38	12.42	11.68	12.26	12.40	12.11
I_{0-60}	ϵ_a (liters)	0.37	0.33	0.27	0.31	0.39	0.30	0.31	0.36
	ϵ_r (%)	20.31	22.80	17.01	16.80	22.34	22.49	19.77	26.57
I_{60-80}	ϵ_a (liters)	0.27	0.23	0.24	0.23	0.18	0.23	0.29	0.21
	ϵ_r (%)	11.35	6.95	9.17	6.56	7.40	7.28	10.86	7.00
I_{80-100}	ϵ_a (liters)	0.19	0.11	0.19	0.13	0.16	0.14	0.17	0.12
	ϵ_r (%)	6.03	4.57	5.96	4.48	5.81	4.62	6.27	4.24
I_{recov}	ϵ_a (liters)	0.42	0.32	0.49	0.34	0.39	0.29	0.48	0.32
	ϵ_r (%)	14.07	12.76	15.26	11.43	15.77	11.32	16.68	12.30

Table 6.3: Inter-subject medians of median and IQR of the fitting errors obtained with the multi-lead, HR, HRV, F_r and multi-parametric approaches. Results concerning the multi-lead approach were achieved considering the leads $V4$, $V6$ and aVF , whereas those of the multi-parametric approach were obtained from a combination of the single-lead and HR approaches (in the single-lead approach, lead II and QRS downslopes were employed). The median and IQR of the absolute and relative error corresponding to the lowest relative error in each stage are highlighted in bold type.

		Multi-lead		HR		HRV		F_r		Multi-parametric	
		Median	IQR	Median	IQR	Median	IQR	Median	IQR	Median	IQR
I_{rest}	ϵ_a (liters)	0.09	0.12	0.10	0.10	0.12	0.10	0.17	0.13	0.16	0.12
	ϵ_r (%)	11.87	14.23	12.74	12.57	16.19	14.10	17.37	16.85	17.61	15.87
I_{0-60}	ϵ_a (liters)	0.39	0.35	0.25	0.22	0.38	0.39	0.56	0.54	0.23	0.25
	ϵ_r (%)	21.86	22.31	15.12	14.36	20.41	25.38	28.85	40.43	12.96	15.87
I_{60-80}	ϵ_a (liters)	0.29	0.22	0.15	0.13	0.27	0.18	0.21	0.23	0.14	0.11
	ϵ_r (%)	11.24	6.80	7.64	5.66	10.98	7.02	9.02	7.49	7.41	4.68
I_{80-100}	ϵ_a (liters)	0.15	0.14	0.16	0.13	0.16	0.14	0.18	0.11	0.14	0.12
	ϵ_r (%)	6.97	5.02	6.14	4.13	5.32	4.03	7.14	4.81	5.06	4.01
I_{recov}	ϵ_a (liters)	0.37	0.31	0.27	0.28	0.54	0.34	0.36	0.35	0.28	0.28
	ϵ_r (%)	15.33	8.66	11.55	12.04	18.58	15.74	13.75	14.61	11.41	12.03

errors of 17.01 and 14.07% respectively. Median IQRs of the estimation error were similar for all the approaches and stages.

Estimation errors obtained with the multi-lead, HR, HRV, F_r and multi-parametric approaches are reflected in Table 6.3. Lowest relative fitting errors were obtained when combining the downslopes series in lead II and the instantaneous HR with the multi-parametric approach, except in I_{rest} , where the multi-lead approach remained the best option. Scatter plots of the performance of the multi-parametric approach for all the subjects and in the different stages are displayed in Fig. 6.4. Nevertheless, similar estima-

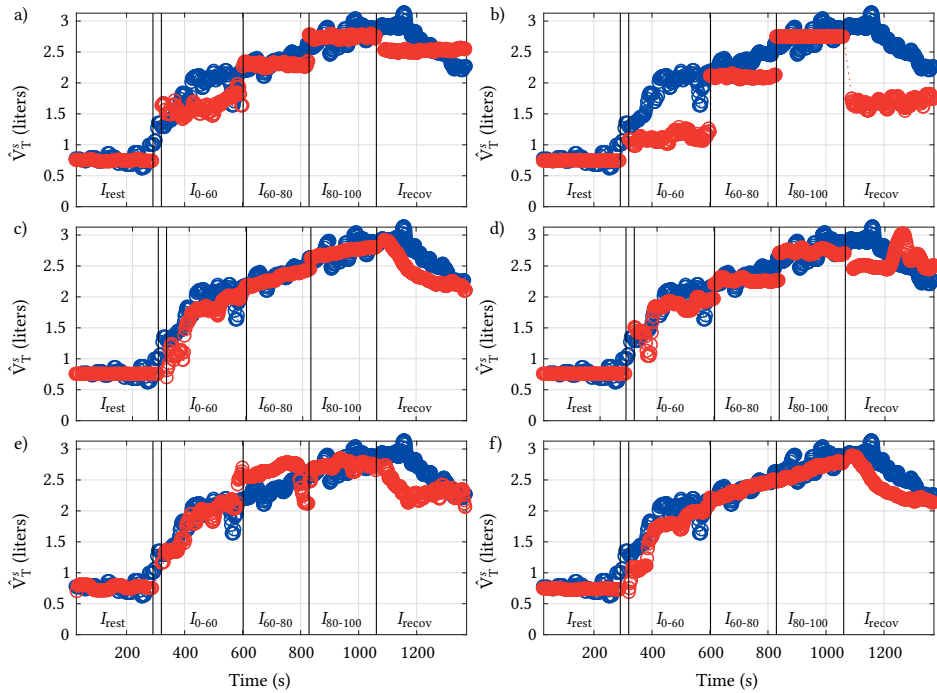


Figure 6.3: Real (blue) and estimated (red) tidal volume (\hat{V}_T^i) for a given subject is displayed. The different estimations were obtained from the best performing lead (*II* in this case) of the single-lead EDR approach (a), the multi-lead EDR approach (b), the instantaneous HR (c) approach, the HRV approach (d), the respiratory rate approach (e) and the best performing feature combination (lead *II* in the EDR approach plus instantaneous HR in this case) of the multi-parametric approach (f).

tion errors were achieved in the multi-lead, HR, F_r and the multi-parametric approaches for all the stages, except for I_{rest} in F_r and the multi-parametric option, and I_{0-60} in F_r and multi-lead, where larger errors were observed. On the other hand, slightly increased errors in most of the stages were obtained for the HRV approach. In most of the cases, median relative error was lower than 14%, being it lower than 7.5% in I_{80-100} for all the approaches, and as low as 5.06% in the multi-parametric approach. Highest estimation errors were generally obtained for HRV and F_r , although their performance is comparable to the other approaches in the majority of the stages. Median IQRs of the estimation error were similar for all the approaches and stages, except for increased values in I_{0-60} for all the approaches excluding the HR and the multi-parametric options.

In Table 6.4, the median value of each coefficient obtained for the subject-independent multi-parametric models, as well as the ratio of the contributions of the downslopes and the HR are summarized. Whereas the contribution of the HR is in median always higher than the contribution of the EDR calculated from the downslopes, the former turns highest during the I_{0-60} and the I_{recov} stages. On the other hand, and since best performance was generally achieved with the multi-parametric model, the subject-independent model was composed by the median of the coefficients of all the subject-specific multi-

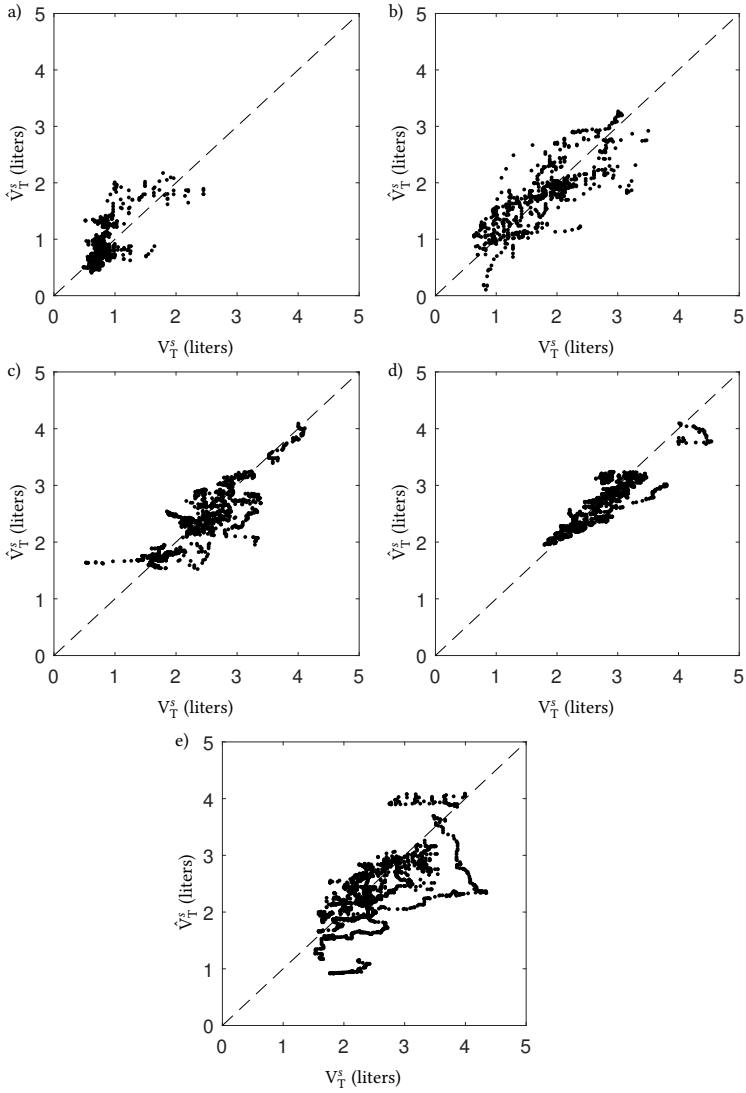


Figure 6.4: Scatter plots of the tidal volume estimated from the multi-parametric approach when combining the downslopes of lead II and the HR (\hat{V}_T^s) against the real one (V_T^s) for all the subjects and each of the stages (a): I_{rest} , b): I_{0-60} , c): I_{60-80} , d): I_{80-100} and e): I_{recov}). Dashed lines indicate $\hat{V}_T^s = V_T^s$.

parametric models, which are those displayed in Table 6.4. The performance of this subject-independent model is also summarized in Table 6.4, where larger absolute and relative errors when compared with the subject-specific model were obtained in all the stages, except from I_{rest} .

Although not displayed in the tables, median F_T estimation error was computed for all the stages in MaxT and SubT independently. Estimation errors lower than 0.035 Hz were obtained for most of the stages in both MaxT and SubT, whilst a maximum error of 0.077 Hz was obtained for I_{0-60} in SubT.

Table 6.4: Median (IQR) of the parameters of the subject-independent multi-parametric model for each stage (parameters of the multi-linear model when the QRS downslopes in lead II and the instantaneous HR are considered, so that $\bar{\alpha}_i$ is the offset, and $\bar{\beta}_i^1$ and $\bar{\beta}_i^2$ are the contributions of the downslopes and the HR respectively). Also the median (IQR) of the absolute and relative errors obtained when estimating the TV using the median model are displayed.

	$\bar{\alpha}_i$	$\bar{\beta}_i^1$	$\bar{\beta}_i^2$	$ \bar{\beta}_i^2/\bar{\beta}_i^1 $	ϵ_a (liters)	ϵ_r (%)
I_{rest}	0.800 (0.232)	0.021 (0.088)	0.036 (0.101)	1.128 (1.594)	0.10 (0.08)	14.04 (11.77)
I_{0-60}	1.734 (0.488)	0.016 (0.070)	0.358 (0.352)	6.186 (21.097)	0.48 (0.28)	22.72 (22.19)
I_{60-80}	2.410 (0.561)	-0.020 (0.042)	0.110 (0.084)	3.076 (4.743)	0.45 (0.14)	18.74 (4.88)
I_{80-100}	2.828 (0.728)	0.001 (0.054)	0.089 (0.1849)	5.791 (14.302)	0.32 (0.14)	10.23 (5.47)
I_{recov}	2.561 (0.942)	0.001 (0.094)	0.230 (0.257)	7.955 (52.689)	0.49 (0.39)	19.75 (12.33)

6.4 Discussion

In this chapter, we addressed the possibility of estimating TV only from ECG recordings. The use of a dataset composed by signals acquired during maximal and submaximal treadmill stress tests results in a challenging but suitable environment for testing the behavior of the proposed methodologies in a highly non-stationary scenario. Also rest periods were considered, thus representing a more stationary situation. Although several different approaches were proposed, all of them are based on a first order lineal model, so that the complexity relies in the selection of adequate ECG-derived features.

Both MaxT and SubT were automatically divided in five stages, according to the exercise onset and offset and different percentages of the maximum reached HR. Afterwards, TV estimation was performed for each stage. For this purpose, we calibrated the parameters of the linear model in Eq. 6.1 using all the samples in the stage of interest of MaxT, and used them for estimating the TV in the same stage of SubT. *Moody et al.* suggested that the amplitude of an EDR signal (calculated using the QRS-complex area) obtained from any set of electrodes should be roughly proportional to the TV [182]. In order to test this hypothesis, we applied four different EDR techniques to all the available leads: the R-S amplitudes [169], and the upslopes, downslopes and angles of the R waves [145]. Although results obtained for all the leads were similar, best estimation accuracy was obtained when using lead II, independently of the employed EDR. When comparing the different EDRs, lowest error was achieved with the downslopes in most of the stages, as displayed in Table 6.2, which might suggest a more linear relationship with TV than the other EDRs. For all the leads and EDRs, a lower performance was observed in the I_{0-60} stage. The most likely explanation for the performance reduction is the fast changes that occur during this stage, with a sudden increase in TV, HR and F_i that are not completely followed by the EDRs or the first-order linear model. Also changes in the position of the electrodes used for ECG acquisition (since both tests were performed in different days, it is probable that they were attached in slightly different places) or in the basal state of the subjects could constitute additional sources of estimation error.

In a second approach, we addressed the possibility of including spatial information by a combination of EDRs extracted from three "quasi-orthogonal" leads (since lead V2 was missing, there were not three leads that were completely orthogonal) through PCA, so that the main variations in those EDRs, which are expected to be produced by respiration, were maximized. Also the option of combining all the available leads was considered, although it did not outperformed the three-lead option. Despite the similar results obtained in the single-lead and multi-lead EDR approaches, median relative error was slightly higher when accounting for spatial information, except for I_{rest} and I_{recov} , probably due to fact that sources of noise such as movement during running may contribute to the first component of PCA. Nonetheless, since the different spatial dimensions of thoracic expansion do not contribute equally to the total TV, most of the information might be obtained from a single lead capturing variations along a preferable dimension. Additionally, the non-standard leads employed by *Lázaro et al.* in [145] were considered, although their performance was not higher than that of the multi-lead approach.

HRV has also been related with TV in the literature, since P_{HF} has been reported to be affected both by TV and respiratory rate [50, 74, 123]. In a previous study using the same dataset, *Hernando et al.* proposed a method for calculating P_{HF} in a time-frequency basis and considering the presence of non-respiratory-related components [122], so we adopted this methodology and used the obtained P_{HF} as a feature for estimating the TV. Results displayed in Table 6.3 revealed that the performance using HRV was similar than for the single-lead EDR approach in I_{80-100} and in I_{0-60} , but fitting error was higher in I_{rest} , I_{60-80} and I_{recov} (although it increased less than a 5% in all the cases). The lowered performance during I_{60-80} and I_{recov} could be related with the fact that HRV is drastically reduced during moderate exercise [17, 67] and so its variations might uncouple from those in TV, thus resulting in an increased estimation error in these stages, whereas during high intensity exercise (as in I_{80-100}) P_{HF} might recover the coupling with TV (possibly due to mechanical stretching of the sinus node [66]), thus resulting in a reduced estimation error. In the case of I_{rest} , decreased performance could have its origin in the fact that low respiratory rates might result in wrong estimations of P_{HF} , due to spectral shift towards low frequency band. Differences in the metabolic demands and in the ANS state (reflected in HRV) from day to day could also contribute to estimation error.

Since metabolic demands of the body increase during exercise, the demanded gas exchange increases as well, so both minute ventilation and HR increase consequently. Due to the very close relation between TV and F_r in the control of \dot{V}_E during exercise [256], F_r was considered for estimating the TV. First, F_r was estimated as proposed by *Lázaro et al.* [145]. Essentially, F_r is calculated from the EDRs derived from the upslopes, downslopes and angles of the R waves of all the available leads, which are combined in a short-term basis when they spectra are peaky enough. Although the same parameters employed in [145] were used in I_{rest} , they were modified during the exercise stages attending to the fast and wide changes observed in F_r in the studied scenario. Median absolute F_r estimation error was generally lower than 0.035 Hz. Results in Table 6.3 reveal a relative error lower than 10% in I_{60-80} and I_{80-100} , lower than 18% in I_{rest} and I_{recov} and higher than 28% in I_{0-60} respectively. The decreased accuracy in the latter stage might be

explained by the different response of the subjects to the increasing ventilation demands, as observed by *Carey et al.* during incremental exercise [55]. Whereas in some subjects F_r increased in parallel with the exercise load, some others satisfied the ventilation demands during moderate exercise by mainly regulating the TV, with a lower contribution of F_r , which increased slowly as exercise became more intense. In order to study the effect of F_r estimation in the results, we repeated the calculations using the original F_r provided by the Oxycon Pro device, concluding that the error in F_r estimation did not contribute noticeably to the error in TV estimation.

On the other hand, HR increases together with exercise intensity. In this way, we observed that the use of HR as TV estimator resulted in low fitting errors, with a median relative error lower than 13% in all the stages except in I_{0-60} , where it increased up to 15.12%. Despite the high performance of this approach (especially in I_{0-60} , when compared with the other approaches), these results should be regarded carefully, since the relation between HR and TV could be not that direct in other scenarios.

Finally, we also considered the combination of several features using a data fusion algorithm such as a multi-linear model. From all the possible feature combinations, lowest fitting errors were obtained when combining the single-lead EDR and the HR approaches. This feature combination outperformed all the other approaches in all the stages, except in I_{rest} , thus highlighting the multi-source origin of the physiological mechanisms underlying the respiratory-related modulation of cardiac activity. In this way, although the EDR and HR signals may share some information regarding respiratory activity, they also contain non-redundant information that is exploited by this multi-parametric approach, thus resulting in a better TV model than any of the considered features separately. However, and as displayed in Table 6.4, the contribution of the HR was always dominant, independently on the considered stage. This dominance was weak during I_{rest} , but increased in the other stages, especially during I_{0-60} and I_{recov} . This behavior is most likely related with the similar profile of the instantaneous HR and the TV during the treadmill tests, so that when abrupt transitions occurs (such as those in I_{0-60} and I_{recov}), HR turns in the best estimator of the TV, whose changes are poorly followed by the other considered features. As displayed in Fig. 6.4, the performance of this approach was similar for all the subjects, with larger variations occurring in I_{rest} , I_{0-60} and I_{recov} . Whereas the presence of outliers in I_{0-60} was to be expected due to abrupt changes in TV, larger performance variations during I_{rest} are most likely due to a lower linear coupling between the target features and the TV during spontaneous breathing in some of the subjects. On the other hand, the subjects behaved distinctly after reaching the maximum HR in MaxT (some of them jumped from the treadmill and started running again), and therefore it is difficult to establish whether large deviations in I_{recov} are explained by this fact or by an uncoupling between TV and the estimation features.

Nevertheless, since the multi-parametric approach was generally the best performing, it was used for estimating a subject-independent model, built as the median of all the previously trained subject-specific models. As summarized in Table 6.4, relative errors lower than 20% were obtained for most of the stages (relative error raised to 23% in I_{0-60}).

As expected, the median absolute and relative errors were larger than in the case of the subject-specific model for all the stages, except in the case of I_{rest} . This is possibly related with the fact that, for those subjects presenting large estimation errors in this particular stage, a median model results in a better approach, given that the average TV during rest is similar for people with similar characteristics.

There are also some limitations that must be highlighted. First, the dataset was composed only by healthy men in a relatively small age range, which were used to aerobic training. In this way, the algorithm performance in subjects with a different age range or physical condition, or with cardiorespiratory disorders remains unknown and should be evaluated in further studies. Regarding the high linear relation between TV and HR, the scope of this work was limited to a treadmill test, and hence this coupling might be reduced in other scenarios.

In summary, we proposed a simple method for estimating TV from only the ECG. Several different features that are related with respiration were considered as TV estimators, and all the methodologies were tested in rest and also in a highly non-stationary scenario such as an effort treadmill test. The promising results with low fitting errors suggest that it might be possible to develop a subject-specific model that could be applied to estimate the TV in a day-independent basis. Nevertheless, further research should be conducted in order to improve TV estimation from the ECG. In this study we only considered estimation during an exercise test, but this method could be useful in many other applications, e.g., in the monitoring of respiratory disorders such as Cheyne-Stokes respiration, COPD or asthma. For this purpose, validation in these scenarios remains crucial. Moreover, the proposed model could be regarded as an interesting tool in several activities that are centered in the control of respiration, like meditation, yoga or mindfulness, and in different fields of sports science.

6.5 Conclusion

A methodology for estimating TV from several features derived from ECG during a treadmill stress test has been presented, considering the possibility to develop a subject-oriented model independent on the measurement day. Recordings from two different days were employed, being the first used for calibrating the model and the second for testing. During exercise, the different proposed approaches led to fitting errors lower than 14% in most of the cases and than 6% in some of them, suggesting that TV can be estimated from the ECG in non-stationary conditions. Best results were obtained when combining the information provided by a single-lead EDR signal based on the downslopes of the R waves and the instantaneous HR.

7

Anaerobic threshold estimation through ventricular repolarization profile analysis

7.1 Motivation		7.2.4 Anaerobic threshold estimation
7.2 Materials and methods		7.2.5 Statistical analysis
7.2.1 Dataset		
7.2.2 Determination of the ventilatory threshold	7.3 Results	
7.2.3 Repolarization dynamics assessment	7.4 Discussion	
	7.5 Conclusion	

7.1 Motivation

During moderate exercise, the aerobic energy production system combines the blood O_2 with carbohydrates, fats and proteins to synthesize adenosine triphosphate (ATP), which is the molecule providing the muscles with energy. However, the rhythm at which ATP is produced through the aerobic pathways results insufficient to maintain muscle activity at higher exercise intensity. In this situation, ATP starts to be produced through the anaerobic pathways, which employ the glycogen stored in the muscles and release lactate and H^+ ions as residuals, resulting in metabolic acidosis [112, 207]. The O_2 consumption

above which anaerobic mechanisms are needed to complement aerobic energy production, thus causing a sustained increase in lactate levels and metabolic acidosis, is referred to as anaerobic threshold (AT) [271]. Apart from representing an inflection point in the way the body obtains energy to maintain its work capacity, the AT is also regarded as the frontier beyond which the cardiovascular system limits the endurance work [270]. In this way, an accurate estimation of the AT remains of large interest in the field of sport sciences, as it can be used to design better training routines, quantify athletes performance or prevent from overtraining. Moreover, it has some clinical applications and, actually, it was initially intended to assess the exercise capacity in cardiac patients [272]. Different methodologies for the estimation of the AT based on the analysis of blood lactate (lactate threshold, LT) and gas exchange (ventilatory threshold, VT) [251] have been proposed in the literature. However, whereas the former requires from repetitive blood samples acquisition, the latter employs cumbersome devices that interfere with natural breathing.

For these reasons, there is a growing interest in the noninvasive estimation of the AT, using ECG-derived parameters such as the HR [124] or HRV [134]. In a recent work by *Hamm et al.* [115], they proposed a methodology for the estimation of the LT based on the analysis of the ventricular repolarization instability and reported a characteristic pattern that was used for estimating the LT in function of its correlation with the HR. However, the use of blood lactate levels as a gold standard for detecting the AT might result in a high uncertainty, given that it can be only assessed in a discrete-time basis, usually with high sampling periods. In this chapter, we addressed the estimation of the AT from the analysis of the ventricular repolarization dynamics, using the VT as a reference, given that it can be assessed in a more continuous-time basis.

On the other hand, *Rizas et al.* proposed the use of periodic repolarization dynamics (PRD), computed from the ventricular repolarization instability analysis, as a novel method for the assessment of sympathetic activity [222]. Given the close relationship between PRD and repolarization instability, we also considered the possibility of estimating the AT from the PRD, under the hypothesis that the VT will also be related with an increased sympathetic activity, due to the need of faster ventilation.

7.2 Materials and methods

7.2.1 Dataset

The same 25 healthy male volunteers recruited for the maximal and submaximal treadmill tests introduced in Ch. 6 (their demographics are displayed in Table 6.1) performed a step incremental cycle ergometer test, divided in three stages. In the first stage, the subjects remained seated and without talking for 5 minutes. Afterwards, they performed the cycle ergometer test, with an initial workload of 75 W that increased 25 W each minute. The cadence frequency was fixed at 80 rpm, and the workload kept on increasing until the

volunteers reached the 90% of their maximum HR (the maximum HR was determined from the maximal treadmill test described in Ch. 6) after what it was kept fixed for 2 more minutes. Finally, they underwent a recovery stage, in which they were asked to keep on pedaling at 75 W for 3 to 5 more minutes. All the volunteers were requested to avoid food, tobacco, alcohol or caffeine in the 3 hours prior to the study, to avoid high intensity physical activity on the day of the test and to drink plenty of fluids during the previous 24 hours.

During the test, high-resolution multi-lead ECG was acquired using a holter device (Mortara 48-hour H12+, Mortara Instrument, Milwaukee, Wisconsin). Leads *I*, *II*, *III*, *aVL*, *aVR*, *aVF*, *V4*, *V5* and *V6* were acquired at 1000 Hz. On the other hand, O_2 and CO_2 consumption (\dot{V}_{O_2} and \dot{V}_{CO_2} , respectively), minute ventilation (\dot{V}_E) and respiratory exchange ratio (RER) were assessed with an Oxycon Pro device (Jaeger/Viasys, Germany). The recordings were performed at University of Zaragoza (Spain), and the protocol was approved by the institutional ethics committee in accordance with the Declaration of Helsinki. Written informed consent was received from all the subjects.

7.2.2 Determination of the ventilatory threshold

The VT was determined by an expert in sport sciences from the ventilatory equivalents of O_2 and CO_2 (\dot{V}_E/\dot{V}_{O_2} and \dot{V}_E/\dot{V}_{CO_2} , respectively) of each subject. In this way, the point at which there was a simultaneous increase in the ventilatory equivalents of O_2 and CO_2 was set as the VT. Also the RER and instantaneous HR were available to the expert. These annotations were used as the gold standard for the estimation of the AT in this work.

7.2.3 Repolarization dynamics assessment

Baseline wander was subtracted from the ECG recordings (it was obtained using a forward-backward low-pass filter with 0.5 Hz cut-off frequency). Afterwards, beat detection and delineation was accomplished using the wavelet-based approach proposed by *Martínez et al.* [167], so that the onset and offset of the T waves (T_{on} and T_{off} , respectively) were obtained. Since there were not three orthogonal leads available and the absence of *V2* did not allow to calculate the Frank's lead configuration, the three most orthogonal leads, namely *V4*, *V6* and *aVF*, were considered. After a low-pass filtering (forward-backward filter with 30 Hz cut-off frequency) for removing HF noise without altering the morphology of the T waves, the T waves were extracted from each lead based on T_{on} and T_{off} . The repolarization dynamics profile, dT , was constructed as follows. First, for each beat i , the T waves of the three employed leads were forced to have a common origin at $0 \mu V$, by subtracting them their first sample. Then, the length of the T waves was truncated to the point when one of them turns zero again, in order to avoid negative values. Finally, the three-dimensional repolarization vector corresponding to beat i was constructed using the mean amplitude of the three T waves as its coordinates, and $dT(i)$ was computed as the angular difference between the repolarization vector of beats i and $i - 1$. An ex-

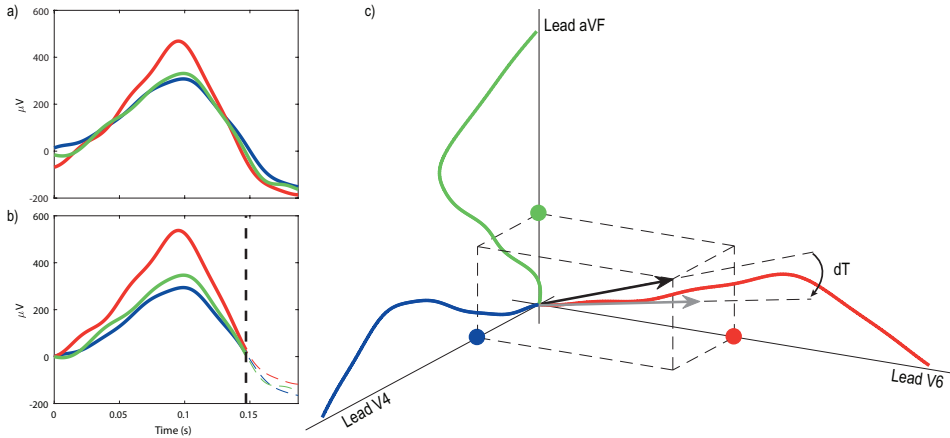


Figure 7.1: Calculation of the dT series. In a), the original T waves of the three considered leads (V4: blue, V6: red, aVF: green) are displayed. In b), they were subtracted their first sample to have a common origin, and they were truncated to the first zero-crossing, marked with a black dashed line. Only the portion of the T waves displayed in bold were used for computing dT . In c), the T waves are displayed along three perpendicular axes, and the values of their mean amplitude (displayed with filled circles) was used to construct the repolarization vector (black arrow). Afterwards, dT was calculated as the angular difference between this vector and the vector corresponding to the previous beat (gray arrow).

ample of this process is displayed in Fig. 7.1. In order to improve the robustness in the computation of $dT(i)$, it was only calculated when the correlation between the T waves corresponding to the beats i and $i-1$ had a correlation coefficient ≥ 0.9 in all the employed leads. However, a visual analysis of the ECG signals revealed that the *aVF* lead was very noisy in approximately half of the recordings during the high-intensity stages, so that dT was estimated from only *V4* and *V6*, in a two-dimensional approach.

On the other hand, the instantaneous HR was computed from the time difference between consecutive beats, and the HR and dT signals were interpolated to 4 Hz and low-pass filtered (forward-backward filter with 0.1 Hz cut-off frequency) in order to obtain the HR and dT profiles (see Fig. 7.2 a)).

Also PRD was assessed. For this purpose, the profile of dT profile was subtracted, and the short-term Fourier transform (STFT) of the resulting detrended dT series was computed (120 s Blackman window, slid sample-by-sample). Afterwards, the time profile of the PRD was computed as the total power within the [0.04 0.15] Hz band in each time instant, and the resulting series was re-sampled to 4 Hz and low-pass filtered as the HR and dT series. An example of the PRD profile of one subject is displayed in Fig. 7.2 b), whereas its corresponding TF distribution is depicted in Fig. 7.3. In order to analyse the effect of the cardiocomotor coupling in the computation of PRD, we also checked if there was any power content in the frequency alias corresponding to $HR(t) - F_c$ and $|2F_c - HR(t)|$ as proposed in [122], where F_c accounts for the pedaling cadence. An example showing the temporal evolution of these components is displayed in Fig. 7.3.

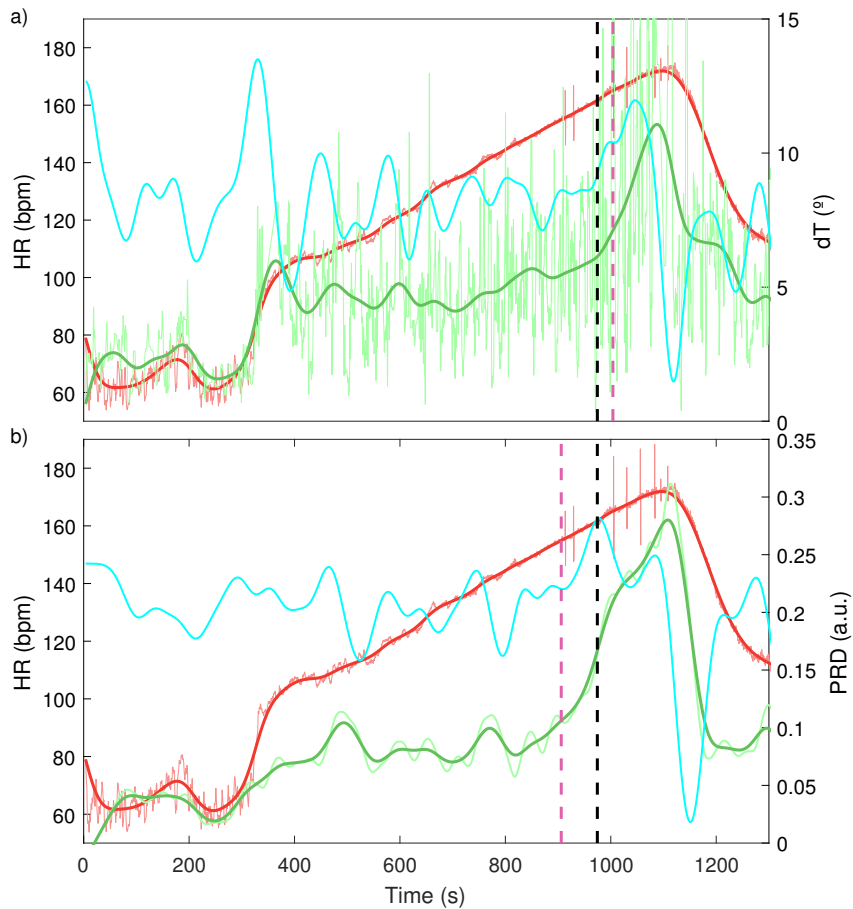


Figure 7.2: a) Instantaneous HR (red, left axis) and dT (green, right axis) during the exercise test for a given subject. The HR and dT profiles are represented in bold. Moreover, the first derivative of the dT profile is displayed (cyan, rescaled for representation purposes). b) Temporal evolution of the PRD (blue), with its profile represented in bold and its first derivative in cyan (rescaled for representation purposes). The dashed black and pink lines represent the occurrence time of the ventilatory threshold and the estimated anaerobic threshold.

7.2.4 Anaerobic threshold estimation

According to the repolarization dynamics profile reported by *Hamm et al.* [115], a visual analysis of the dT profiles revealed a characteristic sudden increase in the repolarization instability in the vicinity of the VT. In the present study, we first located the time instant at which the faster variation in dT occurred from the maximum of its first derivative. The point at which this fast increase in dT started was located as the local minimum preceding the maximum of its first derivative, and this point was selected as an estimation of the AT, being referred to as AT_{dT} . An example showing the estimation of the AT from the derivative of the dT profile is depicted in Fig. 7.2 a). However, in some subjects, only a local maximum of the derivative of dT was found close to the VT, with the absolute maximum occurring close to the onset of exercise (see Fig. 7.2 a)). For this reason, we

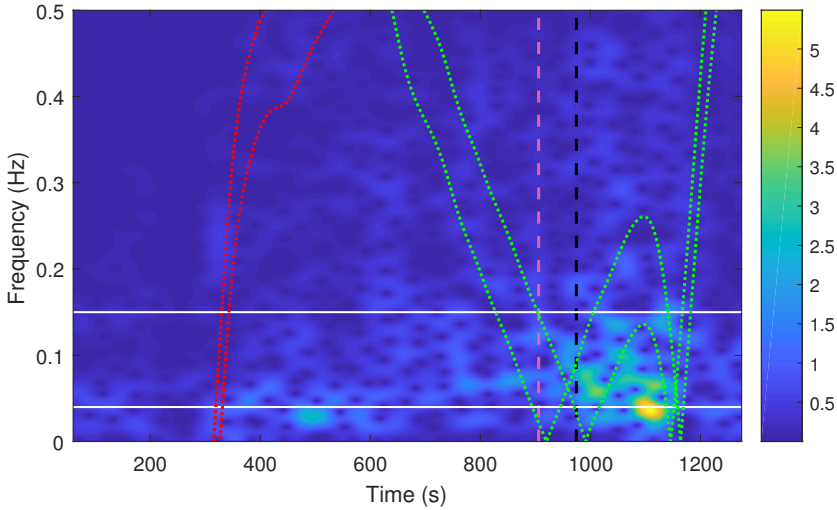


Figure 7.3: Time-frequency distribution of dT (detrended). The dashed black and pink lines represent the occurrence time of the ventilatory threshold and the estimated anaerobic threshold, respectively. The limits of the band used for computing PRD are shown in white, whereas the dotted red and green lines represents the limits of a 0.125 Hz band centered in the alias terms $HR(t) - F_c$ and $|2F_c - HR(t)|$, respectively (F_c , represents the pedaling cadence)

established a lower threshold in the HR, below which we should not expect to see a switch towards the anaerobic pathways. This threshold was set as the 77% of the maximum HR of each subject (measured from a maximal treadmill test, as mentioned above), since a previous study by *Goldberg et al.* [98] revealed that this value was always below the HR measured at the VT, independently on the physical condition. Moreover, it is in accordance with several studies reporting a HR of the 90% of the maximum HR at the training intensity of the AT (assessed either from the VT or the lactate threshold) [190, 274].

Additionally, the possibility of estimating the AT from the PRD profile was also addressed. The same criteria than that described in the case of the dT profile were employed, and an example of the estimation of the AT from the first derivative of the PRD series is displayed in Fig. 7.2 b). In this case, the resulting estimation will be referred to as AT_{PRD} .

7.2.5 Statistical analysis

The performance of the two proposed methodologies for the estimation of the AT was assessed by calculating the error in the VT estimation. All the results are presented in terms of workload, so that they are comparable with previous studies. In this way, the estimations of AT were converted from seconds to watts, assuming a linear increment of the workload.

Since dT was computed using only two leads, we also evaluated the differences in the AT estimation performance with respect to the three-lead approach (only those subjects with good signal quality in the aVF lead were considered in this case).

7.3 Results

From the 25 volunteers enrolled in the study, 5 were discarded because of misleading T wave delineation during the high-intensity exercise, due to the noisy ECG (more than 100 consecutive beats without a correlation index ≥ 0.9 among consecutive T waves), and another one was not included due to missing gas exchange information.

The obtained results and two boxplots accounting for the distribution of the AT estimation error when using the dT and the PRD profiles are displayed in Table 7.1 and Fig. 7.4 a), respectively. In the case of using dT , a median error of -0.6 W and [25th, 75th percentiles] of $[-19.3, 10.8]$ W were achieved, being them 12.9 $[-17.1, 54.4]$ W in the case of employing the PRD series. Since the workload was increased 25 W per minute, the error in the estimation of AT_{dT} was lower than 1 minute for a 63% of the subjects, whereas it was generally kept below 2 minutes in the case of AT_{PRD} . The absolute workload values at VT, AT_{dT} and AT_{PRD} were 330.8 $[282.7, 342.9]$, 313.1 $[287.0, 344.5]$ and 289.6 $[248.3, 325.6]$ W, respectively.

Regarding the dT profile, the behavior shown in Fig. 7.2 a) was shared by the majority of the volunteers, with a sudden increase above the resting level in response to the exercise onset, followed by a plateau-like period and a new increase occurring in the vicinity of the VT. Finally, there was a decrease in dT corresponding to the start of the recovery stage. This behavior was very similar in the case of PRD (Fig. 7.2 b)). In order to assess whether the increase in PRD following the VT could be due to the presence of harmonic components, we studied the alias caused by the cardiocomotor coupling, as displayed in Fig. 7.3. There was not a meaningful power content in the harmonic components for any of the subjects.

Since only two leads were employed in order to maximize the number of subjects available for the analysis (19 subjects when using the two-lead approach versus 11 when considering also the aVF lead), the difference in the estimation performance with respect to the three-lead approach was computed. As displayed in Fig. 7.4 b), the effect was reduced in the case of AT_{dT} , with median and [25th, 75th percentiles] of -6.1 $[-28.4, 3.2]$ W, but it increased to 49.2 $[-4.5, 49.2]$ W for AT_{PRD} , with higher errors when employing the three-lead configuration.

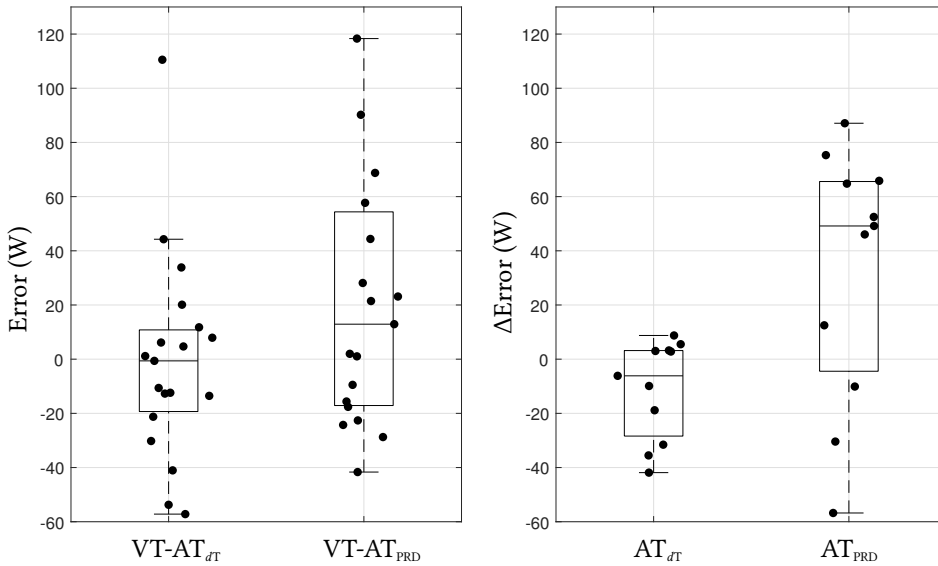


Figure 7.4: a) Boxplots of the error in the estimation of the anaerobic threshold using the dT or the PRD series. b) Difference in the estimation error when using three or two leads, and considering the dT or the PRD series. In both figures, the filled circles represent the values for the different subjects.

Table 7.1: Parameters of interest in the exercise test (median and [25th, 75th percentiles]). The maximum HR refers to that in the test conducted in this study, and not to the maximum HR reached during the maximal treadmill test (see text for details). The percentage of maximum HR was calculated with respect to the maximum HR in the maximal treadmill test. The workloads refer to the test in this study. (VT: ventilatory threshold, AT: estimated anaerobic threshold).

Max. HR (bpm)	171.5 [160.6, 175.6]
% max. HR at VT	89.0 [86.0, 90.8]
Max. workload (W)	350.0 [325.0, 375.0]
% max. workload at VT	85.2 [80.0, 88.2]
VT (W)	330.8 [282.7, 342.9]
AT_{dT}	313.1 [287.0, 344.5]
AT_{PRD}	289.6 [248.3, 325.6]

7.4 Discussion

In this chapter, the AT was estimated during a cycle ergometer test through the study of the ventricular repolarization dynamics. The analysis of the dT and PRD profiles revealed a sudden increase in the repolarization instability, as reflected in abrupt increases in the trends of dT and PRD, in the vicinity of the VT. Therefore, the point at which a change in the repolarization dynamics tendency occurred was employed as an estimation of the AT. The good performance achieved with AT_{dT} and AT_{PRD} suggests that the analysis of either dT or PRD might be suitable for the noninvasive estimation of the AT. Several works have addressed the study of the ventricular repolarization dynamics, aiming to shed some

light on the physiological mechanisms underlying them. *Rizas et al.* proposed the use of dT for deriving PRD, which is regarded as a noninvasive measurement of the effect of sympathetic activity on ventricular myocardial repolarization [222]. They reported an increase in PRD following sympathetic activation, and a decrease after sympathetic blockade. Moreover, they found that PRD was unrelated to HRV and respiratory activity. Other authors have also addressed the study of the low frequency oscillations of the repolarization dynamics, both experimentally [116, 209] and in simulation studies [210, 226], and have suggested that the variability in the repolarization dynamics is increased in response to sympathetic provocation.

The aforementioned results could contribute to the interpretation of the dT and PRD profiles obtained in this work. In Fig. 7.2, there are several well-distinguished stages. During rest, repolarization instability remains low, and it presents a rapid increase following the onset of exercise, due to the surge in sympathetic activity and vagal withdrawal during exercise [45]. Afterwards, the repolarization dynamics present a plateau-like behaviour, suggesting an equilibrium in the sympathetic and vagal control. In this stage, the progressive increase in the blood lactate levels is compensated with the HCO_3^- buffer system. However, in the vicinity of the AT the increase in blood lactate can not be further compensated. According to *Karapetian et al.* [134], the vagal activity reduces at around the 50-60% of the maximum \dot{V}_{O_2} (this range has been related with the LT [63]), so that there is a further increase in the respiratory rate aiming at compensating metabolic acidosis by respiratory alkalosis (CO_2 elimination). The suppression of vagal activity results in an increased sympathetic dominance, reflected as a fast increase in the dT and PRD profiles. Although some authors have reported an increase in the vagal component of HRV at high exercise intensities, this is more likely reflecting the mechanical modulation of cardiac activity due to increased ventilation [66]. Finally, the diminution of the repolarization instability following the end of the exercise test would be associated with a restitution of the sympathovagal control of ventricular repolarization.

The estimation of the AT from the analysis of the ventricular repolarization dynamics was recently proposed by *Hamm et al.* [115], who studied the moving correlation among the instantaneous HR and the trend of dT . The time point at which this correlation was minimum was used as an estimation of the AT. Although initially we tried to replicate the methodology described in [115], we obtained large estimation errors due to the inconsistent correlation profiles of the different subjects. However, there are several differences between our study and the one by *Hamm et al.* that may explain this lower performance. First, the configuration of the exercise test was very different, being it much more exigent in our case, with an initial workload of 75 W followed by increments of 25 W per minute, in comparison with [115], with an initial workload of 40 W and increases of 30 W every 3 minutes. This results in different HR profiles, with a much smoother increase in the case of [115], which could be responsible of the differences in the correlation profiles. Another important difference relies on the lead configuration of the ECG acquisition. Whereas in [115] they employed the orthogonal Frank's leads, in our case the conventional 12-lead ECG configuration was employed (leads V_1 , V_2 and V_3 were not available, since the volunteers were also wearing a chest band during the exercise test). The ab-

sence of $V2$ made it impossible to dispose of three orthogonal leads, so a quasi-orthogonal lead configuration composed of $V4$, $V6$ and aVF was employed. However, due to the bad quality of aVF in several subjects, only $V4$ and $V6$ were used. As displayed in Fig. 7.4 b), the effect of using two leads instead of three resulted in an almost negligible difference for most of the subjects in the case of AT_{dT} , whereas it had a greater impact in AT_{PRD} , being the latter generally higher when employing the three-lead configuration. Possibly, the lower performance when including aVF is due to a generalized lower signal quality, which might not affect the trend of dT , but has an effect on the estimation of the PRD.

On the other hand, the gold standard in the work by *Hamm et al.* was the LT, whilst in this work the VT was employed. In spite of the fact that the LT is largely acknowledged as a good estimator of the physical condition, its use for estimating the AT is not yet unified, so that the accuracy will depend on the methodology and site of the blood extraction and of the employed analysis methods [83]. Moreover, it will also be dependent on the sampling period (in the case of [115] the sampling period was selected as 3 minutes), which is much lower than in the case of the VT, since the signals used for estimating it have a continuous-time nature. Nevertheless, the estimation of the VT might be subjective in some cases, depending on the expert annotator experience and opinion, or in the established criteria in the case of automatic detection.

There are also some limitations in this work that must be discussed. As aforementioned, the VT annotations might have a subjective component, although they are probably more precise than in the case of using the LT, with high sampling periods. Moreover, the use of only 2 leads limits the available information concerning the ventricular repolarization dynamics and, possibly, better results could be obtained if adding a third orthogonal lead in the estimation of dT . Also the use of predefined HR thresholds could result in an overestimation of the VT, although in this case none of the subjects had reached their VT at the 77% of their maximum HR. Additionally, we considered the possibility that the increase in PRD after the AT could be caused by the presence of harmonic cardiocomotor components, but the analysis of the TF maps of dT discarded this possibility. Finally, we only tested the proposed methodologies in subjects used to aerobic training, so further studies in a wider range of physical conditions would be desirable.

7.5 Conclusion

In this chapter, a novel methodology for the estimation of the AT based on the analysis of the ventricular repolarization dynamics profile has been proposed. The analysis of the dT and PRD profiles reflects a rapid increase in sympathetic dominance in the vicinity of the AT, and the high performance with estimation errors lower than 25 W (or 1 minute) for most of the subjects suggests that the AT can be estimated noninvasively, using only ECG recordings.

Part IV

Conclusions

8

Conclusions and future work

8.1 Summary and conclusions

8.1.1 HRV analysis in asthma

8.1.2 HRV analysis in sleep apnea syndrome

8.1.3 Cardiorespiratory signals analysis in sport sciences applications

8.1.4 Conclusion

8.2 Future work

8.1 Summary and conclusions

The main objective of this dissertation was the noninvasive assessment of ANS activity, applied to different respiratory disorders and to the field of sport sciences. For this purpose, this document was divided in three main parts. In the first one, an introduction to the physiology underlying the different considered scenarios was provided, together with a methodological framework for the contextualized analysis of HRV. HRV analysis remains the most extensively employed tool for ANS assessment, although it requires from a proper signal conditioning in order not to hamper the further interpretation. In this way, the presence of noise or other interfering sources, ectopic beats or strong RSA episodes should be considered. In Ch. 2, an algorithm for differentiating between ectopic beats and rhythm changes due to RSA was presented, and it was later employed in Ch. 3 for improving beat detection in two different datasets of asthmatic children, with stronger RSA than in the case of adults.

Also the use of peakness for the assessment of the HF power distribution was addressed, and its potential and relationship with classical frequency domain HRV parameters was evaluated through a simulation study. Moreover, the effect of the respiratory rate on HRV analysis was discussed, contemplating the use of modified HF bands or the removal of the respiratory contribution to HRV. Finally, CRC assessment was considered, and two indexes derived from the TFC map were described. All these tools were employed to a greater or lesser extent in the different sections of this thesis.

In the second part, HRV analysis was applied to three different clinical scenarios, namely child asthma, adult asthma and SAS. In each of these scenarios, the methodology was adapted so that the results of the analysis can be provided with a physiological interpretation. Finally, the third part consisted in the study of cardiorespiratory signals in the context of exercise tests. Two novel methodologies for the estimation of the TV and the AT were proposed and tested during treadmill and cycle ergometer tests, respectively. The methodological details, main results and conclusions of each of the considered scenarios are discussed below.

8.1.1 HRV analysis in asthma

The physiological mechanisms underlying the pathogenesis of asthma have not yet been elucidated. Although airway hyper-responsiveness is one of the most common symptoms of asthma, its origin remains unknown due to the large heterogeneity among asthmatic patients. However, the fundamental role of PNS in the control of bronchomotor tone [184] and bronchoconstriction [151] has attracted some attention to ANS imbalance as a possible source of airway hyper-responsiveness. In this way, it is possible that ANS assessment could add some clinical value for the diagnosis and monitoring of asthma. Under the hypothesis that altered autonomic airway control observed in asthmatics may be also reflected in cardiac vagal activity, in this thesis we proposed the analysis of HRV for ANS evaluation in asthmatic children and adults.

In the case of asthmatic children, we found an increased vagal dominance in those subjects with higher risk of developing asthma in the future, in according with previous studies reporting increased vagal activity in asthmatics [80, 94, 131, 240, 257, 287]. Moreover, increased ρ reflected a peakier HF component, which could suggest a more regular vagal activity in children with higher risk of asthma. Importantly, we included several methodological novelties with respect to previous works, such as the improved detection of ectopic beats taking RSA episodes into account, or the use of modified HF bands for the frequency domain HRV analysis, given the increased respiratory rate observed in children. When analyzing the same parameters in a group of children under ICS treatment for obstructive bronchitis, we observed a decrease in vagal activity and an increase in the sympathovagal balance (as measured from HRV) in those children with less risk of asthma, which might suggest a restoration of the homeostatic autonomic activity. According to *Fryer et al.*, increased vagal activity observed in asthmatics could be caused by a dysfunction of the M_2 muscarinic receptors [90], largely present in the post-ganglionic

nerves innervating the airways. Moreover, a decrease in ρ and CRC was also assessed in this group of children. On the other hand, all these parameters remained unaltered in those children with a worse asthma prognosis, which might be linked to the concept of illness as a state of reduced complexity [99, 212], suggesting that HRV might be more dependent on the respiratory activity in asthma or in subjects with an increased risk of developing asthma. Since the results of both studies were coherent among them and with the literature, and provided that HRV analysis is noninvasive in nature, ANS assessment using HRV might stand out as a feasible option for aiding in the study of the neural mechanisms underlying asthma.

Regarding the study of HRV in asthmatic adults, the objective was to evaluate the added value of ANS assessment in the stratification of asthmatic patients attending to their degree of symptoms control or their disease severity. For this purpose, several HRV, respiratory-derived and clinical features were employed for training various classifiers. Since some of the subjects presented low respiratory rates, respiratory information was removed from the HRV signal using the OSP methodology. We assessed a reduced HRV in the subjects with more severe or uncontrolled asthma with respect to those with a better condition, in concordance with previous studies [160]. Additionally, the classification attending to the asthma severity when including ANS information resulted in a similar performance than using only the clinical features, which were outperformed in some cases, therefore suggesting that ANS assessment through noninvasive cardiorespiratory signals analysis could represent a useful complement in the monitoring and diagnosis of asthma in adults.

8.1.2 HRV analysis in sleep apnea syndrome

SAS has been identified as risk factor for the development of CVD, representing a well-known cause of secondary hypertension, coronary artery disease, cardiac arrhythmias and heart failure [198, 255, 282]. On the other hand, altered HRV has been independently related with SAS and with several conditions that constitute risk factors for the development of CVD. However, and in spite of the fact that the characteristic autonomic response to an apneic episode is shared by most of SAS patients, only some of them will develop CVD. Under the hypothesis that there might be some differences in the autonomic control of SAS patients developing or not cardiac comorbidities, we analyzed the overnight HRV in two datasets composed by SAS patients with a well defined CVD outcome.

Since polysomnographic recordings were available, the effect of the different sleep stages was taken into account, as differences in HRV among sleep stages have been reported [52, 244]. However, and in spite of the well known sympathetic surge following an apneic episode, this effect has been largely ignored in the literature. Given that the increased sympathetic activity due to the presence of apneic events could mimic a chronically increased sympathetic tone, we also studied the effect of removing the apneic episodes from the analysis. Additionally, a preliminary analysis revealed high respi-

ratory rates in some subjects, which could compromise the interpretation of the HF HRV component. For this reason, alternative definitions of the HF band were considered.

When comparing the patients with SAS plus additional cardiac comorbidities with their matched controls (SAS patients without CVD), we found a decreased sympathovagal balance, as assessed by lower values of $R_{LF/HF}^e$ and P_{LFH}^e , suggesting a reduced sympathetic dominance. Additionally, in the SHHS dataset and during NREM, this effect could only be assessed when excluding the apneic events from the analysis, which might imply that the sympathetic surges following apneas could be masking the lowered sympathetic dominance in the group with cardiac comorbidities. This apparent lower sympathetic control could be caused by a desensitization of cardiac β -adrenergic receptors when subjected to a recurrent stimuli [25], such as the continuous sympathetic discharges following apneic episodes, which could point to SAS as a possible precursor of CVD since heart damage has been associated with decreased β -adrenergic receptors density and sensitivity [49]. Moreover, a retrospective analysis in SAS patients also revealed a decreased sympathetic dominance in those subjects that will develop CVD in the future. In this way, the results suggest that SAS patients with a reduced sympathovagal balance could be at higher risk of developing CVD, and the fact that a decreased SNS activity was assessed prior to the arise of cardiac comorbidities encourages further research in the field of autonomic control in sleep apnea, and suggests that HRV could represent a useful tool for improving the screening of SAS patients with increased cardiovascular risk.

8.1.3 Cardiorespiratory signals analysis in sport sciences applications

In Ch. 6 and 7, the noninvasive estimation of the TV and the AT was addressed. Both parameters have a great interest in the field of sports sciences, since they can be used for assessing the physical condition of a subject, for the design of better training routines or to prevent from overtraining. Moreover, they also have clinical value: whereas the TV is drastically reduced in some obstructive respiratory disorders, such as COPD or asthma exacerbations, the AT was initially intended to assess the physical condition of patients with CVD [272].

For the estimation of the TV, several ECG-derived features were extracted from a dataset of 25 volunteers who performed a maximal effort treadmill test. These features were employed for training a linear model, and this model was used to estimate the TV of the same subjects during a submaximal treadmill test performed in a different day. The best results were obtained when combining the information extracted from the instantaneous HR and a single-lead EDR signal derived from the downslopes of the R waves, in a multi-parametric approach. Fitting errors lower than 14% in most of the cases and as low as 6% in some of them suggest that TV can be estimated using only the ECG, and in a non-stationary scenario. Although we only considered an exercise test, TV estimation could be useful in the monitoring of several respiratory disorders, such as Cheyne-Stokes respiration, COPD or asthma. Nevertheless, validation in these scenarios remains crucial.

Regarding the estimation of the AT, the ventricular repolarization dynamics were analyzed from the dT profile, as proposed in previous works. Additionally, and under the hypothesis that the VT should be related with an increased sympathetic activity, also the PRD profile was considered. In both cases, the onset of the characteristic increase in repolarization instability observed at high exercise intensities was employed as an estimation of the AT, yielding to estimation errors lower than 25 W (equivalent to 1 minute in the employed dataset) in most of the subjects. These accurate results suggest that it is possible to estimate the AT in a noninvasive way, using only ECG-derived features.

8.1.4 Conclusion

Cardiorespiratory signal analysis remains the most extensively employed tool for the noninvasive assessment of the ANS. Given the intrinsic variability of ANS activity under different situations or in response to distinct stimuli, it is of paramount importance that the analyses are guided by physiology, so that the results can be provided with a physiological interpretation. In this dissertation, ANS assessment has been applied to several clinical and non-clinical scenarios, and the employed methodology has been contextualized and adapted to the particularities of each of them. In this way, a framework for dealing with several physiological conditions, such as high or low respiratory rates, ectopic beats or the presence of sleep apneas has been provided.

8.2 Future work

Some future research lines derived from the different parts of this thesis are described below.

- The performance of the methodology proposed in Ch. 2 for the accurate detection of ectopic beats in the presence of strong RSA episodes was tested using a simulation study, for which the MIT-BIH dataset was employed. However, this dataset is composed by adults, with a less pronounced RSA than in the case of young children, for who the methodology was proposed. Therefore, its performance should be further tested in populations which are more similar to the target one.
- The use of ϕ for the characterization of the HRV spectra in children with different risk of asthma revealed that not only the power content of the HF band but also the way it is distributed could provide some information regarding the ANS status. In this way, it could be interesting to evaluate this index in a larger set of pathological conditions, such as COPD or bronchitis, for the sake of a better understanding of their relationship with abnormal ANS activity.
- In Ch. 3, the differences in ANS activity of a group of children under ICS treatment were evaluated before and after treatment conclusion. However, no information regarding the children status before the treatment onset was available. The

comparison of autonomic control before and after ICS treatment could shed some light on the effects of the treatment on the ANS. Additionally, the inclusion of information regarding the sleep stages would allow a more detailed analysis of the overnight recordings.

- The main limitation of the study of ANS-related features for the stratification of asthmatic adults was the sample size, with only 30 subjects divided in up to 3 groups. The inclusion of more subjects could improve the feature selection process, and possibly the classification performance. Also the definition of new features derived from respiratory signals which could provide information of the airway status would be desirable. Additionally, it would be of great interest to develop a protocol in which the subjects are subjected to autonomic tests (in the current protocol only basal conditions were considered), so that the response of the different groups can be characterized.
- Although the effect of medication was carefully addressed in Ch. 5, it could not be discarded as a possible confounder of the decreased sympathetic dominance observed in subjects with SAS plus additional cardiac comorbidities. In this way, the inclusion of a larger number of unmedicated subjects would allow to discern to what extent the medication is affecting the results. Moreover, regarding the SHHS dataset, only the baseline but not the follow up session was considered. The analysis of the follow up session could provide some insight into the evolution of ANS activity in those SAS patients at higher risk of developing CVD.
- The TV was only estimated in a dataset of healthy subjects, within a small age and physical condition range. In this way, the validation of this methodology in more heterogeneous datasets remains crucial. Moreover, given its potential application in the monitoring of several respiratory disorders, the proposed methodology should be also tested in patients suffering from the target disorders. The possibility of employing more complex estimation models with more degrees of freedom than the first order linear model proposed here could also represent a future work line. Also adding demographic information could result in more precise and personalized estimation models.
- The main limitation in the analysis of the repolarization dynamics profile for the estimation of the AT was also the small demographic range considered. For this reason, the proposed methodology should be extended to more complete datasets. Additionally, the analysis should be repeated using the Frank's lead configuration for registering the ECG, so that the three-dimensional information was available.

Part V

Appendix

Awards and scientific contributions

Awards

- *Best poster presentation.* Heart Rate Variability Analysis Assessment for Asthma Control Stratification. *XLVI International Conference on Computing in Cardiology*, 2019, Singapore.
- *Semi-finalist of the Rosanna Degani Young Investigators' Awards competition.* On Deriving Tidal Volume From Electrocardiogram During Maximal Effort Test. *XLV International Conference on Computing in Cardiology*, 2018, Maastricht, The Netherlands.
- *Mortara mobility fellowship.* On Deriving Tidal Volume From Electrocardiogram During Maximal Effort Test. *XLV International Conference on Computing in Cardiology*, 2018, Maastricht, The Netherlands.

Scientific contributions

Journal publications

- **Milagro, J.**, Gracia, J., Seppä, V. P., Karjalainen, J., Paassilta, M., Orini, M., Bailón, R., Gil, E. and Viik, J. Noninvasive Cardiorespiratory Signals Analysis for Asthma Evolution Monitoring in Preschool Children. Major revision (*IEEE Trans Biomed Eng*).
- **Milagro, J.**, Hernando, D., Lázaro, J., Casajús, J. A., Garatachea, N., Gil, E., and Bailón, R. Electrocardiogram-Derived Tidal Volume During Treadmill Stress Test. *IEEE Trans Biomed Eng*, 2019. In early access. DOI: 10.1109/TBME.2019.2911351.
- **Milagro, J.**, Deviaene, M., Gil, E., Lázaro, J., Buyse, B., Testelmans, D., P. Borzé, R. Willems, S. Van Huffel, R. Bailón and Varon, C. Autonomic Dysfunction Increases Cardiovascular Risk in the Presence of Sleep Apnea. *Front Physiol*, 2019, vol. 10, n. 620, pp. 1-11.
- **Milagro, J.**, Gil, E., Lázaro, J., Seppä, V. P., Malmberg, L. P., Pelkonen, A. S., Kotaniemi-Syrjänen, A., Mäkelä, M. J., Viik, J. and Bailón, R. Nocturnal Heart Rate Variability Spectrum Characterization in Children with Asthmatic Symptoms. *IEEE J Biomed Health Inform*, 2017, vol. 22, n. 5, pp. 1332-1340.

Journal publications in preparation

- **Milagro, J.**, Soto-Retes, L., Giner, J., Varon, C., Laguna, P., Bailón, R., Plaza, V. and Gil, E. Asthmatic Subjects Stratification Using Autonomic Nervous System Information.
- **Milagro, J.**, Hernández, A., Hernando, D., Garatachea, N., Bailón, R. and Pueyo, E. Estimation of Anaerobic Threshold through Ventricular Repolarization Profile Analysis.

Conference publications derived from the thesis

- **Milagro, J.**, Gracia, J., Seppä, V. P., Karjalainen, J., Paassilta, M., Orini, M., Gil, E., Bailón, R. and Viik, J. Cardiorespiratory coupling in asthmatic children. *XLVI International Conference on Computing in Cardiology*, 2019, Singapore. Accepted for publication.
- **Milagro, J.**, Soto, L., Giner, J., Varon, C., Laguna, P., Plaza, V., Gil, E. and Bailón, R. Heart Rate Variability Analysis Assessment for Asthma Control Stratification. *XLVI International Conference on Computing in Cardiology*, 2019, Singapore. Accepted for publication.
- Morales, J., Deviaene, M., **Milagro, J.**, Testelmans, D., Buyse, B., Willems, R., Orini, M., Van Huffel, S., Bailón R. and Varon C. Evaluation of Methods to Characterize the Change of the Respiratory Sinus Arrhythmia with Age in Sleep Apnea Patients. *41st Annual International Conference of the IEEE Engineering in Medicine & Biology Society (EMBC)*, Berlin, Germany 2019. Accepted for publication.
- **Milagro, J.**, Hernando, D., Lázaro, J., Casajús, J. A., Garatachea, N., Gil, E. and Bailón, R. On Deriving Tidal Volume From Electrocardiogram During Maximal Effort Test. *Proceedings of the XLV International Conference on Computing in Cardiology*, 2018, pp. 1-4, Maastricht, The Netherlands.
- Morales, J., Deviaene, M., **Milagro, J.**, Testelmans, D., Buyse, B., Bailón, R., Willems R., Van Huffel, S. and Varon C. Respiratory Sinus Arrhythmia in Apnea Patients With Apnea Associated Comorbidities. *Proceedings of the XLV International Conference on Computing in Cardiology*, 2018, pp. 1-4 Maastricht, The Netherlands.
- **Milagro, J.**, Gil, E., Garzón-Rey, J.M., Aguiló, J. and Bailón, R. Inspiration and Expiration Dynamics in Acute Emotional Stress Assessment. *Proceedings of the XLIV International Conference on Computing in Cardiology*, 2017, pp. 1-4, Rennes, France.
- **Milagro, J.**, Gil, E., Bolea, J., Seppä, V. P., Malmberg, L. P., Pelkonen, A. S., Kotaniemi-Syrjänen, A., Mäkelä, M. J., Viik, J. and Bailón, R. Nonlinear Dynamics of Heart Rate Variability in Children with Asthmatic Symptoms. *Joint conference of the European*

Medical and Biological Engineering Conference (EMBEC) and the Nordic-Baltic Conference on Biomedical Engineering and Medical Physics (NBC), 2017, pp. 815-818. Springer, Singapore.

- Seppä, V. P., **Milagro, J.**, Pelkonen, A. S., Gil, E., Lázaro, J., Kotaniemi-Syrjänen, A., Mäkelä, M. J., Viik, J., Bailón, R. and Malmberg, L. P. Nocturnal variabilities of tidal airflow and heart rate show mutual association in young children with asthma symptoms. *European Academy of Allergy and Clinical Immunology Congress*, 2017, vol. 72, pp. 9-9, Helsinki, Finland.

Conference publications not related with the thesis

- **Milagro, J.**, Gil, E., Garzón-Rey, J.M., Aguiló, J. and Bailón, R. Inspiration and Expiration Dynamics in Acute Emotional Stress Assessment. *Proceedings of the XLIV International Conference on Computing in Cardiology*, 2017, pp. 1-4, Rennes, France.
- Garzón-Rey, J.M., Lázaro, J., **Milagro, J.**, Gil, E., Aguiló, J. and Bailón, R. Respiration-Guided Analysis of Pulse and Heart Rate Variabilities for Acute Emotional Stress Assessment. *Proceedings of the XLIV International Conference on Computing in Cardiology*, 2017, pp. 1-4, Rennes, France.

List of acronyms

AASM	American Academy of Sleep Medicine
ACh	Acetylcholine
AHI	Apnea Hypopnea Index
ANS	Autonomic Nervous System
ATP	Adenosine Triphosphate
AV	Atrio-Ventricular
AWGN	Additive White Gaussian Noise
BW	Bandwidth
CA	Current Asthma
CA-N	Negative Current Asthma
CA-P	Possible Current Asthma
CA-Y	Positive Current Asthma
COPD	Chronic Obstructive Pulmonary Disease
CRC	Cardiorespiratory Coupling
CSA	Central Sleep Apnea
CVD	Cardiovascular Disease
ECG	Electrocardiogram
EDR	Electrocardiogram-Derived Respiration
GINA	Global Initiative for Asthma
HF	High Frequency
HiR	High Risk
HR	Heart Rate

HRV	Heart Rate Variability
HUH	Helsinki University Hospital
ICS	Inhaled Corticosteroids
IgE	Immunoglobulin E
IL	Interleukin
IP	Impedance Pneumography
IQR	Interquartile Range
LABA	Long Acting β_2 -Agonist
LF	Low Frequency
LoR	Low Risk
mAPI	Modified Asthma Predictive Index
NANC	Non-Adrenergic Non-Cholinergic
NREM	Non-Rapid Eye Movement
NTS	Nucleus Tractus Solitarius
OSA	Obstructive Sleep Apnea
OSAS	Obstructive Sleep Apnea Syndrome
OSP	Orthogonal Subspace Projection
PAP	Positive Airway Pressure
PCA	Principal Component Analysis
PNS	Parasympathetic Nervous System
PRG	Pontine Respiratory Group
PSD	Power Spectral Density
PSG	Polysomnography
REM	Rapid Eye Movement
RSA	Respiratory Sinus Arrhythmia
RTC	Rapid Thoracoabdominal Compression
SA	Sino-Atrial
SAS	Sleep Apnea Syndrome

SDB	Sleep-Disordered Breathing
SHHS	Sleep Heart Health Study
SNR	Signal-to-Noise Ratio
SNS	Sympathetic Nervous System
SPT	Skin Prick Test
TAYS	Tampere University Hospital (Tampereen Yliopistollinen Sairaala)
TF	Time-Frequency
TFC	Time-Frequency Coherence
T_h2	Type 2 Helper
TV	Tidal Volume
TVIPFM	Time-Varying Integral Pulse Frequency Modulation
VRG	Ventral Respiratory Group

List of figures

1.1	Anatomy of the sympathetic (left) and parasympathetic (right) branches of the autonomic nervous system. The effect exerted by each branch over the different organs that they innervate is indicated. Reproduced and modified from [242].	6
1.2	Cardiac electrical conduction system. The morphology and timing of the action potentials generated in different parts of the heart and the surface electrocardiogram resulting from their spatio-temporal combination are displayed. Reproduced from [246].	7
1.3	Characteristic waves and intervals in the electrocardiogram. Reproduced from [246].	8
1.4	Electrodes placement in the standard 12-lead ECG. The dispositions for the acquisition of the bipolar limb leads (<i>I</i> , <i>II</i> and <i>III</i>), the augmented unipolar limb leads (<i>aVF</i> , <i>aVL</i> and <i>aVR</i>) and the unipolar precordial leads (V_1 to V_6) are displayed. Reproduced from [246].	9
1.5	Angular directions covered in the frontal (left) and horizontal (right) planes with the limb and precordial leads, respectively. Reproduced from [246].	9
1.6	Anatomy of the respiratory centers (NTS: nucleus tractus solitarius, PRG: pontine respiratory group, DRG: dorsal respiratory group, VRG: ventral respiratory group, CN: cranial nerves). Reproduced and modified from [242].	10
1.7	Example of the effect of respiratory activity on the ECG. Red and blue segments corresponds to inspiration and expiration respectively. Three different effects are displayed in the figure: amplitude changes (marked with a black dashed line), respiratory sinus arrhythmia (that manifests as decreasing inter-beat intervals during inspiration, t_1 , which increase again during expiration, t_2), and changes in QRS complex morphology (reflected, e.g., as variations in the R wave angle from inspiration, ϕ_1 , to expiration, ϕ_2).	13

- 1.8 Different heart rhythm representations are displayed. In a), an ECG with the beat occurrence times is displayed. Below, the interval tachogram (b)), inverse interval tachogram (c)), interval function (d) and inverse interval function (e)) representations are depicted. The units in the ordinate axes of a) are given in arbitrary units, whereas those in b) and d) are expressed in seconds, and those in c) and e) in hertz. Reproduced and modified from [246]. 15
- 1.9 The inflammatory response in asthma. When the presence of an allergen in the airways is detected, the dendritic cells release cytokines to attract T_H2 cells, which triggers a complex inflammatory response. The T_H2 cells secrete several interleukines which stimulate B cells and mast cells growth, as well as eosinophils and IgE production. The binding of IgE to specific receptors in the eosinophils and mast cells cause the release of a series of pro-inflammatory substances, whose combined effects lead to airway inflammation. 20
- 1.10 An example of the effect of M_2 receptors dysfunction in the presence of eosinophils is displayed. In a) and b), a vagal stimulus triggers the secretion of acetylcholine (ACh) from the vagus nerve. In c), the ACh binds to the M_2 and M_3 receptors, which inhibit the further release of ACh and contract the airway smooth muscle respectively, as in e). During an inflammatory response, the eosinophils release positively charged proteins, such as major basic proteins, which bind to the M_2 receptors (b)), thus blocking the binding of ACh, as in d). This leads to an uncontrolled ACh release (f)), which may result in excessive smooth muscle contraction. This figure has been adapted and modified from [90]. 22
- 1.11 Two different interpretations of the pathogenesis of asthma. In a), inflammation is the direct cause of airway obstruction and hyper-responsiveness. However, this scheme is not enough to explain certain phenotypes of asthma in which inflammation is not a likely underlying cause of hyper-responsiveness. In b), ANS dysfunction (e.g., M_2 receptors dysfunction) is presented as the cause of airway hyper-responsiveness, and it can be originated either by inflammation or by any other cause, thus providing a more complete frame. 23
- 1.12 An example of obstructive sleep apnea and hypopnea is displayed. In a), the upper airways remain open, thus enabling normal breathing. When a partial (b)) or total (c)) obstruction of the respiratory flow takes place, the interruption of normal breathing is referred to as obstructive hypopnea or apnea, respectively. 24

- 1.13 The ventilatory equivalents for O_2 (\dot{V}_E/\dot{V}_{O_2} , green) and CO_2 (\dot{V}_E/\dot{V}_{CO_2} , red) are displayed during an incremental effort test. The point at which \dot{V}_E/\dot{V}_{O_2} starts to increase without an increase in \dot{V}_E/\dot{V}_{CO_2} is identified as the aerobic threshold or VT1, whereas the point at which there is a simultaneous increase in \dot{V}_E/\dot{V}_{O_2} and \dot{V}_E/\dot{V}_{CO_2} is referred to as the anaerobic threshold or VT2. 28
- 1.14 The CO_2 consumption (\dot{V}_{CO_2}) is displayed as a function of the O_2 consumption (\dot{V}_{O_2}). The point at which \dot{V}_{CO_2} increases exponentially with respect to \dot{V}_{O_2} is referred to as the ventilatory threshold (VT). 29
- 2.1 Schematic of the time-varying integral pulse frequency modulation (TVIPFM) model. Reproduced and modified from [19]. 37
- 2.2 A real premature ventricular contraction (a) and some examples showing the effect that ectopic beats exert on HRV spectrum is displayed. The spectra on the right column correspond to the tachograms on their left. In b) and c), the original tachogram and its spectra is shown, whereas in the other examples 1 (d) and e)), 5 (f) and g)), 10 (h) and i)) and 30 (j) and k)) ectopic beats were added. It can be noticed how an increasing number of ectopic beats distort the power distribution of the HRV spectra, thus compromising HRV analysis. 41
- 2.3 Example of a failure in ectopic beat correction. Original R peaks detections are marked with black circles, whereas red crosses indicate the corrected positions after applying the ectopic correction algorithm. The large RR interval in the figure on the left is interpreted as abnormal, so that the beat highlighted with a red dashed line is considered as ectopic and its R peak location is modified. 42
- 2.4 A schematic of the algorithm for RSA episodes detection and correction is displayed. First, the beat labeled as ectopic comes through a morphology analysis, and if it is considered similar to its surrounding beats, the RR interval dynamics are taken into account. If the pattern followed by the tachogram is identified as a RSA episode, beat positions are updated. Otherwise, beat positions obtained from the ectopic correction algorithm are kept unchanged (see text for a detailed description of the algorithm). 43
- 2.5 Three different RSA patterns are displayed. Each RR interval series correspond to the ECG segment displayed at its left. In a) and b), a decelerating pattern is shown, whereas the end and the beginning of two acceleration patterns are displayed at c) and d) and at e) and f) respectively. In the ECG segments, the black circles and the red crosses indicate the original detections and the detections after applying the ectopic correction respectively. The red circles in the RR interval series indicate the RR interval previous to the possible ectopic (RR_{e-1}), and the green ones indicate the RR interval occasioned by it (RR_e). 45

2.6 Differences in the tachograms obtained when varying ectopic and RSA detection and correction thresholds. The same ECG segment is represented in a), d), g) and j), and the tachograms on the right of each ECG representation were obtained from the detection of its R peaks, whereas in c), f), i) and l) the spectrum of each tachogram is shown. Red crosses and dashed lines represent the detections after applying the ectopic correction algorithm and the tachogram obtained from them, respectively, whereas the green crosses and solid lines represent the detections after applying the RSA detection and correction, and the resulting tachograms. In this example, θ_{HR} and θ_{RSA} were fixed at 1 and 1.5 respectively, whereas θ_{morph} was selected as 0 in a), b) and c), 0.5 in d), e) and f), 1 in g), h) and i), and 1.5 in j), k) and l). 47

2.7 Differences in the tachograms obtained when varying ectopic and RSA detection and correction thresholds. The same ECG segment is represented in a), d), g) and j), and the tachograms on the right of each ECG representation were obtained from the detection of its R peaks, whereas in c), f), i) and l) the spectrum of each tachogram is shown. Red crosses and dashed lines represent the detections after applying the ectopic correction algorithm and the tachogram obtained from them, respectively, whereas the green crosses and solid lines represent the detections after applying the RSA detection and correction, and the resulting tachograms. In this example, θ_{HR} and θ_{RSA} were fixed at 2 and 1.5 respectively, whereas θ_{morph} was selected as 0 in a), b) and c), 0.5 in d), e) and f), 1 in g), h) and i), and 1.5 in j), k) and l). 48

2.8 Sensitivity and specificity of the beat classification in normal (a) and c) or ectopics (b) and d)), for the different proposed thresholds. The red lines indicate the results obtained when only ectopic correction is applied, whereas the blue lines indicate the results obtained after applying both ectopic and RSA detection and correction (the results for growing values of θ_{morph} are further from the red line and closer to the green line, the latter indicating the results obtained for the largest value of θ_{morph}). $\theta_{RSA} = 1.15$ was employed. 49

2.9 Sensitivity and specificity of the beat classification in normal (a) and c) or ectopics (b) and d)), for the different proposed thresholds. The red lines indicate the results obtained when only ectopic correction is applied, whereas the blue lines indicate the results obtained after applying both ectopic and RSA detection and correction (the results for growing values of θ_{morph} are further from the red line and closer to the green line, the latter indicating the results obtained for the largest value of θ_{morph}). $\theta_{RSA} = 1.5$ was employed. 50

2.10 Three different simulated HRV spectra with the same P_{HF} but different shapes are displayed. 52

2.11	Scheme followed for studying the relationship of \wp with different parameters (see text for details).	54
2.12	Synthetic HRV spectral with one (a) or several (b)) peaks in the HF band. The frequency bands used for the computation of peakness and the frequency of the component of interest (F_c) are displayed. In the case of the unimodal signal, $\wp = 0.44$, whereas in the multi-modal signal $\wp = 0.24$	56
2.13	Evolution of \wp in function of τ_0 (a)) and BW (b)). \wp is shown for several different values of Δf selected as multiples of the resolution of the Hamming window. Note that in b) the axis of abscissas is represented in logarithmic scale.	57
2.14	Evolution of \wp (a)) and κ (b)) in function of BW. For the computation of \wp , $\Delta f = \Delta H$ was selected. Note that the axes of abscissas are represented in logarithmic scale.	58
2.15	Evolution of \wp (solid line) and $\hat{\wp}(\kappa)$ (dashed line) in function of BW. Both parameters are shown for several different values of Δf selected as multiples of the resolution of the Hamming window. Note that the axis of abscissas is represented in logarithmic scale.	59
2.16	Evolution of \wp and κ in function of the ratio of the amplitudes of two peaks placed within the HF band of HRV spectra. \wp is shown for several different values of Δf selected as multiples of the resolution of the Hamming window.	60
2.17	Evolution of \wp , P_{LF} , P_{HF} and D_2 in function of A_{HF} when only one HF peak is considered. \wp is shown for several different values of Δf selected as multiples of the resolution of the Hamming window.	62
2.18	Evolution of \wp , P_{LF} , P_{HF} and D_2 in function of the ratio of the amplitude of the peak of interest and the sum of the amplitudes of four additional peaks. \wp is shown for several different values of Δf selected as multiples of the resolution of the Hamming window.	63
2.19	The definition of different HF bands for the same HRV spectrum are displayed: the classical HF band (a)), the extended HF band (b)) and a HF band centered in respiration (c)). The green area in each case represents the part of the spectrum that is considered for the calculation of the HF power.	65

- 2.20 Two examples of HRV spectra (a) and c)) and their correspondent respiration spectra (b) and d), respectively) are displayed. Whereas in a) and b) the respiratory rate is above 0.15 Hz (marked with black dashed lines), in c) and d) it lays within the LF band, thus compromising HRV analysis. Orthogonal subspace projection decomposition was applied to the spectra in c) and d), and the respiration (green) and residual (red) components are displayed. 67
- 3.1 Distribution of the subjects in the TAYS dataset attending to their current asthma status (CA-N: no current asthma, CA-P: possible current asthma, CA-Y: current asthma) and their risk of developing asthma as derived from the mAPI (light gray: low risk, dark gray: high risk). This information was not available for 1 of the 68 subjects. 77
- 3.2 Distribution of the subjects in the TAYS dataset attending to the three different classifications. In the figure, CA-N, CA-P and CA-Y refer to the current asthma status (CA-N: no current asthma, CA-P: possible current asthma, CA-Y: current asthma), whereas T-N, T-P and T-E refer to the response to ICS treatment (T-N: not effective, T-P: partially effective, T-E: effective). Dark gray represents the atopic subjects, whilst light gray is used for non-atopics. This information was not available for 2 of the 68 subjects. 78
- 3.3 A five-minute segment of the normalized time-frequency distribution of the heart rate modulating signal (a)) and the impedance pneumography signal (b)) are displayed. In c), the time-frequency coherence distribution is depicted. The black dotted lines represent the limits between which $\hat{\gamma}^2(t, f) \geq \gamma_{TH}(t, f; \alpha)$, defining $\Omega(t)$ (see text for details). 81
- 3.4 Bland-Altman plot for agreement evaluation between ϕ_{HRV}^{IP} and ϕ_{IP}^{IP} . In the figure, μ is the mean of $\phi_{HRV}^{IP} - \phi_{IP}^{IP}$, whereas σ is the standard deviation of these differences. 85
- 3.5 Temporal evolution of the mean values of ϕ_{HRV}^{IP} and P_{LFn} is shown for the LoR (black), HiR (dark gray) and ICS (light gray) groups of the HUH dataset. Boxplots are centered in the intermediate hour of the two-hour interval considered (boxplots for different groups, although plotted separately for interpretation purposes, are calculated with the same time references). * and ** indicate significant differences ($p < 0.05$ and $p < 0.017$ respectively) among groups in the given two-hour interval. 85

- 3.6 Boxplots corresponding to some of the analyzed parameters in R1 (black), R2 (dark gray) and R3 (light gray) in the TAYS dataset, attending to the current asthma status. Each box corresponds to a two-hour window centered in the hour depicted in the figure (although boxes with the same time reference are depicted separately for clarity, same central hour was considered in the analysis). Medians of the boxes corresponding to the same measurement day are connected with solid lines, and statistical significant differences are labeled with * ($p \leq 0.05$). Statistical differences after Bonferroni correction ($p \leq 0.017$) are labeled as **. P_{HF} , as obtained from $m(n)$, is adimensional (ad). In order to improve the readability of the figure, only the interval 00 to 05 a.m. is displayed. 92
- 3.7 Time course of P_{HF} for R1 (black), R2 (dark gray) and R3 (light gray) of three subjects belonging to the different current asthma groups. P_{HF} , as obtained from $m(n)$, is adimensional (ad). 93
- 3.8 Boxplots corresponding to some of the analyzed parameters in R1 (black), R2 (dark gray) and R3 (light gray) in the TAYS dataset. Only the subjects classified as low risk and CA-Y/CA-N are depicted. Each box corresponds to a two hours window centered in the hour depicted in the figure (although boxes with the same time reference are depicted separately for clarity, same central hour was considered in the analysis). Medians of the boxes corresponding to the same measurement day are connected with solid lines, and statistical significant differences are labeled with * ($p \leq 0.05$). Statistical differences after Bonferroni correction ($p \leq 0.017$) are labeled as **. P_{HF} , as obtained from $m(n)$, is adimensional (ad). In order to improve the readability of the figure, only the interval 00 to 05 a.m. is displayed. 94
- 4.1 a) Normalized power spectral density of the modulating signal (blue) and the respiratory effort (pink) in a five-minute segment. Note that the respiratory activity lays below 0.15 Hz (black dashed line). b) Orthogonal subspace projection was applied to separate the respiratory-related (green) and -unrelated (red) components of the modulating signal. 104
- 4.2 A segment of a respiratory effort signal (solid line) and its derivative (dashed line) are displayed, together with the definition of the parameters used for the characterization of the respiratory dynamics. The delineation of a given breath is shown, so that the black facing-up and -down triangles represent its peak and nadir, the pink facing-up and -down triangles mark the points of maximum up and downslope and the green and red circles indicate its onset and offset, respectively. 105

- 4.3 A schematic of the combination of the leave-one-patient-out cross-validation with bootstrapping is displayed. The circles represent the subjects in the dataset (N subjects) whereas their color represent that they belong to different groups. After defining a training (white rectangle) and a test (gray square) set, bootstrapping is applied K times to obtain K different training sets. Then, the median of the performance of the K classifiers is used as a robust measure of the performance of the tested classification model. . . . 106

- 4.4 The accuracy, sensitivity, specificity and F1 score obtained with the different classifiers when the patients were classified based on their asthma severity are displayed. In the case of the accuracy, the squares represent the values obtained when only the cardiorespiratory features were consider in the model, whereas the down-facing triangles account for the results when only the clinical parameters were used and the up-facing triangles represent the performance when all the features were used together. In the other cases, the black, gray and white circles represent the values obtained for the mild, severe controlled and severe uncontrolled groups respectively, when all the features were employed. Linear, quadr, cubic and RBF refer to the kernels employed in the SVM classifier (see text for details). 109

- 5.1 A flowchart of the data analysis performed for each subject is displayed. First, the modulating signal was divided in periods corresponding to NREM (black) and REM (gray) sleep. Afterwards, two different HRV analyses were performed in each of the sleep stages: one including the apneic episodes (red) and one excluding them (the one-minute period after the apneic episodes are included in the segments highlighted in red). The HRV analyses were performed over five-minute windows of available signal. 119

- 5.2 Average spectra for all the NREM segments (excluding those with apneic episodes) of a control subject of the UZ Leuven dataset (black) and his match (gray) are displayed. An increased sympathetic dominance can be noticed in the control subject, as reflected by the relative higher low frequency power content. The dashed black lines indicate the boundaries of the low frequency band. The number of averaged 5 minute segments was 50 and 36 for the control and the match respectively. As estimated from the modulating signal, the power spectral density is given in arbitrary units (a.u.). 121

- 5.3 Boxplots of the differences in \overline{NN} ($\Delta\overline{NN}$) and P_{LFn}^e (ΔP_{LFn}^e) between the control subjects of the UZ Leuven dataset and their matches under or not under medication intake (during NREM sleep and excluding apneic episodes). Whereas $\Delta\overline{NN}$ was decreased in the group under medication intake when compared with the group without medication ($p < 0.05$, indicated with *), no differences in ΔP_{LFn}^e were assessed. 122
- 6.1 Stage segmentation for MaxT, a), and SubT, b), of one subject is shown. Vertical lines indicate onset and offset of the different stages for each test, whereas horizontal lines mark the different percentages of maximum HR used for segmentation. In both cases, there is a 30-second interval between I_{rest} and I_{0-60} , and between I_{80-100} and I_{recov} , in order to exclude the transition from rest to exercise and from exercise to recovery respectively. . . . 133
- 6.2 Derivation of the amplitude difference series using R-S amplitude as EDR. In a), R (green circles) and S (red circles) waves were detected in the ECG signal, and the difference between them was calculated for each beat to obtain a R-S amplitude series. $x_{EDR}(t)$ is a low-pass filtered version of this series (b)). Finally, the peaks and nadirs in $x_{EDR}(t)$ were detected (pink and blue circles respectively), and the series generated from the difference between them was resampled at the times when breaths occur and smoothed with a 10-sample median filter. The result, $\theta^m(k)$ (c)), was used as a feature for our linear model. 134
- 6.3 Real (blue) and estimated (red) tidal volume (\hat{V}_T^s) for a given subject is displayed. The different estimations were obtained from the best performing lead (lead II in this case) of the single-lead EDR approach (a)), the multi-lead EDR approach (b)), the instantaneous HR (c)) approach, the HRV approach (d)), the respiratory rate approach (e)) and the best performing feature combination (lead II in the EDR approach plus instantaneous HR in this case) of the multi-parametric approach (f)). 139
- 6.4 Scatter plots of the tidal volume estimated from the multi-parametric approach when combining the downslopes of lead II and the HR (\hat{V}_T^s) against the real one (\hat{V}_T^s) for all the subjects and each of the stages (a): I_{rest} , b): I_{0-60} , c): I_{60-80} , d): I_{80-100} and e): I_{recov}). Dashed lines indicate $\hat{V}_T^s = V_T^s$ 140

- 7.1 Calculation of the dT series. In a), the original T waves of the three considered leads ($V4$: blue, $V6$: red, aVF : green) are displayed. In b), they were subtracted their first sample to have a common origin, and they were truncated to the first zero-crossing, marked with a black dashed line. Only the portion of the T waves displayed in bold were used for computing dT . In c), the T waves are displayed along three perpendicular axes, and the values of their mean amplitude (displayed with filled circles) was used to construct the repolarization vector (black arrow). Afterwards, dT was calculated as the angular difference between this vector and the vector corresponding to the previous beat (gray arrow). 148
- 7.2 a) Instantaneous HR (red, left axis) and dT (green, right axis) during the exercise test for a given subject. The HR and dT profiles are represented in bold. Moreover, the first derivative of the dT profile is displayed (cyan, rescaled for representation purposes). b) Temporal evolution of the PRD (blue), with its profile represented in bold and its first derivative in cyan (rescaled for representation purposes). The dashed black and pink lines represent the occurrence time of the ventilatory threshold and the estimated anaerobic threshold. 149
- 7.3 Time-frequency distribution of dT (detrended). The dashed black and pink lines represent the occurrence time of the ventilatory threshold and the estimated anaerobic threshold, respectively. The limits of the band used for computing PRD are shown in white, whereas the dotted red and green lines represents the limits of a 0.125 Hz band centered in the alias terms $HR(t) - F_c$ and $|2F_c - HR(t)|$, respectively (F_c , represents the pedaling cadence) 150
- 7.4 a) Boxplots of the error in the estimation of the anaerobic threshold using the dT or the PRD series. b) Difference in the estimation error when using three or two leads, and considering the dT or the PRD series. In both figures, the filled circles represent the values for the different subjects. 152

List of tables

2.1	Sensitivity and specificity of the detection of normal and ectopic beats in the MIT-BIH arrhythmia dataset (see test for details) with the proposed methodology. The results obtained for different combinations of thresholds are displayed.	51
3.1	Characteristics of the children in the HUH dataset. (Whereas continuous variables are expressed as median (min-max), integer variables are displayed as n (%). BMI: Body Mass Index, SPT: Skin Prick Test.)	76
3.2	Median value between 02 and 04 a.m. of the presented parameters for each of the groups of the HUH dataset (median [25 th , 75 th percentiles]). * and ** indicate differences with LoR ($p < 0.05$ and $p < 0.017$ respectively). Since P_{LF} , P_{HF} and TP are calculated from $m(n)$ and not directly from RR interval series, they are adimensional (ad). Nonlinear indexes were calculated from a filtered version of the RR intervals (band-pass filter centered in the respiratory rate).	84
3.3	Median and [25 th , 75 th percentiles] of the most relevant time domain HRV parameters obtained from a two-hour window centered at 04 a.m. in the TAYS dataset. Results for each recording day attending to their current asthma status, atopy and response to treatment are displayed. Statistical significant differences with R1 are indicated with * ($p \leq 0.05$), whereas differences with R2 are labeled with † ($p \leq 0.05$). Statistical differences after Bonferroni correction ($p \leq 0.017$) are labeled as ** or ‡.	88
3.4	Median and [25 th , 75 th percentiles] of the most relevant frequency domain HRV parameters obtained from a two-hour window centered at 04 a.m. in the TAYS dataset. Results for each recording day attending to their current asthma status, atopy and response to treatment are displayed. Statistical significant differences with R1 are indicated with * ($p \leq 0.05$), whereas differences with R2 are labeled with † ($p \leq 0.05$). Statistical differences after Bonferroni correction ($p \leq 0.017$) are labeled as ** or ‡.	89

3.5	Median and [25 th , 75 th percentiles] of the proposed cardiorespiratory coupling parameters obtained from a two-hour window centered at 04 a.m. in the TAYS dataset. Results for each recording day attending to their current asthma status, atopy and response to treatment are displayed. Statistical significant differences with R2 are indicated with † ($p \leq 0.05$) or ‡ (after Bonferroni correction, $p \leq 0.017$).	90
4.1	Demographics and clinical parameters of the subjects classified based on their asthma severity and control. The values are displayed as median [25 th , 75 th percentiles] for the continuous variables (* and † indicate $p < 0.05$ with respect to the mild and severe controlled groups respectively, whereas ** and ‡ indicate $p < 0.017$. On the other hand, # indicates $p < 0.05$ between the controlled and the severe uncontrolled groups. BMI: body mass index, Eos: eosinophilia, Inflam: upper airway inflammation.)	102
4.2	Median [25 th , 75 th percentiles] of the parameters that were significantly different among groups. (* and † indicate $p < 0.05$ with respect to the mild and severe controlled groups respectively, whereas ** and ‡ indicate $p < 0.017$. On the other hand, # indicates $p < 0.05$ between the controlled and the severe uncontrolled groups.)	107
4.3	Median [25 th , 75 th percentiles] of the accuracy, sensitivity, specificity and F1 score obtained with the different classification algorithms when the subjects were classified based on their degree of asthma control. The sensitivity, specificity and F1 score were computed considering the uncontrolled asthma group as the positive class. The results correspond to the case of combining cardiorespiratory and clinical features, or using any of them separately.	108
4.4	Features selected for each of the classification approaches and methodologies, when considering all the features or only the clinical or cardiorespiratory ones separately. When the classification was performed attending to the asthma control, the criteria for the feature selection algorithm was to maximize the F1 score of the uncontrolled group. When the classification was based on the asthma severity, the total accuracy was maximized.	108
5.1	Anthropometric data of the UZ Leuven dataset. In the cardiac comorbidity group, subjects under medication intake can be treated with various distinct drugs simultaneously. (BMI: Body Mass Index, AHI: Apnea Hypopnea Index, ACE: Angiotensin Converting Enzyme.)	116
5.2	Anthropometric data of the SHHS dataset. (BMI: Body Mass Index, AHI: Apnea Hypopnea Index.)	117

5.3	Results of HRV analysis for the UZ Leuven dataset. Results are displayed as median (IQR), except for the number of subjects. Significant differences with the same sleep stage of the control group are marked with † ($p < 0.05$). Significant differences between NREM and REM sleep within each group are marked with * ($p < 0.05$).	122
5.4	Results of HRV analysis for the SHHS dataset. Results are displayed as median (IQR), except for the number of subjects. Significant differences with the same sleep stage of the control group are marked with † ($p < 0.05$). Significant differences between NREM and REM sleep within each group are marked with * ($p < 0.05$).	123
6.1	Demographics of the subjects in the presented dataset. All the values are given as mean \pm standard deviation, except from the number of subjects (N) and the maximum heart rate (the latter is provided as median [25 th , 75 th percentiles] since it was not normally distributed). (BMI: Body Mass Index).	131
6.2	Inter-subject medians of median and IQR of the fitting errors obtained with the single-lead EDR approach. Best results were achieved for lead <i>II</i> , so results obtained in lead <i>II</i> with each of the considered EDRs are displayed. The median and IQR of the absolute and relative error corresponding to the lowest relative error in each stage are highlighted in bold type.	138
6.3	Inter-subject medians of median and IQR of the fitting errors obtained with the multi-lead, HR, HRV, F, and multi-parametric approaches. Results concerning the multi-lead approach were achieved considering the leads <i>V4</i> , <i>V6</i> and <i>aVF</i> , whereas those of the multi-parametric approach were obtained from a combination of the single-lead and HR approaches (in the single-lead approach, lead <i>II</i> and QRS downslopes were employed). The median and IQR of the absolute and relative error corresponding to the lowest relative error in each stage are highlighted in bold type.	138
6.4	Median (IQR) of the parameters of the subject-independent multi-parametric model for each stage (parameters of the multi-linear model when the QRS downslopes in lead <i>II</i> and the instantaneous HR are considered, so that $\bar{\alpha}_i$ is the offset, and $\bar{\beta}_i^1$ and $\bar{\beta}_i^2$ are the contributions of the downslopes and the HR respectively). Also the median (IQR) of the absolute and relative errors obtained when estimating the TV using the median model are displayed.	141

-
- 7.1 Parameters of interest in the exercise test (median and [25th, 75th percentiles]). The maximum HR refers to that in the test conducted in this study, and not to the maximum HR reached during the maximal treadmill test (see text for details). The percentage of maximum HR was calculated with respect to the maximum HR in the maximal treadmill test. The workloads refer to the test in this study. (VT: ventilatory threshold, AT: estimated anaerobic threshold). 152

References

- [1] Acharya, U. R., *et al.* Heart rate variability: a review. *Med Biol Eng Comput* 44(12):1031–1051, 2006.
- [2] Agertoft, L. and S. Pedersen. Effects of long-term treatment with an inhaled corticosteroid on growth and pulmonary function in asthmatic children. *Respir Med* 88:373–381, 1994.
- [3] Ahmed, T., J. Garrigo, and I. Danta. Preventing bronchoconstriction in exercise-induced asthma with inhaled heparin. *N Engl J Med* 329:90–95, 1993.
- [4] Akselrod, S. Components of heart rate variability: Basic studies. *Heart Rate Variability* pp. 147–163, 1995.
- [5] AL-Khalidi, F. Q., *et al.* Respiration rate monitoring methods: A review. *Pediatr Pulmonol* 46:523–529, 2011.
- [6] Alcalay, M., *et al.* Paradoxical pharmacodynamic effect of atropine on parasympathetic control: a study by spectral analysis of heart rate fluctuations. *Clin Pharmacol Ther* 52(5):518–527, 1992.
- [7] Ali-Melkkilä, T., *et al.* Effects of glycopyrrolate and atropine on heart rate variability. *Acta Anaesthesiol Scand* 35(5):436–441, 1991.
- [8] Altman, D. G. and J. M. Bland. Measurement in medicine: the analysis of method comparison studies. *J R Stat Soc Series D (Statistician)* 32(3):307–317, 1983.
- [9] American Academy of Sleep Medicine Task Force. Sleep-related breathing disorders in adults: recommendations for syndrome definition and measurement techniques in clinical research. *Sleep* 22:667–689, 1999.
- [10] Anandan, C., *et al.* Is the prevalence of asthma declining? Systematic review of epidemiological studies. *Allergy* 65(2):152–167, 2010.
- [11] Anderson, G. P. Endotyping asthma: new insights into key pathogenic mechanisms in a complex, heterogeneous disease. *Lancet Respir Med* 372(9643):1107–1119, 2008.
- [12] Antelmi, I., *et al.* Influence of age, gender, body mass index, and functional capacity on heart rate variability in a cohort of subjects without heart disease. *Am J Cardiol* 93(3):381–385, 2004.

- [13] Arai, Y., *et al.* Modulation of cardiac autonomic activity during and immediately after exercise. *Am J Physiol Heart Circ Physiol* 256(1):H132–H141, 1989.
- [14] Aurora, R. N., *et al.* Updated adaptive servo-ventilation recommendations for the 2012 AASM guideline: “The treatment of central sleep apnea syndromes in adults: practice parameters with an evidence-based literature review and meta-analyses”. *J Clin Sleep Med* 12(5):757–761, 2016.
- [15] Aydin, M., *et al.* Cardiac autonomic activity in obstructive sleep apnea: time-dependent and spectral analysis of heart rate variability using 24-hour holter electrocardiograms. *Tex Heart Inst J* 31(2):132–136, 2004.
- [16] Bailly, S., *et al.* Obstructive sleep apnea: a cluster analysis at time of diagnosis. *PLoS One* 11(6):e0157318, 2016.
- [17] Bailón, R., *et al.* Influence of running stride frequency in heart rate variability analysis during treadmill exercise testing. *IEEE Trans Biomed Eng* 60(7):1796–1805, 2013.
- [18] Bailón, R., *et al.* Analysis of heart rate variability using time-varying frequency bands based on respiratory frequency. in *Proceedings of the 29th Annual International Conference of the IEEE Engineering in Medicine and Biology Society*, pp. 6674–6677, IEEE, 2007.
- [19] Bailón, R., *et al.* The integral pulse frequency modulation model with time-varying threshold: application to heart rate variability analysis during exercise stress testing. *IEEE Trans Biomed Eng* 58(3):642–652, 2011.
- [20] Bailón, R., *et al.* Analysis of heart rate variability during exercise stress testing using respiratory information. *Biomed Signal Process Control* 5(4):299–310, 2010.
- [21] Bailón, R., *et al.* A robust method for ECG-based estimation of the respiratory frequency during stress testing. *IEEE Trans Biomed Eng* 53(7):1273–1285, 2006.
- [22] Ballard, R. D., *et al.* Effect of sleep on nocturnal bronchoconstriction and ventilatory patterns in asthmatics. *J App Physiol* 67(1):243–249, 1989.
- [23] Barnes, P. J. Neural mechanisms in asthma. *Br Med Bull* 48(1):149–168, 1992.
- [24] Barnes, P. J. Circadian variation in airway function. *Am J Med* 79(6):5–9, 1985.
- [25] Barnes, P. J. Beta-adrenergic receptors and their regulation. *Am J Respir Crit Care Med* 152(3):838–860, 1995.
- [26] Barnes, P. J. Neuroeffector mechanisms: the interface between inflammation and neuronal responses. *J Allergy Clinical Immunol* 98(5):S73–S83, 1996.
- [27] Bayly, E. J. Spectral analysis of pulse frequency modulation in the nervous systems. *IEEE Trans Biomed Eng* (4):257–265, 1968.

- [28] Beaver, W. L., K. Wasserman, and B. J. Whipp. A new method for detecting anaerobic threshold by gas exchange. *J Appl Physiol* 60:2020–2027, 1986.
- [29] Bekheit, S., *et al.* Use of heart rate spectral analysis to study the effects of calcium channel blockers on sympathetic activity after myocardial infarction. *Am Heart J* 119(1):79–85, 1990.
- [30] Bellia, V., *et al.* Relationship of nocturnal bronchoconstriction. *Am Rev Respir Dis* 140(2):363–367, 1989.
- [31] Ben-Tal, A., S. Shamailov, and J. Paton. Evaluating the physiological significance of respiratory sinus arrhythmia: looking beyond ventilation–perfusion efficiency. *J Physiol* 590(8):1989–2008, 2012.
- [32] Ben-Tal, A., S. S. Shamailov, and J. F. Paton. Central regulation of heart rate and the appearance of respiratory sinus arrhythmia: New insights from mathematical modeling. *Math Biosci* 255:71–82, 2014.
- [33] Bendstrup, K. and J. Jensen. Inhaled heparin is effective in exacerbations of asthma. *Respir Med* 94(2):174–175, 2000.
- [34] Berger, R. D., *et al.* An efficient algorithm for spectral analysis of heart rate variability. *IEEE Trans Biomed Eng* (9):900–904, 1986.
- [35] Bergmann, M. M., *et al.* Agreement of self-reported medical history: comparison of an in-person interview with a self-administered questionnaire. *Eur J Epidemiol* 19(5):411–416, 2004.
- [36] Bernardi, L., *et al.* Effects of controlled breathing, mental activity and mental stress with or without verbalization on heart rate variability. *J Am Coll Cardiol* 35(6):1462–1469, 2000.
- [37] Berry, R. B., *et al.* The AASM manual for the scoring of sleep and associated events: rules, terminology and technical specifications: version 2.3. *American Academy of Sleep Medicine*, 2016.
- [38] Berry, R. B., *et al.* The AASM manual for the scoring of sleep and associated events: rules, terminology and technical specifications: version 2.4. *American Academy of Sleep Medicine*, 2017.
- [39] Berry, R. B., *et al.* The AASM manual for the scoring of sleep and associated events: rules, terminology and technical specifications. *American Academy of Sleep Medicine*, 2012.
- [40] Beydon, N., *et al.* An official American Thoracic Society/European Respiratory Society statement: pulmonary function testing in preschool children. *Am J Respir Crit Care Med* 175(12):1304–1345, 2007.

- [41] Birkett, C., M. Kienzle, and G. Myers. Interpolation over ectopic beats increases low frequency power in heart rate variability spectra. *in Proceedings of the Computers in Cardiology Conference*, pp. 257–259, IEEE, 1991.
- [42] Blain, G., O. Meste, and S. Bermon. Influences of breathing patterns on respiratory sinus arrhythmia in humans during exercise. *Am J Physiol Heart Circ Physiol* 288(2):H887–H895, 2005.
- [43] Bolea, J., *et al.* Methodological framework for estimating the correlation dimension in HRV signals. *Comput Math Methods Med*, 2014.
- [44] Bolea, J., *et al.* Pulse rate and transit time analysis to predict hypotension events after spinal anesthesia during programmed cesarean labor. *Ann Biomed Eng* 45(9):2253–2263, 2017.
- [45] Borresen, J. and M. I. Lambert. Autonomic control of heart rate during and after exercise. *Sports Med* 38(8):633–646, 2008.
- [46] Boulet, L.-P., *et al.* Adherence: the goal to control asthma. *Clin Chest Med* 33(3):405–417, 2012.
- [47] Braman, S. S. The global burden of asthma. *Chest* 130(1):4S–12S, 2006.
- [48] Breiman, L. Random forests. *Mach Learn* 45(1):5–32, 2001.
- [49] Bristow, M. R., *et al.* Decreased catecholamine sensitivity and β -adrenergic-receptor density in failing human hearts. *N Engl J Med* 307(4):205–211, 1982.
- [50] Brown, T. E., *et al.* Important influence of respiration on human RR interval power spectra is largely ignored. *J Appl Physiol* 75(5):2310–2317, 1993.
- [51] Browning, I. B., G. E. D’Alonzo, and M. J. Tobin. Importance of respiratory rate as an indicator of respiratory dysfunction in patients with cystic fibrosis. *Chest* 97(6):1317–1321, 1990.
- [52] Bušek, P., *et al.* Spectral analysis of heart rate variability in sleep. *Physiol Res* 54(4):369–376, 2005.
- [53] Busse, W., *et al.* Expert panel report 3: Guidelines for the diagnosis and management of asthma. *J Allergy Clin Immunol* 120(Suppl 5):S94–S138, 2007.
- [54] Caples, S. M., A. Garcia-Touchard, and V. K. Somers. Sleep-disordered breathing and cardiovascular risk. *Sleep* 30(3):291–303, 2007.
- [55] Carey, D., G. Pliego, and R. Raymond. How endurance athletes breathe during incremental exercise to fatigue: interaction of tidal volume and frequency. *J Exerc Physiol Online* 11(4):44–51, 2008.
- [56] Carey, D. G., *et al.* Respiratory rate is a valid and reliable marker for the anaerobic threshold: implications for measuring change in fitness. *J Sports Sci Med* 4(4):482, 2005.

- [57] Casolo, G., *et al.* Decreased spontaneous heart rate variability in congestive heart failure. *Am J Cardiol* 64(18):1162–1167, 1989.
- [58] Castro-Rodriguez, J. A. The asthma predictive index: a very useful tool for predicting asthma in young children. *J Allergy Clin Immunol* 126(2):212–216, 2010.
- [59] Caudri, D., *et al.* Predicting the long-term prognosis of children with symptoms suggestive of asthma at preschool age. *J Allergy Clin Immunol* 124(5):903–910, 2009.
- [60] Cavkaytar, O., *et al.* Evidence of hypothalamic-pituitary-adrenal axis suppression during moderate-to-high-dose inhaled corticosteroid use. *Eur J Pediatr* 174(11):1421–1431, 2015.
- [61] Charbonneau, M., *et al.* Changes in obstructive sleep apnea characteristics through the night. *Chest* 106(6):1695–1701, 1994.
- [62] Chesné, J., *et al.* IL-17 in severe asthma. Where do we stand? *Am J Respir Crit Care Med* 190(19):1094–1101, 2014.
- [63] Chwalbinska-Moneta, J., *et al.* Threshold for muscle lactate accumulation during progressive exercise. *J Appl Physiol* 66(6):2710–2716, 1989.
- [64] Citterio, G., *et al.* Decay of inspiratory muscle activity in chronic airway obstruction. *J Appl Physiol* 51(6):1388–1397, 1981.
- [65] Cockcroft, D., *et al.* Bronchial reactivity to inhaled histamine: a method and clinical survey. *Clin Exp Allergy* 7(3):235–243, 1977.
- [66] Cottin, F., C. Médigue, and Y. Papelier. Effect of heavy exercise on spectral baroreflex sensitivity, heart rate, and blood pressure variability in well-trained humans. *Am J Physiol Heart Circ Physiol* 295(3):H1150–H1155, 2008.
- [67] Cottin, F. and Y. Papelier. Regulation of the cardiovascular system during dynamic exercise: integrative approach. *Crit Rev Phys Rehabil Med* 14(1):53–81, 2002.
- [68] Cysarz, D., *et al.* Oscillations of heart rate and respiration synchronize during poetry recitation. *Am J Physiol Heart Circ Physiol* 287(2):H579–H587, 2004.
- [69] Dahl, R. Systemic side effects of inhaled corticosteroids in patients with asthma. *Respir Med* 100(8):1307–1317, 2006.
- [70] Davis, K. F., K. P. Parker, and G. L. Montgomery. Sleep in infants and young children: Part one: normal sleep. *J Pediatr Health Care* 18(2):65–71, 2004.
- [71] De Burgh Daly, M. Interactions between respiration and circulation. *Compr Physiol* pp. 529–594, 2011.
- [72] Dergacheva, O., *et al.* Respiratory modulation of premotor cardiac vagal neurons in the brainstem. *Respir Physiol Neurobiol* 174(1-2):102–110, 2010.

- [73] Douglas, N., *et al.* Respiration during sleep in normal man. *Thorax* 37(11):840–844, 1982.
- [74] Eckberg, D. L. Human sinus arrhythmia as an index of vagal cardiac outflow. *J Appl Physiol* 54(4):961–966, 1983.
- [75] Eckberg, D. L. Point: counterpoint: respiratory sinus arrhythmia is due to a central mechanism vs. respiratory sinus arrhythmia is due to the baroreflex mechanism. *J Appl Physiol* 106(5):1740–1742, 2009.
- [76] Eckert, D. J., *et al.* Central sleep apnea: pathophysiology and treatment. *Chest* 131(2):595–607, 2007.
- [77] Eckert, D. J., *et al.* Defining phenotypic causes of obstructive sleep apnea. Identification of novel therapeutic targets. *Am J Respir Crit Care Med* 188(8):996–1004, 2013.
- [78] Efron, B. and R. J. Tibshirani. An introduction to the bootstrap. *CRC Press*, 1994.
- [79] Eigen, H., *et al.* Spirometric pulmonary function in healthy preschool children. *Am J Respir Crit Care Med* 163(3):619–623, 2001.
- [80] Emin, O., *et al.* Autonomic nervous system dysfunction and their relationship with disease severity in children with atopic asthma. *Respir Physiol Neurobiol* 183(3):206–210, 2012.
- [81] Epstein, L. J., *et al.* Clinical guideline for the evaluation, management and long-term care of obstructive sleep apnea in adults. *J Clin Sleep Med* 5(3):263–276, 2009.
- [82] Fajt, M. L. and S. E. Wenzel. Asthma phenotypes and the use of biologic medications in asthma and allergic disease: the next steps toward personalized care. *J Allergy Clin Immunol* 135(2):299–310, 2015.
- [83] Faude, O., W. Kindermann, and T. Meyer. Lactate threshold concepts. *Sports Med* 39(6):469–490, 2009.
- [84] Fenech, A., *et al.* Mutation screening of the muscarinic M₂ and M₃ receptor genes in normal and asthmatic subjects. *Br J Pharmacol* 133(1):43–48, 2001.
- [85] Fieselman, J. F., *et al.* Respiratory rate predicts cardiopulmonary arrest for internal medicine inpatients. *J Gen Intern Med* 8(7):354–360, 1993.
- [86] Findley, L. J., *et al.* Apnea duration and hypoxemia during rem sleep in patients with obstructive sleep apnea. *Chest* 87(4):432–436, 1985.
- [87] Finley, J. P. and S. T. Nugent. Heart rate variability in infants, children and young adults. *J Auton Nerv Syst* 51(2):103–108, 1995.
- [88] Flandrin, P. Time-frequency signal analysis and processing. *Elsevier*, pp. 160–167, 2003.

- [89] Fleming, S., *et al.* Normal ranges of heart rate and respiratory rate in children from birth to 18 years of age: a systematic review of observational studies. *Lancet Respir Med* 377(9770):1011–1018, 2011.
- [90] Fryer, A. D. and D. B. Jacoby. Muscarinic receptors and control of airway smooth muscle. *Am J Respir Crit Care Med* 158(Suppl 2):S154–S160, 1998.
- [91] Galletly, D. and P. Larsen. Cardioventilatory coupling during anaesthesia. *Br J Anaesth* 79(1):35–40, 1997.
- [92] Garcia, G., *et al.* Anti-interleukin-5 therapy in severe asthma. *Eur Respir Rev* 22(129):251–257, 2013.
- [93] Garcia III, A. J., *et al.* Cardiorespiratory coupling in health and disease. *Auton Neurosci* 175(1-2):26–37, 2013.
- [94] Garrard, C. S., *et al.* Spectral analysis of heart rate variability in bronchial asthma. *Clin Auton Res* 2(2):105–111, 1992.
- [95] Giardino, N. D., L. Chan, and S. Borson. Combined heart rate variability and pulse oximetry biofeedback for chronic obstructive pulmonary disease: preliminary findings. *Appl Psychophysiol Biofeedback* 29(2):121–133, 2004.
- [96] Giardino, N. D., *et al.* Respiratory sinus arrhythmia is associated with efficiency of pulmonary gas exchange in healthy humans. *Am J Physiol Heart Circ Physiol* 284(5):H1585–H1591, 2003.
- [97] Global initiative for asthma. Global strategy for asthma management and prevention. Available from <https://ginasthma.org/>.
- [98] Goldberg, L., D. L. Elliot, and K. S. Kuehl. Assessment of exercise intensity formulas by use of ventilatory threshold. *Chest* 94(1):95–98, 1988.
- [99] Goldberger, A. L. Fractal variability versus pathologic periodicity: complexity loss and stereotypy in disease. *Perspect Biol Med* 40(4):543–561, 1997.
- [100] Goldberger, A. L., *et al.* PhysioBank, PhysioToolkit, and PhysioNet: components of a new research resource for complex physiologic signals. *Circulation* 101(23):e215–e220, 2000.
- [101] Goldie, R., *et al.* In vitro responsiveness of human asthmatic bronchus to carbachol, histamine, beta-adrenoceptor agonists and theophylline. *Br J Clin Pharmacol* 22(6):669–676, 1986.
- [102] Goldsmith, R. L., *et al.* Long-term carvedilol therapy increases parasympathetic nervous system activity in chronic congestive heart failure. *Am J Cardiol* 80(8):1101–1104, 1997.
- [103] Goren, Y., *et al.* Individual time-dependent spectral boundaries for improved accuracy in time-frequency analysis of heart rate variability. *IEEE Trans Biomed Eng* 53(1):35–42, 2006.

- [104] Grassberger, P. and I. Procaccia. Characterization of strange attractors. *Phys Rev Lett* 50(5):346, 1983.
- [105] Gravelyn, T. R. and J. G. Weg. Respiratory rate as an indicator of acute respiratory dysfunction. *JAMA* 244(10):1123–1125, 1980.
- [106] Grossman, P. and E. W. Taylor. Toward understanding respiratory sinus arrhythmia: relations to cardiac vagal tone, evolution and biobehavioral functions. *Biol Psychol* 74(2):263–285, 2007.
- [107] Grossman, P., F. Wilhelm, and M. Spoerle. Respiratory sinus arrhythmia, cardiac vagal control, and daily activity. *Am J Physiol Heart Circ Physiol* 287(2):H728–H734, 2004.
- [108] Guilbert, T. W., *et al.* Atopic characteristics of children with recurrent wheezing at high risk for the development of childhood asthma. *J Allergy Clin Immunol* 114(6):1282–1287, 2004.
- [109] Guilbert, T. W., *et al.* Long-term inhaled corticosteroids in preschool children at high risk for asthma. *N Engl J Med* 354(19):1985–1997, 2006.
- [110] Guilleminault, C., *et al.* Cyclical variation of the heart rate in sleep apnoea syndrome: mechanisms, and usefulness of 24 h electrocardiography as a screening technique. *Lancet Respir Med* 323(8369):126–131, 1984.
- [111] Gula, L. J., *et al.* Heart rate variability in obstructive sleep apnea: a prospective study and frequency domain analysis. *Ann Noninvasive Electrocardiol* 8(2):144–149, 2003.
- [112] Guyton, A. and J. Hall. Textbook of medical physiology. 12th ed. *Saunders*, 2011.
- [113] Guzzetti, S., *et al.* Heart rate variability in chronic heart failure. *Auton Neurosci* 90(1-2):102–105, 2001.
- [114] Guzzetti, S., *et al.* Sympathetic predominance in essential hypertension: a study employing spectral analysis of heart rate variability. *J Hypertens* 6(9):711–717, 1988.
- [115] Hamm, W., *et al.* Dynamic changes of cardiac repolarization instability during exercise testing. *Med Sci Sports Exerc* 51(7):1517–1522, 2019.
- [116] Hanson, B., *et al.* Oscillatory behavior of ventricular action potential duration in heart failure patients at respiratory rate and low frequency. *Front Physiol* 5:414, 2014.
- [117] Hayano, J. and F. Yasuma. Hypothesis: respiratory sinus arrhythmia is an intrinsic resting function of cardiopulmonary system. *Cardiovasc Res* 58(1):1–9, 2003.
- [118] Hayano, J., *et al.* Respiratory sinus arrhythmia: a phenomenon improving pulmonary gas exchange and circulatory efficiency. *Circulation* 94(4):842–847, 1996.

- [119] Heffler, E., *et al.* Inhaled corticosteroids safety and adverse effects in patients with asthma. *J Allergy Clin Immunol* 6(3):776–781, 2018.
- [120] Heinzer, R., *et al.* Prevalence of sleep-disordered breathing in the general population: the HypnoLaus study. *Lancet Respir Med* 3(4):310–318, 2015.
- [121] Hernando, A., *et al.* Inclusion of respiratory frequency information in heart rate variability analysis for stress assessment. *IEEE J Biomed Health Inform* 20(4):1016–1025, 2016.
- [122] Hernando, D., *et al.* Methodological framework for heart rate variability analysis during exercise: application to running and cycling stress testing. *Med Biol Eng Comput* 56(5):781–794, 2018.
- [123] Hirsch, J. A. and B. Bishop. Respiratory sinus arrhythmia in humans: how breathing pattern modulates heart rate. *Am J Physiol Heart Circ Physiol* 241(4):H620–H629, 1981.
- [124] Hofmann, P., *et al.* Heart rate threshold related to lactate turn point and steady-state exercise on a cycle ergometer. *Eur J Appl Physiol Occup Physiol* 69(2):132–139, 1994.
- [125] Huikuri, H. V., *et al.* Reproducibility and circadian rhythm of heart rate variability in healthy subjects. *Am J Cardiol* 65(5):391–393, 1990.
- [126] Huikuri, H. V., *et al.* Heart rate variability in systemic hypertension. *Am J Cardiol* 77(12):1073–1077, 1996.
- [127] Julien, C., *et al.* Comments on point: counterpoint: respiratory sinus arrhythmia is due to a central mechanism vs. respiratory sinus arrhythmia is due to the baroreflex mechanism. *J Appl Physiol* 106(5):1745–1749, 2009.
- [128] Juniper, E., *et al.* Development and validation of the mini asthma quality of life questionnaire. *Eur Resp J* 14(1):32–38, 1999.
- [129] Kabir, M. M., *et al.* Cardiorespiratory phase-coupling is reduced in patients with obstructive sleep apnea. *PLoS One* 5(5):e10602, 2010.
- [130] Kaliner, M., *et al.* Autonomic nervous system abnormalities and allergy. *Ann Intern Med* 96(3):349–357, 1982.
- [131] Kallenbach, J., *et al.* Reflex heart rate control in asthma: evidence of parasympathetic overactivity. *Chest* 87(5):644–648, 1985.
- [132] Kamath, M. V. and E. L. Fallen. Correction of the heart rate variability signal for ectopics and missing beats. *Heart Rate Variability* pp. 75–85, 1995.
- [133] Kantz, H. and T. Schreiber. Nonlinear time series analysis, volume 7. *Cambridge university press*, 2004.

- [134] Karapetian, G., H. Engels, and R. Gretebeck. Use of heart rate variability to estimate LT and VT. *Int J Sports Med* 29(8):652–657, 2008.
- [135] Karemaker, J. M. Counterpoint: respiratory sinus arrhythmia is due to the baroreflex mechanism. *J Appl Physiol* 106(5):1742–1743, 2009.
- [136] Kasai, T., J. S. Floras, and T. D. Bradley. Sleep apnea and cardiovascular disease: a bidirectional relationship. *Circulation* 126(12):1495–1510, 2012.
- [137] Kau, A. L. and P. E. Korenblat. Anti-interleukin 4 and 13 for asthma treatment in the era of endotypes. *Curr Opin Allergy Clin Immunol* 14(6):570, 2014.
- [138] Kim, H. C., *et al.* Sleep-disordered breathing and neuropsychological deficits: a population-based study. *Am J Respir Crit Care Med* 156(6):1813–1819, 1997.
- [139] Kleiger, R. E., *et al.* Decreased heart rate variability and its association with increased mortality after acute myocardial infarction. *Am J Cardiol* 59(4):256–262, 1987.
- [140] Klion, A. D., *et al.* Familial eosinophilia: a benign disorder? *Blood* 103(11):4050–4055, 2004.
- [141] Korkushko, O., *et al.* Autonomic control of cardiac chronotropic function in man as a function of age: assessment by power spectral analysis of heart rate variability. *J Auton Nerv Syst* 32(3):191–198, 1991.
- [142] Krieger, B., *et al.* Continuous noninvasive monitoring of respiratory rate in critically ill patients. *Chest* 90(5):632–634, 1986.
- [143] Kurukulaaratchy, R., *et al.* Predicting persistent disease among children who wheeze during early life. *Eur Respir J* 22(5):767–771, 2003.
- [144] Laguna, P., G. B. Moody, and R. G. Mark. Power spectral density of unevenly sampled data by least-square analysis: performance and application to heart rate signals. *IEEE Trans Biomed Eng* 45(6):698–715, 1998.
- [145] Lázaro, J., *et al.* Electrocardiogram derived respiratory rate from QRS slopes and R-wave angle. *Ann Biomed Eng* 42(10):2072–2083, 2014.
- [146] Lázaro, J., *et al.* Deriving respiration from photoplethysmographic pulse width. *Med Biol Eng Comput* 51(1-2):233–242, 2013.
- [147] Lee, M.-Y. and S.-N. Yu. Improving discriminability in heart rate variability analysis using simple artifact and trend removal preprocessors. *in Proceedings of the 32nd Annual International Conference of the IEEE Engineering in Medicine and Biology Society*, pp. 4574–4577, IEEE, 2010.
- [148] Lehrer, P., Y. Sasaki, and Y. Saito. Zazen and cardiac variability. *Psychosom Med* 61(6):812–821, 1999.

- [149] Lenis, G., *et al.* Separating the effect of respiration on the heart rate variability using Granger's causality and linear filtering. *Biomed Signal Process Control* 31:272–287, 2017.
- [150] Leung, R. S. and T. Douglas Bradley. Sleep apnea and cardiovascular disease. *Am J Respir Crit Care Med* 164(12):2147–2165, 2001.
- [151] Lewis, M., A. Short, and K. Lewis. Autonomic nervous system control of the cardiovascular and respiratory systems in asthma. *Respir Med* 100(10):1688–1705, 2006.
- [152] Lezmi, G., *et al.* Airway remodeling in preschool children with severe recurrent wheeze. *Am J Respir Crit Care Med* 192(2):164–171, 2015.
- [153] Liao, D., *et al.* Age, race, and sex differences in autonomic cardiac function measured by spectral analysis of heart rate variability—the aric study. *Am J Cardiol* 76(12):906–912, 1995.
- [154] Lim, S., *et al.* Relationship between exhaled nitric oxide and mucosal eosinophilic inflammation in mild to moderately severe asthma. *Thorax* 55(3):184–188, 2000.
- [155] Lin, J.-L., *et al.* Long-term β -blocker therapy improves autonomic nervous regulation in advanced congestive heart failure: a longitudinal heart rate variability study. *Am Heart J* 137(4):658–665, 1999.
- [156] Lippman, N., K. M. Stein, and B. B. Lerman. Comparison of methods for removal of ectopy in measurement of heart rate variability. *Am J Physiol Heart Circ Physiol* 267(1):H411–H418, 1994.
- [157] Lipponen, J. A. and M. P. Tarvainen. A robust algorithm for heart rate variability time series artefact correction using novel beat classification. *J Med Eng Tech* 43(3):173–181, 2019.
- [158] Lum, S., *et al.* Early detection of cystic fibrosis lung disease: multiple-breath washout vs. raised volume tests. *Thorax* 62(4):341–347, 2006.
- [159] Lum, S., *et al.* Potential misinterpretation of infant lung function unless prospective healthy controls are studied. *Pediatr Pulmonol* 45(9):906–913, 2010.
- [160] Lutfi, M. F. Patterns of heart rate variability and cardiac autonomic modulations in controlled and uncontrolled asthmatic patients. *BMC Pulm Med* 15(1):119, 2015.
- [161] Mainardi, L. T., *et al.* Pole-tracking algorithms for the extraction of time-variant heart rate variability spectral parameters. *IEEE Trans Biomed Eng* 42(3):250–259, 1995.
- [162] Malfatto, G., *et al.* Effects of cardiac rehabilitation and beta-blocker therapy on heart rate variability after first acute myocardial infarction. *Am J Cardiol* 81(7):834–840, 1998.

- [163] Malliani, A. The pattern of sympathovagal balance explored in the frequency domain. *Physiology* 14(3):111–117, 1999.
- [164] Malliani, A., *et al.* Cardiovascular neural regulation explored in the frequency domain. *Circulation* 84(2):482–492, 1991.
- [165] Malmberg, L. P., *et al.* Measurement of tidal breathing flows in infants using impedance pneumography. *Eur Respir J* 49(2):1600926, 2017.
- [166] Martinez, F. D., *et al.* Asthma and wheezing in the first six years of life. *N Engl J Med* 332(3):133–138, 1995.
- [167] Martínez, J. P., *et al.* A wavelet-based ECG delineator: evaluation on standard databases. *IEEE Trans Biomed Eng* 51(4):570–581, 2004.
- [168] Masoli, M., *et al.* for Asthma (GINA) Program. The global burden of asthma: executive summary of the GINA Dissemination Committee report. *Allergy* 59(5):469–478, 2004.
- [169] Mason, C. and L. Tarassenko. Quantitative assessment of respiratory derivation algorithms. in *Proceedings of the 23rd Annual International Conference of the IEEE Engineering in Medicine and Biology Society*, pp. 1998–2001, IEEE, 2001.
- [170] Massaroni, C., *et al.* Contact-based methods for measuring respiratory rate. *Sensors* 19:908, 2019.
- [171] Mateo, J. and P. Laguna. Improved heart rate variability signal analysis from the beat occurrence times according to the IPFM model. *IEEE Trans Biomed Eng* 47(8):985–996, 2000.
- [172] Mateo, J. and P. Laguna. Analysis of heart rate variability in the presence of ectopic beats using the heart timing signal. *IEEE Trans Biomed Eng* 50(3):334–343, 2003.
- [173] McCorry, L. K. Physiology of the autonomic nervous system. *Am J Pharm Educ* 71(4):78, 2007.
- [174] McGrath, K. W., *et al.* A large subgroup of mild-to-moderate asthma is persistently noneosinophilic. *Am J Respir Crit Care Med* 185(6):612–619, 2012.
- [175] McNames, J., T. Thong, and M. Aboy. Impulse rejection filter for artifact removal in spectral analysis of biomedical signals. in *Proceedings of the 26th Annual International Conference of the IEEE Engineering in Medicine and Biology Society*, pp. 145–148, IEEE, 2004.
- [176] Médigue, C., *et al.* Relationship between pulse interval and respiratory sinus arrhythmia: a time- and frequency-domain analysis of the effects of atropine. *Pflügers Archiv* 441(5):650–655, 2001.
- [177] Merri, M., *et al.* Sampling frequency of the electrocardiogram for spectral analysis of the heart rate variability. *IEEE Trans Biomed Eng* 37(1):99–106, 1990.

- [178] Milagro, J., *et al.* Noninvasive cardiorespiratory signals analysis for asthma evolution monitoring in preschool children. *IEEE Trans Biomed Eng.* Major revision.
- [179] Minette, P., *et al.* A muscarinic agonist inhibits reflex bronchoconstriction in normal but not in asthmatic subjects. *J Appl Physiol* 67(6):2461–2465, 1989.
- [180] Mirmohamadsadeghi, L., J.-M. Vesin, M. Lemay, and O. Dériaz. The respiration pattern as an indicator of the anaerobic threshold. in *Proceedings of the 37th Annual International Conference of the IEEE Engineering in Medicine and Biology Society*, pp. 546–549, IEEE, 2015.
- [181] Moody, G. B. and R. G. Mark. The impact of the MIT-BIH arrhythmia database. *IEEE Eng Med Biol Mag* 20(3):45–50, 2001.
- [182] Moody, G. B., *et al.* Derivation of respiratory signals from multi-lead ECGs. in *Proceedings of the Computers in Cardiology Conference*, pp. 113–116, IEEE, 1985.
- [183] Moors, J. J. A. The meaning of kurtosis: Darlington reexamined. *Am Stat* 40(4):283–284, 1986.
- [184] Morrison, J., S. Pearson, and H. Dean. Parasympathetic nervous system in nocturnal asthma. *Br Med J (Clin Res ed.)* 296(6634):1427, 1988.
- [185] Nadel, J. A. and P. J. Barnes. Autonomic regulation of the airways. *Annu Rev Med* 35(1):451–467, 1984.
- [186] Nagashima, M., *et al.* Cardiac arrhythmias in healthy children revealed by 24-hour ambulatory ECG monitoring. *Pediatr Cardiol* 8(2):103–108, 1987.
- [187] Nardelli, M., *et al.* Recognizing emotions induced by affective sounds through heart rate variability. *IEEE Trans Affect Comput* 6(4):385–394, 2015.
- [188] Narkiewicz, K., *et al.* Contribution of tonic chemoreflex activation to sympathetic activity and blood pressure in patients with obstructive sleep apnea. *Circulation* 97(10):943–945, 1998.
- [189] Navarro-Verdugo, A. L., *et al.* A modified Boltzmann sigmoidal model for the phase transition of smart gels. *Soft Matter* 7(12):5847–5853, 2011.
- [190] Neder, J. A. and R. Stein. A simplified strategy for the estimation of the exercise ventilatory thresholds. *Med Sci Sports Exerc* 38(5):1007, 2006.
- [191] Niizeki, K. and T. Saitoh. Incoherent oscillations of respiratory sinus arrhythmia during acute mental stress in humans. *Am J Physiol Heart Circ Physiol* 302(1):H359–H367, 2011.
- [192] Niwa, K., *et al.* Prevalence of arrhythmias and conduction disturbances in large population-based samples of children. *Cardiol Young* 14(1):68–74, 2004.

- [193] Oh, C. K., *et al.* A randomized, controlled trial to evaluate the effect of an anti-interleukin-9 monoclonal antibody in adults with uncontrolled asthma. *Respir Res* 14(1):93, 2013.
- [194] Orini, M., *et al.* A multivariate time-frequency method to characterize the influence of respiration over heart period and arterial pressure. *EURASIP J Adv Signal Process* 2012(1):214, 2012.
- [195] Orini, M., *et al.* Characterization of dynamic interactions between cardiovascular signals by time-frequency coherence. *IEEE Trans Biomed Eng* 59(3):663–673, 2012.
- [196] Pagani, M., *et al.* Power spectral analysis of heart rate and arterial pressure variabilities as a marker of sympatho-vagal interaction in man and conscious dog. *Circ Res* 59(2):178–193, 1986.
- [197] Pearson, K. Das Fehlgengesetz und seine Verallgemeinerungen durch Fechner und Pearson. A Rejoinder. *Biometrika* 4:169–212, 1905.
- [198] Peker, Y., *et al.* Increased incidence of cardiovascular disease in middle-aged men with obstructive sleep apnea: a 7-year follow-up. *Am J Respir Crit Care Med* 166(2):159–165, 2002.
- [199] Penzel, T., *et al.* Comparison of detrended fluctuation analysis and spectral analysis for heart rate variability in sleep and sleep apnea. *IEEE Trans Biomed Eng* 50(10):1143–1151, 2003.
- [200] Peppard, P. E., *et al.* Longitudinal association of sleep-related breathing disorder and depression. *Arch Intern Med* 166(16):1709–1715, 2006.
- [201] Peppard, P. E., *et al.* Increased prevalence of sleep-disordered breathing in adults. *Am J Epidemiol* 177(9):1006–1014, 2013.
- [202] Peppard, P. E., *et al.* Prospective study of the association between sleep-disordered breathing and hypertension. *N Engl J Med* 342(19):1378–1384, 2000.
- [203] Pesant, C., *et al.* Spirometric pulmonary function in 3-to 5-year-old children. *Pediatr Pulmonol* 42(3):263–271, 2007.
- [204] Pin, I., *et al.* Use of induced sputum cell counts to investigate airway inflammation in asthma. *Thorax* 47(1):25–29, 1992.
- [205] Pincus, S. M., I. M. Gladstone, and R. A. Ehrenkranz. A regularity statistic for medical data analysis. *J Clin Monit* 7(4):335–345, 1991.
- [206] Plaza, V. M., *et al.* GEMA (4.0). Guidelines for asthma management. *Arch Bronconeumol* 51(Suppl 1):2–54, 2015.
- [207] Porcari, J., C. Bryant, and F. Comana. *Exerc Physiol. FA Davis*, 2015.

- [208] Porta, A., *et al.* Conditional self-entropy and conditional joint transfer entropy in heart period variability during graded postural challenge. *PLoS One* 10(7):e0132851, 2015.
- [209] Porter, B., *et al.* Beat-to-beat variability of ventricular action potential duration oscillates at low frequency during sympathetic provocation in humans. *Front Physiol* 9:147, 2018.
- [210] Pueyo, E., *et al.* Interactive effect of beta-adrenergic stimulation and mechanical stretch on low-frequency oscillations of ventricular action potential duration in humans. *J Mol Cell Cardiol* 97:93–105, 2016.
- [211] Quan, S. F., *et al.* The sleep heart health study: design, rationale, and methods. *Sleep* 20(12):1077–1085, 1997.
- [212] Que, C.-L., *et al.* Homeokinesis and short-term variability of human airway caliber. *J Appl Physiol* 91(3):1131–1141, 2001.
- [213] Reinaux, C. M. A., *et al.* Tidal volume measurements in infants: Opto-electronic plethysmography versus pneumotachograph. *Pediatr Pulmonol* 51(8):850–857, 2016.
- [214] Reinhard, U., P. Müller, and R.-M. Schmölling. Determination of anaerobic threshold by the ventilation equivalent in normal individuals. *Respiration* 38(1):36–42, 1979.
- [215] Reljin, N., B. A. Reyes, and K. H. Chon. Tidal volume estimation using the blanket fractal dimension of the tracheal sounds acquired by smartphone. *Sensors* 15(5):9773–9790, 2015.
- [216] Reyes, B. A., *et al.* Tidal volume and instantaneous respiration rate estimation using a volumetric surrogate signal acquired via a smartphone camera. *IEEE J Biomed Health Inform* 21(3):764–777, 2017.
- [217] Reyes del Paso, G. A., *et al.* The utility of low frequency heart rate variability as an index of sympathetic cardiac tone: a review with emphasis on a reanalysis of previous studies. *Psychophysiology* 50(5):477–487, 2013.
- [218] Richman, J. S. and J. R. Moorman. Physiological time-series analysis using approximate entropy and sample entropy. *Am J Physiol Heart Circ Physiol* 278(6):H2039–H2049, 2000.
- [219] Riedl, M., *et al.* Cardio-respiratory coordination increases during sleep apnea. *PloS One* 9(4):e93866, 2014.
- [220] Ritz, T., E. Simon, and A. F. Trueba. Stress-induced respiratory pattern changes in asthma. *Psychosom Med* 73(6):514–521, 2011.

- [221] Ritz, T., M. Thöns, and B. Dahme. Modulation of respiratory sinus arrhythmia by respiration rate and volume: Stability across posture and volume variations. *Psychophysiology* 38(5):858–862, 2001.
- [222] Rizas, K. D., *et al.* Sympathetic activity–associated periodic repolarization dynamics predict mortality following myocardial infarction. *J Clin Invest* 124(4):1770–1780, 2014.
- [223] Rompelman, O., A. Coenen, and R. Kitney. Measurement of heart-rate variability: part 1 - comparative study of heart-rate variability analysis methods. *Med Biol Eng Comput* 15(3):233, 1977.
- [224] Sackner, M. A., *et al.* Periodic sleep apnea: chronic sleep deprivation related to intermittent upper airway obstruction and central nervous system disturbance. *Chest* 67(2):164–171, 1975.
- [225] Sakakibara, M., S. Takeuchi, and J. Hayano. Effect of relaxation training on cardiac parasympathetic tone. *Psychophysiology* 31(3):223–228, 1994.
- [226] Sampedro-Puente, D. A., *et al.* Mechanisms underlying interactions between low-frequency oscillations and beat-to-beat variability of cellular ventricular repolarization in response to sympathetic stimulation: Implications for arrhythmogenesis. *Front Physiol* 10:916, 2019.
- [227] Sandrone, G., *et al.* Effects of beta blockers (atenolol or metoprolol) on heart rate variability after acute myocardial infarction. *Am J Cardiol* 74(4):340–345, 1994.
- [228] Sassi, R., *et al.* Advances in heart rate variability signal analysis: joint position statement by the e-Cardiology ESC Working Group and the European Heart Rhythm Association co-endorsed by the Asia Pacific Heart Rhythm Society. *Europace* 17(9):1341–1353, 2015.
- [229] Saul, J. P., *et al.* Transfer function analysis of the circulation: unique insights into cardiovascular regulation. *Am J Physiol Heart Circ Physiol* 261(4):H1231–H1245, 1991.
- [230] Sayadi, O., *et al.* An optimized method for estimating the tidal volume from intracardiac or body surface electrocardiographic signals: implications for estimating minute ventilation. *Am J Physiol Heart Circ Physiol* 307(3):H426–H436, 2014.
- [231] Schäfer, C., *et al.* Heartbeat synchronized with ventilation. *Nature* 392(6673):239, 1998.
- [232] Schatz, M., *et al.* The relationship of asthma impairment determined by psychometric tools to future asthma exacerbations. *Chest* 141(1):66–72, 2012.
- [233] Scheinin, H., *et al.* Spectral analysis of heart rate variability as a quantitative measure of parasympatholytic effect-integrated pharmacokinetics and pharmacodynamics of three anticholinergic drugs. *Ther Drug Monit* 21(2):141–151, 1999.

- [234] Schleich, F. N., *et al.* Distribution of sputum cellular phenotype in a large asthma cohort: predicting factors for eosinophilic vs neutrophilic inflammation. *BMC Pulm Med* 13(1):11, 2013.
- [235] Schulz, S., *et al.* Cardiovascular and cardiorespiratory coupling analyses: a review. *Philos Trans Royal Soc A Math Phys Eng Sci* 371(1997):20120191, 2013.
- [236] Seppä, V.-P., *et al.* Tidal breathing flow measurement in awake young children by using impedance pneumography. *J Appl Physiol* 115(11):1725–1731, 2013.
- [237] Seppä, V.-P., *et al.* Tidal flow variability measured by impedance pneumography relates to childhood asthma risk. *Eur Resp J* 47(6):1687–1696, 2016.
- [238] Seppä, V.-P., J. Viik, and J. Hyttinen. Assessment of pulmonary flow using impedance pneumography. *IEEE Trans Biomed Eng* 57(9):2277, 2010.
- [239] Shaffer, F. and J. Ginsberg. An overview of heart rate variability metrics and norms. *Front Public Health* 5:258, 2017.
- [240] Shah, P. K., *et al.* Clinical dysautonomia in patients with bronchial asthma: study with seven autonomic function tests. *Chest* 98(6):1408–1413, 1990.
- [241] Shee, C., Y. Ploy-Song-Sang, and J. Milic-Emili. Decay of inspiratory muscle pressure during expiration in conscious humans. *J Appl Physiol* 58(6):1859–1865, 1985.
- [242] Silverthorn, D. U. Human physiology: An integrated approach. 6th ed. *Pearson*, 2016
- [243] Smeeton, N. C., *et al.* Agreement between responses to a standardized asthma questionnaire and a questionnaire following a demonstration of asthma symptoms in adults. *Am J Epidemiol* 163(4):384–391, 2006.
- [244] Somers, V. K., *et al.* Sympathetic-nerve activity during sleep in normal subjects. *N Engl J Med* 328(5):303–307, 1993.
- [245] Somers, V. K., *et al.* Sleep apnea and cardiovascular disease: An American Heart Association/American College of Cardiology Foundation scientific statement from the American Heart Association Council for High Blood Pressure Research Professional Education Committee, Council on Clinical Cardiology, Stroke Council, and Council on Cardiovascular Nursing in collaboration with the National Heart, Lung, and Blood Institute National Center on Sleep Disorders Research (National Institutes of Health). *J Am Coll Cardiol* 52(8):686–717, 2008.
- [246] Sörnmo, L. and P. Laguna. Bioelectrical signal processing in cardiac and neurological applications, volume 8. *Academic Press*, 2005.
- [247] Soutar, C., M. Carruthers, and C. Pickering. Nocturnal asthma and urinary adrenaline and noradrenaline excretion. *Thorax* 32(6):677–683, 1977.

- [248] Stanojevic, S., A. Wade, and J. Stocks. Reference values for lung function: past, present and future. *Eur Respir J* 36(1):12–19, 2010.
- [249] Stein, P. K. and Y. Pu. Heart rate variability, sleep and sleep disorders. *Sleep Med Rev* 16(1):47–66, 2012.
- [250] Suzuki, Y. J., *et al.* Oxidative stress and oxidant signaling in obstructive sleep apnea and associated cardiovascular diseases. *Free Radic Biol Med* 40(10):1683–1692, 2006.
- [251] Svedahl, K. and B. R. MacIntosh. Anaerobic threshold: the concept and methods of measurement. *Can J Appl Physiol* 28(2):299–323, 2003.
- [252] Task Force of the European Society of Cardiology and the North American Society of Pacing and Electrophysiology. Heart rate variability: Standards of measurement, physiological interpretation, and clinical use. *Eur Heart J* 17:354–381, 1996.
- [253] Teran-Santos, J., *et al.* The association between sleep apnea and the risk of traffic accidents. *N Engl J Med* 340(11):847–851, 1999.
- [254] Thayer, J. F., S. S. Yamamoto, and J. F. Brosschot. The relationship of autonomic imbalance, heart rate variability and cardiovascular disease risk factors. *Int J Cardiol* 141(2):122–131, 2010.
- [255] Tietjens, J. R., *et al.* Obstructive sleep apnea in cardiovascular disease: A review of the literature and proposed multidisciplinary clinical management strategy. *J Am Heart Assoc* 8(1):e010440, 2019.
- [256] Tipton, M. J., *et al.* The human ventilatory response to stress: rate or depth? *J Physiol* 595(17):5729–5752, 2017.
- [257] Tokuyama, K., *et al.* Beat-to-beat variation of the heart rate in children with allergic asthma. *J Asthma* 22(6):285–288, 1985.
- [258] Tregear, S., *et al.* Obstructive sleep apnea and risk of motor vehicle crash: systematic review and meta-analysis. *J Clin Sleep Med* 5(6):573–581, 2009.
- [259] Tzeng, Y., *et al.* Human sinus arrhythmia: inconsistencies of a teleological hypothesis. *Am J Physiol Heart Circ Physiol* 296(1):H65–H70, 2009.
- [260] Van De Borne, P., *et al.* Absence of low-frequency variability of sympathetic nerve activity in severe heart failure. *Circulation* 95(6):1449–1454, 1997.
- [261] Van Ganse, E., *et al.* Effects of antihistamines in adult asthma: a meta-analysis of clinical trials. *Eur Respir J* 10(10):2216–2224, 1997.
- [262] Vanninen, E., *et al.* Cardiac sympathovagal balance during sleep apnea episodes. *Clin Physiol* 16(3):209–216, 1996.
- [263] Varon, C., *et al.* A novel algorithm for the automatic detection of sleep apnea from single-lead ECG. *IEEE Trans Biomed Eng* 62(9):2269–2278, 2015.

- [264] Varon, C., *et al.* Unconstrained estimation of HRV indices after removing respiratory influences from heart rate. *IEEE J Biomed Health Inform* (Early Access), 2018.
- [265] Varon, C. and S. Van Huffel. Complexity and nonlinearities in cardiorespiratory signals in sleep and sleep apnea. *In: Complexity and Nonlinearity in Cardiovascular Signals*, pp. 503–537, Springer, 2017.
- [266] Vega, J., *et al.* Validation of the spanish version of the asthma control test (ACT). *J Asthma* 44(10):867–872, 2007.
- [267] Veiga, J., *et al.* Approximate entropy as a measure of the airflow pattern complexity in asthma. *in Proceedings of the 32th Annual International Conference of the IEEE Engineering in Medicine and Biology Society*, pp. 2463–2466, IEEE, 2010.
- [268] Voss, A., *et al.* Short-term heart rate variability–influence of gender and age in healthy subjects. *PloS One* 10(3):e0118308, 2015.
- [269] Wang, Y., *et al.* Altered cardiac autonomic nervous function in depression. *BMC Psychiatry* 13(1):187, 2013.
- [270] Wasserman, K. The anaerobic threshold measurement to evaluate exercise performance. *Am Rev Respir Dis* 129(2P2):S35–S40, 1984.
- [271] Wasserman, K. The anaerobic threshold: definition, physiological significance and identification. *Adv Cardiol* 35:1–23, 1986.
- [272] Wasserman, K. and M. B. McIlroy. Detecting the threshold of anaerobic metabolism in cardiac patients during exercise. *Am J Cardiol* 14(6):844–852, 1964.
- [273] Welch, P. The use of fast fourier transform for the estimation of power spectra: a method based on time averaging over short, modified periodograms. *IEEE Trans Audio Electroacoust* 15(2):70–73, 1967.
- [274] Weltman, A., *et al.* Percentages of maximal heart rate, heart rate reserve and VO₂max for determining endurance training intensity in male runners. *Int J Sports Med* 11(3):218–222, 1990.
- [275] Wennerblom, B., *et al.* Patients with uncomplicated coronary artery disease have reduced heart rate variability mainly affecting vagal tone. *Heart* 83(3):290–294, 2000.
- [276] Wenzel, S. E. Asthma phenotypes: the evolution from clinical to molecular approaches. *Nat Med* 18(5):716, 2012.
- [277] Westfall, P. H. Kurtosis as peakedness, 1905–2014. R.I.P. *Am Stat* 68(3):191–195, 2014.
- [278] White, D. P. Pathogenesis of obstructive and central sleep apnea. *Am J Respir Crit Care Med* 172(11):1363–1370, 2005.

- [279] Widdicombe, J. Autonomic regulation: i-NANC/e-NANC. *Am J Respir Crit Care Med* 158(Suppl 2):S171–S175, 1998.
- [280] Widjaja, D., *et al.* Separation of respiratory influences from the tachogram: a methodological evaluation. *PloS One* 9(7):e101713, 2014.
- [281] Widjaja, D., E. Vlemincx, and S. Van Huffel. Stress classification by separation of respiratory modulations in heart rate variability using orthogonal subspace projection. in *Proceedings of the 35th Annual International Conference of the IEEE Engineering in Medicine and Biology Society*, pp. 6123–6126, IEEE, 2013.
- [282] Yacoub, M., *et al.* Cardiovascular disease risk in obstructive sleep apnea: an update. *J Sleep Disord Ther* 7(1), 2017.
- [283] Yaffe, K., *et al.* Sleep-disordered breathing, hypoxia, and risk of mild cognitive impairment and dementia in older women. *JAMA* 306(6):613–619, 2011.
- [284] Yoshimura, K., *et al.* Dynamics of cardiorespiratory response during and after the six-minute walk test in patients with heart failure. *Physiother Theory Pract* pp. 1–12, 2018.
- [285] Young, S., *et al.* The association between early life lung function and wheezing during the first 2 yrs of life. *Eur Respir J* 15(1):151–157, 2000.
- [286] Young, T., *et al.* The occurrence of sleep-disordered breathing among middle-aged adults. *N Engl J Med* 328(17):1230–1235, 1993.
- [287] Zahorska-Markiewicz, B., *et al.* Circadian heart rate variability in asthma. *Med Sci Monit* 3(1):CR52–CR56, 1997.
- [288] Zinchuk, A. V., *et al.* Phenotypes in obstructive sleep apnea: a definition, examples and evolution of approaches. *Sleep Med Rev* 35:113–123, 2017.
- [289] Zulli, R., *et al.* QT dispersion and heart rate variability abnormalities in Alzheimer’s disease and in mild cognitive impairment. *J Am Geriatr Soc* 53(12):2135–2139, 2005.

